Advanced Materials Research Group,

Faculty of Engineering

Developing a Novel *In-situ* Polymerisation Process for Fully Bioresorbable Fibre Reinforced Composites

By

Menghao Chen

(BEng)

Thesis submitted to the University of Nottingham for the degree of Doctor of Philosophy

August 2017

To the love of my life, Jiawa Lu,

Who will always be in the deepest place of my heart.

To my parents, Xin Chen & Li Meng,

With all the support and love in the world.

To my grandfather in law, a man who lived with courage,

strength and resolution.

Xianxiang Meng, dedicated to you.

I miss you so much.

‘An investment in knowledge pays the best interest.’

Benjamin Franklin

ABSTRACT

In recent decades, fully bioresorbable polymer composites with appropriate biocompatibility and mechanical properties have provided an exciting opportunity to replace conventional metal alloy implants. This work explores the development of a novel, one-step *in-situ* polymerisation (ISP) process for the manufacture of fully bioresorbable phosphate based glass fibre (PGF) reinforced composites with matrix materials of polycaprolactone (PCL), polycaprolactone-polylactic acid copolymer (PLA-PCL) and polylactic acid (PLA). Composites produced via conventional laminate stacking (LS) process were used as the comparison to demonstrate the advantages that ISP can provide in composites quality. *In-vitro* degradation in phosphate buffered saline (PBS) at 37 °C, flexural property retention and cytocompatibility were investigated for both LS and ISP composites. Additionally, the composites were degraded under representative flexural loading for high cycle fatigue analysis to understand and predict their lifetime in service and their likely mechanisms of failure.

Significantly more robust fibre/matrix interface and uniform fibre distribution along the cross section of the composites were achieved via ISP compared to LS. These enhancements resulted in considerably higher initial mechanical properties (~450 MPa and ~24 GPa for flexural strength and modulus, close to the upper range of human cortical bone properties), prolonged mechanical retention, less and slower water uptake and mass loss profiles for the ISP composites. The flexural fatigue life of the ISP composites was at least 10 times longer than the LS composites counterpart within both dry and wet (within PBS at 37 °C) testing environments. Furthermore, positive cytocompatibility was also

found for both the LS and ISP PLA/PGF composites. Conclusively, ISP composites exhibited considerably enhanced mechanical retention and drastically improved media resistance, making those fully bioresorbable composites significantly more favourable as materials for bioresorbable bone fracture fixation devices.

LIST OF PUBLICATIONS

Peer Reviewed Paper:

- Chen M, Parsons AJ, Felfel RM, Rudd CD, Irvine DJ, Ahmed I. *In-situ* polymerisation of fully bioresorbable polycaprolactone/phosphate glass fibre composites: *In-vitro* degradation and mechanical properties. Journal of the mechanical behaviour of biomedical materials 2016; 59:78-89.
- Chen M, Lu J, Felfel RM, Parsons AJ, Irvine DJ, Rudd CD, Ahmed I. Wet and dry flexural high cycle fatigue behaviour of fully bioresorbable glass fibre composites: *In-situ* polymerisation versus laminate stacking. Composites Science and Technology 2017; 150:1-15.
- Chen M, Lu J, Patel U, Felfel RM, Parsons AJ, Irvine DJ, Rudd CD, Ahmed I. 2017. Heated *In-situ* Polymerisation *vs.* Laminate Stacking for Fully Bioresorbable PGF Reinforced PLA Based Polymer Composites: *In-vitro* Degradation, Mechanical retention and Cytocompatibility behaviour. Under review.
- Xi G, Chen M, Lu J, Xiaogang Y, Lee TH, Ahmed, I. 2017. High cycle fatigue life prediction of glass fibre reinforced composites using the continuum damage mechanics coupled with a cohesive zone approach. International journal of mechanical sciences. Under review.

Conferences:

- Chen M, Parsons AJ, Felfel RM, Rudd CD, Irvine DJ, Ahmed I. 2015. Developing an *in-situ* polymerisation process for biocomposite manufacturing. 20th International Conference on Composite Materials. Copenhagen: ICCM20 Organizing Committee.
- Xi G, Chen M, Lu J, Xiaogang Y, Lee TH, Ahmed I. 2017. Elastic properties of a representative volume element of glass fibre reinforced composites using finite element method. 21th International Conference on Composite Materials. Xian, China: ICCM21 Organizing Committee.
- *In-situ* polymerisation method for polycaprolactone and polylactide/phosphate based glass fibre composites. UK society for Biomaterials UKSB 13th Annual Conference, University of Birmingham, 2013 (Poster presentation).

ACKNOWLEDGEMENTS

Firstly, I would like to express my gratitude to my principal supervisors and mentors, Prof Christopher Rudd and Dr Ifty Ahmed, for their complete support and guidance throughout my PhD. They have been extremely kind and patient with me, and encouraged me for pushing forward. I would also like to thank my supervisors, Dr Derek Irvine and Dr Andrew Parsons for their professional support and valuable advices.

Special thanks are given to Dr Reda Felfel for his scrupulous and friendly support, with very knowledgeable discussions during my PhD. Many thanks to Dr Tom Turner and Dr Richard Brooks (retired), who are my kind internal assessors. Great thanks also go to all my colleagues and friends in the polymer composites and biocomposites research group, with their constant support and friendship. Acknowledgements are also given to all the technicians in the ITRC composites lab and the Wolfson labs, especially to Paul Johns for his kind assistance in the labs all around.

Most importantly, my highest gratitude is given to Jiawa Lu, for her everyday support and understanding during my time in the UK. Life was full of fun and love with her and she made me much better in both professional and personal ways. My heart always goes with my parents with their limitless and eternal love and care.

Finally, I would like to give my thanks to the University of Nottingham for awarding me the Dean of Engineering Research Scholarship for International Excellence during my PhD.

ABBREVIATIONS

ACE	Active chain end
AM	Activated monomer
CAS	Critical applied stress
CIM	Catalyst insertion mechanism
CL	ε-caprolactone
CP	Condensation polymerisation
DDW	Double distilled water
DMEM	Dulbecco‘s Modified Eagle Media
DSC	Differential scanning calorimetry
FCS	Foetal calf serum
FDA	Food and drug administration USA
FRC	Fibre reinforced composites
GMT	Glass fibre mats reinforced sheet
GPC	Gel permeation chromatography
HA	Hydroxyapatite
ISP	*In-situ* polymerisation
LA	Di-lactide
LS	Laminate stacking
MTM	Monomer transfer moulding
M_w	Weight averaged molecular weight
M_n	Number averaged molecular weight
NMR	Nuclear magnetic resonance
NR	Neutral red
PBS	Phosphate buffered saline
PCL	Polycaprolactone
PDI	Polydispersity index
PE	Polyethylene
PEEK	Polyetheretherketone
PET	Poly(ethylene terephthalate)
PGA	Polyglycolide
PGF	Phosphate based glass fibre
PLA	Polylactic acid

PLA-PCL	Copolymer of polylactic acid and polycaprolactone
PLGA	Poly(lactic-co-glycolic acid)
PMMA	Polymethylmethacrylate
PS	Polystyrene
PTFE	Polytetrafluoroethylene
PU	Polyurethane
PVC	Polyvinylchloride
RM	Random mat
RTM	Resin transfer moulding
ROP	Ring opening polymerisation
SBF	Simulated body fluid
SDC	Specific damping capacity
SEM	Scanning electron microscopy
S-N	Stress – fatigue life
SRTM	Structural resin transfer moulding
TCA	Tricaboxylic acid cycle
THF	Tetrahydrofuran
T_g	Glass transition temperature
UD	Unidirectional
UFS	Ultimate flexural strength
V_f	Fibre volume fraction

TABLE OF CONTENTS

LIST OF FIGURES

LIST OF TABLES

Chapter 1. Introduction

1.1. Overview

There is significant scope for improving and developing current load bearing devices for hard tissue repair. The main complications concerning current metal implant materials, such as stainless steel, titanium and cobalt chromium alloys, are corrosion, stress shielding and, in Europe, the necessity for secondary surgery to remove metal implants [1-3]. The ideal internal bone fixation device should have excellent biocompatibility, be fully bioresorbable, have adequate initial mechanical properties to sustain the mechanical stresses experienced during surgical procedures and to support bone healing through the early stages, followed by a gradual decline of its mechanical properties in order to transfer the stress to the healing bone [4, 5].

Fully bioresorbable polymer composites provide a highly attractive opportunity to improve and replace traditional metal implants and are an active research field due to their potential use in load-bearing applications. The biocompatibility of polycaprolactone (PCL), polylactic acid (PLA) (approved by FDA) and phosphate based glass fibre (PGF) has been well investigated and these materials are known to be bioresorbable, which makes them favourable candidates for bone repair applications [6-11]. PGF has been used as reinforcement for developing fully bioresorbable polymer composites in the Biocomposites Group at Nottingham [5, 12, 13]. PGFs are able to dissolve completely within aqueous media and their dissolution rate can be adjusted by altering the glass composition [5]. Fibres with mechanical properties between 500-1200 MPa and 60-80 GPa, for tensile strength and modulus respectively, have been achieved, which the

modulus is comparable to commercially available E-glass fibre [13-15]. The biocompatibility and mechanical properties of the composites have been studied extensively with various matrix polymers, fibre compositions and architecture combinations, which are reported to have achieved flexural strength and modulus between 180-350 MPa and 14-21 GPa respectively [16-21]. As an example, PLA/unidirectional (UD) PGF composite plates with fibre volume fractions (V_f) of 35% and 50% have been produced, which showed flexural strength values of ~216 MPa, ~270 MPa and flexural modulus values of ~16 GPa and ~19 GPa, respectively [16, 19].

It is the key aim to match the degradation rate of the composites with the bone healing process, which achieving satisfactory adhesion and retention of the fibre and matrix interface has been the main challenge in developing fully bioresorbable composites. The most frequently used manufacturing process adapted for bioresorbable polymer/fibre composites is laminate stacking (LS) followed by hot compression moulding [22-24]. However, a number of studies have seen a rapid loss in mechanical properties of these composites after immersion in an aqueous environment [5, 16, 18, 25]. It is believed that rapid reduction in fibre/matrix interfacial bonding occurred, which reduced adhesion and prevented efficient stress transfer between matrix and reinforcement.

Due to the high viscosity of the polymer melt, it is difficult to gain a good impregnation and wet-out of the fibre surfaces by using the LS process, which often results in poor fibre/matrix adhesion. Poor interfacial bonding is more vulnerable to fluid ingress through the interfaces in aqueous environments, which leads to the rapid loss of mechanical properties and early stage failure of the composites [26]. As such, it is of paramount importance for bioresorbable fibre

reinforced composites to achieve strong fibre/matrix adhesion for their successful application in the field of hard tissue repair.

1.2. Aims and objectives

The main aim of the work was to develop a one-step ISP process for PGF reinforced fully bioresorbable composites manufacturing, and to characterise the performance of the ISP composites and compare them to the LS equivalents.

This process was to be applied to PCL and PLA matrix composites. PCL and PLA were both chosen as the matrix material because of their favourable biocompatibility and the available cytotoxicity data in the literature [27-29]. ISP process requires the monomer of the matrix material to be in a low-viscous liquid state to work effectively. The monomer of PCL is naturally a low viscosity liquid, which is hugely beneficial for the application of the ISP process. Conversely, the monomer of PLA is a solid material with a melting point of ~95 °C, which extensive melting is necessary before utilising during the ISP process. However, PLA is mechanically much stronger than PCL, which makes PLA more advantageous for the loading bearing application. PLA-PCL copolymer was also investigated as a potential matrix material to reduce the meting requirement as well as to retain the mechanical properties of PLA as much as possible.

The objectives set to achieve these aims are listed below:

I. Establish an effective catalyst system and in situ polymerisation mechanism for PCL based matrix materials. Develop a room temperature ISP manufacturing system for phosphate glass fibre reinforced PCL composites.

II. Fabricate PGF reinforced PCL composites via both LS and ISP processes with various V_f. Characterisation of the resulting PCL/PGF composites via *in-vitro* degradation, flexural mechanical tests, molecular weight analysis and long-term environmental fatigue analysis. Compare the results between the LS and ISP composites to illustrate the advantages of using the ISP process.

III. Once the effectiveness of the room temperature ISP process is determined, develop the room temperature injection equipment to enable a heated injection process for PLA based composites manufacturing.

IV. Investigate the use of PLA-PCL monomer mixtures as a means of depressing the melting point in comparison to neat PLA monomer. This would reduce the required temperature rating of the heated injection system whilst retaining most of the characteristics of PLA.

V. Following the development of PLA-PCL *in-situ* copolymerisation, enhance the heated ISP system for neat PLA/PGF composites production, to achieve optimum mechanical properties and retention of the fully bioresorbable PGF reinforced composites.

VI. Fabricate PGF reinforced PLA-PCL copolymer and then neat PLA composites. Characterise the composites via *in-vitro* degradation, flexural mechanical tests, thermal analysis, molecular weight analysis and cytocompatibility study. Compare the results of the copolymer and neat polymer systems.

1.3. Thesis structure

The structure of the thesis is presented:

Chapter 2 presents a literature review on: bone structure, bone fracture and the need for improvements in current metal fracture fixation devices; bioresorbable polymers; manufacture of phosphate based glass and glass fibre; fully bioresorbable polymer composite implants and their manufacturing processes.

Chapter 3 describes all the materials and methods used throughout this thesis, which offers an understanding of the flow for the development of this work. This includes the phosphate based glass and glass fibre production; LS process for PCL and PLA composites production; room temperature ISP process development for PCL/PGF composites production; heated ISP process development for PLA-PCL/PGF and then PLA/PGF composites production; high cycle fatigue analysis of PCL/PGF composites; characterisation protocols for both LS and ISP composites.

Chapter 4 looks at the mechanical properties and degradation behaviour of the PCL/PGF composites manufactured via both LS and ISP. Mechanical retention and degradation profiles over 28 days in phosphate buffered saline (PBS) at 37 °C are reported for LS and ISP composites.

Chapter 5 illustrates for the first time the environmental fatigue behaviour of PCL/PGF composites produced via both LS and ISP. High cycle flexural fatigue tests were performed on both LS and ISP composites in dry and wet (in PBS at 37 °C) environments.

Chapter 6 presents the mechanical properties, degradation and cytocompatibility behaviour of PLA-PCL/PGF and then PLA/PGF composites produced via LS and

ISP. Reaction mechanisms and polymerisation methods for PLA and PLA-PCL are discussed. Degradation was performed in PBS at 37 °C over 28 days.

Chapter 7 gives a summary of the major conclusions from this work and highlights recommendations for future work related to the manufacture of fully bioresorbable composites.

Chapter 2. Literature Review

2.1. Introduction

Fixation of fractures or replacement of damaged or missing bone are always required by congenital deformity, trauma and tumour removal [30]. The orthopaedic market has increased significantly from ~$5 billion in 1993 to ~$35 billion revenue generation at the end of 2008. It was also expected that around 167 million people of the global population will suffer from orthopaedic problems, such as fractures, arthritis and osteoarthritis, of which ~78% cases will be related to fractures [31].

The development and manufacture of fully bioresorbable, load-bearing polymer composites with appropriate biocompatibility and mechanical properties has become an exciting research area in recent decades. These composites have great potential to serve as the implant material in hard tissue repair and reconstruction [32, 33]. Aliphatic polyesters, such as PCL and PLA, are often chosen as the matrix material due to their favourable biocompatibility. However, reinforcements are usually required as the virgin mechanical properties of these polymers are not sufficient for load-bearing applications. Novel phosphate based glass fibre (PGF) developed in the biocomposites group at Nottingham is chosen as the reinforcement material in this work to produce fully bioresorbable polymer composites.

The conventional manufacturing process adapted for bioresorbable polymer composites is laminate stacking and hot press moulding (LS). However, due to the high viscosity of the polymer melt, using this process is difficult to gain a good impregnation and wet-out of the fibres. Poor interfacial bonding between the fibre

and the matrix could result in low mechanical properties and early stage failure of the composites. This is the potential reason for the poor success of fully bioresorbable polymer composites in load bearing implant applications. Based on these considerations, a novel manufacturing process comprising *in-situ* polymerisation (ISP) for fully bioresorbable PCL and PLA polymer composites is being developed during this work. ISP process of PCL composites was initially established in the biocomposites group at Nottingham [34, 35]. However, a different catalyst system of PCL polymerisation and novel moulding system design were used in this work. Moreover, PCL and PLA have very similar polymerisation mechanisms, as such potentially the same or similar catalyst systems should work for both of them. PCL was investigated first in this work as its monomer ε-caprolactone (CL) is in liquid state at room temperature, which is hugely beneficial for injection. The polymerisation mechanism is then imitated and used onto PLA *in-situ* polymerisation. Monomer of PLA, di-lactide (LA), has a melting point around 95°C, which high temperature is required before mixing with catalysts and injecting into moulds. High melting point resulted in high viscosity during the mixing and the injection. It also affects the wet-out and impregnation of fibres during the injection. The mixing, injection and impregnation mechanisms are the main limitations of PLA *in-situ* polymerisation.

This chapter reviews the literature on the structure and mechanical properties of bone, load-bearing implant materials, characteristics of PBG, characteristics and polymerisation mechanism of PCL and PLA, conventional and ISP manufacture processes adapted to fully bioresorbable polymer composites.

2.2. Human bone

Bone is the main constituent of the skeletal system and differs from the connective tissues in rigidity and hardness. The main functions of bones are to enable the skeleton to maintain the shape of the body, to protect the soft tissues and internal organs from injury, to supply the framework for the bone marrow and to transmit the forces of muscular contraction from one part of the body to another during movements [36]. Bones also have several metabolic functions, which are supporting haematopoiesis (formation of blood cells), serve as the reservoir of ions and contribute to the regulation of blood calcium levels [36, 37].

2.2.1. Bone structure

Bones are naturally composite materials consisting of 65% inorganic minerals, 35% organic matrix and 8% cells and water [36]. A typical bone comprises a hard and compact outer shell, which surrounds and protects the bone marrow inside the cavity (see Figure 2.1). They are classified into cortical (compact) and cancellous (spongy) bone. The mineral is largely impure hydroxyapatite (HA), $Ca_{10}(PO_2)_6(OH)_2$, containing constituents, such as calcium carbonate, magnesium, fluoride, strontium and citrate. The mineral phase provides bones with the mechanical strength, whilst the collagen fibres, which are the organic phase, are responsible for the ductility of bones [36, 38]. Cortical bone has a compact and much denser structure than cancellous bone, whilst, cancellous bone has a highly porous structure. 80% of the human skeletal system is made up by cortical bone.

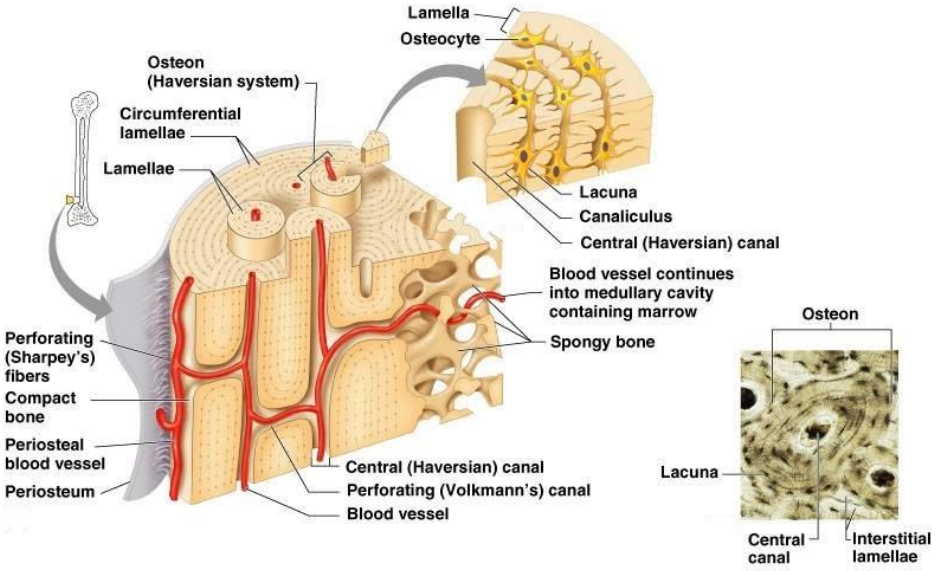

Figure 2.1 *Typical structure of human bone*

2.2.2. Bone cells

Bone is a dynamic material that continuously renews and remodels itself. It has four main types of cells, which are osteoclasts, osteoblasts, osteocytes and lining cells (see Figure 2.2). Osteoclasts are responsible for the resorption of bone tissues. They resorb the bone by means of local acidification and secretion of specific proteases. Osteoblasts are the bone forming cells, which they synthesis the organic matrix by secretion of a wide varieties of extracellular matrix proteins. Moreover, they contribute to the mineralisation process and regulate the osteoclasts function [39]. At the end of the differentiation stage of osteoblasts, they are entrapped by their self-produced bone matrix and they are recognized as osteocytes. Osteocytes are the most abundant type of cells in bone and they are very sensitive to mechanical strains [40]. They maintain the bone remodelling by sensing the applied mechanical strains and interpret them into biochemical signals of resorption or formation associated to the intensity and distribution of the strains [41]. In addition, Osteoblastic differentiation also forms another type

of bone cell, lining cells. Lining cells are located at the bone surfaces and thus separate the bone surfaces from the bone marrow.

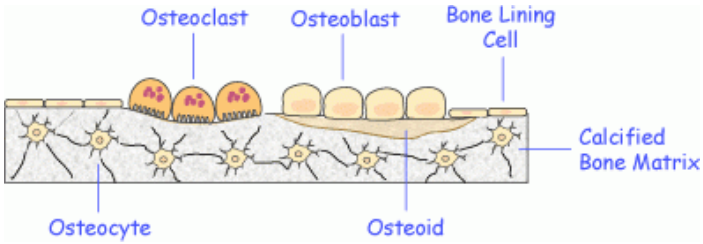

Figure 2.2 *Sketch of major bone cells*

2.2.3. Bone fractures and bone repair

Bone fractures usually occur due to the exposure to high impact force during accidents, such as sports injury and traffic accidents. Typical long bone fracture can be classified into the following types (see Figure 2.3):

a) Simple, skin is intact at the fracture site;

b) Compound, broken bone protrudes through the skin;

c) Greenstick, breaks in bones along only one side of the bone;

d) Complete, bone splits into two fragments;

e) Communicated, bone is broken into more than two fragments;

f) Transverse, bone is fractured at the right angle with respect to bone axis;

g) Spiral, helical fractures result from twisting of the bone;

h) Oblique, these fractures occur at 45° to the axis of the bone.

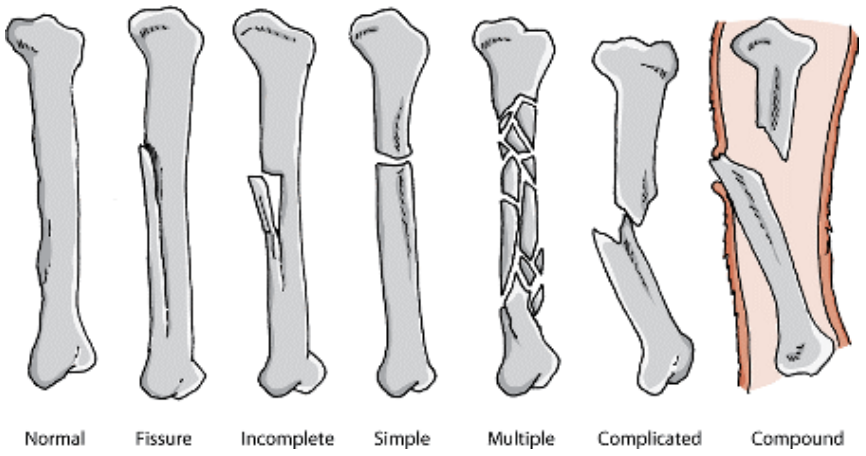

Figure 2.3 *Classifications of bone fractures*

The bone healing process follows the sequence of inflammation, formation of callus and bone remodelling in the final stage [42]. When fracture happens, the fracture site bleeds and then is covered by the freshly formed cartilage and dense connective tissue to form a fibro-cartilaginous callus to stabilize and bind the fractured parts. In the meantime, osteoblasts deposit and form new bone adjacent to both ends of the fracture site, occupying the callus and replacing it with a bony callus structure. After the bony callus is formed and is enough to bridge the fracture ends, the original shape of the bone is restored gradually by remodelling [43]. In addition, there are several methods to stimulate and accelerate bone healing process, such as electrical, electromagnetic, ultrasound and mechanical stimulation. The rate of bone healing is also related to the minerals inside the body, such as calcium, phosphorus and magnesium [44].

Bone healing process can last from 4 to 24 weeks depending on the age, health and types of bone (4-6 weeks for cancellous and 8-24 weeks for cortical bone) [27]. To support bone healing, fixation devices can be used to stabilize the bone fracture and accelerate the healing process. It is essential for bone healing to reduce the interfragmentary mobility under external forces. Therefore, fixation

methods are assessed regarding to their capability to control the motions of the fractured bone segments [45]. Both external fixation and internal fixation methods can be employed to keep the fragments at position during the healing process.

Internal fixation devices are implanted inside the fractured bone to stabilize the fragments [45]. The most common materials are stainless steel, titanium and cobalt chromium alloys. There are four kinds of internal fixation devices, which are wires, intramedullary rods or nails, plate and screws (see Figure 2.4). They are targeted at different types of fracture and can be combined to promote effective healing of the fractured bone.

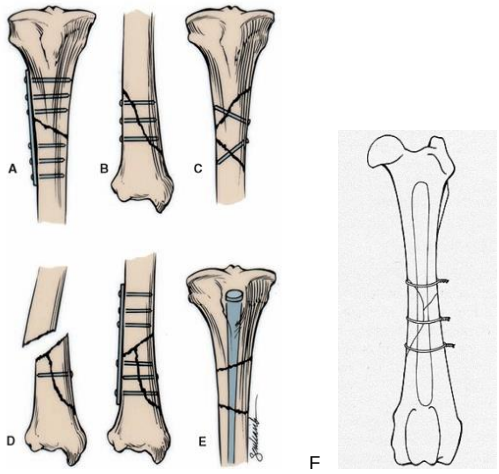

Figure 2.4 *Typical internal fixation devices for bone fractures: A), B), C) and D) are bone plates and screws fixation; E) is intramedullary nail; F) is wire fixation.*

2.2.4. Mechanical properties of bones

The mechanical properties of bones can be measured by testing the whole bone unit or isolated parts of the bone via uniaxial tensile or compressive tests and 3 or 4-point bending tests. Mechanical properties of both the cortical and cancellous bone are summarized in Table 2.1. Both types of bone exhibit a high degree of anisotropy. The large range of values was resulted from different bone locations, testing conditions (dry/wet, temperature), sex, age and health.

Table 2.1 *Mechanical properties of human cortical and cancellous bone [46-48]*

Mechanical properties	**Cortical bone**		**Cancellous bone**	
	Modulus (GPa)	Strength (MPa)	Modulus (GPa)	Strength (MPa)
Tensile	7~34	90~190	0.4~1.5	7~20
Compressive		130~295		1.5~38
Flexural	5~23	35~280	0.05~0.34	1~9

2.3. Load bearing implant materials

Biomedical implants are devices manufactured to enhance, restore, support or replace the biological structures that are performing below a satisfactory level. Biomaterials used to produce implants are defined as any synthetic or natural materials that are intended for use to interact with biological system in order to maintain, replace or improve the function of bodies [49]. Consequently, the essential parameters in selecting biomaterials for biomedical implants should include good biocompatibility, appropriate mechanical properties, reliable corrosion, wear and fatigue resistance [50]. In terms of biocompatibility, the material should not cause any toxic, allergenic or carcinogenic reactions to the biological host.

The most commonly used biomaterials are metals, ceramics and some biocompatible polymers. Further to these, two categories of materials can be combined to form composites materials, which is a relatively new category of biomaterials. In addition, biomaterials can be identified as three different generations. The first-generation biomaterials are bioinert and have similar physical properties with the replaced tissue. The second generation are as

bioactive and bioresorbable. Finally, the third generation biomaterials are bioactive, bioresorbable and biofunctional, such that their degradation should stimulate and promote tissue growth [51].

2.3.1. Metals

Metal alloys have been used for biomedical implants, such as bone fixation devices, since early 1900s mainly due to their excellent mechanical properties (see Table 2.2) and durability and corrosion resistances [52]. Three main classes of metal alloys have been utilised in orthopaedic devices, which are stainless steel, titanium and its alloys and cobalt chromium alloys (Vitallium and CoNiCrMo). Despite metal alloys offer acceptable biocompatibility and good stability for bone fractures, several complications were also raised:

a) Secondary removal surgery may be required across European area;
b) Stress shielding resulted from huge elastic mismatch between metal alloys (see Table 2.2) and human bones (see Table 2.1);
c) Corrosion of metal alloys inside human body and the corrosion products can be toxic;
d) Interference with certain modern imaging process, such Magnetic Resonance Imaging (MRI);
e) Relatively high density, which could cause elevated stresses around the implant sites;
f) Lack of bioactivity.

Table 2.2 *Mechanical properties of metallic biomaterials for orthopaedic applications*

Materials	Tensile Modulus (GPa)	Tensile Strength (MPa)
Stainless steel	190-210	465-950
Cobalt chromium alloys	210-230	600-1785
Titanium and its alloys	105-119	785-1021

The high stiffness of metal alloys allows them to carry the majority of the load from the fractured bone, which will support the initial stage of bone healing process [22]. However, bone is a dynamic material, which remodels itself by sensing the applied stress environment to achieve and maintain its density and structure thickness [49]. Therefore, the lack of applied force to the bone could result in forming weak bone structures (bone atrophy), particularly around the implant sites. Moreover, subsequent removal of metallic devices can leave the bone temporarily deficient in structure strength and prone to re-fracture [44].

2.3.2. Ceramics

Ceramics are inorganic materials, which have high stiffness and strength, good corrosion and wear resistance and relatively low density compared to metal alloys. These properties have made ceramics favourable for a broad range of biomedical applications [2]. The main applications include crowns for dentistry, joint and bone segment replacement and temporary bone repair devices. Furthermore, ceramics can serve as coatings for other biomedical materials to provide a biocompatible interface [53]. Two most common ceramics in biomaterials are alumina and calcium phosphates (main composition hydroxyapatite). They both have

excellent biocompatibility/bioactivity, high wear resistance and good chemical stability in physiologic environment.

2.3.3. Polymers

A wide range of polymers have been successfully used as biomaterials in many different applications within human body. They also have a broad range of mechanical and physical properties and can be fabricated easily into films, textiles, rods and fibres [54].

Biomedical polymers can be classified into two categories based on their durability in biological environment, which are biostable and biodegradable [55]. Examples of common biostable polymers include Polyethylene (PE), Polyurethane (PU), polyvinylchloride (PVC), Polymethylmethacrylate (PMMA), polytetrafluoroethylene (PTFE), and polyetheretherketone (PEEK). They have been employed in various applications, such as dental, cardiovascular, sutures, orthopaedic (hip replacement) and drug delivery [22]. Lots of attention have been paid on the biodegradable polymers, such as poly(ε-caprolactone) (PCL), polylactic acid (PLA) and poly(lactic-co-glycolic acid) (PLGA) due to their great potential in bone fixation devices. There are several advantages of biodegradable polymers over the metallic and ceramic biomaterials concerning bone fixation applications:

a) Secondary removal surgery is eliminated as they are biodegradable;
b) Ease of fabrication, can be made into different forms;
c) Mechanical properties degrade over time, allows the applied stress to gradually transfer to the healing bone (no stress shielding);

d) Degradation products are biocompatible and can be excreted through natural pathways.

However, these polymers do not have sufficient mechanical properties to serve as load-bearing applications, which reinforcements are usually required to produce composites material.

2.4. Biodegradable polymers

Biodegradable polymers are the specific type of polymers that breaks down in the biological environment into biocompatible products after their intended purpose. The degradation of these polymers usually takes place through random chain and chain-end scission via thermal, mechanical, hydrolytic, enzymatic, oxidation, photolysis and radiation activations [42]. However, hydrolytic and oxidative degradation are the most common degradation modes inside the biological system where living cells and microorganisms are present around the polymer [56]. It is also called the absorbable or resorbable polymer [57].

Extensive researches have been carried out in recent years owing to their increasing applications within the field of medical care and environmental concerns of polymeric waste. To maintain and improve the global environment, it is necessary to replace the biostable polymers with biodegradable polymers in a wide range of applications, such as agricultural mulch films and packaging. Furthermore, there are several important applications in the medical field that involves the use of biodegradable polymers, including sutures, drug release agents, orthopaedic fixation devices and tissue engineering. In particular, attentions have been paid on PCL and PLA for low-load internal bone fixation devices due to their favourable biocompatibility.

2.4.1. Aliphatic polyesters

Aliphatic polyesters are among the most important class of synthetic biodegradable polymers for biomedical applications owing to their degradation mechanism and generally high biocompatibility. Conventional aliphatic polyesters are semi-crystalline, hydrophobic solids [58]. There are lots of different types of aliphatic monomers. Table 2.3 summarized the monomer structure and some physical properties of the most common aliphatic polyesters. By using different types of initiator and catalyst systems, ring opening polymerisation (ROP) of lactones and lactides can provide macromolecules with advanced molecular architectures. Different molecular structures of the aliphatic polyesters offered a wide range of physical properties and the possibility to regulate their degradation rate, which significantly expanded its potential applications in the biomedical field [59]. Two kinds of the most commonly used aliphatic polyesters and their polymerisation mechanism were reviewed below, including Poly(ε-caprolactone) (PCL) and Polylactic acid (PLA).

Table 2.3 *Monomer structure and physical properties of the most common aliphatic polyesters (AM. Refers to amorphous, T_g for glass transition temperature, T_m for melting temperature) [20, 60]*

Monomer		Polymer		
		Abbreviation	T_g (°C)	T_m (°C)
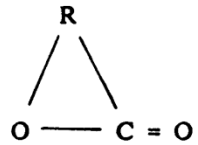	R=$(CH_2)_2$, β-propiolactone	PβPL	-24	93
	R=$(CH_2)_3$, γ-butyrolactone	PγBL	-59	65

	R=$(CH_2)_4$, δ-valerolactone	PδVL	-63	60
	R=$(CH_2)_5$, ε-caprolactone	PCL	-60	60
	R=$(CH_2)_2$-O-CH_2, p-dioxanone	PDO	-15-8	110
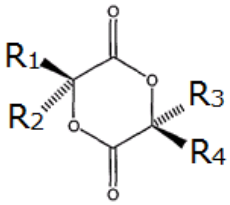	R_1=R_2=R_3=R_4= H, glycolide	PGA	34	225
	R_1=R_4=CH_3, R_2=R_3=H, L-lactide	PLLA	55-60	175-178
	R_1=R_4=H, R_2=R_3=CH_3, D-lactide	PDLA	55-60	170
	R_1=R_3=CH_3, R_2=R_4=H, Meso-lactide	PmesoLA	45-55	AM.
	DLA/LLA=50/50	PDLLA	45-55	AM.

2.4.2. Poly(ε-caprolactone) (PCL) and its monomer

PCL can be synthesised from both condensation polymerisation (CP) and ring opening polymerisation (ROP) of its monomer ε-caprolactone. ROP mechanism is usually used in order to yield high molecular weight PCL (see Scheme 2.1).

Its monomer, ε-caprolactone, is a cyclic ester belongs to the family of lactone, with a formula of $(CH_2)_5CO_2$ (see Scheme 2.1). It is a colourless liquid that miscible with most organic solvent. Its low viscosity liquid feature at room temperature is very beneficial for monomer transfer during *ISP process*. ε-caprolactone is prepared industrially by Baeyer-Villiger oxidation of cyclohexanone with peracetic acid [61]. The majority of ε-caprolactone is consumed as a precursor to caprolactam, which is a precursor to Nylon 6 (a widely used synthetic polymer) [62].

PCL is a highly crystalline polyester that has a long degradation period of at least two years [44]. Some reports also stated that PCL acquires 4 years to be fully absorbed by human body [60]. Due to the relatively long degradation period, it has been developed for long term implantation applications and drug delivery applications. A successful biomedical application of PCL is the contraceptive implant drug delivery system named as Capronor ® [63]. The other applications of PCL range from packaging to bioresorbable sutures, tissue engineering and bone graft substitutes [64-66].

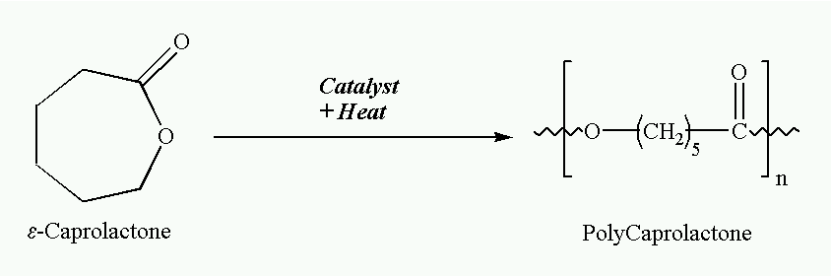

Scheme 2.1 *Polymerisation of ε-caprolactone*

PCL has relatively low mechanical properties compared to other common aliphatic polyesters, such as PLA (see Table 2.4). Its mechanical properties are known to be sufficient for non-load bearing applications, such as maxillofacial

fracture repairs. However, for load bearing applications, such as internal bone fixation devices, reinforcements are required to provide higher mechanical properties. Although PCL has a slow degradation rate, it has the potential to yield a wide spectrum of degradation rates by suitable routes to accelerate the degradation rate. The ROP mechanism of PCL is reviewed below.

Table 2.4 *Mechanical properties of PCL and PLA [27, 67, 68]*

Mechanical property	**PCL**	**PLLA**	**PDLLA**
Elastic modulus (GPa)	0.2-0.4	3-6	1-3.5
Flexural strength (MPa)	16-29	109-145	95-130
Tensile strength (MPa)	20-35	50-80	20-60
Degradation time (Month)	24-48	24-72	12-16

2.4.3. ε-caprolactone polymerisation

Carothers [69] first polymerised ε-caprolactone in the research of polymerisation reactions at 150°C without any catalyst in the 1930s. However, he also indicated that there were no methods to control the molecular weight. Later in the 1950s, it was discovered by Young and Hostettler [70] that the molecular weight could be controlled by the use of initiators containing active hydrogen, such as amines and alcohols. Active hydrogen initiators are necessary in order to provide good control over both the molecular weight and the nature of the end groups [70]. Since 1950s, various catalysts and initiators were developed to accelerate the polymerisation process, including protic acids, metal alkoxides, metal carboxylates and organometallic compounds, such as those of tin, aluminium and zinc.

The polymerisation of lactones and lactides should follow the mechanisms similar to the catalysed reactions of simple esters. The attack sites of the monomer that can leads to ring-opening polymerisation (ROP) could be carbonyl carbon, carbonyl oxygen, alkyl oxygen and α-carbon to the alkyl oxygen as a result of their electron rich or deficient characteristic (see Figure 2.5) [71]. Therefore, the polymerisation mechanism of the catalyst system could be cationic, anionic or coordination depending on the reagents and the experimental conditions.

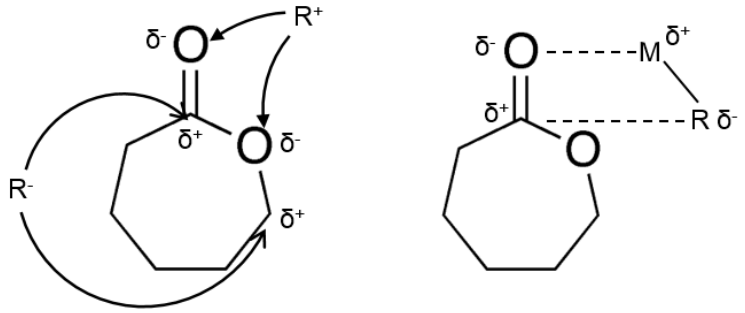

Anionic (R-) or Cationic (R+) Coordination Insertion

Figure 2.5 *Schematic diagram of potential ε-caprolactone attack sites for different polymerisation mechanism*

2.4.3.1. Cationic mechanism

For cationic polymerisation mechanism, typical catalysts and initiators used are compounds that can provide cationic species to attack the exocyclic (carbonyl) oxygen or the endocyclic (alkyl) oxygen of the monomer ε-caprolactone, such as protonic acids, alkylating agents, acylating agents and Lewis acids [72]. There are two nucleophilic centres in the ε-caprolactone molecules for cationic mechanism as indicated in Figure 2.5. Two different types of polymerisation propagation centres can be formed depending on the attack sites and the subsequent bond scissions. However, Kricheldorf [73] studied the polymerisation mechanism of β-propiolactone and ε-caprolactone in 1984 using both alkylating

and acylating agents as the catalysts and characterised the end-groups using ^{1}H NMR, ^{13}C NMR (nuclear magnetic resonance) and inferred spectroscopy (IR). He then concluded that all cationic polymerisations proceed via alkyl-oxygen bond scission of the lactone involving an electrophilic attack at the endocyclic oxygen of the monomer (see Scheme 2.2) [74].

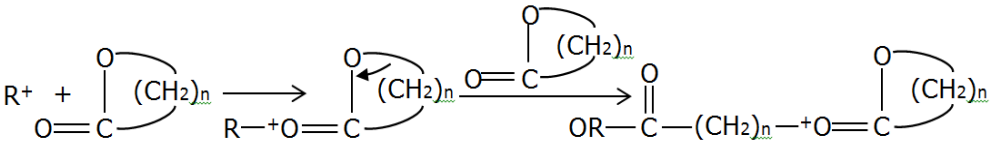

Scheme 2.2 *Cationic species R^{+} attacks exocyclic oxygen of lactones to initiate polymerisation*

This mechanism is noted as the active chain end (ACE) mechanism and has been accepted since then. This mechanism is a logical outcome of the fact that the exocyclic oxygen is much more nucleophilic than the endocyclic one and that the delocalisation of the positive charge here strongly contributes to their stabilisation [73].

There is also an alternative cationic mechanism when the polymerisation proceeds in the presence of alcohol, which is noted as activated monomer (AM) mechanism. Belen'kaya and Okamoto [75, 76] investigated this mechanism separately and led to the same conclusion. In the AM mechanism, alcohol alone cannot initiate the cationic polymerisation. The cationic catalyst reacts with the alcohol first to release a hydrogen ion, which then transfers to the exocyclic oxygen of a monomer molecule. Thus, the monomer molecule is activated and then the hydroxyl oxygen of alcohol molecule attacks the carbonyl carbon to open the ring. Polymer molecule is then formed by subsequent chain propagation. In addition, the ACE mechanism often forms ring oligomers due to the active chain

end attacking the ester group in its own chain (back-biting). In contrast, AM mechanism can supress back-biting reactions owing to the non-existence of active chain ends.

2.4.3.2. Anionic mechanism

In the anionic mechanism, the attack sites may be carbonyl carbon or the alkyl carbon as shown in Figure 2.5. Typical anionic initiators are tertiary amines, metal alkoxides and carboxylate salts, such as CH_3OK and CH_3COOK. Penczek [77] investigated the lactone anionic polymerisation in the early 1980s by end group analysis using NMR. He determined that the anionic polymerisation of ε-caprolactone was via the attack of alcoholate to the carbonyl carbon and then underwent acyl-oxygen bond scission to form alcoholate anions. The reaction scheme is shown in Scheme 2.3.

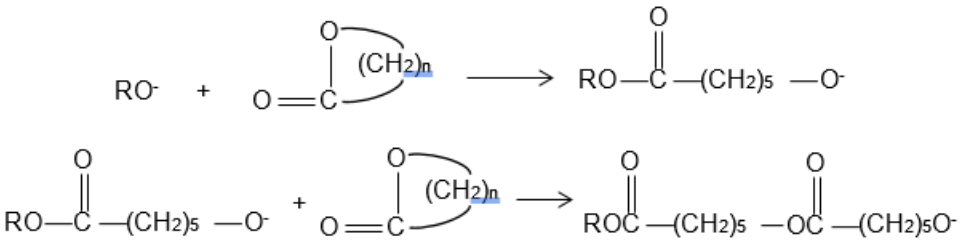

Scheme 2.3 *Initiation and propagation reaction of the alkoxide initiated ε-caprolactone anionic polymerisation mechanism*

Anionic polymerisation is also known as the 'living' polymerisation due to the highly active chain ends formed during the reactions. Back-biting reactions of the chain end to ester group in the chain extensively forms ring molecules, which terminates the chain growth. This characteristic also presents in the ACE mechanism of cationic polymerisation.

2.4.3.3. Coordination mechanism

The cationic and anionic polymerisation mechanism of lactones is often disturbed and terminated by inter-or intra-molecular transesterifications. These undesirable side reactions were caused by the highly active chain ends as discussed previously. However, for the coordination insertion mechanism, the initiator is not strong enough to form ionic active species, but to coordinate with carbonyl groups of lactone molecules, then to let the monomers insert into the metal-alkyl or metal-alkoxide bonds [71]. As a result, the side reactions are suppressed significantly and close control of the molecular weight becomes possible as well.

The most commonly used catalysts are organometallic compounds of transition metals or elements from groups III and IV, such as zinc, titanium and tin [71]. Recent researches also concentrated on the organometallic compounds of rare earth metal in order to narrow the polydispersity of the synthesised polymers, including Ln, Sc and La [78]. The most frequently used catalyst is stannous octoate ($Sn(Oct)_2$) [67, 79]. The reaction mechanism is shown in scheme 2.4. The monomer first coordinate with the initiator, and then the monomer is inserted into the Sn-O bond in such a way that the growing chain remains attached to tin through an alkoxide bone [80].

Coordination insertion mechanism is applied when using stannous octoate as the pre-catalyst and benzyl alcohol as the initiator. Stannous octoate is chosen owing to the availability of its cytotoxicity data and its extensive applications for preparing PCL for medical applications [63]. Benzyl alcohol was chosen since it makes easier to identify the chain ends and monitor the polymerisation process.

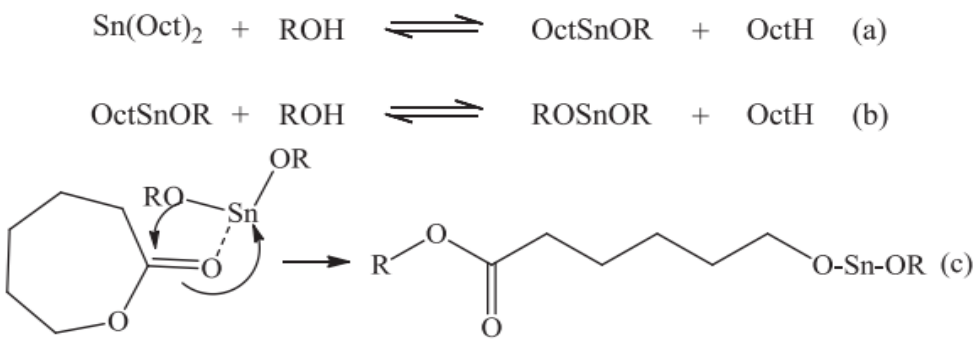

Scheme 2.4 *Initiation and propagation reactions for coordination insertion polymerisation mechanism of ε-caprolactone*

2.4.4. Polylactic Acid (PLA) and its monomer

PLA can be obtained either by CP of lactic acid or by ROP of the cyclic dimer lactide (see Scheme 2.5). PLA has a rigidity and clarity similar to polystyrene (PS) or poly(ethylene terephthalate) (PET) [81]. Its mechanical properties are relatively high comparing to other common biodegradable polyesters (see Table 2.4). End uses of PLA are in biomedical sutures, rigid packaging, flexible film packaging, cutlery, bottles, injection moulded products, extrusion coatings and so on [81]. It is also the most popular bioresorbable polymer for internal bone fixation devices owing to its relatively good mechanical properties, appropriate degradation rate (~1 year for complete degradation), favourable biocompatibility and availability in different chemical forms [82].

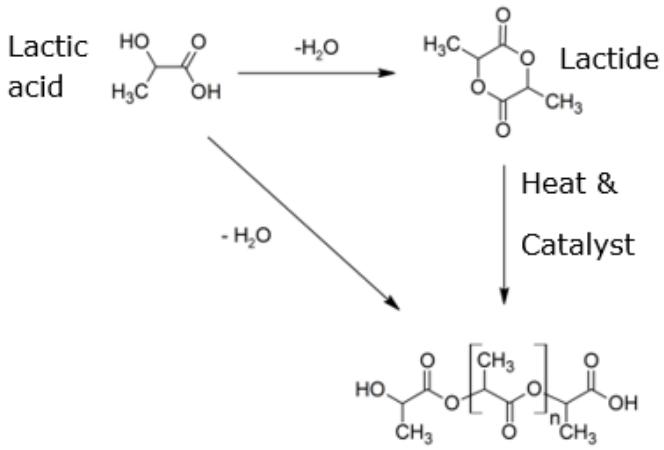

Scheme 2.5 *Polymerisation of lactic acid and lactide*

Its monomer, lactic acid, is a naturally occurring acid and can be extracted from natural sources, such as starch and sugar [83]. Lactic acid is a carboxylic acid with a chemical formula $C_3H_6O_3$. It has a chiral carbon atom and exists in two enantiomeric forms, which are usually referred as L-(+)-lactic acid or (S)-lactic acid and the other, its mirror image, is D-(−)-lactic acid or (R)-lactic acid (see Figure 2.6). Its molecule has a hydroxyl and an acid functional group, which may trigger intermolecular and intramolecular esterification reactions. The dehydrated cyclic dimer of lactic acid is commonly referred as di-lactide (3,6-dimethyl-1,4-dioxane-2,5-dione) (see Scheme 2.5). Due to the two asymmetric carbon atoms in the molecule, di-lactide exists in the three different forms (see Figure 2.7). In addition to the three diastereomeric structures, there is also a racemic of $_D$-lactide and $_L$-lactide, often referred as rac-lactide or $_{DL}$-lactide. Di-lactide is produced by thermal catalytic depolymerisation of lactic acid using tin catalysts (see Figure 2.8). Di-lactide and low molecular weight oligomers are both formed during the CP and reaction equilibrium is also formed between the oligomer and the di-

lactide. In order to pull the reaction towards the lactide side, di-lactide must be withdrawn from the system constantly [84, 85].

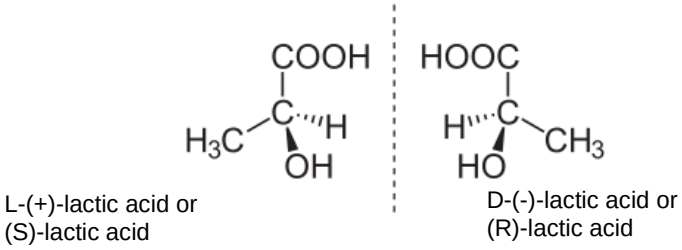

Figure 2.6 *Enantiomers of lactic acid*

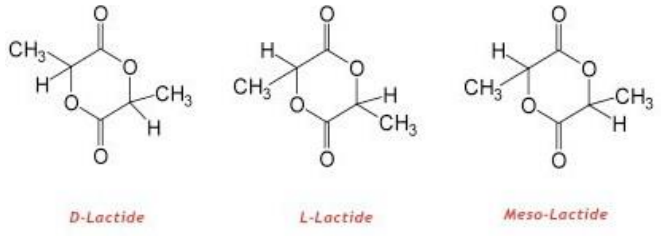

Figure 2.7 *Lactide diastereomeric structures*

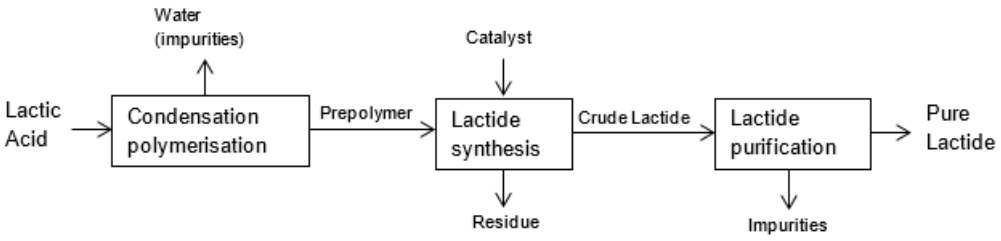

Figure 2.8 *Lactide manufacture via thermal catalytic depolymerisation*

Since there are two isomers for PLA monomer, PLA can be polymerised into poly($_L$-lactic acid) (PLLA 100% $_L$-lactide), poly($_D$-lactic acid) (PDLA 100% $_D$-lactide) and poly($_{D,L}$-lactic acid) (PDLLA) as a copolymer with different L to D ratios [86]. Four different stereoisomers of PLA are presented in Figure 2.9. Molecular weight, degradation rate and physical and mechanical properties of the PDLLA all depend on L/D ratio [87, 88].

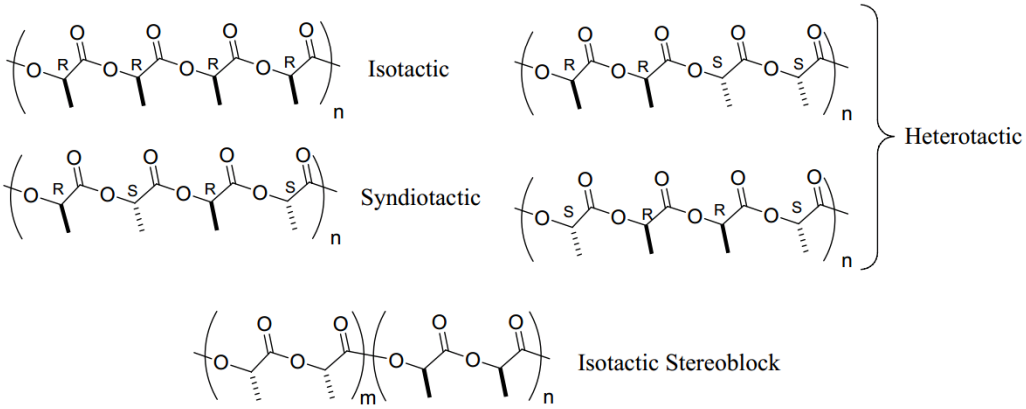

Figure 2.9 *Stereoisomers of PLA*

PLA can be either semi-crystalline or amorphous depending on the stereo purity of the polymer backbone [89]. PLLA and PDLA have a high crystallinity, and the crystallinity of PDLLA is dependent on the amount of D-lactide. The crystallinity decreases as the D content increases and it is highly crystallized when the D content drops to 2% [90]. In addition, polymerisation of the rac-lactide usually leads to the synthesis of amorphous PDLLA. Commercial PLA is usually prepared by L-lactide because the resulting polymer, PLLA, is semi-crystalline with a relatively high melting and glass transition temperature (T_g) (see Table 2.3). The mechanical properties can be retained very near to its melting temperature [91]. PLLA has been used as the biodegradable scaffolds in tissue engineering. However, PLA has certain shortcomings that limit its use in load-bearing biomedical applications: it is a relatively brittle polymer that fails at very low elongation and its virgin mechanical properties is not sufficient for load-bearing applications [92]. Biomedical bone fixation implants should have strong mechanical properties to avoid implant failure until the fractured bone has fully healed. Consequently, reinforcement of these polymers is essential in order to produce composites implant with mechanical properties comparable to cortical bone.

2.4.5. Di-lactide polymerisation

High molecular weight PLA is most commonly made by ROP of the cyclic dimer lactide. As mentioned previously, lactide production is related to significant cost. However, preparation of high molecular weight PLA by direct dehydrated CP is not feasible as the reaction equilibrium does not favour the high molecular weight polymer [91]. PLA prepared by CP usually has low molecule weight and is not suitable for many applications. Moreover, ROP also provides the possibility of an accurate control of chemistry, and thus varying the properties of the resulting polymers in a more controlled manner. ROP of lactide have been successfully carried out via melt polymerisation, bulk polymerisation, solution polymerisation and suspension polymerisation processes. Despite each of these processes have its own advantages and disadvantages, melt polymerisation is considered as the most simple and reproducible process and will be reviewed below [93].

From the pioneers' works, same ROP mechanisms as ε-caprolactone were investigated and summarized for lactide, including cationic mechanism (ACE and AM), anionic mechanism and coordination insertion mechanism [94-97]. However, significant racemization and inter- or intra transesterification reactions often hinder the polymerisation process for cationic and anionic ROP mechanisms (see Figure 2.10). Coordination insertion mechanism is the best method in terms of supressing the undesired side reactions and gets a close control over the PLA molecular weight [96]. Therefore, only coordination insertion mechanism of lactide is reviewed below.

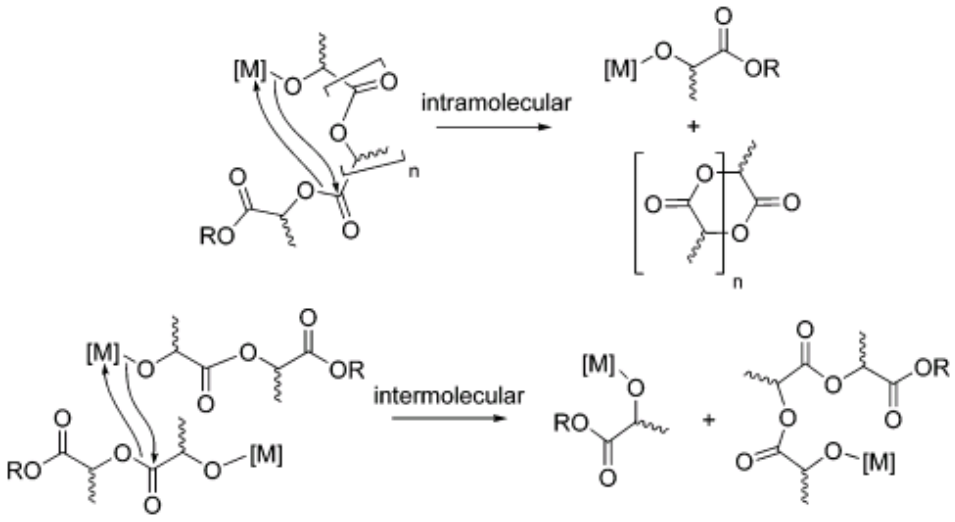

Figure 2.10 *Inter- and intra-transesterification reactions during lactide ROP*

A vast number of catalyst systems have been investigated for coordination insertion ROP of lactide, of which the most studied were the carboxylates and alkoxides of Sn and Al [80, 94-99]. Among all the catalysts, stannous octoate ($Sn(Oct)_2$) is the most intensively studied and used. $Sn(Oct)_2$ is commercially available, easy to handle, and soluble in common organic solvents and in melt monomers. It is highly effective during polymerisation and allows for preparation of high molecular weight PLA (10^5 or even 10^6 Da in the presence of alcohol) [100]. However, the low-level toxicity related to tin compounds is a drawback for biomedical applications. Regarding to Al alkoxides, $Al(Oi\text{-}Pr)_3$ has been largely used for mechanistic study. Compare to $Sn(Oct)_2$, it has been revealed to be significantly less active and the general molecular weight is less than 10^5 Da [100]. Furthermore, since aluminium does not belong to the family of human metabolism, Al alkoxides were much less used for preparing biodegradable polyesters. Therefore, recent researches have also been devoted to investigate zinc, calcium, iron and magnesium derivatives as potential non-toxic catalysts [101-107]. So far, the best outcomes regarding to lactide conversion and the degree of

polymerisation were obtained by zinc(II) lactate. However, the polymerisation efficiency and the molecular weight were still not as good as $Sn(Oct)_2$ [98].

Dittrich and Schulz [108] first formulated the three step coordination-insertion mechanism for ROP of cyclic esters in 1971. It was proved experimentally in the $Al(Oi\text{-}Pr)_3$-initiated polymerisation of lactide, for such a mechanism independentlyby Kricheldorf and Teyssiė [74, 80] in the late 1980s. Recently, further experimental as well as theoretical proofs have been provided [109, 110]. It was found that $Sn(Oct)_2$ can provide more effective and better controlled polymerisation when it was combined with a protic reagent, such as an alcohol. It is generally accepted that alcohols react with $Sn(Oct)_2$ to form covalent tin(II) alkoxides, this coordination step can occur with either retention of the octanoate ligands (see Equation 1, Scheme 2.6) or with liberation of octanoic acid (see Equation 2, Scheme 2.6) [96, 111]. The reaction conditions (in terms of temperature, alcohol-to-tin ratio, solvent) are believed to strongly influence these processes. It is also widely accepted that impurities present in the monomer (alcohols, lactic acid, water) may act as co-initiators, especially when $Sn(Oct)_2$ is used without protic additives. Finally, it should not be underestimated that besides their involvement in polymerisation initiation, protic agents may also be involved in reversible chain transfer with the growing chain (see Equation 3, Scheme 2.6), making it essential that the alcohol to $Sn(Oct)_2$ ratio must be carefully optimized [112].

$$\mathrm{Sn(Oct)_2 + ROH \rightleftharpoons (ROH)Sn(Oct)_2} \quad (1)$$

$$\mathrm{Sn(Oct)_2 + ROH \rightleftharpoons (RO)Sn(Oct) + OctH} \quad (2)$$

$$\mathrm{RO{-}(lactide)_n{-}Sn(Oct) + ROH \rightleftharpoons (RO)Sn(Oct) + RO{-}(lactide)_n{-}H} \quad (3)$$

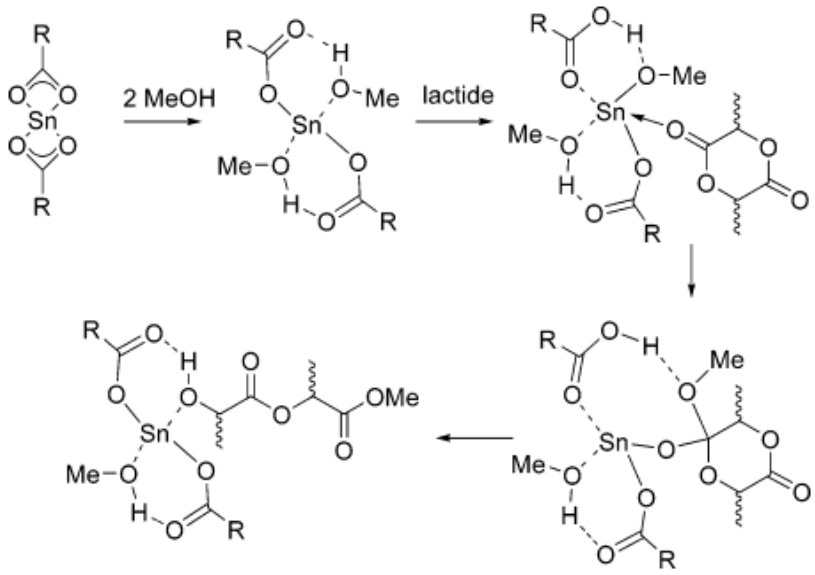

Scheme 2.6 *Coordination-insertion mechanism for ROP of lactide initiated by alcohol and stannous octoate*

2.4.6. Degradation mechanisms and absorbable pathways of aliphatic polyesters

Among all types of synthetic biodegradable polymers, aliphatic polyesters have received special attentions in biomedical applications as they are sensitive to hydrolytic degradation, a feature of interest when compared with the fact that biological systems function in aqueous media. Besides hydrolytic degradation, aliphatic polyesters can also be degraded through enzymatic degradation, thermal degradation, photodegradation and radiation degradation. For biomedical applications of aliphatic polyesters, hydrolytic degradation is of paramount importance.

The hydrolytic degradation behaviour, rate and mechanism depend on material and environment factors, such as temperature, pH and catalytic species. Thus, the hydrolytic degradation behaviour, rate and mechanism can be controlled by varying these factors. The hydrolytic degradation rate of biodegradable polyesters, such as PCL and PLA, should be engineered and optimised for biomedical applications. Generally speaking, there are two hydrolytic degradation mechanisms for biodegradable polymers, which are bulk degradation and surface degradation. Bulk degradation polymer degrades all over its cross section and has degradation kinetics that are non-linear and are usually characterised by a discontinuity. The degradation or erosion of a surface degradation polymer is limited to the surface of the polymer only. The kinetics of the mass loss should be theoretically linear when it is normalised to the surface area. The molecular weight of the polymer should be constant if the hydrolytic degradation is the only mechanism that controls the process. Polyanhydrides serves as a good example of surface degradation polymer [113].

Aliphatic polyesters are typical bulk degradation polymers. However, some research has shown that the degradation is non-uniform across their cross sections. The degradation of lactic and glycolic copolymers of varying sample thickness were investigated by Li *et al.* [114]. For thick samples, the degradation rate of the inner part of the polymer was found to be much faster than the outer surfaces resulted from the acid concentration gradient from the centre to the surface, which the acid is produced by hydrolysis of the polymer. Therefore, material thickness is an important factor for determining the hydrolytic degradation mechanisms. Both PCL and PLA breaks down by hydrolysis into lactic acid and ε-caprolactone, which then converts to carbon dioxide and water

though the tricaboxylic acid cycle (TCA) [27, 115]. Both their degradation rate can be engineered to match with the growth of fractured bone to support the bone healing process.

2.5. Phosphate based glass

2.5.1. Introduction

Phosphate glasses were developed around 100 years ago [116]. They have high refractive indices, low optical dispersion and high UV transparency. During the middle of the last century, phosphate glasses with modified compositions were introduced to industrial applications such as water treatment, pigments manufacturing and solid-state lasers. Iron phosphate glasses were investigated as hosts for nuclear waste due to their low processing temperatures and high chemical durability [117, 118]. Phosphate based glasses are a promising material for biomedical applications due to their unique characteristics [119, 120]:

a) They are totally soluble in aqueous environment;
b) Their chemical composition can be similar to the mineral phase of bone (calcium phosphate);
c) Biocompatible;
d) Can be formed into fibres, have good mechanical properties in fibre form;
e) Controllable and predictable dissolution rates (from hours, days, and months to years) by altering their composition.

Based on these advantages for phosphate glasses, they have various potential medical applications. They have also been trail-applied for hard tissue applications such as bone fracture in the form of reinforcement for bioresorbable polymers [121, 122].

2.5.2. Structure

There are three common glass former oxides (SiO_2, B_2O_3 and P_2O_5). Phosphorus pentoxide (P_2O_5) is the former for phosphate glasses and the basic structural unit is a tetrahedral phosphate anion (PO_{4}^{-3}) (see Figure 2.11) [118, 123].

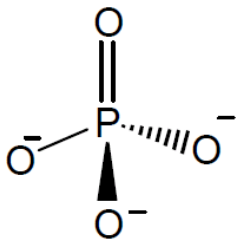

Figure 2.11 *Structure of the tetrahedral phosphate anion*

Tetrahedra are classified based on Q_i terminology into Q_3, Q_2, Q_1 and Q_0 where 'i' represents the number of bridging oxygen per tetrahedron (i.e. number of P-O-P links of a PO_4 tetrahedron) (see Figure 2.12) [124]. Vitreous P_2O_5 consists of a three dimensional network (Q_3) and use of pure vitreous P_2O_5 glasses is extremely limited due to their hygroscopic nature [118, 122]. Addition of modifiers (MO/M_2O) results in depolymerisation of the phosphate network by creation of terminal oxygens at the expense of bridging oxygens. Different oxides such as sodium oxide (Na_2O), calcium oxide (CaO), magnesium oxide (MgO), iron oxide (Fe_2O_3) and titanium oxide (TiO_2) have been used as modifiers to suit varying end applications [125]. Figure 2.12 shows the transformation from one species to another via addition of monovalent cations (M^+). Phosphate glasses can be classified into binary, ternary, quaternary and complex glass systems based on the number of oxides within the composition. CaO and Na_2O are the most common modifiers in the preparation of binary phosphate glasses. Binary glasses ($x\ M_{2/v}O – (1- x)\ P_2O_5$) can be divided into three groups based on the composition, where 'v' is the valance of the metal cation [118, 122, 123, 126]:

a) Ultraphosphates ($0 \leqslant x<0.5$): structure is based on Q_3 and Q_2 species,

b) Metaphosphates ($x=0.5$): structure consists of infinity long chains of Q_2,

c) Polyphosphates ($x>0.5$): structure of polyphosphate glasses can be divided into four subgroups according to x ratio:

1) ($0.5<x<0.67$): structure contains mixture of Q_2 and Q_1 species,
2) Pyrophosphates ($x=0.67$): structure dominated by phosphate dimers (two Q_1 species sharing a bridging oxygen atom),
3) ($0.67<x<0.75$): Structure contains a mixture of Q_1 and Q_0 species,
4) Orthophosphate ($x =0.75$): structure consists of isolated Q_0 units.

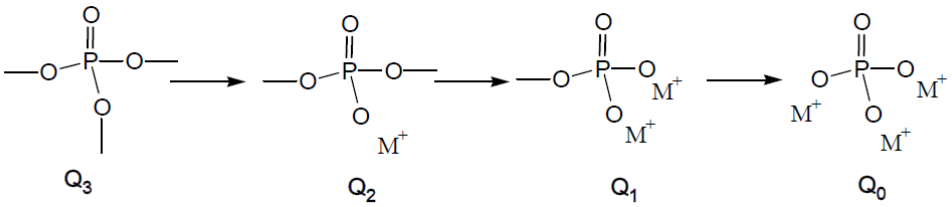

Figure 2.12 *Effects of addition of monovalent cation (M+) on the Q structure of the P_2O_5*

Structure of quaternary phosphate glasses (P_2O_5 – CaO – Na_2O – MgO) were investigated using ^{31}P MAS-NMR spectroscopy by Walter *et al.* [127]. Good agreement was seen with the theoretical and experimental Q structure (see Figure 2.13). Similar findings were demonstrated by Brauer *et al.*[128].

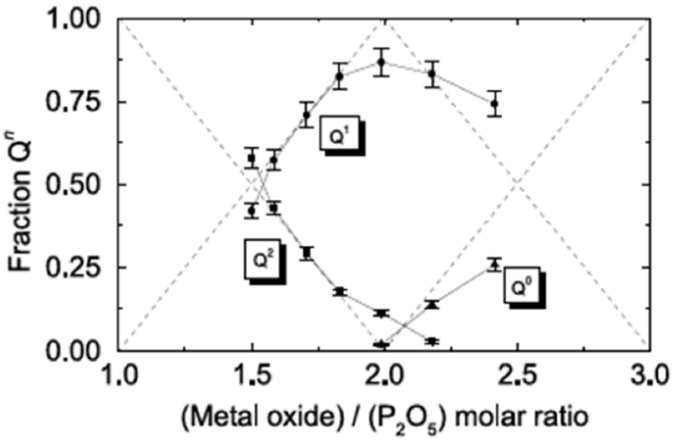

Figure 2.13 *The Q structure for P_2O_5 – CaO – Na_2O – MgO glass [127]*

2.5.3. Dissolution

The poor chemical durability of phosphate glasses in aqueous environments restricted their industrial applications. It was the main motivation for their use in medical applications such as temporary bone fracture fixation devices [122, 129]. Dissolution rate or resorption time of the implant could be adjusted according to the requirements of end applications. Degradation rate of PGF does not only depend on the chemical composition but also on the pH of the degradation medium, degradation temperature, thermal history and ratio of surface area to volume [130]. Based on their structure, polyphosphate glasses are more durable than metaphosphate due to a decrease in the fraction of highly hydrolysable Q_2 species [131]. It was found that the degradation rate for phosphate glasses in stimulated body fluid (SBF) was lower than that in deionised water. This was attributed to the fact that SBF is a buffering solution, whilst pH for the water would decrease due to degradation of the glasses causing acceleration of the process with ions leaching into the media [129, 130].

The degradation process of phosphate glass is divided into two steps [132, 133]:

(i) Hydration reaction: during this stage, the outer layer of the glass (i.e. at the interface with the surrounding medium) would be hydrated due to ion exchange reaction. The glass exchanges the cations (Na^+) with hydrogen ion (H^+) form the water.

(ii) Network breakage: the hydrated layers would be attacked by the water (hydrolysis) resulting in cleavage of the P-O-P bonds and breakdown of the network structure. Consequently, phosphate chains with different lengths would be released into the medium.

2.5.4. Biocompatibility

Biocompatibility of the implant materials is essential to avoid adverse or inflammatory reactions after implantation. Incorporation of PGF into the matrix (PLA) has been shown to improve both biological response as well as the material mechanical properties [5, 25, 134].

Since the mineral phase of bone is composed mainly of calcium (Ca) and phosphorus (P), they should have an essential role in the bone remodelling process. Therefore, it was expected that PBGs would have good potential for hard tissue applications such as bone repair. PBG showed capability of stimulating the new bone formation via release of ions (mainly Ca, Mg and P) during their degradation. The rate of ion release is controllable to avoid the cytotoxicity effect [135].

Biological response of P_2O_5 – CaO – Na_2O ternary glasses to human osteoblast cells were investigated [136]. It was reported that cell proliferation was adversely affected by glasses containing high amounts of Na_2O. Cell proliferation enhanced by increasing the amount of CaO at the expense of Na_2O (less soluble glass).

These findings were supported by Bitar *et al.* [137] and Navarro *et al.* [138] in their studies on human osteoblast and fibroblast cells interaction with P_2O_5 – CaO – Na_2O ternary glasses. Therefore, it can be argued that the dissolution rate of the glass had a direct influence (inversely) on their biological performances.

Biocomptability was assessed for 50 P_2O_5 – 30 CaO – (20 – x)Na_2O – x TiO_2 (x varied from 0 to 15 mole %) glasses using cell viability and cell proliferation tests with human osteosarcoma cells by Abou Neel *et al.* [128, 131, 139]. The cell proliferation viability and attachment for glasses containing 3 mol% or higher of TiO_2 was greater than the titanium free composition. Glasses containing titanium maintained cell viability greater than 99% over the period of the study (7 days). Enhancement of biocompatibility for the glasses by inclusion of titanium oxides was associated with decrease in solubility of the glasses.

2.5.5. Phosphate based glass fibre (PGF)

Glass fibres can be drawn from molten glass via melt spinning process. The existence of strong bonds within molten glass is required to produce continuous thread. These bonds should withstand the applied tensile stresses during the pulling process at high temperatures [140]. Continuity of the fibres depends also on composition and structure of the glasses. Heat treatment (annealing) of the prepared fibres is essential for releasing internal stresses which are created by the rapid cooling of the pulled fibres [141]. The internal stresses were ascribed to broken bonds and stretched bonds greater than the original length at equilibrium state. The stretched bonds create bonding stress as they try to restore to equilibrium state, which then turned into the internal stress. Annealing of glass fibres around the glass transition temperature would stabilise their structure by reforming broken bonds and allowing some bonds to reach a more stable state.

However, the mechanical strength of the fibres might slightly decrease by annealing. In addition, it is also difficult to perform the annealing of the fibres within the furnaces without damaging the fibres.

Cozien-Cazuc *et al.* investigated the effect of annealing on dissolution and mechanical retention of quaternary phosphate glass fibres (40 P_2O_5-20 Na_2O- 16 CaO-24 MgO – in mol%) [142, 143]. However, the initial tensile strength for the annealed fibres decreased due to formation of flaws at the fibre surface as a result of annealing in a humid environment. The fibres failed during the tensile test by fracture which originated from surface flaws. Interestingly, they found that the annealed fibres recovered the as-prepared (non-annealed) fibres strength after 3 days of degradation in distilled water at 37°C. The increase in tensile strength for the annealed fibres was ascribed to peeling off of the outer tensile layer with its inherent flaws. Removal of the outer layer of the fibres was seen by using scanning electron microscopy (SEM). Conversely, non-annealed fibres lost ~ 25 % of their initial value due to hydrolysis and pitting corrosion at the surface. Approximately 50% decrease in dissolution rate for the fibres was seen after annealing.

Thermal, mechanical, structure and dissolution properties for glass fibres differ greatly from those for bulk glass. This difference is due to the preparation method, drawing parameters (temperature, speed, viscosity) and fibre diameter. Ahmed *et al.* [119] compared degradation properties for P_2O_5 – CaO – Na_2O ternary phosphate glass fibres with bulk glass. They found that the degradation rate for fibres significantly increased in comparison to the bulk glasses due to the huge increase in surface area. Furthermore, the degradation rate for fibres decreased with increasing fibre diameter due to surface area effect also. It was reported that

the strength of phosphate glass fibres decreased by 15% to 34% of the freshly pulled fibres after exposure to air (around 10 days). This reduction was attributed to be due to degradation as a result of moisture [117, 144].

2.6. Fibre reinforced polymer composite

A composite material is defined as material made from at least two constituent materials with distinctly different chemical and/or physical properties, which the combined material results in characteristics different from the individual components. The continuous phase within the composites is named matrix and the stiffer, dispersed phase is the reinforcement. Fibre reinforcement can be either chopped strand or continuous fibre strand, depending on the fibre length. Fibre orientations could be random, angled or preferentially aligned, which greatly affect the properties of the composites [145, 146]. It should be noted that one of the key factors controlling the properties of the composites is the strength of the fibre/matrix interfaces [147]. There are many types of fibres being used in the field of orthopaedic applications, such as carbon fibre [20, 148-150], bioglass fibre [149, 151-156] and phosphate based glass fibre [132, 136, 157-159].

Biocomposites are composite materials which are used to be implanted inside human bodies to repair or place the function of certain living tissues, such as cancellous or cortical bone [49]. Fibre reinforced polymer biocomposites (FRC) provide the possibility to achieve wide ranges of biological and mechanical properties, which could potentially mimic the structure and properties of human bones [1, 160]. Biocomposites can be broadly divided into three categories based on their biodegradability: non-bioresorbable, semi-bioresorbable and fully bioresorbable.

2.6.1. Non/semi bioresorbable composites

Both the matrix and reinforcement material must be biotolerable and/or biostable to be counted as non/semi-resorbable composites. There are many studies on both thermoplastic and thermoset polymers for their applications as non-resorbable composites materials [161]. However, toxic effects from the monomer of epoxy (common matrix material for thermoset composites) was found to be considerably harmful to human bodies, which greatly reduced the research interests in the thermoset polymer composites [161, 162]. This encouraged the counterpart development in thermoplastic fibre composites, such as PMMA/carbon fibre [163], PP/carbon fibre [164], PE/carbon fibre [22] and most commonly PEEK/carbon fibre [165, 166].

The non-bioresorbable polymer composite implant should be stable in vivo with no or minimum variations in mechanical properties during applications. The well-designed mechanical properties of those composites can support the healing process of bone fractures, but stress shielding is still unavoidable due to the stiffness mismatch between the fracture bones and the non-bioresorbable polymer composites, which weakens the tissue around the fracture site and increases the probability of re-fracture [134]. It is highly desirable that the healing bones are subject to a gradually increasing stress to reduce the influences of stress shielding [17, 18]. Therefore, semi-bioresorbable composites have been investigated, which evolves around fully bioresorbable matrix (PLA, PCL, etc) with the addition of various kinds of non-bioresorbable fibre reinforcement (carbon fibre, bioglass fibre, etc) [22]. Although it reduces the effects of stress shielding, there are several associated complications, including cytotoxicity and inflammation of the surrounding tissue due to the fibre or fibre particles from the

reinforcement phase [161]. As such, the development of a fully bioresorbable polymer composites with well-engineered degradation profiles are called for to eliminate the issues mentioned above.

2.6.2. Phosphate based glass fibre reinforced composites

Both the matrix and reinforcement phase must be fully bioresorbable for the resulted composites to be accounted as fully bioresorbable composites. For fibre reinforced fully bioresorbable polymer composites with intended applications in bone fracture fixation, PGF reinforced composites have attracted most of the attentions and being heavily studied in our research group [16, 18, 159, 167, 168].

PGF reinforced composites demonstrated relatively high range of mechanical properties and the chemical composition of PGF is similar to the inorganic component of human bones [157, 169]. Positive results were also reported on the biocompatibility of PGF reinforced composites [167, 170]. It has been reported that with the addition of relatively small amounts of modifying oxides, such as TiO_2, $B2O_3$ and Fe_2O_3, to the composition of PGF, the composites successfully promoted cell proliferation and attachment [13, 138]. The biocompatibility of PGF reinforced methacrylate-modified oligo-lactide based polymer composites was investigated by Brauer *et al.* using MC3T3-H1 ore-osteoblast cells and the growth of continuous cell layers was found [19]. Ahmed *et al.* also studied the *in-vitro* cell response of PLA/PGF composites using MG63 cells, which high cell viability was maintained by the composites throughout the investigation [16].

The flexural properties of PGF reinforced polymer composites have been extensively studied with various polymer matrix, fibre compositions and

architectures combinations, which reported to have achieved initial (non-degraded) flexural strength and modulus between 100-210 MPa and 11-21 GPa respectively [16-20]. Those mechanical properties were well within the range of the properties for human cortical bone. The developments gained considerable attention from many biomedical companies, which Corbion Purac already invested in development of bioresorbable fibre reinforced composites implant (FibreLive technology) for hard tissue repairs [171]. However, many studies reported a rapid deterioration of mechanical properties for PGF reinforced polymer composites during degradation inside aqueous environment [17, 18, 158, 159]. It is due to the fluid attack at fibre/matrix interfaces, which decreased the adhesion dramatically and prohibited effective stress transfer. Table 2.5 summarised the flexural properties of the PGF reinforced composites with various matrix material, fibre composition and fibre volume fractions.

Table 2.5 *Flexural strength and modulus of selected PGF reinforced polymer composites with various matrix materials, fibre compositions, types and fibre volume fractions (RM = Random mat, UD = Unidirectional)*

Matrix materials & fibre form	PGF formulation	Fibre volume fraction (%)	Flexural strength (MPa) & Modulus (GPa)	Reference
PLA & UD	$45P_2O_5$-$5B_2O_3$-16CaO-24MgO-$7Na_2O$-$3Fe_2O_3$	19	184; 12	[170]
PLA & UD	$45P_2O_5$-16CaO-24MgO-$12Na_2O$-$3Fe_2O_3$	22	150; 11	[170]
PLA & UD	$45P_2O_5$-$5B_2O_3$-16CaO-24MgO-$10Na_2O$	17	160; 12	[170]
PLA & UD	$45P_2O_5$-16CaO-24MgO-$15Na_2O$	18	131; 10	[170]
PLA & RM	$40P_2O_5$-16CaO-24MgO-$16Na_2O$-$4Fe_2O_3$	37	210; 21	[172]
PLA & RM		14	115; 9	[173]
PLA & UD		45	120; 10	[5]
PLA & UD		37	106; 7	[173]
PLA & RM	$50P_2O_5$-40CaO-$5Na_2O$-$5Fe_2O_3$	32	150; 11	[174]
PLA & RM		25	112; 9	[169]
PLA & UD		30	105; 9	[175]
PLA & UD		14	80; 5	[16]
PCL & RM	$50P_2O_5$-50CaO	17	30; 3	[157]
PCL & RM	$40P_2O_5$-16CaO-24MgO-$16Na_2O$-$4Fe_2O_3$	10	72; 2	[176]

2.7. Manufacturing process for PGF composites

Aliphatic polyesters, such as PCL and PLA, belong to the family of thermoplastics. Therefore, their dominated PGF reinforced polymer composites manufacturing process is conventional thermoplastic composites manufacturing process, which is laminate stacking (LS) followed by hot press moulding.

The conventional manufacturing processes for thermoplastic composites involve combining the reinforcements and polymer. The processes need intermediate forms of materials manufactured from the raw fibres and polymer matrix. The intermediate materials are usually in the forms of short or long fibre reinforced granules, glass fibre mats reinforced sheet (GMT), unidirectional tapes, ribbons or sheets of pre-impregnated glass roving or fabric. These intermediate materials then undergo various processes to produce composites. There are four basic steps for conventional thermoplastic composites manufacturing processes: wetting/impregnation (exclude processes using pre-pregs), lay-up, consolidation and solidification. LS and *in-situ* polymerisation (ISP) processes were briefly reviewed.

2.7.1. Laminate stacking (LS) and hot press moulding

LS process requires the fibre and polymers to be in intermediate forms, which usually is fibre prepregs and thin polymer films. The prepregs of the fibres in the form of continuous aligned sheets or woven cloth were stacked with polymer thin films in the required position and hot pressed to form the final products (see Figure 2.14). The temperature of the moulds is usually set to the minimum necessary for the matrix to melt and flow sufficiently for consolidation to occur. This process is limited to simple shapes due to poor drapability of the prepreg. High viscosity of the polymer melt often forms polymer rich zone and leads to

poor interfacial bonding. This process is currently used in our group to manufacture fibre reinforced polymer composites.

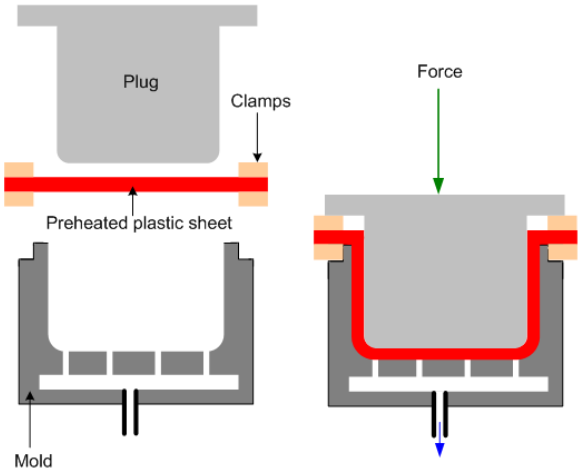

Figure 2.14 *Hot press moulding*

2.7.2. *In-situ* polymerisation (ISP)

It is well established that the use of continuous fibre can provide the most effective mechanical reinforcements. However, two major challenges still present in manufacturing biodegradable continuous PGF reinforced thermoplastic composites. On the one hand, it is difficult to obtain a good fibre wet-out and impregnation due to the relatively high viscosity of the thermoplastic melt. On the other hand, implants with specific complex shapes cannot be manufactured via conventional thermoplastic composites manufacturing processes. To overcome these complications, *in-situ* polymerisation, a variant of liquid transfer moulding based on the monomer transfer moulding (MTM) process, was investigated in this work. Similar approaches, such as resin transfer moulding (RTM) and structural resin transfer moulding (SRTM) in the thermoset composites manufacturing is well developed. However, the counterpart in the thermoplastic composites manufacturing is rarely reported.

For the ISP process, the monomer of aliphatic polyesters is polymerised directly around the reinforcement materials within a closed, shaped mould to form the biodegradable polymer composites. A schematic set-up diagram for the ISP process is shown Figure 2.15. Since the viscosity of the monomer is much lower compare to its polymer melt, good reinforcement impregnation and stronger fibre/matrix interfacial bonding are theoretically promoted by this process, thus leading to improved mechanical properties of the resulted biodegradable composites. Moreover, moulds with specific complex shaped cavity can be made to produce complicated shaped implants. This ability to produce a moulding of complex shapes is essential in many biomedical applications, such as repair of face and skull structures.

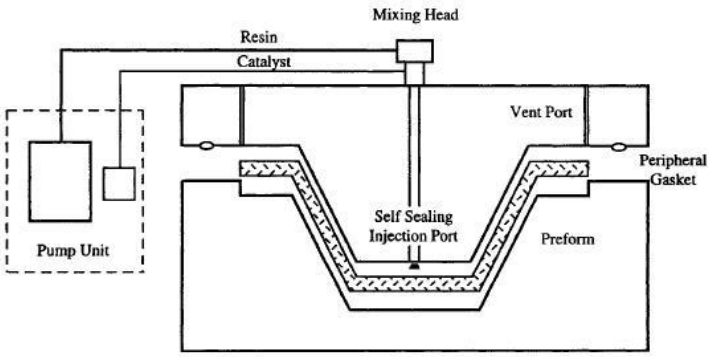

Figure 2.15 *Sechmatic diagram for ISP mould setup*

The essential operation procedures for the ISP process are as follows: pre-treated glass fibre is put into the mould cavity first, then the mould is sealed and placed in a vacuum oven overnight to drive off any moisture. The reaction mixture (monomer and catalyst) is injected into the mould through the injection port, allowing polymerisation to take place at proper temperature and for a certain duration of polymerisation time. After the polymerisation is complete, the mould is allowed to cool down and the resulted composites is taken out.

In this work, novel ISP process for manufacturing PCL/PGF and PLA/PGF fully bioresorbable polymer composites is being established and developed. From the literature review above, it can be concluded that the PGF reinforced PCL and PLA composites processed excellent potential for the development of the appropriate fully bioresorbable bone fixation devices. However, due to the limitations of the current manufacture processes, PGF reinforced composites suffered from rapid reductions of mechanical properties within aqueous environment, which were resulted from the poor fibre/matrix interfacial bonding.

Therefore, it is necessary to promote stronger fibre/matrix interfacial bonding by developing the manufacturing processes, thus the required enhancement for the degradation and mechanical retention behaviour of the fully bioresorbable composites can be achieved.

Chapter 3. Material and Methodology

3.1. Summary

This chapter describes all the materials and methods used throughout the whole work. Manufacturing methods for the phosphate based glass, the PGF fibre, and the PGF reinforced composites (LS and ISP) were presented. The development of the room temperature ISP manufacturing process for PGF reinforced PCL composites firstly, and then the heated ISP process for PLA-PCL copolymer and neat PLA composites were detailed and emphasised. The main characterisations performed on the resulted polymer and polymer composites were the polymerisation kinetic studies and degradation studies, followed by various of chemical, thermal, imaging, mechanical (including long-term fatigue tests) and cytocompatibility analysis. The specifications and procedures for the characterisations are all detailed in this chapter, which are referred by later results chapters.

It should be emphasised that there were many subtle challenges in developing the heated ISP process for the manufacture of the PGF reinforced PLA based polymer composites. The ISP process is limited to the use of monomer in a low viscosity liquid state, such as ε-caprolactone at room temperature (naturally as a low viscosity liquid). In this work, a first-time, novel heated ISP process was developed for the manufacturing of PLA based polymer composites, which the monomer di-lactide has a melting point of ~95 °C. To achieve a suitable melt viscosity of di-lactide for monomer transfer and fibre impregnation during ISP, a high temperature operating system is essential. To overcome the difficulties posted by the high operating temperature during the development, specific

heating system, monomer transfer system and moulding system were designed and tested. The flow of this work is centred around this heated ISP process development, and as such, this work is followed by a carefully designed manner around this matter to achieve the proposed objectives.

3.2. Flow of work

Since this work is primarily concerned about developing manufacturing processes for PGF reinforced composites, a well-studied phosphate based glass composition was selected and its fibre was produced, which the degradation behaviour and the mechanical properties of this specific PGF were accurately investigated and reported previously [119, 172].

PCL was chosen as the matrix material for the initial development of the monomer transfer system and composites moulding design for the room temperature ISP process. The monomer of PCL, ε-caprolactone, is liquid at room temperature, which is extensively beneficial for the ISP method development. As such, ISP process for PCL was established firstly and PCL/PGF composites with various V_f were produced via the established ISP process. In the meantime, PCL/PGF composites with matching V_f were produced via conventional LS process, which served as the control and comparison group for the ISP composites. The resulted LS and ISP composites were characterised and the benefits and improvements that the ISP process brought in was demonstrated via the property comparisons. At this point, the initial polymerisation mechanism, liquid transfer system and composite moulding designs for the room temperature ISP process were well established, which served as the foundation system design for the novel heated ISP method development.

In order to overcome the poor mechanical properties and long degradation period (>2 years for complete degradation) within aqueous environment that PCL possesses, PLA based polymer matrix was investigated as PLA has significantly higher virgin mechanical properties than PCL and considerably faster degradation rate (~1 year for complete degradation) [9, 59, 67, 177, 178]. Moreover, since PLA and PCL both belongs to the family of aliphatic polyesters, their polymerisation mechanism are similar, which suggests the established PCL ISP process is appropriate as the base for further development of the PLA ISP process. As discussed earlier, the monomer of PLA, di-lactide, has a melting point of ~95 °C, which heating was required to perform the monomer transfer and fibre impregnation. Based on the PCL ISP system, a bespoke heated pressure pot with vacuum aid was designed for the automatic monomer transfer system. The moulding design was also modified to fit in with the required heating elements and heated pipelines were set up for the molten monomer transfer. Temperature control and monitoring system was electrically wired into each of the ISP systems. Many trails were performed to tune all the systems and establish solid standard operating procedures. This system was initially used to *in-situ* copolymerise PLA-PCL copolymer/PGF composites with two different compositions (9:1 and 8:2 for mass ratio between PLA to PCL). The use of a copolymerisation system was intended to reduce the required temperature to liquefy the monomer mixture, therefore making processing easier, whilst retaining as high a proportion as possible of the matrix material that has greater mechanical properties (PLA in this case). With the successful development of PLA-PCL *in-situ* copolymerisation and to pursue the optimal mechanical properties of the PGF composites, ISP for manufacture of PGF reinforced neat PLA composites was performed later.

Characterisations and comparisons were then performed on the resulted ISP composites to investigate the performance of the novel heated ISP process.

Figure 3.1 presented a flow chart for the organization of this work.

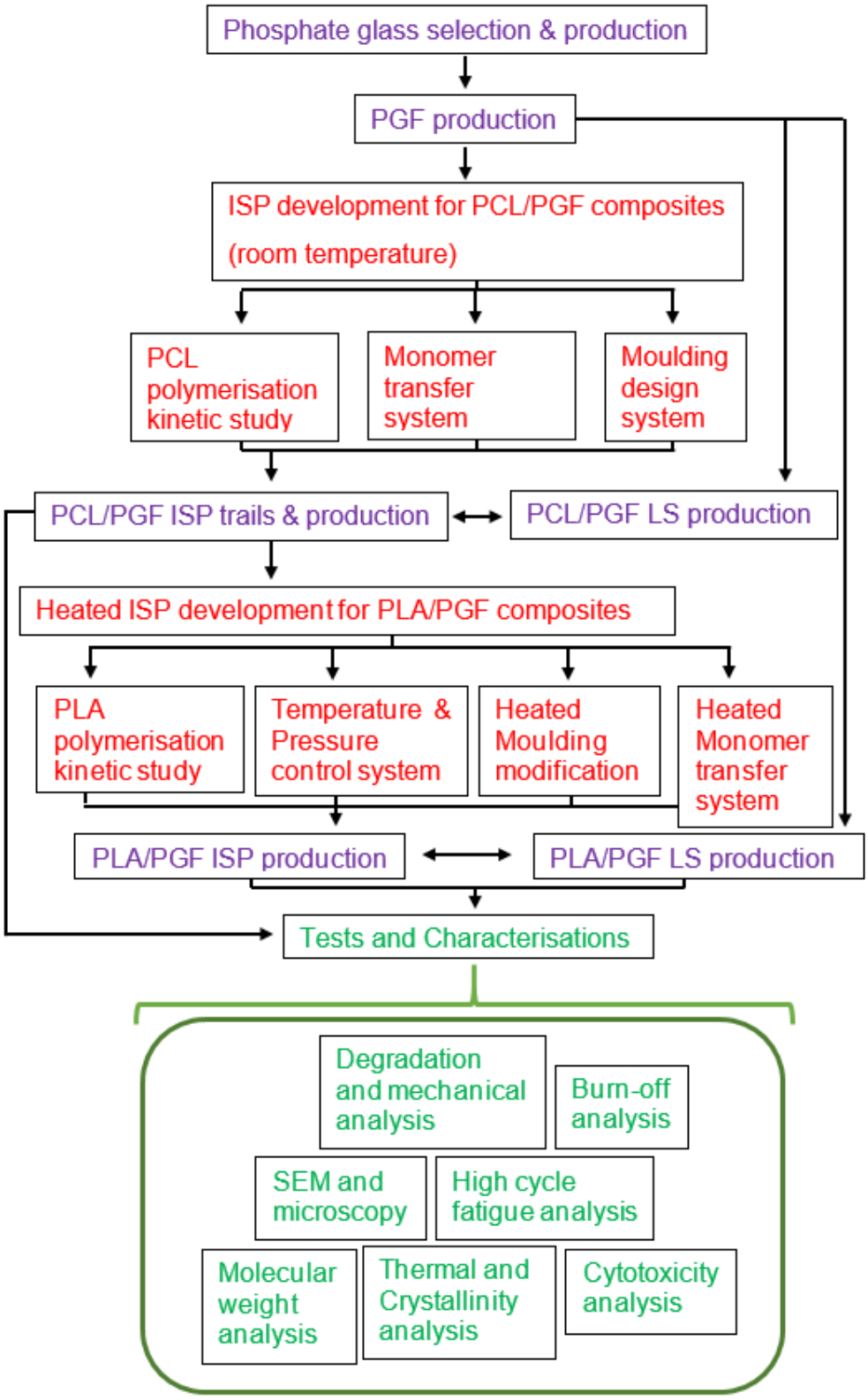

Figure 3.1 *Flow chart for the organization of this work (Colour scheme: Purple for manufacturing* process*; Red for manufacturing process development; Green for materials analysis.)*

3.3. Materials

The monomer ε-caprolactone, 3,6-dimethyl-1,4-dioxane-2,5-dione (di- lactide), catalyst $Sn(Oct)_2$ and initiator benzyl alcohol were all purchased from Sigma Aldrich (UK), with purities reported as 97%, 99.5%, 92.5%~100% and 99.8% respectively. All the above chemical components were used as purchased. PCL granules used were purchased from Sigma Aldrich (UK) and reported to have a weight average molecular weight (M_w) of ~65,000 g/mol and number average molecular weight (M_n) of ~42,500 g/mol. PLA granules (3251D Injection moulding grade) were purchased from NatureWorks (UK) and reported to have a M_w of ~80,000 g/mol and a M_n of ~65,000 g/mol. The granules were dried at 50 °C in a vacuum oven for 48 hours before processing.

3.4. Phosphate based glass production

The precursors used to prepare the glass were sodium hydrogen phosphate (NaH_2PO_4), calcium hydrogen phosphate ($CaHPO_4$), magnesium hydrogen phosphate tri-hydrate ($MgHPO_4 \cdot 3H_2O$), iron(III) phosphate di-hydrate ($FePO_4 \cdot 2H_2O$) and phosphorous pentoxide (P_2O_5), which were all purchased from Sigma Aldrich (UK) and used as received. The glass formulation used in this work (with its respective glass code) is reported in Table 3.1. The precursors were mixed together and then transferred into a 100 ml Pt/5% Au crucible (Birmingham Metal Company, UK). The crucible was then placed in a preheated oven (350 °C) for 30 minutes to remove any water within the mixture. The salt mixtures were then melted and reacted at 1150 °C for 1.5 hours in a furnace. Molten glass was poured onto a steel plate to cool down.

Table 3.1 *Phosphate glass code and formulation*

Glass code	P_2O_5 content (mol%)	CaO content (mol%)	Na_2O content (mol%)	MgO content (mol%)	Fe_2O_3 content (mol%)
P45Fe5	45	16	10	24	5
Drying temp/time (°C/h): 350/0.5; Melting temp/time (°C/h): 1100/1.5.					

3.5. Phosphate glass fibre (PGF) production

The in-house designed fibre rig contains a furnace (Lenton Furnaces, UK) with a Pt/10% Rh crucible (Johnson Matthey, UK) consisting of a bushing with an approximate 1 mm hole and a tip 15 mm long (see Figure 3.2). Glass was placed into the crucible and left to melt and homogenise for 30 minutes. The temperature of the furnace was then adjusted to achieve a viscosity suitable for fibre drawing. Different fibre diameters can be obtained by pulling the glass at different speeds. In order to produce the unidirectional fibre mats, the collecting drum was adjusted to move transversely at constant speed, covering the drum evenly with fibre. After the fibre mat had reached a certain thickness, the fibre drawing was stopped and the drum was taken to a fume hood. To maintain the integrity of the fibre mat alignment, a solution of PCL dissolved in chloroform (5% concentration) was sprayed onto the fibre mat to coat them. Afterwards, the drum was left inside the fume hood for 24 hours to let the chloroform evaporate. Finally, the coated fibre mat was removed from the drum and PGFs were produced of parallel filaments without any twist.

Figure 3.2 *Fibre drawing system*

3.6. Laminate stacking (LS)

PCL/PGF composites with three different targeted fibre volume fractions (V_f, 20%, 35% and 50%) were produced via LS process. PLA/PGF composites with 35% targeted V_f was produced via LS.

3.6.1. LS production for PCL/PGF composites

Thin sheets PCL (thickness ~0.2 mm) were prepared by hot press moulding of 4~5 g PCL granules. The granules were placed between metal plates, with PTFE coated glass fabric sheets used as release film (see Figure 3.3). The whole assembly and granules were heated to 120 °C within the hot press for 10 minutes and then pressed at 3 bar pressure for 1 minute. The assembly was then transferred to a cold press at room temperature to cool down under the same pressure.

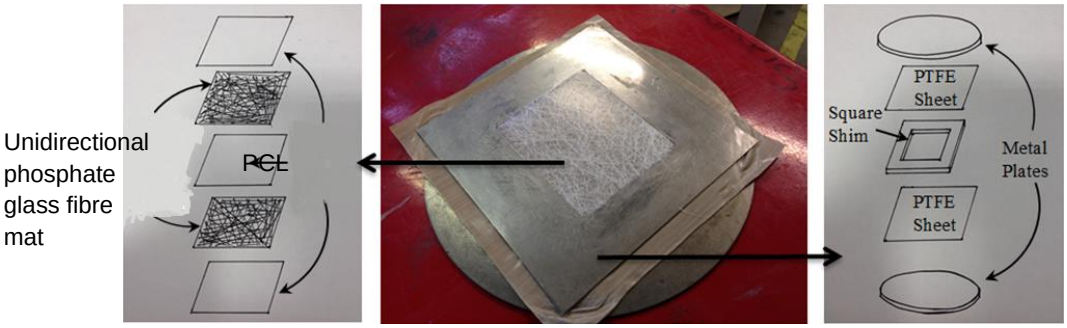

Figure 3.3 *Laminate stacking assembly for hot compression moulding*

All PCL films and fibre mats were dried in a 50 °C vacuum oven for 24 hours prior to use. The PCL/PGF laminates were prepared by LS process. Both PCL laminates and PGFs were cut to fit the mould cavity. The assembly was then heated to 120 °C within the hot press for 15 minutes, pressed under 30 bars pressure for 10 minutes. The stack was then transferred immediately to a cold press at room temperature to cool down under the same pressure for 15 minutes.

3.6.2. LS production for PLA/PGF composites

Similar LS procedures to PCL/PGF composites production were used for PLA/PGF composites production. Thin sheets of PLA (~0.2 mm thickness) were produced via hot compression moulding, where the detailed procedures stood the same as stated in Section 3.6.1. The moulding temperature was increased to 180 °C since PLA has a higher melting temperature, where the melting, pressure and cooling scheme for PLA thin sheet production remained the same.

24-hour vacuum oven drying at 50 °C was also performed on all PLA thin sheets and PGF mats before composites production. The stacking, melting, pressure and cooling scheme were the same as the PCL/PGF composites LS production (see Section 3.6.1), only which the melting temperature was raised to 180 °C.

3.7. Room temperature ISP process development

Two key studies were performed to establish the ISP processes for PCL/PGF composites production, including polymerisation kinetic study, monomer transfer and composites moulding system design.

3.7.1. PCL polymerisation kinetic study

3.7.1.1. PCL polymerisation chemistry

PCL can be synthesised from both condensation polymerisation (CP) and ring opening polymerisation (ROP). Because of the difficulty in getting rid of the water during CP, ROP is usually used to yield high molecular weight polymers. ROP of ε-caprolactone is chosen here and the reaction follows the coordination insertion mechanism using $Sn(Oct)_2$ as the pre-catalyst and benzyl alcohol as the initiator. The reaction mechanism is illustrated in Figure 3.4. $Sn(Oct)_2$ first reacts with benzyl alcohol to form the active catalyst species for ROP. The monomer then coordinates with the active catalyst, which induces strain in the monomer ring. The monomer is finally inserted into the Sn-O bond by acly-oxygen bond scission in such a way that the growing chain remains attached to tin through an alkoxide bond.

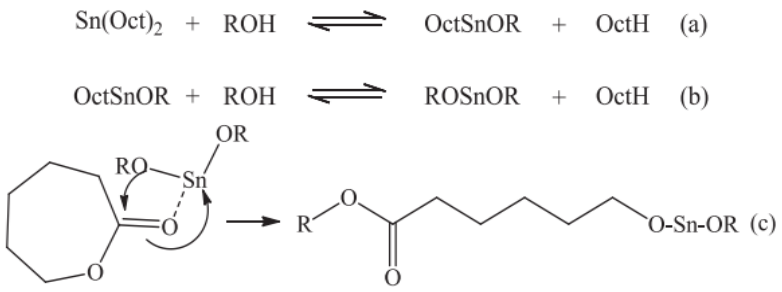

Figure 3.4 *Initiation and propagation reactions for CIM polymerisation of ε-caprolactone (a and b are reactions between pre-catalyst and initiator to form the active catalyst, c is the PCL polymerisation)*

3.7.1.2. Kinetic study of PCL polymerisation

The molecular weight and polydispersity of the PCL synthesised by ISP are dependent on several manufacturing parameters, which are reaction temperature, reaction time under heating, extent of impurities, and catalyst and initiator concentrations. It is believed that higher molecular weight and lower polydispersity (≥1) of the polymer can increase its virgin mechanical property. Meanwhile, more consistent and homogenous performance can also be achieved when the polymer serves as the matrix material of the composites. To determine the most suitable polymerisation environment, a kinetic study to simulate the reaction conditions inside the mould and to monitor the polymerisation behaviour is performed. In this study, 5ml glass vials are used to replace the mould as it is difficult to take the sample out of the sealed mould during the polymerisation.

ε-caprolactone was treated with predetermined amount of $Sn(Oct)_2$ and benzyl alcohol under a dry blanket of nitrogen in a 100 ml two neck boiling flask. Detailed molar ratios and reaction conditions are stated in Table 3.2. All the glassware was dried in a 50 °C oven for 24 hours before use. The reaction mixture was mixed using a magnetic stirrer on hot plate until homogeneous (~5 mins). After the mixing was completed, 2 ml of the mixture was then injected into each vial by a syringe. The glass vials were then transferred into an oven at the predetermined temperature. At each time point (every 30 minutes in this case), one glass vial was then taken out of the oven, and a sample was collected for the chemical analysis.

Table 3.2 *Reaction parameters for PCL polymerisation kinetic study*

Reaction parameters	Molar Ratio: [ε-caprolactone : Benzyl alcohol : $Sn(Oct)_2$]; Reaction Temperature (°C)		
Alter $Sn(Oct)_2$ amount only	[1000:1:1]; 130	[1000:1:0.5]; 130	[1000:1:0.1]; 130
Alter Benzyl alcohol amount only	[1000:1.25:0.5]; 130	[1000:1:0.5]; 130	[1000:0.625:0.5]; 130
Alter reaction temperature only	[1000:1:0.5]; 110	[1000:1:0.5]; 130	[1000:1:0.5]; 150
All reactions are monitored up to 24 hours			

3.7.2. ISP moulding design for PCL/PGF composites

To perform ISP for PCL/PGF composites, moulds were designed and made by PTFE and aluminium (see Figure 3.5). PTFE was chosen as the material because it is chemically inert, thermally stable and easy for sample de-moulding. Each mould consists of a female half and a male half PTFE block, and two aluminium blocks, which act as the outer shells to protect the PTFE moulds. The aluminium blocks also helped to flatten the PTFE moulds as PTFE is prone to distortion under stress and heating. The mould halves were assembled using long screws and nuts. Two injection ports were located on the male half, one for liquid injection and one for degassing. The plate-shaped cavity was positioned on the female half and surrounded by an O-ring cord groove to provide a tight seal. O-rings were also incorporated around the injection ports.

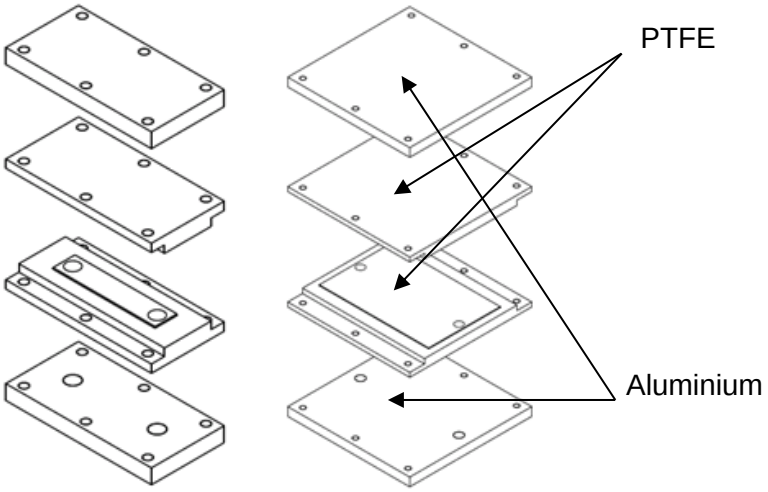

Figure 3.5 *ISP moulding design for PCL/PGF composites production (scale 1:10)*

3.8. ISP manufacture for PCL/PGF composites

The mould assembly used to perform the room temperature ISP, mixing and injection apparatus were all dried at 70°C for 24 hours in the vacuum oven before processing. Unidirectional (UD) PGF mats were carefully trimmed to fit in the cavity of the mould (70mm*15mm*2mm). The trimmed fibre mats were also dried under the same condition with the moulds. ε-caprolactone was treated with predetermined amount of $Sn(Oct)_2$ and benzyl alcohol (molar ratio: [ε-caprolactone : benzyl alcohol : $Sn(Oct)_2$] = [1000 : 1 : 0.1]) under a dry blanket of nitrogen in a 100ml two neck boiling flask. The reaction mixture was mixed by a magnetic stirrer on hot plate until homogeneous (~5 mins). After the mixing was completed, the mixture was then injected into the moulds by a syringe. Each injection port was connected with one syringe by PTFE tubing, one with chemical mixture and one empty. The reaction mixture was injected backwards-forwards from one syringe to another to eliminate air bubbles in the moulds and to ensure a solid monomer impregnation around the PGF fibres (see Figure 3.6). During

the injection, the whole mould assembly was placed on a rotating whirl mixer to help removing the trapped air inside the mould. After the injection has completed, two tubing clamps were used to seal the tubing and syringes were then removed. The mould assembly was then transferred into a preheated oven (130 °C for PCL polymerisation) for 24 hours to complete the polymerisation reactions. Finally, moulds were disassembled and samples were taken out of the moulds.

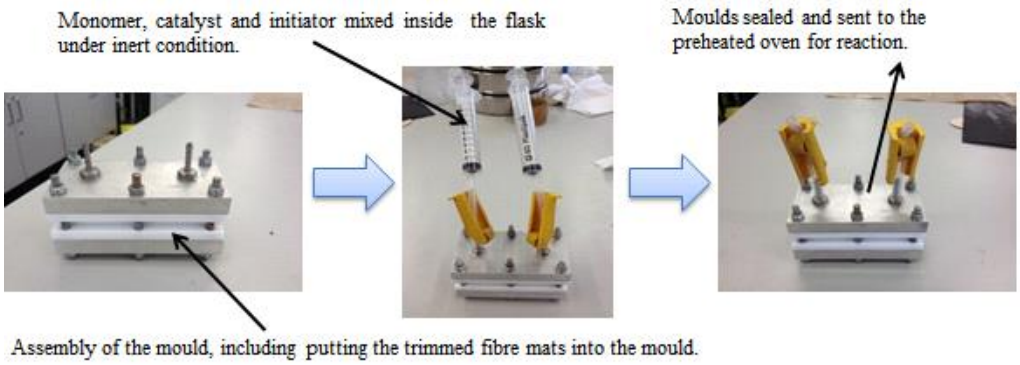

Figure 3.6 *ISP procedures for PCL/PGF composites production*

3.9. Heated ISP process development

Based on the basic design from the room temperature ISP process, further developments were made to establish the heated ISP process for PLA-PCL copolymer and PLA composites production. Polymerisation kinetic study on PLA and PLA-PCL copolymers were performed. Modifications to fit in the required heating elements were conducted in the moulding design. Novel heated monomer transfer system with pressure and vacuum assist was developed, with accurate temperature and pressure control system.

3.9.1. PLA and PLA-PCL polymerisation kinetic study

3.9.1.1. PLA and PLA-PCL polymerisation chemistry

Figure 3.7 illustrated the reaction mechanism for the PLA-PCL random copolymerisation and then the PLA polymerisation mechanism. ROP from di-lactide and ε-caprolactone was used to yield PLA-PCL copolymers and neat PLA.

For PLA-PCL copolymerisation, as both monomers were present in the mould to polymerise at the same time, random ring opening copolymerisation of PLA-PCL was expected. For PLA polymerisation, as di-lactide and ε-caprolactone both belongs to the same group of aliphatic polyesters, they undergo the same ROP mechanism when reacted with pre-catalyst $Sn(Oct)_2$ and initiator benzyl alcohol [96, 179]. More details of the reaction mechanism were presented in Section 3.7.1.1. Chemical equation I and II described the pre-reactions between $Sn(Oct)_2$ and benzyl alcohol to form the active catalyst (ROSnOR) for the ROP. Chemical equation III illustrated the random copolymerisation of di-lactide and ε-caprolactone, which the sequence of the PLA and PCL segments within the resulted copolymer was random. Meanwhile, ROP of di-lactide was demonstrated in chemical equation IV.

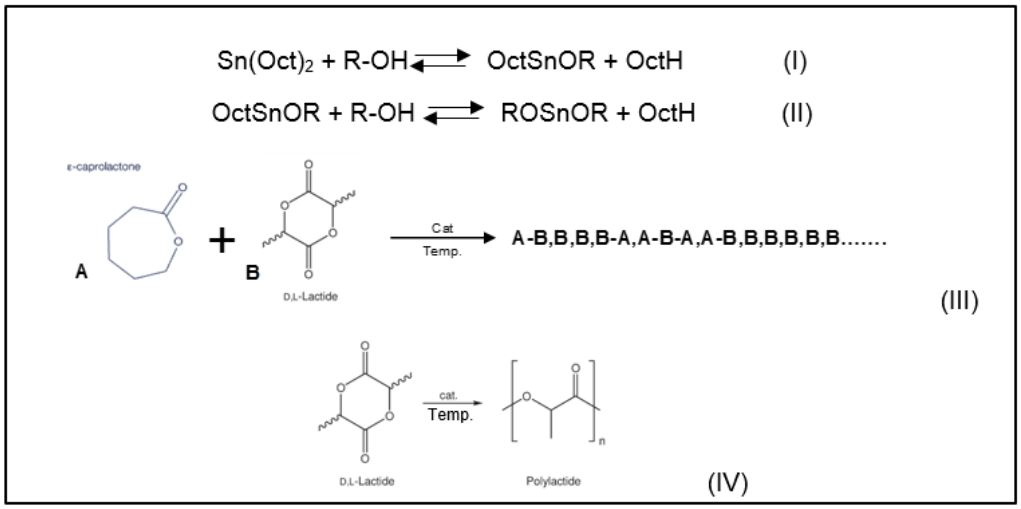

Figure 3.7 *Reaction mechanism for PLA-PCL and PLA polymerisation: (I) and (II) showed the pre-reaction of catalyst and initiator; (III) Random ring opening copolymerisation of PLA-PCL copolymer; (IV) PLA ring opening polymerisation*

3.9.1.2. Kinetic study of PLA and PLA-PCL polymerisation

Similar kinetic study to PCL polymerisation (see Section 3.7.1.2) was performed to determine the appropriate reaction parameters for both PLA polymerisation and PLA-PCL copolymerisation, including reaction temperature, ratio between ε-caprolactone and di-lactide, concentration of initiator and catalyst. 5ml glass vials are used to replace the mould as it is difficult to take the sample out of the sealed mould during the polymerisation. Di-lactide was melted (and mixed with ε-caprolactone for PLA-PCL copolymerisation) before treated with predetermined amount of $Sn(Oct)_2$ and benzyl alcohol under a dry blanket of nitrogen in a 100ml two neck boiling flask. After the mixing was completed, 2ml of the mixture was transferred into each vial. The glass vials were then transferred into an oven at the predetermined temperature. One glass vial was then taken out every 30 minutes, and a sample was collected for the chemical analysis to track the course of the polymerisation.

Detailed molar ratios and reaction conditions are stated in Table 3.3 and Table 3.4. Kinetic study of neat PLA polymerisation was performed first, which appropriate reaction parameters were determined for neat PLA polymerisation. With the reaction parameters determined for both neat PCL and PLA polymerisation, the kinetic study for PLA-PCL copolymerisation was performed, which appropriate molar ratio among the monomers, catalyst and initiator was chosen based on the neat PCL and PLA kinetic studies. As such, the key parameters of concern for PLA-PCL copolymerisation was solely the ratio between ε-caprolactone and di-lactide. This guaranteed the consistency of the resulted molecular weight for PLA-PCL copolymers and provided comparable results for this kinetic study.

Table 3.3 *Reaction parameters for neat PLA kinetic study*

Reaction parameters	Molar Ratio: [Di-lactide : Benzyl alcohol : $Sn(Oct)_2$]; Reaction Temperature (°C)		
Alter $Sn(Oct)_2$ amount only	[1000:0.1:0.1]; 160	[1000:0.1:0.5]; 160	[1000:0.1:1]; 160
Alter Benzyl alcohol amount only	[1000:0.05:1]; 160	[1000:0.1:1]; 160	[1000:0.5:1]; 160
Alter reaction temperature only	[1000:0.1:1]; 120	[1000:0.1:1]; 140	[1000:0.1:1]; 160
All reactions are monitored up to 24 hours			

Table 3.4 *Reaction parameters for PLA-PCL kinetic study*

Molar Ratio: [Di-lactide : ε-caprolactone]	
[8 : 2]	[9 : 1]
For all polymerisations: Molar ratio of [Monomers : Benzyl alcohol : $Sn(Oct)_2$] = [1000 : 0.1 : 1]; Reaction temperature = 160 °C.	

3.9.2. Viscosity study

Although the above heating system was designed for PLA ISP process, working at around 160 °C was still difficult, time consuming and potentially dangerous. To work at lower temperature, it was suggested that mixing di-lactide with ε-caprolactone to induce copolymerisation was an efficient method since di-lactide is slightly miscible with ε-caprolactone. To confirm if the drop-in transfer temperature is sufficient enough to give good fibre impregnation, and also to monitor suitable viscosity of both the copolymerisation mixture and pure di-lactide for heated monomer transfer, a viscosity study was performed for the copolymerisation mixture and pure di-lactide. An overhead Brookfield DV II-PRO viscometer was used to perform the tests, with suitable mass spindle selected for each mixture. The mass spindles used were chosen based on the shear stress range, which model RV-1 and RV-2 were used. Temperature range used for this study was from 95 °C (melt point for di-lactide) to 170 °C. Di-lactide was melted using a hot oil bath before ε-caprolactone was added. The weight ratio of di-lactide and ε-caprolactone used in this study is presented in Table 3.5.

Table 3.5 *Weight ratio of di-lactide and ε-caprolactone for viscosity study*

Weight ratio: [Di-lactide : ε-caprolactone]			
[0 : 10]	[8 : 2]	[9 : 1]	[10 : 0]

3.9.3. Heated ISP moulding system

3.9.3.1. Automated monomer transfer system

Since di-lactide required high temperature melting, automated monomer transfer system must be developed to replace the simple syringe injection system. In this work, a heated pressure pot was used to store and transfer the melted di-lactide, which controllable pressure was applied by putting dried nitrogen gas into the pot. Vacuum assistance was also used via a pump to help the transfer of the melted monomer and ensure good impregnation of the PGF mats. A capture pot was connected between the composite moulds and the pump, which was designed to prevent the melted di-lactide from getting into the pump. The designed system was automatic and effective in monomer transfer at high temperature.

3.9.3.2. Heating system

Heating was applied to the composite moulds, connecting piping and the pressure pot. Silicone heating mats were used to heat up the moulds and the pressure pot to the required temperature. Meanwhile, rope heaters were wrapped around all the connecting piping and kept them at the required temperature. High temperature silicone oil was inside the pressure pot to keep the di-lactide melted, where the di-lactide was contained inside a glass round bottom flask inside the oil.

3.9.3.3. Degassing system

To achieve thorough fibre impregnation and solid fibre/matrix interface, good degassing system must be developed to minimise or eliminate small air bubbles (voids) inside the ISP composites. Since the moulds were heated, manual degassing cannot be carried out. Vacuum degassing of the sealed moulds was conducted before the monomer transfer, which was effective to remove big pockets of air. To further remove the potential development of the voids, sealed moulds was put on a vibration table, where effective, controlled vibration were applied to the moulds during and after the monomer transfer.

3.9.3.4. Temperature and pressure control system

A central power control system was used to connect all the heating elements in the heated ISP system, where individual PID temperature controller was applied to each heater. Thermometers with accuracy of ± 1 °C were embedded into the centre of the moulds, the transfer piping and within the silicone oil inside the pressure pot. Pressure gauge of the accuracy within 3% was used for the pressure pot to provide essential control of the monomer transfer rate.

3.10. Heated ISP manufacture for PLA-PCL, PLA/PGF composites

A novel heated ISP system was specifically designed to manufacture PLA-PCL copolymer firstly followed by neat PLA fibre reinforced composite plates. The setup developed was based on a modified design of the room temperature ISP system developed for PCL composite production, for which a detailed description can be found in Section 3.7.

Figure 3.8 illustrates the heated ISP process developed, which consists of power control, heating elements, vacuum pump, mould assembly and monomer transfer

system. PGF mats were placed inside the plate-shaped mould cavity and then the mould was assembled and sealed. The mould was evacuated using the vacuum pump, which remained sealed until the monomer mixtures were transferred into it. The vacuum process was performed to reduce the possibility of void formation within the composites as well as to control the moisture contacts with the chemical mixture during the monomer transfer. A stainless-steel stand was placed inside the pressure pot to hold the one-neck flask (containing the molten monomer mixture) in place, which ensured that the monomer mixture did not come into contact with the heated silicone oil inside the pressure pot and maintained the mixture at the required temperature (mixture temperature was monitored via a thermocouple constantly). The stand also kept the one-neck flask in the designated position, to accurately fit with the PTFE tubing used for the monomer transfer to achieve maximum transfer efficiency.

PTFE tubing was also used to connect the mould with the pressure pot and the capture pot, which was heated to 160 °C using rope heaters. Both the tubing and the mould (heated by silicone heating mats, see Figure 3.8) were pre-heated (to 120 °C for 8-2 mixture; 140 °C for 9-1 mixture and 160 °C for neat di-lactide) to ensure that the mixture remained molten and did not form a blockage during the monomer transfer process. Pressure was applied by introducing dried nitrogen gas (dried by passing through a drying column tightly packed with molecular sieves) into the pressure pot to pump the molten mixture through the PTFE tubing and into the mould. Mixture transfer continued until it reached the capture pot and degassing was performed simultaneously by applying controlled vibrations to the moulds. The controlled vibration was applied using a vibration table (frequency controllable, up to 3000 rpm), where the mould assembly was sitting on top of the

vibration table during the monomer transfer (see Figure 3.8). After the polymerisation was complete, the heaters were switched off and the mould was left to cool to room temperature, before the resulted plate was demoulded.

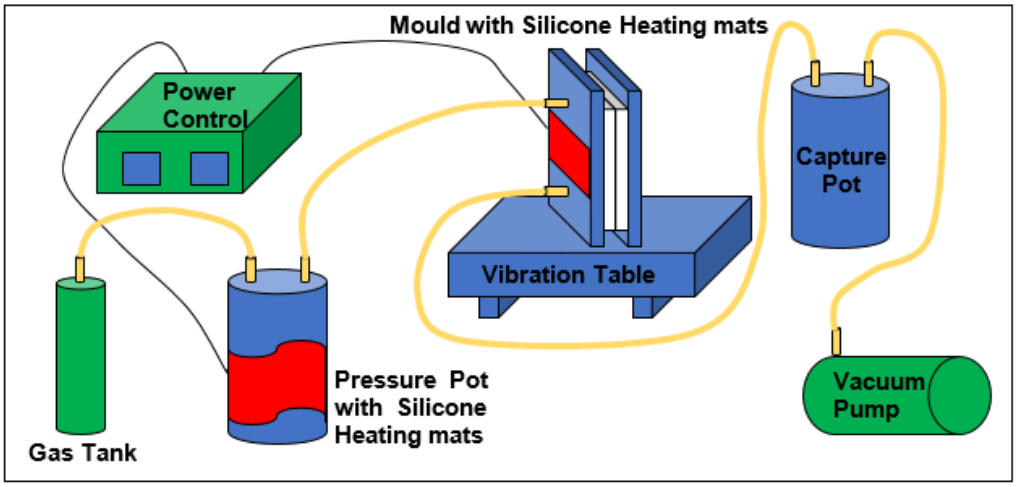

Figure 3.8 *Graphic illustration of the heated ISP system for PLA-PCL copolymer, neat PLA and their fibre reinforced composites production (Red represents the silicone heating mats; Yellow lines represent the PTFE tubing coupled with rope heaters for molten monomer transfer; Stainless-steel stand was placed within the pressure pot and the pressure pot was filled with silicone oil bath; White blocks represent the PTFE moulds with plate-shaped cavity inside; Black lines represent the electrical cables connecting each heating element to the power control system)*

3.11. High cycle flexural fatigue analysis for PCL/PGF composites

Flexural fatigue tests were conducted on a Bose ElectroForce® Series II 3330 testing machine under load-control mode. Constant amplitude loads were applied in a sinusoidal waveform at a frequency of 5 Hz. In accordance with BS ISO 13003:2003, at least 5 specimens were tested to failure at a minimum of five stress levels for the determination of the composites stress-lifetime diagram. All the composites were tested in 3-point bending mode (bending-bending condition) with a stress ratio of R = 0.1. The specimen dimension was 40 mm in length, 15

mm in width and 2 mm in thickness. Figure 3.9 presents an example load waveform used during fatigue tests, showing definition of terms and illustration of R-value. Calculations for flexural stress and strain were performed according to BS EN ISO 14125:1998. Shear effects were taken into consideration for the stress and strain calculations since the defection of the specimens during the fatigue tests was relatively large.

When the measured deflection was less than 10% of the sample span length, the flexural stress and strain were calculated via equation 1 and 2. When the measured deflection was larger than 10% of the sample span length, equation 3 and 4 below were used:

$$\sigma_f = \frac{3FL}{2bh^2} \qquad (1)$$

$$\varepsilon = \frac{6sh}{L^2} \qquad (2)$$

$$\sigma_f = \frac{3FL}{2bh^2}\left\{1 + 6\left(\frac{s}{L}\right)^2 - 3\left(\frac{sh}{L^2}\right)\right\} \qquad (3)$$

$$\varepsilon = \frac{h}{L}\left\{6\frac{s}{L} - 24.37\left(\frac{s}{L}\right)^3 + 62.17\left(\frac{s}{L}\right)^5\right\} \qquad (4)$$

where σ_f is the flexural stress, ε is the strain, s is the beam mid-point deflection, F is the load, L is the span length, h is the thickness of the specimen and b is the width of the specimen.

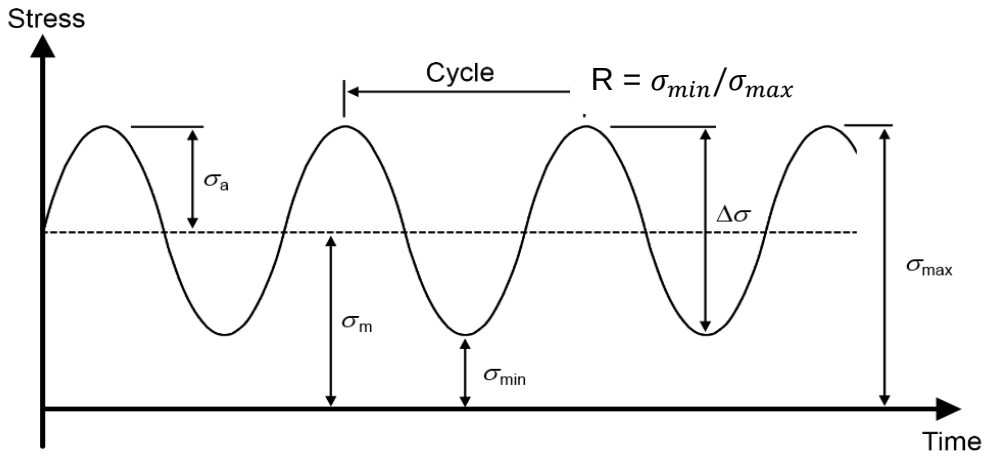

Figure 3.9 *Example of sinusoidal constant amplitude load waveforms with term definition and R value*

Fatigue tests were performed in both dry and wet testing conditions. Testing the dry composites at room temperature was known as the dry testing condition and wet testing condition referred to testing the submersed composites in PBS solution and at 37 °C. Composite samples were immersed in PBS solution at 37 °C for ~10 mins before performing the fatigue test. A KTJ TA318 thermometer & hygrometer was used to measure the temperature and relative humidity of the dry testing conditions, which were in the range of 15 °C - 22 °C and 44% - 53% respectively. Stress levels for all fatigue tests were 80%, 70%, 60%, 50%, 40% and 30% of the corresponding Ultimate Flexural Strength (UFS) for each type of composite.

Figure 3.10 shows an example of the stress strain variation of a composite sample during fatigue test. The loading cycle plotted were selected 1 out of every 1000 loading cycles and each loop in Figure 3.10 represents a full loading cycle. Flexural stiffness of the composites can be calculated from each loading cycle and the variation in their strain can also be recorded.

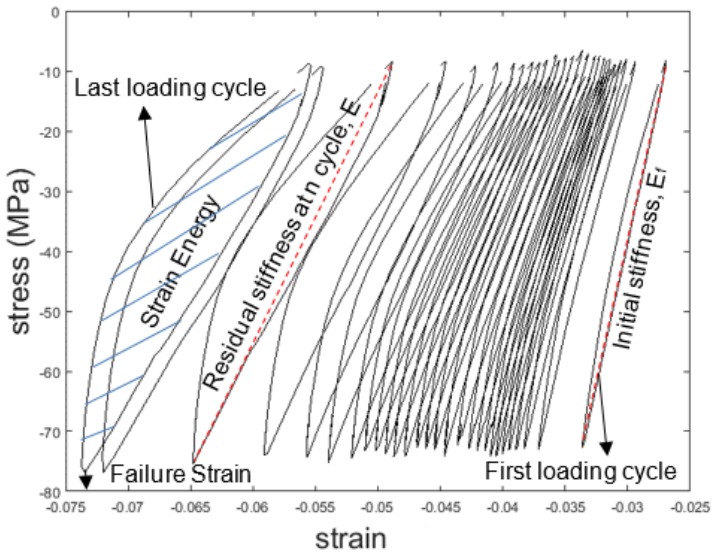

Figure 3.10 *Example stress strain variation during the fatigue tests (the negative sign only indicated the direction as downwards)*

3.12. Fatigue characterisation for PCL/PGF composites

3.12.1. Stress-Life (S-N) diagram

As illustrated in Figure 3.11, a typical Wohler Stress-Life (S-N) diagram [180] is plotted as stress amplitude (σ_a, see Figure 3.9) against number of fatigue cycles to failure (N_f). S-N curves are normally fitted with a power regression relationship, named Basquin's equation (Equation 5) [180].

$$\sigma = aN_f{}^b \qquad (5)$$

where σ is a generic term describing cyclic stress (in this case σ_a, see Figure 3.11), N_f is generic term describing fatigue life (in this case cycles to failure) and *a* & *b* are material constants specific to each material. The constant 'b' is used as an important parameter in this study to indicate the sensitivity of the fatigue life to the applied stress. The value of 'b' represents the slope of the S-N curve, thus the decline rate of fatigue strength.

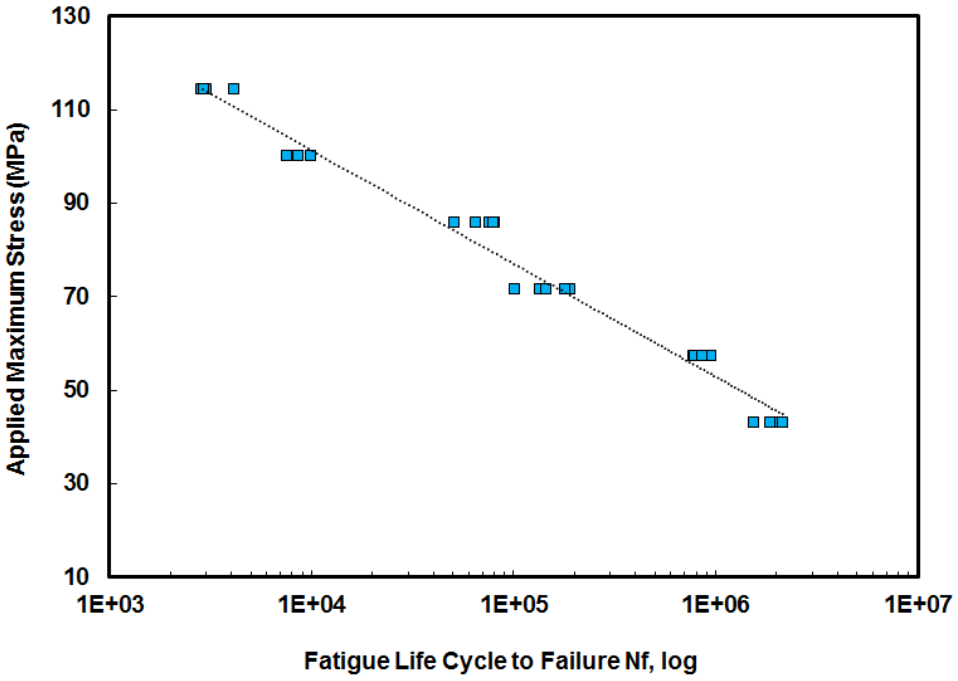

Figure 3.11 *Typical S-N diagram with example data*

3.12.2. Specific damping capacity (SDC)

To study and monitor the progress of composite damage during the fatigue tests, SDC was used as a sensitive indicator throughout this study. As damage progresses, the composite specimens shows reductions in strength and modulus as well as a significant increase in their own damping [181, 182]. Changes in material damping capacity can be monitored as a function of the increasing stress levels during the fatigue tests [183]. An example is illustrated graphically in Figure 3.12.

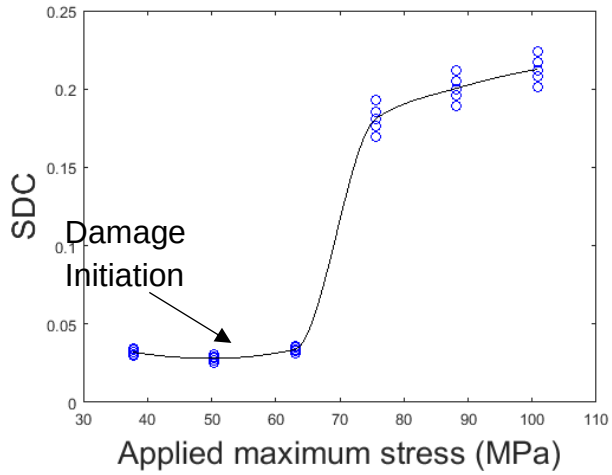

Figure 3.12 *Example of Specific Flexural Damping Capacity vs. Applied Maximum Stress for dry LS35 composites*

In this work, SDC was measured to determine the critical applied stress (CAS) for damage initiation of both the LS and ISP composites within 10^4 fatigue loading cycles. This cycle number (10^4) was chosen since it is the general divider between low and high cycle fatigue behaviour, and this divider is determined as the majority of engineering materials (metals, plastics and composites) fail before 10^4 cycles during low cycle fatigue test [180]. A similar method was used by Gassan *et al.* to measure the CAS values for studying fatigue damage behaviour of fibre reinforced composites [182]. The CAS is an important factor for load bearing applications, such as fracture fixation devices, as it sets the limitations of the composite loading capacity under cyclic loading conditions. Any applied cyclic stress higher than the measured CAS would imply material damage within 10^4 loading cycles.

In order to obtain SDC values for the composites, a fatigue test is performed using constant values of stress level, R and frequency (R=0.1, 5 Hz) for a defined number of load cycles (10^4 cycles in this case). Fresh LS and ISP PCL/PGF composites (non-degraded) were used for the SDC study. Subsequently, the

fatigue test was repeated for the same number of load cycles at a higher stress levels. This continued until the specimen failed. A minimum of n=5 samples were tested for each category of composites. Tests were carried out in both dry and wet testing conditions, using the stress levels specified in Section 3.11. The value of SDC was then calculated using Equation 6 [182, 184]:

$$SDC = \Delta U/U = (U_I - U)/U \qquad (6)$$

where *U* is the maximum strain energy stored by the specimen during one loading cycle, ΔU is the energy dissipated only by the specimen during one loading cycle (such as friction damping caused by de-bonding, crack and delamination) and U_I is the input energy from the system to the specimen during one cycle. Strain energy was calculated by integrating the area within the loading loop (see Figure 3.10 shaded area) at defined number of load cycles. Input energy was calculated by integrating the loading and displacement history from the fatigue tests.

3.13. Characterisation

3.13.1. Degradation study

The degradation study was performed according to the standard BS EN ISO 10993-13. All neat polymer, copolymer and their composites were cut into specimens with dimensions of 40mm × 15mm × 2mm. The weight of each specimen was recorded before placing them into a 30-ml glass vial individually. 30 ml of PBS (pH=7.4 ± 0.2) was added to each vial to fully immerse the specimen. Vials were kept at 37 °C for 28 days. At various time points (0, 1, 3, 7, 11, 15, 21 and 28 days), specimens were extracted and blot dried before measuring the wet weight. pH of the degradation media was also monitored at each time point using a bench-top pH meter (pH 212, Hanna Instruments, UK). The solution was replaced by fresh PBS solution at each time point. The extracted specimens were

dried at 50 °C for 48 hours to evaluate their mass loss. The specimen mass loss (M_d) and media uptake (W) were calculated using the following equations:

$$M_d = \frac{m_d - m_i}{m_i} \times 100\% \quad (7)$$

$$W = \frac{m - m_d}{m_d} \times 100\% \quad (8)$$

where m is the mass of the blot dried specimen at each time point, m_i is the initial dry mass and m_d is the mass of degraded sample after drying at 50 °C for 48 hours within a vacuum oven.

3.13.2. 3-point bending flexural tests

Monotonic 3-point bending tests were conducted on a Bose ElectroForce® Series II 3330 testing machine. The testing machine is equipped with an environmental chamber, which enables tests within liquid at various temperatures (see Figure 3.13). All flexural tests were performed according to standard BS EN ISO 14125:1998. Specimen dimensions of 40mm × 15mm × 2mm, a cross-head speed of 1 mm/min and a 3 kN load cell was used. Tests were performed in triplicate (n=3). Flexural properties of the composites were tested in two environments: at ambient temperature and in dry condition (dry environment) and at 37 °C submerged in PBS solution (wet environment). The samples were immersed in PBS heated to 37°C for 5 minutes to allow PBS and testing temperature equilibrate prior to testing.

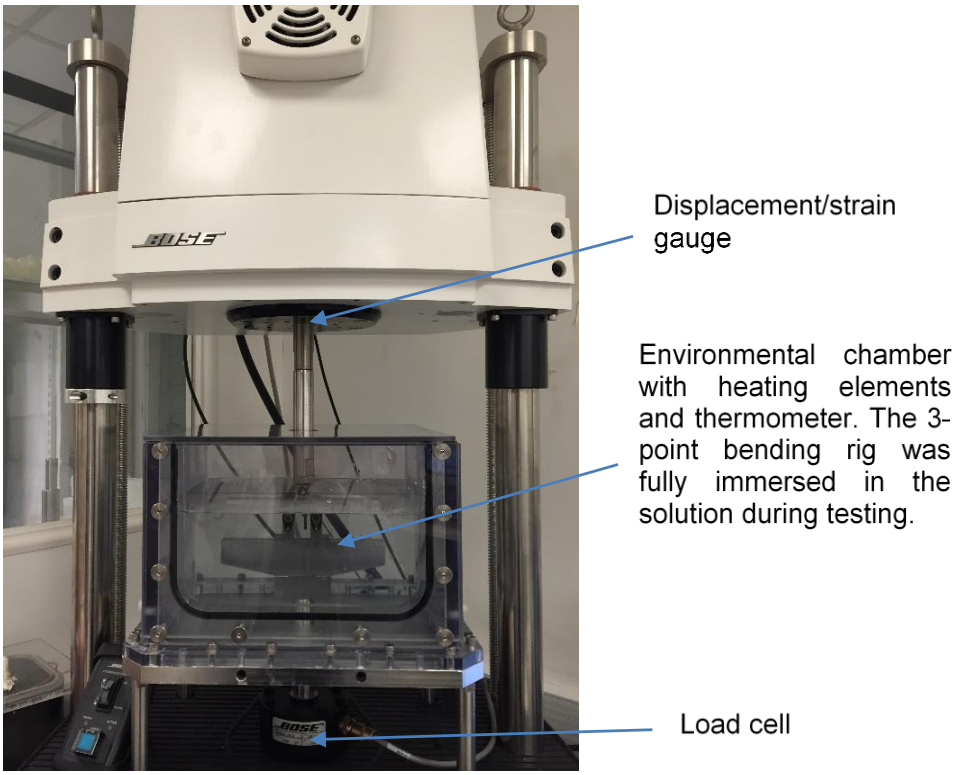

Figure 3.13 *Bose ElectroForce® Series II 3330 testing machine equipped with environmental chamber*

3.13.3. Gel permeation chromatography (GPC)

GPC was carried out to measure the molecular weight variation of the samples during the degradation study. The GPC was an Agilent Technologies 1260 Infinity GPC system with mixed D columns at 40 °C, a refractive index detector and a viscometer. Tetrahydrofuran (THF) was used as the mobile phase at a flow rate of 1.0 cm^3/min. Calibration was conducted using polystyrene standards for all neat PCL and PLA samples. A specific calibration using the viscometer against polystyrene was performed to establish testing standards for PLA-PCL copolymers with different compositions. The calibration range of the GPC was between 10 and 17.35 minutes of elution time, corresponding to molecular weights from 580 g/mol to 377,400 g/mol. Sample concentration was ~5 mg/ml.

3.13.4. Nuclear magnetic resonance (NMR)

The molecular structure and monomer conversion rate of PCL, PLA and PLA-PCL copolymer were monitored by NMR process. 1H spectra were recorded in deuterated chloroform solution by using a Bruker DPX 300 MHz spectrometer. Sample concentration was 5% for the 1H spectra.

3.13.5. Scanning electron microscopy (SEM)

After flexural testing, SEM analysis was conducted on the cross sections of the composite samples after sputter-coating with platinum (utilising a SC500, Emscope) to assess the quality of the fibre/matrix interface. Samples were examined using an XL 30 scanning electron microscope (Philips, UK) with secondary electron mode at a voltage of 10 kV.

3.13.6. Burn off test

Burn-off tests were performed on all composites samples to determine the actual V_f. Tests were performed according to standard BS EN ISO 2782-10. The initial weight of each sample was taken. Then all composite samples were burned off at 450 °C for 2 hours before the burn-off weight of each sample was taken. 5 samples were tested for each kind of the composites (n=5).

3.13.7. Rule of mixture

Theoretical Young's modulus of fibre reinforced composites can be predicted using the following equation:

$$E = \eta_L \eta_o E_f V_f + E_m(1 - V_f) \qquad (9)$$

where η_L and η_o represented fibre length correction and orientation efficiency factors. For unidirectional fibre composites, both η_L and η_o equal 1. E_f and E_m are Young's modulus for the fibres and polymer matrix. Young's modulus of

unidirectional fibre reinforced composites can be predicted by using properties of fibre and matrix along with fibre volume fraction data.

3.13.8. Differential scanning calorimetry (DSC)

A DSC Q10 (TA instrument, USA) was initially calibrated by indium and then utilised to determine the glass transition temperatures (T_g) of ISP PLA-PCL copolymer and PLA samples (~10 mg) using aluminium pans. The test was carried out through heating & cooling cycles ranging from 60 °C to 150 °C at 10 °C/min under argon gas (50 ml/min), where two cycles were performed for each test. The first run was performed to remove the thermal history of the samples. The T_g was measured on the second run as the point of inflection. Results were analysed by TA universal analysis 2000 software.

T_g estimation for PLA-PCL copolymers were performed using Flory-fox equation (see Equation 10 below), which could act as an indication for the compositions of the copolymer.

$$\frac{1}{T_g} = \frac{w_1}{T_{g1}} + \frac{w_2}{T_{g2}} \qquad (10)$$

where w_1 and w_2 are weight fractions of the component 1 and 2 (in this case PCL and PLA) respectively, T_{g1} and T_{g2} are the glass transition temperature for component 1 and 2 separately, and T_g is the glass transition temperature of the copolymer.

3.13.9. Neutral red cytocompatibility study

A cytocompatibility test for elution products from the degraded samples (in this case polymer and their composites) was performed with neutral red uptake by viable cells. This study was repeated twice to access the accuracy and consistency of the results. All 9mm x 2mm thick samples (n = 5) were eluted in

Dulbecco's Modified Eagle Media (DMEM) supplemented with 10% foetal calf serum (FCS), 2% HEPES Buffer, 2% antibiotics-antimycotis agents, 1% L-glutamine, 1% non–essential amino acids (Gibco Invitrogen, UK) and 0.85 mM of ascorbic acid (Sigma Aldrich, UK), and incubated at 37 ºC in a humidified atmosphere of 5% CO_2 for the following time points; day 1, 3, and 7. All eluted media was immediately frozen after each time point until use.

MG63 cells were seeded at a density of 40,000 cells/cm^3 in a 48 well plate and tissue culture to form a sub-confluent monolayer. After 24 hours of incubation, the culture medium was removed and cells were exposed for 24 hours to the elution products (all eluted media was first gently defrosted in a 37 ºC incubator in a humidified atmosphere of 5% CO_2).

Neutral Red (NR) stock was made by adding a ratio of 4mg of neutral red dye to 1ml of deionised water. A NR Medium was made using the stock by diluting with culture medium at a ratio of 1:100 under sterile conditions and kept warm at 37 ºC. The NR Medium was centrifuged before use. 100 µl of NR medium was added to the cells and the plates were incubated for 3 hours. De-stain was made by mixing 50% pure ethanol, 49% deionised water and 1% acetic acid.

The NR medium was then discarded and cells were washed once with PBS before adding 150 µl de-stain to the cells. Subsequently plates were shaken for 10 minutes and NR absorption was measured at ex490 and em630m using an ELx800 Microplate Colorimeter (BioTek Instruments Inc).

3.13.10. Statistical analysis

Data were presented graphically as mean ± standard deviation. Measured data were analysed by Microsoft Excel using Student's unpaired t-test, assuming

equal variance with Microsoft Excel. Statistical significance ranking was defined as $p>0.05$ (statistically insignificant), $p<0.05$ (statistically significant), $p<0.01$ (very statistically significant) and $p<0.0001$ (extremely statistically significant).

Chapter 4. Room Temperature *In-situ* Polymerisation *vs.* Laminate Stacking for Fully Bioresorbable PCL/PGF Composites: Reaction Kinetic Mechanism, *In-vitro* Degradation and Mechanical Properties

4.1. Summary

This chapter investigates PCL/PGF composites with 20%, 35% and 50% fibre volume fractions (V_f) manufactured via an ISP process and a conventional LS process followed by hot press moulding, where their degradation profiles and mechanical retention were monitored.

The initial (without degradation) flexural properties of ISP composites were substantially higher ($p<0.0001$) than those of the LS composites. During the degradation study, statistically higher flexural property retention profiles ($P<0.01$) were also seen for the ISP composites compared to LS composites. SEM micrographs of fracture surfaces for the LS composites revealed dry fibre bundles and poor fibre dispersion with polymer rich zones. In contrast, evenly distributed fibres without dry fibre bundles or polymer rich zones, were observed for the ISP composite samples, which showed that a superior fibre/matrix interface was achieved with highly improved adhesion by ISP process.

4.2. Introduction

The mechanical and degradation behaviour of PCL/PGF composites with different phosphate based glass formulations, V_f and manufacturing methods have been investigated previously [17, 157, 168, 176, 185, 186]. The common

process for the manufacture of bioresorbable composites, including PCL/PGF composites, is LS process. Due to the high viscosity of the PCL polymer melt, it is difficult to gain a good wet-out of the fibre surface by using the LS process, which often result in poor fibre/matrix adhesion. However, it is of paramount importance for bioresorbable fibre reinforced composites to achieve strong fibre/matrix adhesion for their successful application in the field of hard tissue repair.

In this chapter, room temperature ISP process was developed and investigated to manufacture fully bioresorbable PCL/PGF composites. Instead of using resin, a reaction mixture (monomer and catalyst) was injected into moulds and polymerised in situ to form the matrix directly around the reinforcement within a single step. Since the viscosity of the monomer (ε-caprolactone at room temperature: 1.07 mPa s) is much lower in comparison to the polymer melt (PCL melt: 12,650 Pa s), good fibre impregnation and significantly enhanced interfacial bonding could be obtained by ISP [18]. Fully bioresorbable PCL/PGF composites with V_f of 20%, 35% and 50% were manufactured via both LS and ISP (first time) to compare between the reinforcing efficiency of both manufacturing processes. A degradation study was performed on the composites in PBS up to 4 weeks at 37 °C, in which their mechanical property retention, pH, media up-take and weight loss were monitored. Change in molecular weight and polydispersity were also monitored via GPC and SEM micrographs revealed the fibre distribution and fibre/matrix interfaces.

4.3. Materials and methods

4.3.1. Materials

Please refer to Section 3.3 for details.

4.3.2. Kinetic study

The detailed procedures of kinetic study were described in Section 3.7.1.2. The molecular weight and monomer conversion of PCL were monitored via GPC and NMR respectively, which the procedures were detailed in Section 3.13.3 and Section 3.13.4 respectively.

4.3.3. Phosphate based glass and glass fibre production

The glass composition, the production process of the glass, its glass fibre, and fibre mats were all detailed in Section 3.4 and 3.5 respectively.

4.3.4. PCL/PGF composites production

Please refer to Section 3.6.1 for the LS process and Section 3.8 for the ISP process, which specified the details of the composites production.

4.3.5. Degradation study

The details for the specimen preparation and property measurement were listed in Section 3.13.1. The equipment and specifications for flexural testing were detailed in section 3.13.2. The molecular weight variation during the degradation study was also monitored via the GPC, which was detailed in Section 3.13.3.

4.3.6. Scanning electron microscopy (SEM)

SEM was detailed in Section 3.13.5. Rule of mixture was applied to estimate the flexural modulus of the LS and ISP composites. Please refer to Section 3.13.7.

4.3.7. Burn off tests

Actual V_f of the composites were confirmed via the burn off tests in Section 3.13.6.

4.3.8. Statistical analysis

Please refer to Section 3.13.10.

4.4. Results

4.4.1. Kinetic study of PCL polymerisation

4.4.1.1. Effects of catalyst concentration

Figure 4.1 shows that the PCL monomer conversion reached ~98% after ~120 mins and ~180 mins when the $Sn(Oct)_2$ concentration was 0.0174 mol/L and 0.00868 mol/L respectively (reaction temperature and initiator benzyl alcohol concentration were kept constant). Meanwhile, when the $Sn(Oct)_2$ concentration was 0.00174 mol/L (lowest), the monomer conversion only reached ~17% at ~360 mins, and the polymerisation did not start until 1 hour of heating.

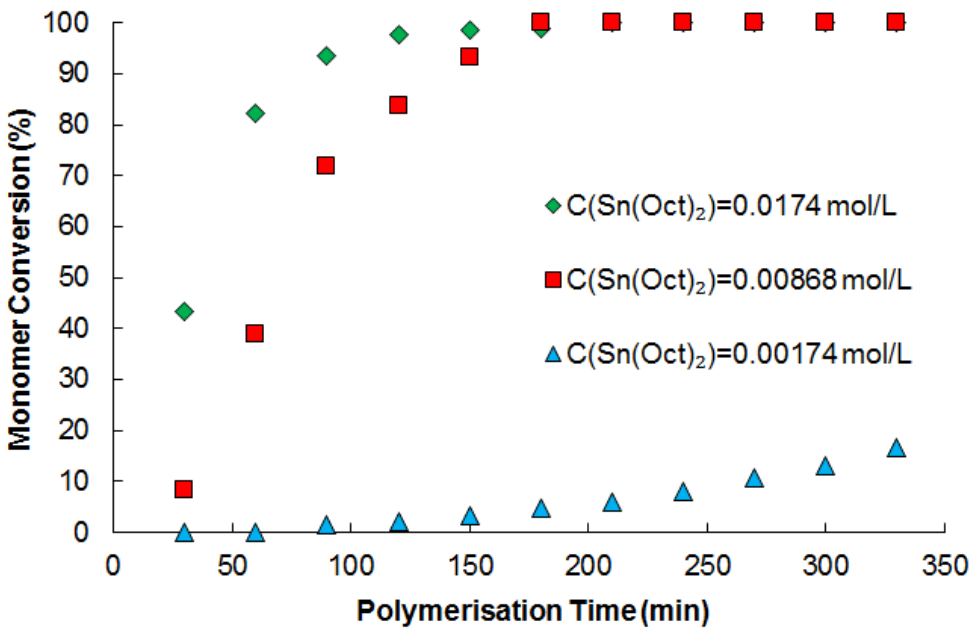

Figure 4.1 *Monomer conversion rate at various $Sn(Oct)_2$ concentrations (Benzyl alcohol concentration kept at 0.01159 mol/L and the polymerisation temperature kept at 130 °C)*

Figure 4.2 depicts the change of molecular weight (M_w) and polydispersity (PDI, indicates how broad the molecular weight is for the investigated polymer) at each time point with varying catalyst $Sn(Oct)_2$ concentration. With $Sn(Oct)_2$ concentration of 0.0174 mol/L, the molecular weight & PDI achieved values of

~30000 Da & ~1.6 respectively. Meanwhile, ~38000 Da & ~1.4 was seen for polymerisation with 0.00868 mol/L $Sn(Oct)_2$ concentration, and only ~3000 Da & ~1.2 was observed with 0.00174 mol/L $Sn(Oct)_2$ concentration.

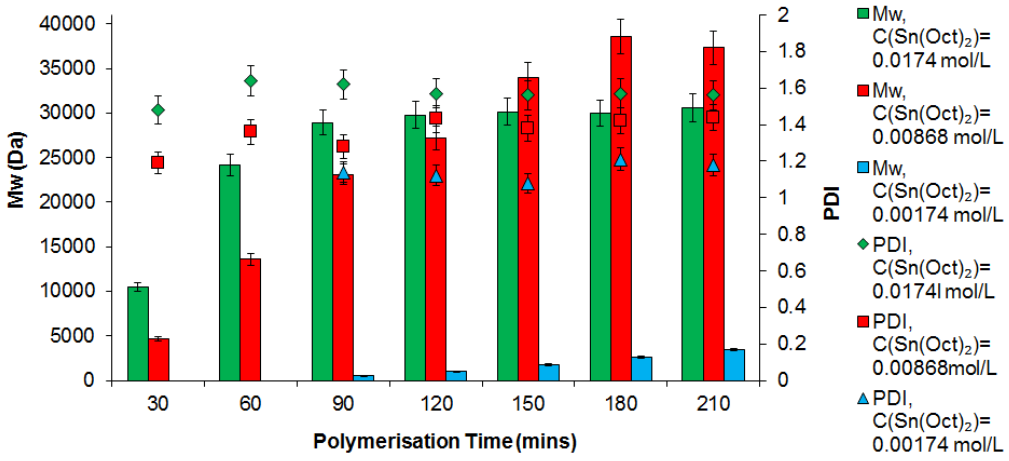

Figure 4.2 *M_w and PDI at various $Sn(Oct)_2$ concentrations (benzyl alcohol concentration kept at 0.01159 mol/L and the polymerisation temperature kept at 130 °C)*

4.4.1.2. Effects of initiator concentration

As can be seen in Figure 4.3, the PCL monomer conversion reached ~98% at ~180 mins for both 0.01159 mol/L and 0.0145 mol/L initiator benzyl alcohol concentration (reaction temperature and $Sn(Oct)_2$ concentration kept constant). Meanwhile, with the lowest benzyl alcohol concentration 0.00724 mol/L, the monomer conversion reached ~98% at ~240 mins.

Regarding Figure 4.4, the M_w was proportional to the initiator concentration in the polymerisation system, which produced molecular weights of ~20000 Da, ~35000 Da and ~45000 Da with decreasing benzyl alcohol concentrations. The PDI for all polymerisations was seen to be ~1.4.

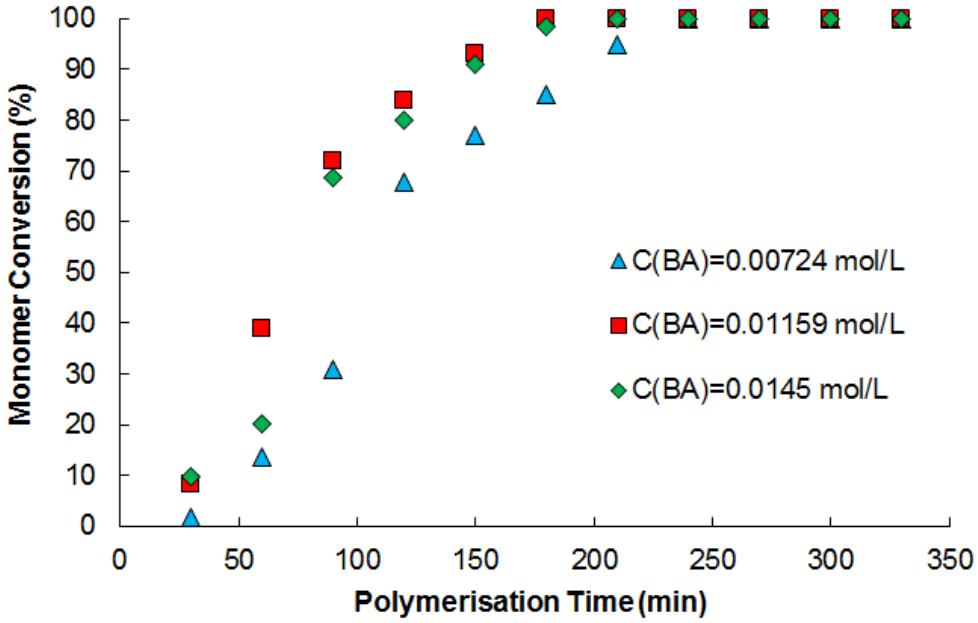

Figure 4.3 *Monomer conversion at various benzyl alcohol concentrations ($Sn(Oct)_2$ concentration kept at 0.00868 mol/L and the polymerisation temperature kept at 130 °C)*

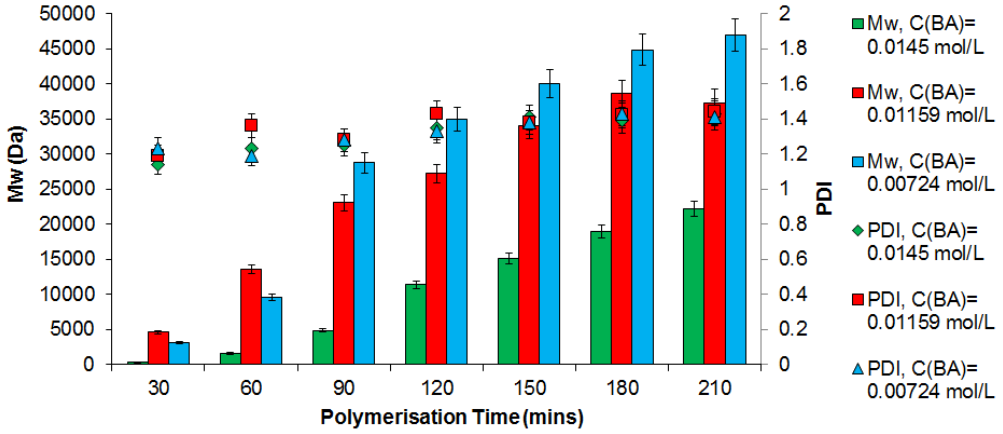

Figure 4.4 *M_w and PDI at various Benzyl alcohol concentrations ($Sn(Oct)_2$ concentration kept at 0.00868 mol/L and the polymerisation temperature kept at 130 °C)*

4.4.1.3. Effects of polymerisation temperature

Figure 4.5 shows the relationship between the PCL monomer conversion and the polymerisation temperature ($Sn(Oct)_2$ and benzyl alcohol concentration kept at constant). With increasing polymerisation temperature, the monomer conversion

rate increased, which ~98% was reached at ~ 90 mins and ~180 mins for 150 °C and 130 °C respectively, meanwhile 110 °C only reached ~20% monomer conversion after 300 mins (polymerisation did not take place until 2 hours).

Figure 4.6 revealed that the PDI level and M_w variation with increasing reaction temperature, which the polymerisation at 150 °C reached ~30000 Da & ~1.6 PDI, 130 °C reached ~38000 Da & ~1.4 PDI and 110 °C only reached ~5000 Da & ~1.2 PDI respectively.

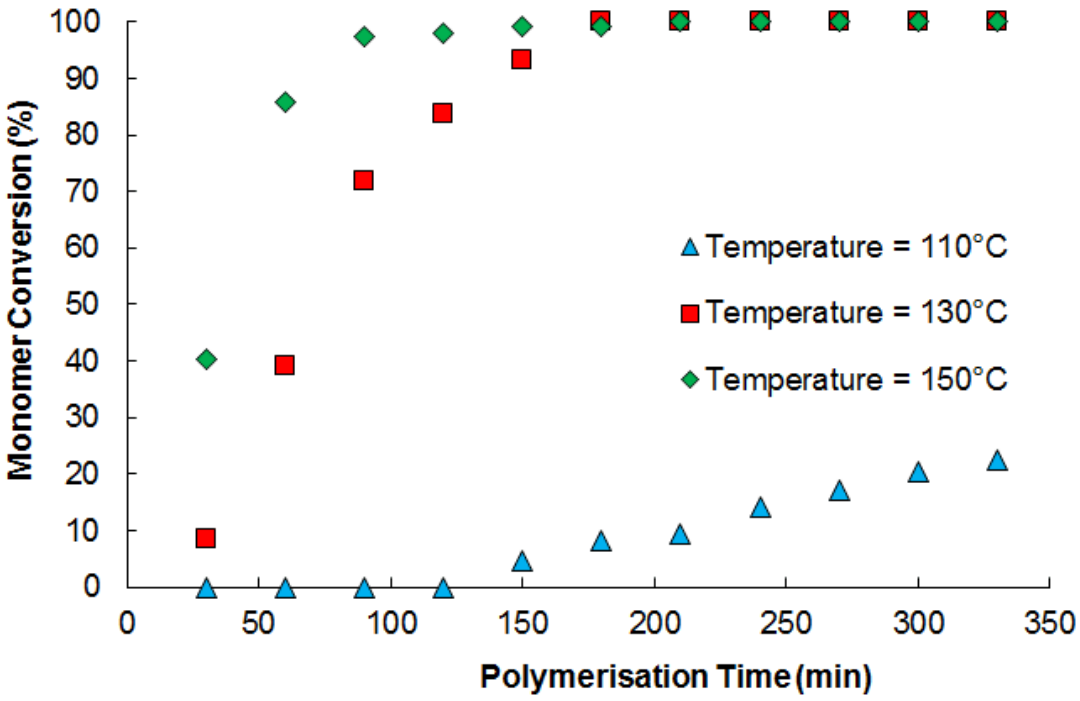

Figure 4.5 *Monomer conversion at various reaction temperatures ($Sn(Oct)_2$ concentration kept at 0.00868 mol/L and benzyl alcohol concentration kept at 0.01159 mol/L)*

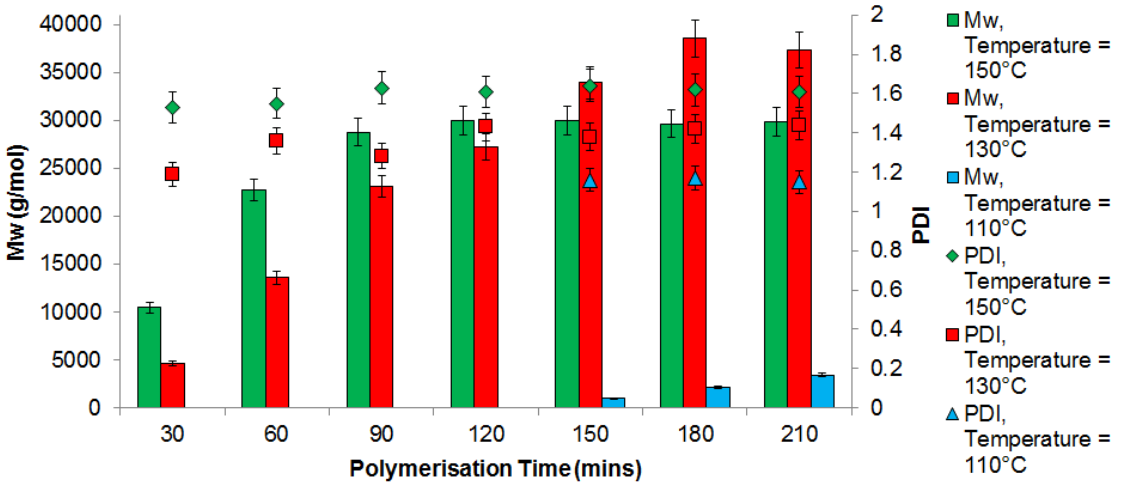

Figure 4.6 *M_w and PDI at various reaction temperatures ($Sn(Oct)_2$ concentration kept at 0.00868 mol/L and benzyl alcohol concentration kept at 0.01159 mol/L)*

4.4.2. Degradation and mechanical retention behaviour

Table 4.1 shows the sample codes and fibre V_f for all the composites produced in this chapter.

Table 4.1 *PCL/PGF composites volume fraction and codes*

Manufacture process	Composite codes	Targeted V_f	Actual V_f
Laminate Stacking (LS)	LSPCL	N/A	PCL only
	LS20	20%	23.0% ± 1.2%
	LS35	35%	29.1% ± 0.6%
	LS50	50%	49.0% ± 0.5%
***In-situ* Polymerisation (ISP)**	ISPPCL	N/A	PCL only
	ISP20	20%	19.6% ± 2.1%
	ISP35	35%	31.5% ± 1.0%
	ISP50	50%	51.9% ± 1.8%

4.4.2.1. Media uptake

Figures 4.7a and b shows the change in percentage of media uptake versus degradation time for PCL and PCL/PGF composites manufactured via LS and ISP processes during degradation in PBS at 37 °C for 28 days. Both LSPCL and ISPPCL (see Table 4.1 for the sample code) maintained a constant media uptake (~0.5%) throughout the 28 days of immersion. By comparing the media uptake profiles for LS20, LS35 and LS50, it was seen that amounts of media uptake increased by increasing fibre volume fraction over the same immersion time (similar trend was observed for ISP20, ISP35 and ISP50).

By comparing Figure 4.7a and b, the media uptake profiles of the LS and ISP PCL/PGF composites with the same fibre volume fractions exhibited very similar trends. An approximately linear increase was observed up to 21 days of immersion followed by a reduction in the rate of media uptake till the end of the study. However, in absolute terms, significantly higher amounts of media were absorbed ($p<0.05$) by the LS composites in comparison to the ISP composites at all time points. The LS20, LS35 and LS50 composites absorbed approximately 43%, 44% and 42% more media than their respective ISP equivalents at day 28.

(a)

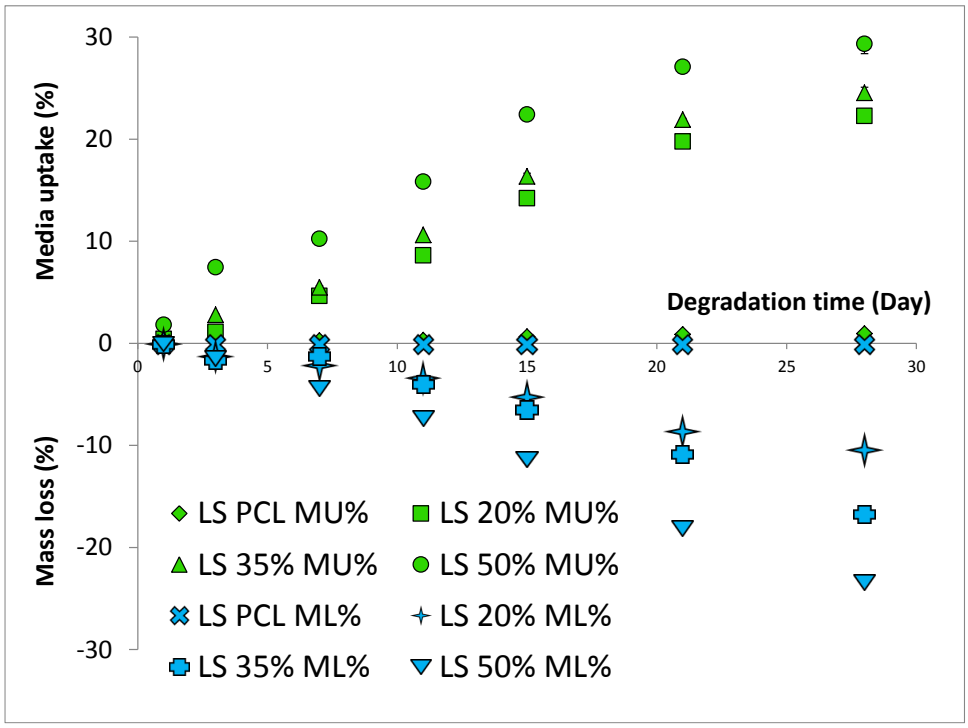

(b)

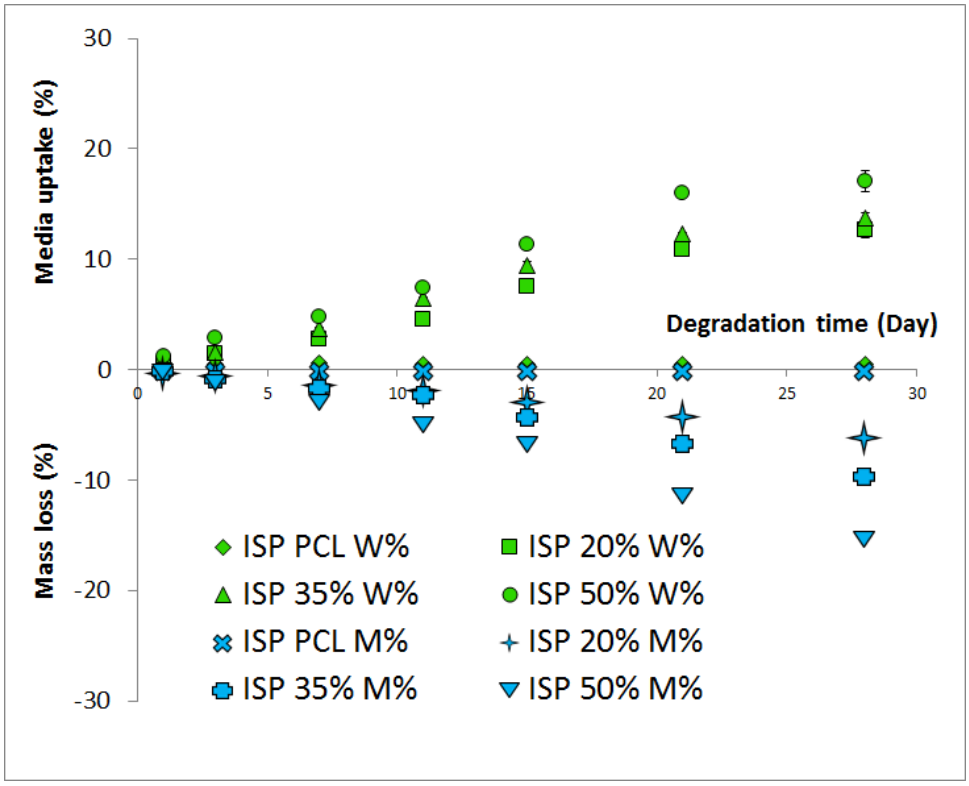

Figure 4.7 *Variation of percentage media uptake and mass loss of the (a) LS PCL and PCL/PGF composites, (b) ISP PCL and PCL/PGF composites. Degradation study conducted in PBS at 37 °C. LS = Laminate stacking, ISP = In-situ polymerisation, Fibre volume fraction = 20%, 35% and 50%. MU% = % media uptake; ML% = % mass loss.*

4.4.2.2. Mass loss

Figure 4.7a and b also show the percentage of mass loss against degradation time for PCL and PCL/PGF composites manufactured via LS and ISP. Both neat LSPCL and ISPPCL showed no significant mass loss throughout the degradation period. Similar profiles of mass loss curves between LS and ISP composites were observed, in which an initial mass loss after 1-day immersion (~0.2%) was recorded, followed by a linear increase up to the end of the study (28 days). By comparing LS and ISP composites with the same V_f, it can be seen that LS composites showed a significantly higher mass loss ($p<0.01$) than the ISP composites. At the end of the degradation study (28 days), LS composites with V_f of 20%, 35% and 50% had lost approximately 41%, 42% and 35% more mass than their respective ISP composites.

4.4.2.3. pH variation

The variation of pH values of the PBS solution for PCL and PCL/PGF composites manufactured via LS and ISP are presented in Figure 4.8a and b respectively. The pH for LSPCL and ISPPCL remained neutral at 7.4 ± 0.2 till the end of the degradation study. However, the pH profiles for all composites remained stable at 7.4 ± 0.2 until the 11-day interval, after which a gradual decrease was observed up to 28 days. At the same V_f, LS composites showed significantly larger pH reduction ($p<0.05$) than ISP composites between 11 and 28 days of immersion.

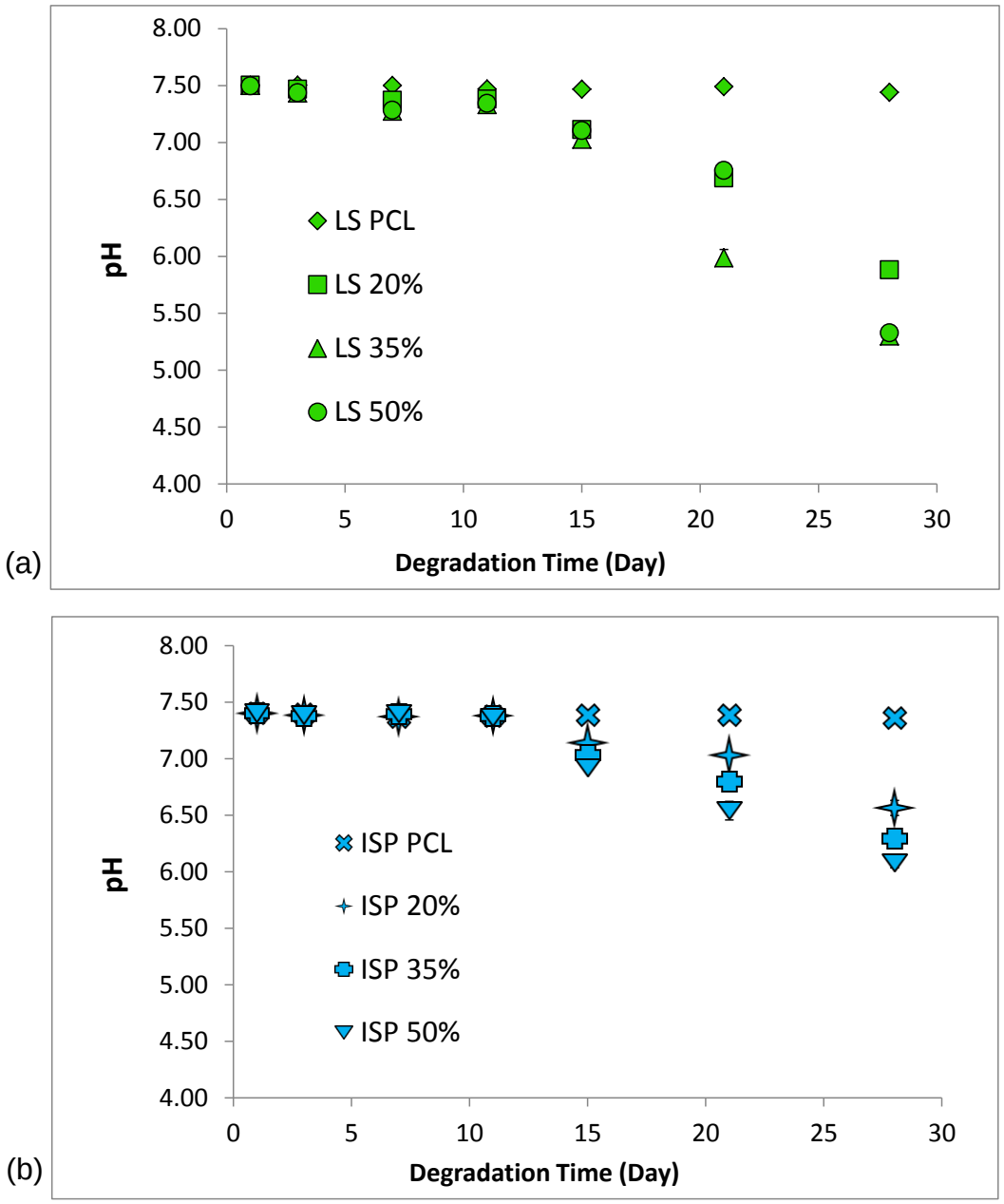

Figure 4.8 *Variations in the pH values of PBS media during degradation for (a) Laminate stacked PCL and PCL/PGF composites, (b) In-situ polymerised PCL and PCL/PGF composites. Degradation study conducted in PBS at 37 °C. LS = Laminate stacking, ISP = In-situ polymerisation, Fibre volume fraction = 20%, 35%, 50% (Error bars fall within the dimension of the markers).*

4.4.2.4. Molecular weight and distribution variation

Change in M_w against degradation time for PCL and PCL/PGF composites produced by LS and ISP are shown in Figure 4.9a. There was no significant difference ($p>0.05$) seen in M_w between non-degraded neat LSPCL and LS

composites. The values of M_w for LSPCL and LS20 did not show any significant change ($p>0.05$), whilst both LS35 and LS50 gradually decreased by ~7% by the 28-day interval, where the reduction in M_w was found to be statistically significant ($p<0.05$). Similarly, the M_w of ISPPCL remained stable for the 28-day study, meanwhile the M_w of ISP20, ISP35 and ISP50 gradually decreased by ~6%, ~10% and ~7% respectively ($p<0.05$). Moreover, only the non-degraded ISPPCL exhibited a similar M_w to the LSPCL and LS composites (~90,000 g/mol), which was considerably higher ($P<0.0001$) than the M_w of the ISP composites (~45,000 g/mol for ISP20, ISP35 and ISP50). Figure 4.9b exhibited the polydispersity index (PDI) data of all the LS and ISP specimens over 28 days of immersion. It can be seen that the PDI of all specimens was similar (1.2~1.4) and no significant variation ($p>0.05$) was observed over the whole period of study. However, it was noticed that the PDI of ISPPCL (~1.2) stayed slightly lower than all other composites over the 28-day period.

(a)

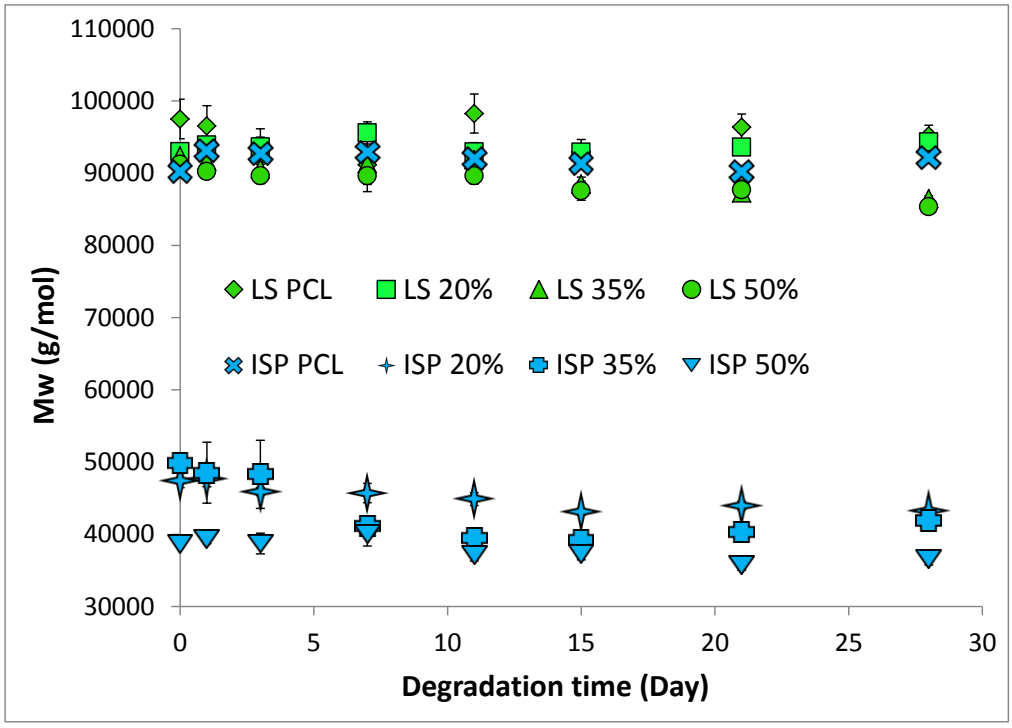

(b)

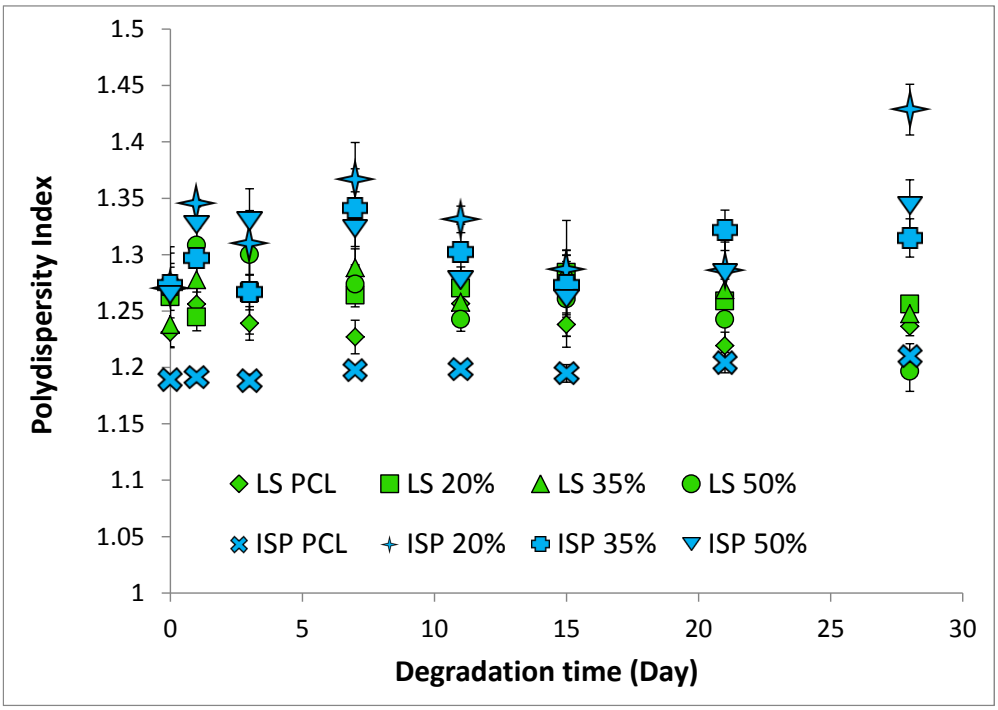

Figure 4.9 *Variation of (a) Molecular weight (b) Polydispersity of LS and ISP PCL and PCL/PGF composites; Degradation study conducted in PBS at 37 °C. LS = Laminate stacking, ISP = In-situ polymerisation; Fibre volume fraction = 20%, 35% and 50%.*

4.4.2.5. Flexural properties

Figures 4.10a and b show that the flexural strength and modulus decreased with immersion time for all PCL/PGF composites. However, both LSPCL and ISPPCL maintained their flexural strength and modulus for the whole degradation period, with no statistically significant difference found between the flexural properties of the LSPCL and ISPPCL specimens ($p>0.05$, ~20 MPa and ~0.35 GPa for flexural strength and modulus respectively).

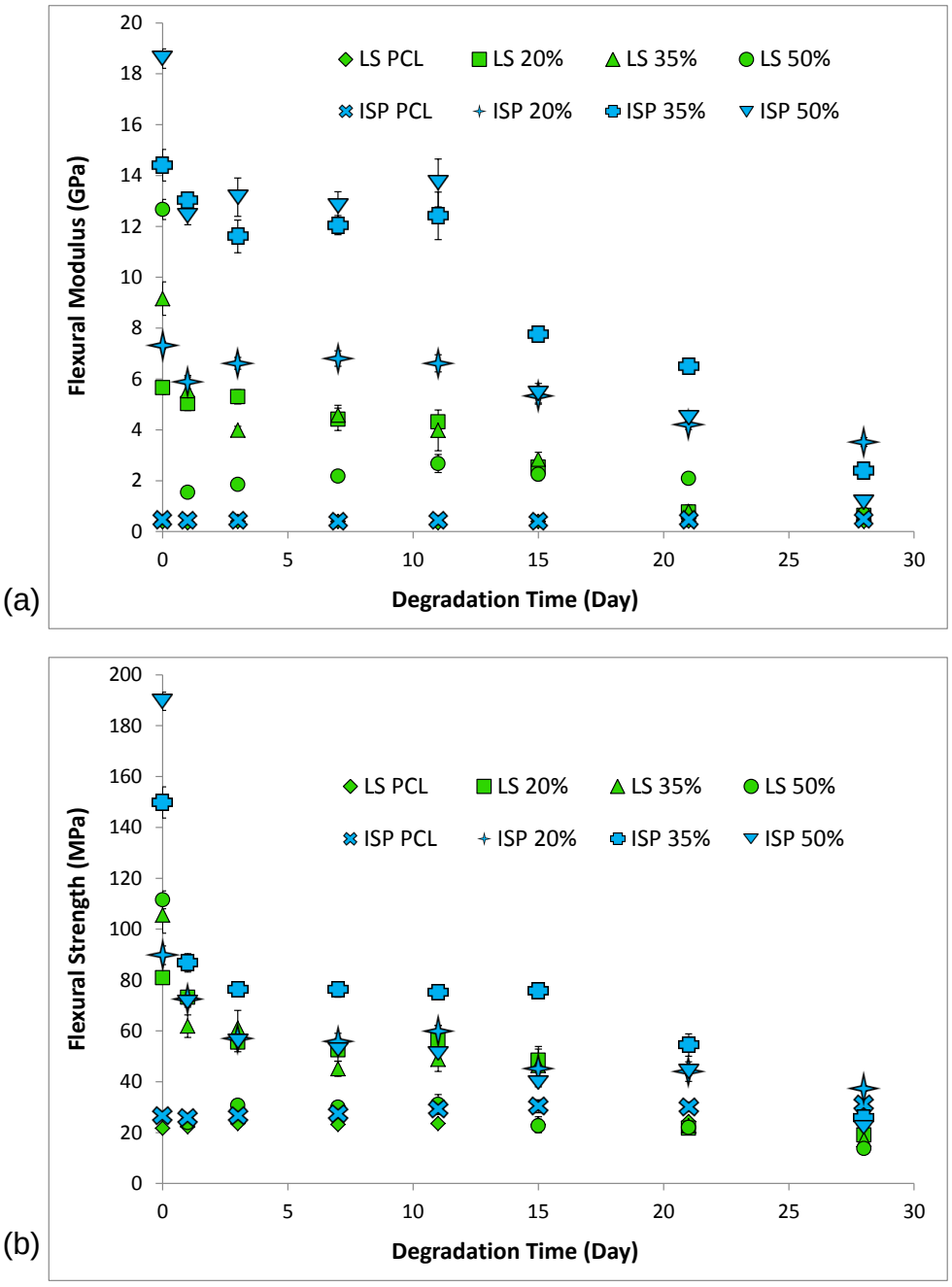

Figure 4.10 *Variations of (a) flexural strength (b) flexural modulus of LS and ISP PCL and PCL/PGF composites; degradation study conducted in PBS at 37 °C for 28 days. LS = Laminate stacking, ISP = In-situ polymerisation. Fibre volume fraction = 20%, 35% and 50%.*

By comparing the initial (non-degraded) flexural strength and modulus values between LS and ISP composites with the same V_f, it can be seen that ISP composites had significantly higher ($p<0.001$) flexural properties than LS composites, with increases of ~11%, ~30% and ~42% in flexural strength and

~28%, ~36% and 37% in modulus observed for ISP20, ISP35 and ISP50 composites in comparison to LS20, LS35 and LS50 respectively. It was also noticed that ISP35 (V_f=35%) had significantly higher ($p<0.05$) degradation profiles (exclude day 0, non-degraded) of flexural strength and modulus than the ISP50 (V_f=50%) composites. Similar profiles of flexural properties were obtained for all LS and ISP composites, a sharp decrease after 1-day immersion in PBS followed by a plateau until day 11 for modulus and day 15 for strength, after which a further drop was seen until the end of study. Furthermore, the flexural properties of ISP composites remained statistically higher ($p<0.01$) than all LS composites with same V_f after 28 days of degradation.

The flexural strength for all LS composites was significantly lower ($p<0.05$) than LSPCL after 21 days of immersion, whilst all ISP composites maintained a higher strength than ISPPCL. However, it was also noted that after 28 days of immersion, only ISP20 exhibited higher flexural strength than pure PCL, whilst all other composites showed significantly lower ($P<0.05$) flexural strength than pure PCL. In addition, all composites (LS and ISP) maintained a significantly higher ($P>0.05$) flexural modulus than pure PCL until the end of the study (28 days).

4.4.2.6. SEM analysis

Figure 4.11 shows the two kinds of composites SEM micrographs: freeze fractured and cut polished surfaces of non-degraded LS35 and ISP35 composites. SEM micrographs of composites with 20% and 50% V_f were very similar. The LS35 and ISP35 composites were selected to represent and illustrate the reinforcing effect of the LS and ISP composites that were produced. From Figure 4.11a and c, the individual layers of PCL and UD PGF mats can be seen clearly, with polymer rich zones between the fibre layers and extensive areas of dry fibre

within the fibre layers. In contrast, uniform fibre distributions were observed in Figure 4.11b and d throughout the entire cross-sectional area of the ISP35 composites. No obvious polymer rich zones or dry fibres were detected in the composites manufactured via the ISP process.

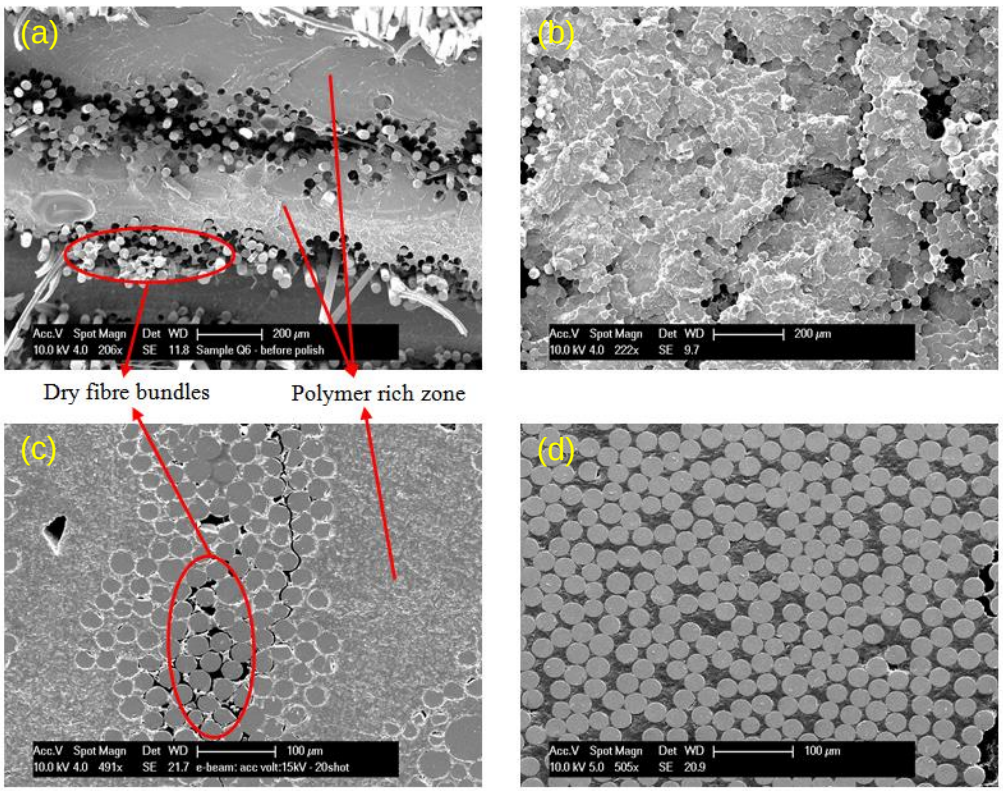

Figure 4.11 *SEM micrographs of composites specimens before degradation: freeze fractured surface of (a) LS35, (b) ISP35; cut polished surface of (c) LS35, (d) ISP35 (marker bar length 200 um for 'a' & 'b', 100 um for 'c' & 'd')*

SEM micrographs of freeze fractured surfaces for LS35 and ISP35 composites at selected degradation time points (1, 15 and 28 days of degradation) are presented in Figure 4.12. Different phenomena can be seen from the micrographs: micro tubes resulting from fibre degradation (see Figure 4.12c and 4.12f), fibre pull out sites in LS35 composites (see Figure 4.12a and 4.12b) and fibre fracture with no pull out in ISP35 composites (see Figure 4.12d and 4.12e).

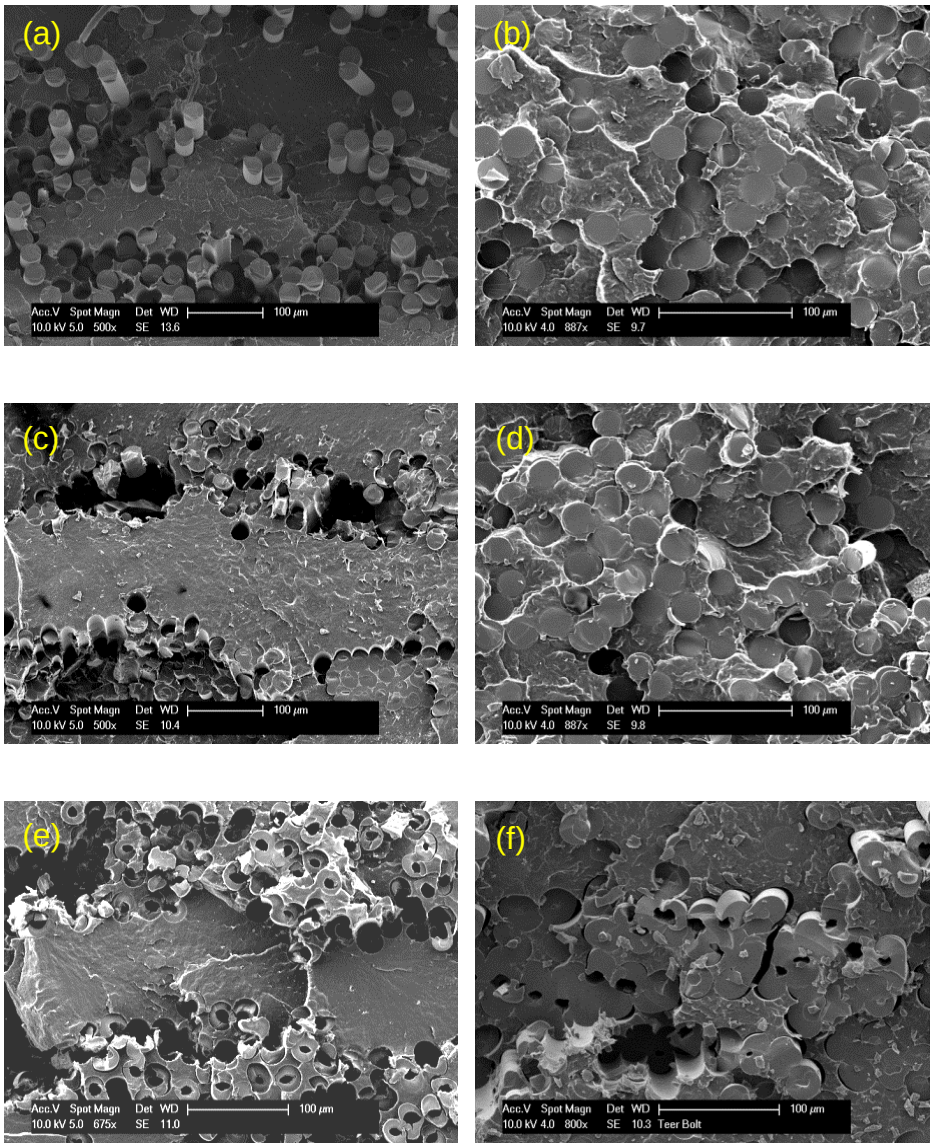

Figure 4.12 *SEM micrographs of freeze fractured surfaces for LS35 samples post immersion in PBS at 37°C: (a) 1 day, (b) 15 days, (c) 28 days interval. In comparison ISP35 samples post immersion was shown (d) 1 day, (e) 15 days, (f) 28 days.*

4.5. Discussion

4.5.1. Effects of catalyst concentration on ε-caprolactone polymerisation

It can be seen from Figure 4.1 that monomer conversion only reached ~17% after 6 hours with the lowest concentration of 0.00174 mol/L. With increasing catalyst concentration, the monomer conversion also increased significantly, which 0.0174 mol/L and 0.00868 mol/L reached ~98% at 120 mins and 180 mins

respectively. When the reaction temperature and the initiator concentration were kept at the same level, the catalyst ($Sn(Oct)_2$) concentration revealed the ability to accelerate polymerisation rate of the ε-caprolactone polymerisation. It was also noted from Figure 4.1 that polymerisation didn't take place within the first 60 mins with the lowest catalyst concentration. This has been referred as the polymerisation induction time, in which the pre-catalyst ($Sn(Oct)_2$) and the initiator (benzyl alcohol) reacts to form the active catalyst for PCL polymerisation (see Figure 3.4 in Section 3.7.1.1). By increasing the catalyst concentration, the induction time was also shortened significantly (<30mins).

However, as the catalyst concentration increased from 0.00868 mol/L to 0.0174 mol/L, the resulted PCL molecular weight decreased significantly (~25%, $P<0.01$) and the PDI also increased, which indicated that the polymer chain lengths were becoming shorter and broader. It is known that excessive catalyst in the ring opening polymerisation system can induce extensive inter- and intra-molecular transesterifications due to the excessive active chain ends formed by the catalyst, which could considerably lower the molecular weight and increase the PDI [74]. Therefore, to minimize polymerisation time, the catalyst concentration is kept as high as possible without jeopardising the molecular weight and polydispersity, which in this case 0.00868 mol/L was selected as the catalyst concentration.

4.5.2. Effects of initiator concentration on ε-caprolactone polymerisation

Figure 4.3 indicated that the initiator concentration did not have any significant effect on the monomer conversion rate. Kricheldorf *et al.* [74] stated that initiator alone (without catalyst) could not initiate the PCL polymerisation process, thus the initiator concentration should not have any effect on the polymerisation rate. However, it was also noticed that when the concentration of benzyl alcohol was

reduced to 0.00724 mol/L, the polymerisation reached ~98% at 240 minutes, which was 30 mins slower than polymerisation with higher benzyl alcohol concentrations. This was suggested to be due to the interference from water inside the reaction mixtures acting as a competitive initiator for the ε-caprolactone polymerisation, since both water and benzyl alcohol molecules have active hydroxyl groups, which could react and initiate the polymerisation process. As the concentration of benzyl alcohol decreased, the corresponding concentration of water compared to benzyl alcohol increased, thus water could then be more actively involved in the polymerisation process and in turn have a significant effect on the polymerisation rate [73]. As such, removing water in all of the reactants was stressed going forward and freeze-pump-thaw process was carried out for the ε-caprolactone in this work in order to minimize the water content within the monomer before use.

There was no significant difference in the PDI data (see Figure 4.4) with different initiator concentrations. It can also be observed from Figure 4.4 that the molecular weight of PCL increased with decreasing amount of initiator within the polymerisation reactions, which indicated that the molecular weight of PCL can be directly controlled by varying the initiator concentration during polymerisation. Overall, targeted molecular weight could be achieved by varying the concentration of benzyl alcohol in the ε-caprolactone polymerisation mechanism. However, the initiator concentration should also not be too low to allow water molecules to act as competitive initiator, which in this case, 0.01159 mol/L was chosen as the initiator concentration for the PCL polymerisation.

4.5.3. Effects of reaction temperature on ε-caprolactone polymerisation

A similar trend with changing catalyst concentrations (see Figure 4.1 and 4.2) was observed for varying the polymerisation temperature, which the reaction rate increased with increasing reaction temperature. Figure 4.5 indicated that the monomer conversion reached ~98% at 90 mins and 180 mins when the reaction temperature was 150 °C and 130 °C respectively. Meanwhile, at 110°C, the monomer conversion only reached ~22% after 6 hours and polymerisation induction time was also observed up to 2 hours (see Figure 4.5), which suggested that increase the reaction temperature can increase the polymerisation rate considerably.

According to studies in the literature, side reactions (inter- and intra-transesterification reactions) are sensitive not only to catalyst concentrations (see Figure 4.4), but also to reaction temperatures [73, 74, 179]. It can be seen from Figure 4.6 that the molecular weight of PCL decreased by ~27% when the polymerisation temperature increased from 130 °C to 150 °C, which indicated considerable amount of side reactions has happened at 150 °C and in turn reduced the molecular weight. Kricheldorf *et al.* [74] reported that the molecular weight of PCL produced via ROP almost halved by increasing the reaction temperature from 85°C to 100°C.

Therefore, polymerisation temperature for PCL was optimised to achieve the optimum balance between increasing molecular weight and decreasing polymerisation time, which 130 °C was used in this work.

Consequently, it was necessary to optimise the polymerisation rate as well as the molecular weight and PDI by choosing the appropriate combination of

polymerisation parameters (reaction temperature, $Sn(Oct)_2$ and benzyl alcohol concentrations). The final reaction parameters chosen for effective PCL ISP process to yield well-balanced reaction time and polymer quality was molar ratio of [1000:0.1:1;130 ºC] ([Monomer : Initiator : Catalyst ; Reaction temperature]), which is the equivalent of $Sn(Oct)_2$ and benzyl alcohol concentrations to be 0.00868 mol/L and 0.01159 mol/L respectively. The reaction time for complete PCL polymerisation (>98% monomer conversion) was chosen as 24 hours according to the kinetic study.

4.5.4. Degradation and mechanical retention behaviour of LS and ISP PCL/PGF composites

In this chapter, fully bioresorbable PGF reinforced PCL composites were produced via both LS and ISP manufacturing processes. The aim of this chapter was to develop the ISP process for bioresorbable composite manufacturing and investigate the reinforcing efficiency in comparison to conventional LS processes. Jiang *et al.* [35] reported that the ISP process could significantly enhance the fibre/matrix adhesion and interfacial bonding for PCL/continuous bioglass fibre composites, which indicated its potential in improving the degradation profile of PCL/PGF composites.

The formation of extensive dry fibre bundles and polymer rich zones (evident from SEM cross sections, see Figure 4.11a and c) in LS composites were resulted from the high viscosity of the polymer melt during the LS process. This meant that the molten polymer only had limited flow under pressure, making it very difficult to achieve sufficient wet-out and impregnation around and within the fibre mats. As such, the presence of these dry fibre bundles led to lack of interfacial bonding, which only provided limited reinforcement and transfer of stress within

these composites. Thus, the mechanical properties of the composites were significantly below expectation due to the poor efficiency of fibre reinforcement. These composites also tend to fail via delamination at the early stages of load-bearing due to the lack of reinforcement within the polymer rich zones [22, 187].

In contrast, SEM micrographs of the non-degraded ISP35 composites (see Figures 4.11b and d) suggested that a more robust fibre/matrix interfacial bonding and even fibre distribution had successfully been achieved via the ISP process as no noticeable dry fibre bundles and polymer rich zones were observed. The viscosity of the monomer was significantly lower than the polymer melt, which allowed improved flow properties within and between the fibre bundles, thus resulted in significantly enhanced the fibre wet-out and impregnation [35, 188]. Furthermore, the direct polymerisation also allowed for a one-step net shape production of composites, whereas making polymer films was the pre-requisite for the LS process. The enhanced fibre reinforcement also correlated well with the results from rule of mixtures. It can be seen in Table 4.2 (presented below) that the theoretical and experimental values of flexural modulus were very similar ($p>0.05$) for the ISP composites, whilst the theoretical flexural modulus for the LS composites were significantly lower ($P<0.001$) than the experimental data. This suggested that robust interfacial bonding via the ISP process with complete fibre impregnation had been achieved (see Figure 4.11b and d).

It has been established that ISP process achieved significantly more complete and stronger physical bonding via more effective fibre impregnation. Since no coupling agent was applied to the fibre surfaces, the bonding achieved between the fibre and the matrix during the LS process should be almost purely physical [185, 189]. In contrast to the LS process, ISP process utilised active

polymerisation reaction while *in-situ* forming the fibre/matrix interfacial bonding. Aside from the physical bonding formed, it can be argued that chemical bonding can take place between the surface of the fibre and the polymer matrix. Hydroxy groups are commonly presented on the surface of the fibre, which can act as active initiator for the ring opening polymerisation of PCL [35, 188, 190]. It was seen from Figure 4.9a that the molecular weight of neat ISPPCL was nearly twice as high as the PCL polymerised for the composites. Therefore, it is clear that the presence of the fibre affected the polymerisation significantly, and the reduction of the molecular weight is a potential indicator that the hydroxy groups on the surface of the fibre partially initiated the PCL polymerisation, thus the decreased the molecular weight. However, it should be noted that there is no definitive confirmation of the existence of the chemical bonding between the fibre surface and the PCL matrix. Jiang [35]chemically extracted the fibres after the polymerisation and used XPS to quantify the hydroxy bonding on the fibre surfaces, a slight increase (~12%) of the hydroxy bonding was found compared to the virgin fibre. He argued that the increase might indicate the existence of the chemical bonding, but the increase might also be induced by the chemical extraction.

Table 4.2 *Comparison between experimental and theoretical flexural modulus for LS and ISP composites (range of values for theoretical flexural modulus calculated from the range of fibre volume fractions, see Table 4.1)*

Sample code	Experimental flexural modulus (GPa)	Theoretical flexural modulus range (GPa)
LS20	5.6 ± 0.3	8.5 – 9.4
LS35	9.2 ± 0.7	10.9 – 11.3
LS50	12.7 ± 0.4	18.0 – 18.4
ISP20	7.3 ± 0.2	6.9 – 8.5
ISP35	14.4 ± 0.6	13.8 – 14.6
ISP50	18.6 ± 0.4	18.9 - 20.2

In addition, Figure 4.13 (presented below) showed that the strain at failure of LS20 (ε = ~1.05%) was significantly lower than that of ISP20 (ε = ~1.55%), which indicated early failure of LS composites due to poor interfacial bonding (LS35 and LS50 exhibited a similar trend). ISP20 also showed significantly higher yield stress than LS20, indicating higher mechanical performance was achieved via ISP process. The profile of the stress strain curves also indicated very different failure mechanisms between the LS and ISP composites. The LS composites showed a more ductile failure mechanism, suggesting progressive fibre pull-out had occurred. Whilst, a brittle failure mode was observed for the ISP composites and the stress was seen to increase linearly until composite failure. The difference in failure mechanisms also correlated well with the SEM micrographs of the fracture surfaces (see Figure 4.11 and 4.12), where fibre pull-outs were observed for the LS composites and clean fibre breakages were seen for the ISP composites.

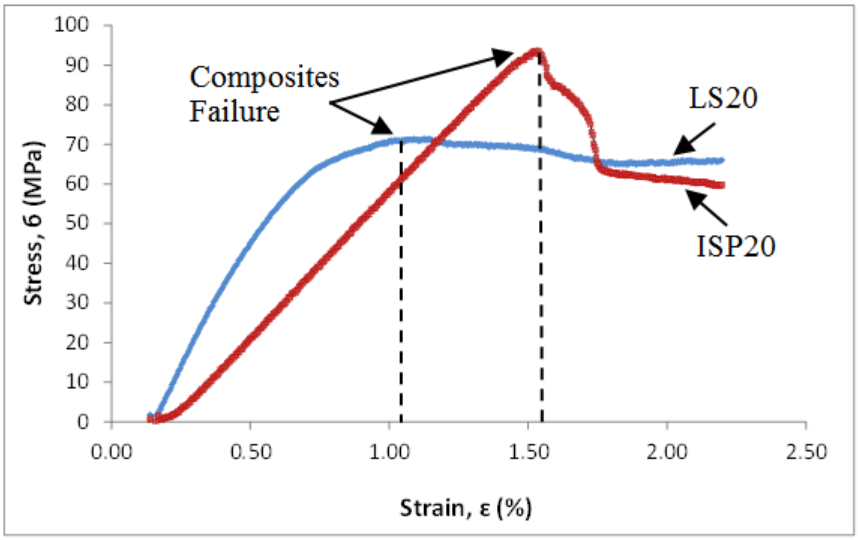

Figure 4.13 *Stress strain curve of flexural tests for non-degraded LS20 and ISP20 composites*

The media uptake of composites is usually higher than for the polymer alone, since the media is more prone to diffusion along the fibre/matrix interfaces by capillary action (see Figure 4.7a and b). The fibres within the composite samples were exposed at the edges and hence the fibre/matrix interfaces were directly exposed to the aqueous environment during immersion, where wicking effects could occur and are known to be responsible for the increase of media uptake in the composites [191]. It was also seen that the amount of media absorbed by composites increased with higher V_f, which was as ascribed to the increase in the amount of interfacial area with increasing V_f. When comparing the media uptake profiles of the LS composites with ISP composites at the same V_f, it was seen that ISP composites absorbed significantly less media than LS composites ($p<0.05$). This correlated well with the stronger interfacial bonding promoted by ISP process compared to the LS process, in which there were less voids or channels for media to pass through. Additionally, the rapid increase in media uptake as degradation proceeded was attributed to fibre degradation itself, clear evidence for fibre degradation was seen at later time points (see Figure 4.12c

and f). The media uptake profiles for all composites exhibited a tendency to decrease after day 21, which indicated that the media was getting saturated within the composites and most, if not all, of the fibre/matrix interfaces had been degraded, followed by a reduction in degradation of the fibres.

For both LS and ISP composites, increasing V_f resulted in an increasing amount of mass loss within the same degradation time (see Figure 4.7a and b). This was suggested to be due to the larger amount of fibres within the composites, which also increased the contact surface areas between fibre and PBS, hence more fibre degradation occurred. For LS and ISP composites with the same V_f, significantly less mass loss ($p<0.001$) was seen for ISP composites throughout the degradation study, which indicated that the ISP composites were more resistant to PBS ingression than LS composites. The stronger interface of ISP composites protected more PGF fibres from contacting PBS for longer period of time, thus leading to less fibre degradation, which correlated well with media uptake profile as less media was absorbed by ISP composites. Ahmed *et al.* [157] investigated the degradation behaviour of a binary calcium phosphate-based glass fibre reinforced PCL composites (V_f = ~6% and ~14%) within deionized water at 37°C for up to 900 hours. They reported similar mass loss profiles that exhibited a linear mass degradation up to 250 hours.

From Figure 4.8, the reduction of pH for both LS and ISP composites started from day 11, whilst the mass loss was shown to be linear with degradation time. This would suggest that there is a delayed loss of acidic materials that could be due to the buffering effect of PBS and progressive dissolution of fibre. The resulting acidity of the degradation media was attributed to phosphate ions from the fibres being released from the composite into solution, forming phosphoric acid (H_3PO_4)

[16]. The relatively higher pH of the ISP composites compared to the LS composites suggested that less degradation has occurred, hence the slower fibre degradation rate for the ISP composites. The pH started to drop faster from day 21 for all composites, which suggested major fibre degradation, and leaving behind micro tubes within the composites at the end of the study (See Figure 4.12c and f).

Both neat LSPCL and ISPPCL did not show any reduction in molecular weight over 28 days of immersion (see Figure 4.9a). However, all the PGF/PCL composites manufactured via LS and ISP exhibited significant decrease ($p<0.05$) in molecular weight after 28 days of immersion (see Figure 4.9a). Degradation of PCL within PBS often occurs through hydrolysis and chain scission [192]. This indicated that the inclusion of PGFs accelerated the hydrolytic degradation of PCL as a result of the acidic breakdown products from PGF glass fibre catalysing the hydrolysis process. Similar molecular weight variations were observed by Haltia *et al.* [193]. They monitored the hydrolytic degradation of self-reinforced poly(ester-amide) rods within PBS at 37°C and reported that degradation at the fibre/matrix interfaces was faster than in the matrix and the diffusion of PBS through the fibre/matrix interfaces accelerated the degradation of the matrix by hydrolysis.

All the specimens manufactured via LS exhibited an initial (non-degraded) molecular weight of ~90,000 g/mol (see Figure 4.9a), meanwhile only ISPPCL showed a similar ($p>0.05$) initial molecular weight. The ISP20, ISP35 and ISP50 exhibited approximately half the molecular weight in comparison to LS composites (~45,000 g/mol). The ISP of all PCL and PCL/PGF composite specimens were performed with the same reaction parameters. The large

difference in molecular weight was attributed to excess moisture content in the reaction system presumably introduced via the PGF mats. Kinetic studies of PCL polymerisation found that the reaction system was highly sensitive to moisture, where excess water in the reaction system could act as a competitive initiator for the ε-caprolactone polymerisation, since both water and benzyl alcohol molecules have active hydroxyl groups. PGF mats were dried in the 50°C vacuum oven 48 hours prior to use to remove any excess moisture. However, it is suspected that some moisture content remained on the PGFs which caused the decrease in molecular weight of the polymer in the ISP composites. In addition, the PGF mats were bound together using a PCL coating solution, for which the PCL utilised had a specified molecular weight. It is also possible that the PCL used in the binding solution could have been thermally degraded under heating during the ISP process, and the degradation products could have hindered the ISP PCL polymerisation reaction.

The flexural strength and modulus of all PCL/PGF composite specimens in this study exhibited an initial reduction after immersion in PBS for 1 day, which was suggested to be due to plasticisation of the fibre/matrix interface by the diffused PBS within the composite specimens [18, 23, 194]. The diffused PBS might also cause micro cracks and stress concentration sites on the fibre surfaces and led to the reduction in composites mechanical properties [5]. A further decrease in the flexural properties was observed after 11 to 15 days of immersion for all composites, which was attributed to the partial degradation of PCL and PGFs themselves, and the degradation of the fibre/matrix interfaces. This is well supported by the pH profiles (see Figure 4.8) as the pH reduced considerably between 11 and 15 days of degradation, indicated significant fibre degradation

occurred during that degradation period. The degradation profile of PLLA composites with different types of fibres within PBS were studied by Slivka *et al.* [191]. They reported that an increasing interfacial gap was seen during 30 days of immersion within PBS using a laser confocal microscope, which confirmed that interface degradation had occurred during the study. Lin *et al.* [144] also found a similar reduction in mechanical properties for calcium phosphate glass fibre reinforced PLLA composites (V_f = ~55%). They found that the initial flexural strength and modulus as ~350 MPa and ~28 GPa, which decreased to ~84 MPa and ~3.8 GPa respectively after 1 week of immersion in PBS at 37°C. They stated that the observed decrease was ascribed to the breakdown of the fibre/matrix interface and fibre degradation.

From Figure 4.10a and 4.10b, the initial (non-degraded) flexural strength and modulus values for all ISP composites were statistically higher ($p<0.01$) than the LS composites with same V_f at all time points throughout the study. All the composites exhibited initial properties which were within the range of the flexural properties of cortical bone (E = 5-23 GPa, σ = 35-250 MPa) [195, 196]. It is well known that the strength of the fibre/matrix interface is critical to the mechanical properties of fibre reinforced composites [14, 197-199]. Although the molecular weight of the ISP composites was much lower than that of LS composites, the flexural properties of the ISP composites were still significantly higher, which proved that ISP process delivered a significantly enhanced interfacial bonding and adhesion. This also suggests that if the ISP process can yield higher molecular weight of the PCL matrix, then further enhancements of the mechanical properties for the resulted composites could be achieved. Furthermore, it was seen that only ISP20 had higher flexural strength than pure PCL after 28 days

degradation (see Figure 4.10a), which indicated that fibre reinforcements were no longer contributing to the mechanical properties of all the other composites. The degradation of the fibres was effectively developing pores/channels inside the matrix, which could further intensify the PCL matrix degradation.

In summary, the PCL/PGF composites manufactured via ISP process revealed superior mechanical properties, improved degradation profiles and prolonged mechanical property retention in comparison to those manufactured via the LS process.

4.6. Conclusions

Results from polymerisation kinetic studies have suggested that the ε-caprolactone polymerisation rate was sensitive to the reaction temperature and the amount of the catalyst. Higher reaction temperature and larger amount of catalyst could accelerate the polymerisation rate of ε-caprolactone. Moreover, the initiator concentration was found to be the key factor in controlling the molecular weight of the polymer produced. Lower initiator concentration could effectively increase the molecular weight. Careful controls over those three factors were necessary to effectively yield PCL with high molecular weight and narrow polydispersity. Moreover, the polymerisation system became more sensitive to moisture when the initiator concentration was low as water could also act as a competitive initiator in this mechanism. Therefore, it is of paramount importance to get rid of any excessive moisture within the ISP system before reaction.

SEM micrographs of fractured cross sections of the LS composites revealed dry fibre bundles and poor fibre dispersion with extensive polymer rich zones. Conversely, even fibre distributions with no dry fibre bundles or polymer rich

zones were observed for the ISP composites. Via the ISP manufacturing process, the bioresorbable PCL/PGF composites also had significantly prolonged and higher retention of mechanical properties over the 28-day degradation study within PBS at 37 °C. These differences showed that a robust and significantly stronger fibre/matrix interface had been achieved via the ISP process.

An enhanced fibre/matrix interface resulted in a significant decrease of voids or channels within the composites, leading to reduced degradation rate for all the ISP composites. This correlated well with the media uptake and mass loss profiles, which showed that the ISP composites had significantly lower levels of media absorption and mass loss ($p<0.001$ for both data) during the degradation period. Molecular weight and distribution did not show any significant variation for neat PCL over 28 days, meanwhile significant decrease ($p<0.05$) was noted for all PCL/PGF composites. The accelerated degradation of the matrix was attributed to the acidic breakdown products from fibre degradation, which could have catalysed matrix hydrolysis. Overall the ISP process showed significant advantages over the LS process in manufacturing fully bioresorbable PCL/PGF composites.

Chapter 5. Wet and Dry High Cycle Flexural Fatigue Behaviour of Fully Bioresorbable PCL/PGF Composites: *In-situ* Polymerisation *vs.* Laminate Stacking

5.1. Summary

This chapter investigated for the first time the environmental (dry and wet condition) flexural fatigue behaviour of fully bioresorbable PCL/PGF composites. Significantly longer flexural fatigue life ($p<0.0001$) and superior fatigue damage resistance were observed for ISP composites as compared to the LS composites in both dry and wet conditions, indicating that the ISP process promoted considerably stronger interfacial bonding than the LS process. Immersion in fluid during the flexural fatigue tests resulted in significant reduction ($p<0.0001$) in the composites fatigue life, earlier onset of fatigue damage and faster damage propagation. Regardless of testing conditions, increasing fibre content led to shorter fatigue life for the PCL/PGF composites. Among all the composites that were investigated, ISP35 (35% fibre volume fraction) composites showed a minimum fatigue life of 10^5 and 10^6 cycles up to 50% testing stress level in dry and wet conditions respectively. It also maintained at least 50% of its initial stiffness (~6.5 GPa) by the end of fatigue tests in both conditions, which is comparable to the flexural properties of human cortical bone (5–23 GPa).

5.2. Introduction

The majority of previous studies on fibre reinforced composites have indicated that elevated humidity and temperature generally severely shortened their fatigue

life [200-203]. Damage mechanisms in flexural fatigue of fibre reinforced composites, in general, involve matrix cracking, fibre breakage and interface failure [180, 204]. The diffusion and growth of composites fatigue damage resulting from crack bridging and/or fibre/matrix de-bonding is governed by the behaviour of fibre/matrix interaction [180, 205-207]. The diffuse damage growth often results in a gradual decrease of the composite's stiffness with growing loading cycles, which is coupled with a significant increase in the composite's material damping [208]. Both stiffness evolution and material damping are often used as sensitive indicators to study the damage mechanisms of composites [209-213].

Fatigue properties are of paramount importance for their intended application, where components are subjected to various loading and environmental parameters, which vary with time over the period of service. The target properties of the composites were within the properties reported for human cortical bone, i.e. 5-23 GPa and 35-250 MPa for flexural modulus and strength respectively [46]. However, up to the best of the authors knowledge, cyclic fatigue response of the fully resorbable composites has not been explored yet.

In this chapter, PCL/PGF composites with V_f of 35% and 50% were produced using LS and ISP processes. Environmental flexural fatigue tests were performed on these composites in both dry conditions at ambient temperature and in wet conditions immersed in PBS solution at 37 °C. The wet conditions were intended to mimic the physiological nature of the human body. Both stiffness reduction and SDC were used as sensitive indicators to monitor the damage initiation of the composites during cyclic loading. The influences of solution immersion, fibre

content and fibre-matrix adhesion on the performance of the PCL/PGF composites were investigated by comparing their fatigue behaviour.

5.3. Materials and methods

5.3.1. Materials

Please refer to Section 3.3 for details.

5.3.2. Phosphate based glass and glass fibre production

The glass composition, the production process of the glass, its glass fibre, and fibre mats were all detailed in Section 3.4 and 3.5.

5.3.3. PCL/PGF composites production

Please refer to Section 3.6.1 for the LS process and Section 3.8 for the ISP process, which specified the details of the composites manufacture.

5.3.4. Flexural testing

5.3.4.1. Monotonic loading

Please refer to Section 3.13.2 for the detailed specifications.

5.3.4.2. High cycle flexural fatigue loading

Details were stated in Section 3.11.

5.3.5. Fatigue data analysis

5.3.5.1. Stress-Life (S-N) diagram

Please refer to Section 3.12.1 for all the details.

5.3.5.2. Specific damping capacity (SDC)

. Please refer to Section 3.12.2 for the specifications.

5.3.6. Scanning electron microscopy (SEM)

Procedures were detailed in Section 3.13.5.

5.3.7. Burn off tests

Procedures were detailed in Section 3.13.6.

5.3.8. Statistical analysis

Please refer to Section 3.13.10.

5.4. Results

5.4.1. Composites fibre content and static flexural properties

PCL/PGF composites with 35% and 50% fibre volume fraction (V_f) were produced via both LS and ISP in this chapter. Details of the composites with their respective codes are listed in Table 5.1 as below.

Table 5.1 *PCL/PGF composites codes (D/W refers to dry or wet testing conditions)*

Manufacture process	**Composites codes**	**Fibre Orientation**
Laminate Stacking (LS)	(D/W)-LS35	Unidirectional (UD)
	(D/W)-LS50	
In-situ Polymerisation (ISP)	(D/W)-ISP35	
	(D/W)-ISP50	

Table 5.2 below shows the fibre volume fractions, static flexural strength and modulus for all the LS and ISP composites tested in both dry and wet testing conditions.

Table 5.2 *Static flexural properties for all composite specimens*

Composites Code	Actual V_f (%)	Ultimate Flexural Strength (UFS) (MPa)	Flexural Stiffness (E_f) (GPa)
D-LS35	34 ± 1	126 ± 2	9.1 ± 0.7
W-LS35	32 ± 1	110 ± 3	6.2 ± 0.3
D-LS50	51 ± 1	143 ± 2	12.7 ± 0.4
W-LS50	50 ± 1	105 ± 1	6.3 ± 0.3
D-ISP35	36 ± 1	172 ± 3	14.4 ± 0.6
W-ISP35	35 ± 1	141 ± 2	13.0 ± 0.2
D-ISP50	49 ± 2	210 ± 3	18.6 ± 0.4
W-ISP50	50 ± 1	123 ± 1	12.4 ± 0.4

5.4.2. S-N diagram

Figure 5.1 shows the variation of the fatigue life for each of the composites tested versus increasing stress levels in both dry and wet testing conditions. Basquin's equation (see Equation 5, Section 3.12.1) gives a good fit to the experimental fatigue data, with R^2-value > 0.9 for all regressions. Table 5.3 shows the values of *'b'* obtained from curve fitting the experimental fatigue data using the Basquin's equation.

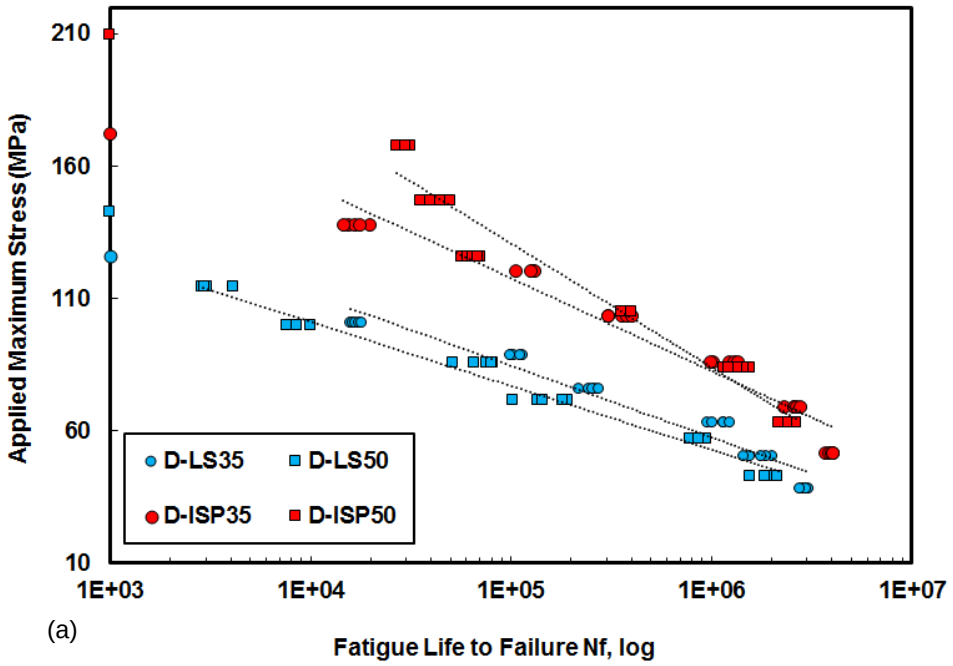

(a)

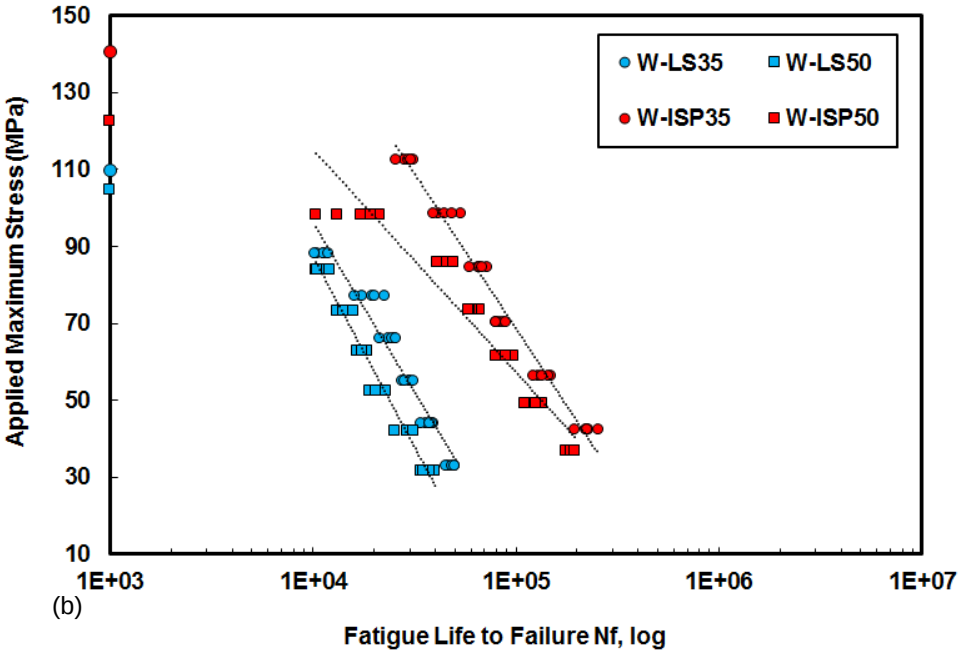

(b)

Figure 5.1 *S-N diagram of PCL/PGF composites in dry and wet environments plotted in power-law regression scale (points on the y-axis indicate the monotonic flexural strength of the composites): (a) Comparison of composites made by LS and ISP in dry environment; (b) Comparison of composites made by LS and ISP in wet environment. The circles represent 35% V_f whereas the square points are representative of 50% V_f samples.*

Table 5.3 *Values of* 'b' *from S-N curve fitting for LS and ISP composites*

Sample Code	D-LS35	D-LS50	W-LS35	W-LS50	D-ISP35	D-ISP50	W-ISP35	W-ISP50
b	-0.089	-0.071	-0.497	-0.661	-0.101	-0.131	-0.241	-0.244

A gradual decrease in fatigue life with increasing stress levels was observed for all composites, as expected. It was also observed that the 35% V_f composites showed a significantly longer fatigue life ($p<0.01$) than their equivalent 50% V_f composites (see Figures 5.1a and b). In dry conditions at the same stress level, D-LS35 and D-ISP35 showed ~29% and ~34% longer fatigue lives respectively, when compared to D-LS50 and D-ISP50. Meanwhile, in wet conditions, the W-LS35 and W-ISP35 showed ~20% and ~23% longer fatigue life than W-LS50 and W-ISP50.

Comparing Figures 5.1a and 5.2b, immersion in PBS solution at 37 °C substantially decreased the fatigue life for both LS and ISP composites. At the same stress level, the D-LS35 and D-LS50 samples showed approximately 10 times longer fatigue life than the W-LS35 and W-LS50 samples respectively. For example, D-LS35 exhibited ~3 million cycles to failure at 30% UFS stress level, whilst the wet W-LS35 samples lasted only ~50,000 cycles. Similarly, D-ISP35 and D-ISP50 exhibited approximately 9 times longer fatigue life than W-ISP35 and W-ISP50 (i.e. ~4 million and ~230,000 cycles to failure for D-ISP35 and W-ISP35 respectively at 30% UFS stress level).

Regardless of the testing conditions, the ISP composites showed a significantly longer fatigue life ($p<0.0001$) than the LS composites of equivalent V_f. When

tested in a dry environment and at the same stress level, the D-ISP35 and D-ISP50 showed ~25% and ~19% longer fatigue life than D-LS35 and D-LS50 respectively (see Figure 5.1a). Similarly, in wet conditions, the W-ISP35 and W-ISP50 exhibited ~85% and ~74% longer fatigue life than W-LS35 and W-LS50 (see Figure 5.2b).

5.4.3. Failure strain variation

Figures 5.2a and 5.2b show the variation of failure strain versus the stress levels tested. Vertical dotted line presents threshold stress level that the failure strains increase significantly ($p<0.01$).

The LS composites showed significantly lower failure strain profiles ($p<0.01$) than ISP composites in both dry and wet conditions. By comparing ISP and LS composites (identical V_f) in dry conditions (see Figure 5.2a), no significant difference ($p>0.01$) was found in the increase rate of failure strain with increasing stress levels. However, in wet conditions, the W-ISP50 samples showed a significantly faster increase rates of failure strain than the W-LS50 (see Figure 5.2b).

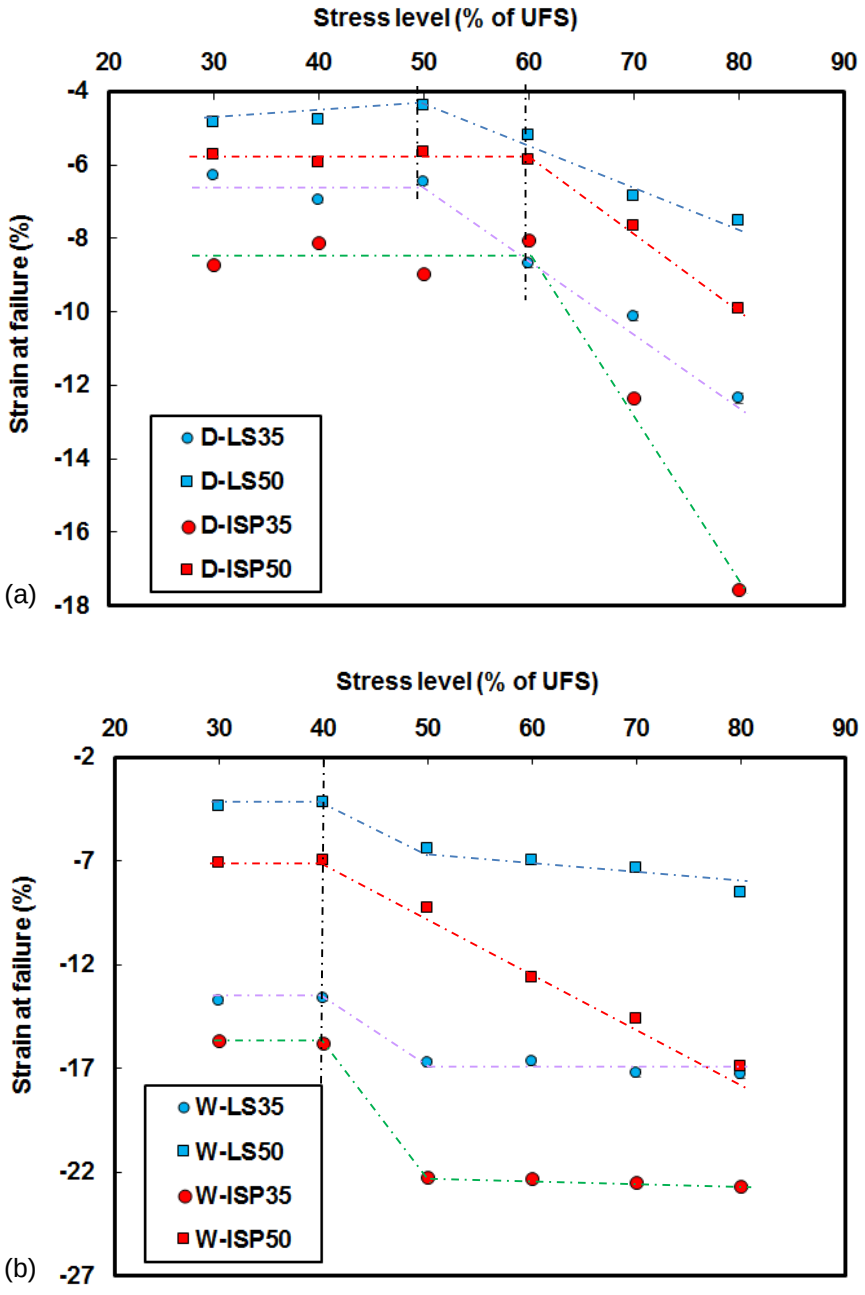

Figure 5.2 *Strain at fatigue failure ('-' as downwards) against tested stress levels: (a) LS and ISP composites tested dry; (b) LS and ISP composites tested wet; Error bars fall within the dimension of the markers. Vertical dotted line presents threshold stress level that the failure strains increase significantly, other dotted lines are given as guides to the eyes.*

When tested in the same conditions, both LS and ISP composites with 50% V_f showed significantly lower ($p<0.01$) failure strain values in comparison to

composites with 35% V_f for all stress levels. Figures 5.2a and b also showed that the LS and ISP composites had significantly higher failure strain value profiles ($p<0.01$) in dry conditions compared to wet conditions. When tested dry, the failure strain value of D-LS35 and D-LS50 started to increase significantly at 50% UFS stress level, meanwhile 60% UFS stress level (see the dotted vertical line in Figure 5.2) was observed for D-ISP35 and D-ISP50. However, in wet conditions, the significant increase was observed from 40% UFS stress level for all LS and ISP composites.

5.4.4. Stiffness evolution

The stiffness evolution profiles are presented in Figures 5.3a and b below, which show gradual decline of the composites' stiffness during their fatigue life at a specific stress level (40% of UFS). The initial stiffness E_f was determined from the first loading cycle and the residual stiffness, *E* at *n* cycles, was determined from the peak-to-peak values in the loading/unloading cycle loop (see Figure 3.10 in Section 3.11).

Substantial differences were observed when comparing the stiffness at failure, following the trend of D-ISP35 > D-LS35 > D-ISP50 > D-LS50 > W-ISP35 > W-LS35 > W-ISP50 > W-LS50 for all stress levels investigated. For example, at 40% UFS stress level, D-ISP35 exhibited ~60% of initial stiffness at failure whilst W-LS50 demonstrated ~30% residual stiffness at failure.

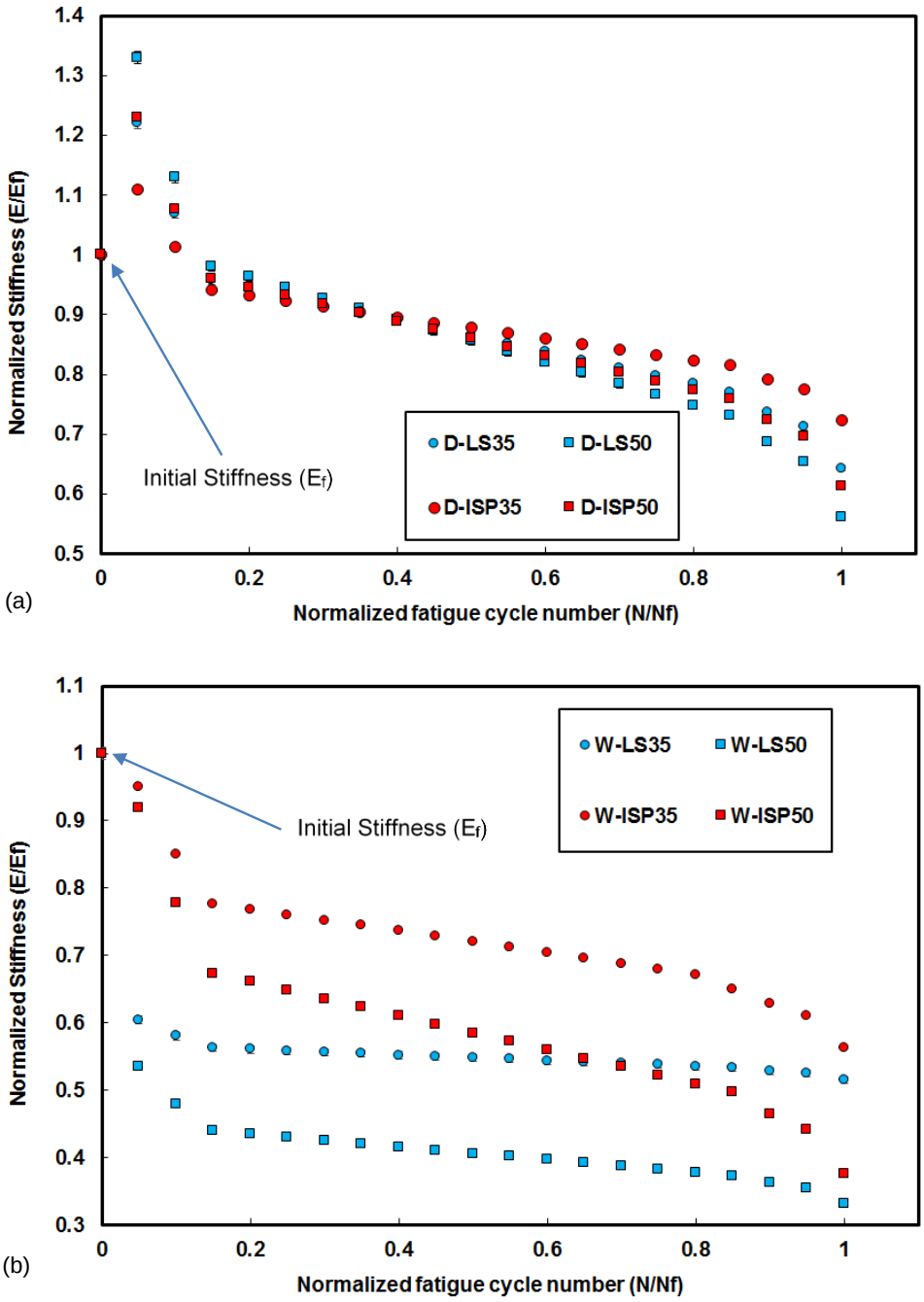

Figure 5.3 *Normalised stiffness against normalised cycle number for composites tested at 40% of UFS in: (a) Dry Environment, inner graph for dry composites tested at 60% of UFS; (b) Wet Environment; Error bars fall within the dimension of the markers.*

Comparing Figures 5.3a and b, the ISP composites revealed significantly higher stiffness profiles ($p<0.01$) than the LS composites through their entire fatigue life.

Moreover, composites with 35% V_f showed considerably higher stiffness profiles throughout the fatigue life and slower stiffness reduction rate than composites with 50% V_f in the same testing condition. The change from dry to wet condition resulted in significantly lower stiffness profiles ($p<0.01$) and faster stiffness reduction rate ($p<0.01$) for all the LS and ISP composites.

According to Figure 5.3a, there was a distinct increase in stiffness at the beginning of the composites fatigue life in dry conditions. Meanwhile, in wet conditions, the stiffness profiles showed a gradual decline from the beginning of the fatigue life (see Figure 5.3b). Moreover, in dry testing conditions, it was found that with tests performed at stress levels over 50% of respective UFS, no initial increase was seen and a gradual decline from the beginning of the fatigue tests was also observed.

5.4.5. Specific damping capacity (SDC)

Figure 5.4 shows the variation of SDC versus increasing maximum applied stress for both LS and ISP composites tested in dry and wet conditions. The critical applied stress (CAS) for damage initiation of the composites was estimated as the stress where SDC starts to increase significantly ($p<0.01$) and they are indicated by arrows in Figure 5.4 [182].

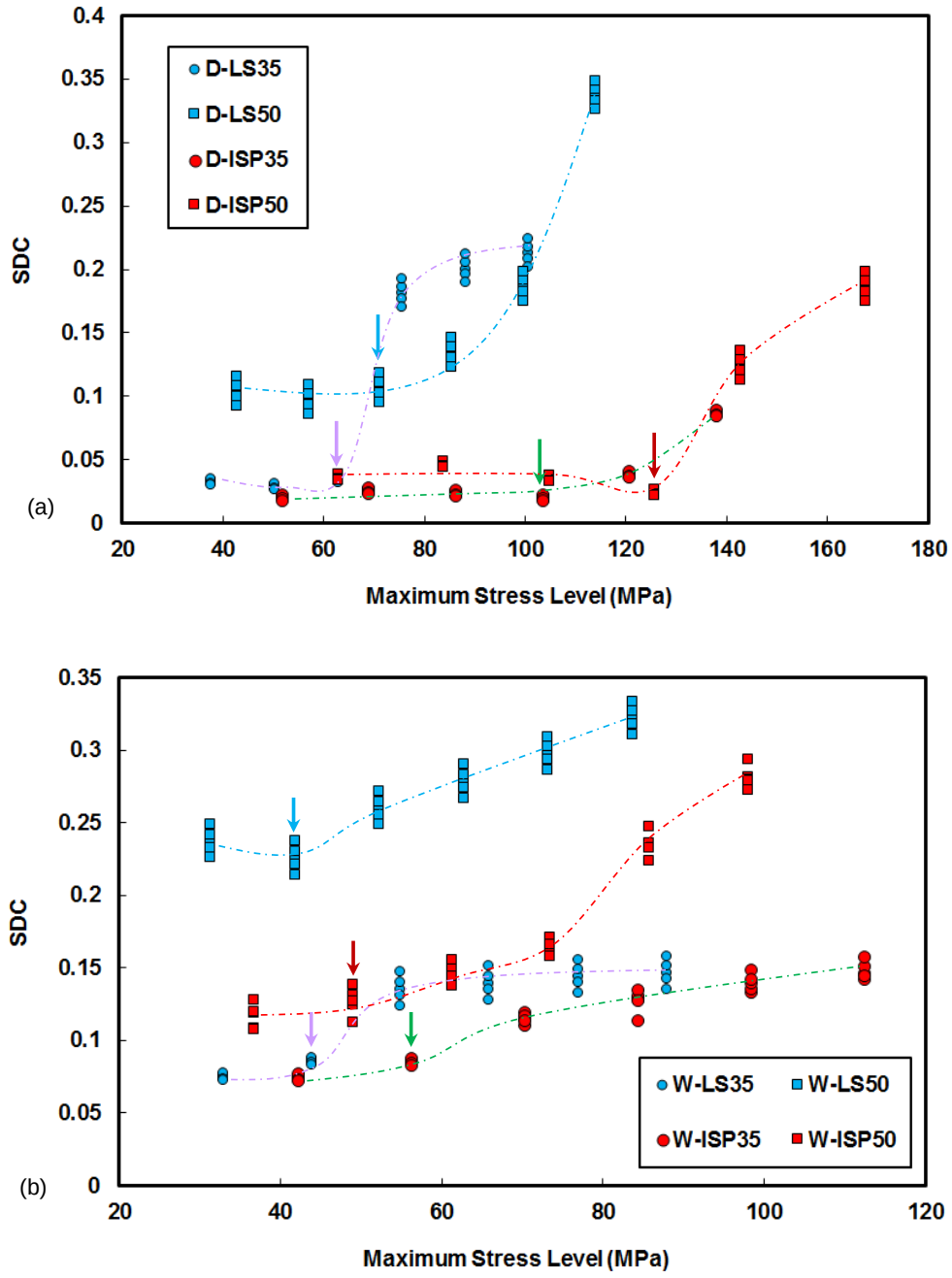

Figure 5.4 *Specific flexural damping capacity verses applied maximum load for LS and ISP composites: (a) in dry conditions; (b) in wet conditions; Arrows point to the CAS values of the composites. The dotted lines are given as guides to the eye.*

Table 5.4 showed the CAS values for all composites tested. Regardless of the testing environment, significantly higher CAS ($p<0.01$) values can be seen for ISP composites than for the LS composites. Moreover, with same manufacturing

method and in dry conditions, composites with 35% V_f showed significant higher CAS ($p<0.01$) than composites with 50% V_f. Meanwhile, 50% composites also showed lower CAS values than 35% composites in wet conditions. In dry conditions (see Figure 5.4a), only D-LS50 had significantly higher SDC profile ($p<0.01$) against increasing applied stress than other composites. However, in a wet condition (see Figure 5.4b), both W-LS35 and W-LS50 showed distinctly higher SDC profiles ($p<0.01$) than W-ISP35 and W-ISP50 respectively. By comparing Figures 5.4a and b, the CAS values for W-LS35, W-LS50, W-ISP35 and W-ISP50 were ~30%, ~41%, ~41% and ~49% lower than D-LS35, D-LS50, D-ISP35 and D-ISP50 respectively.

Table 5.4 *Values of Critical Applied Stress (CAS) for LS and ISP composites*

Sample Code	**D-LS35**	**D-LS50**	**D-ISP35**	**D-ISP50**	**W-LS35**	**W-LS50**	**W-ISP35**	**W-ISP50**
CAS (MPa)	63	71	103	126	44	42	56	49

5.4.6. SEM analysis

Figure 5.5 compared the cross sections of the composite fracture surfaces between LS and ISP composites tested within both dry and wet conditions. Clear polymer rich zones and fibre pull-outs were seen from the SEM micrographs of LS35 and LS50 (see Figure 5.5a, e and c, g respectively). Meanwhile, clean fibre fractures with no visible polymer rich zones were observed from the SEM micrographs of ISP35 and ISP50 (see Figure 5.5b, f and d, h respectively).

Figure 5.6 displayed the typical fatigue failure modes of the LS and ISP composites tests in both dry and wet conditions. In dry conditions, LS composites showed compressive delamination and interlaminar shear fracture failure modes (see Figure 5.6a and b), whilst ISP composites showed clean centre fracture (see Figure 5.6c). In wet conditions, the LS composites showed softening behaviour with interlaminar shear fracture failure mode (see Figure 5.6d and e), whilst the ISP composites showed fibre pultrusion behaviour with centre fracture failure mode (see Figure 5.6f).

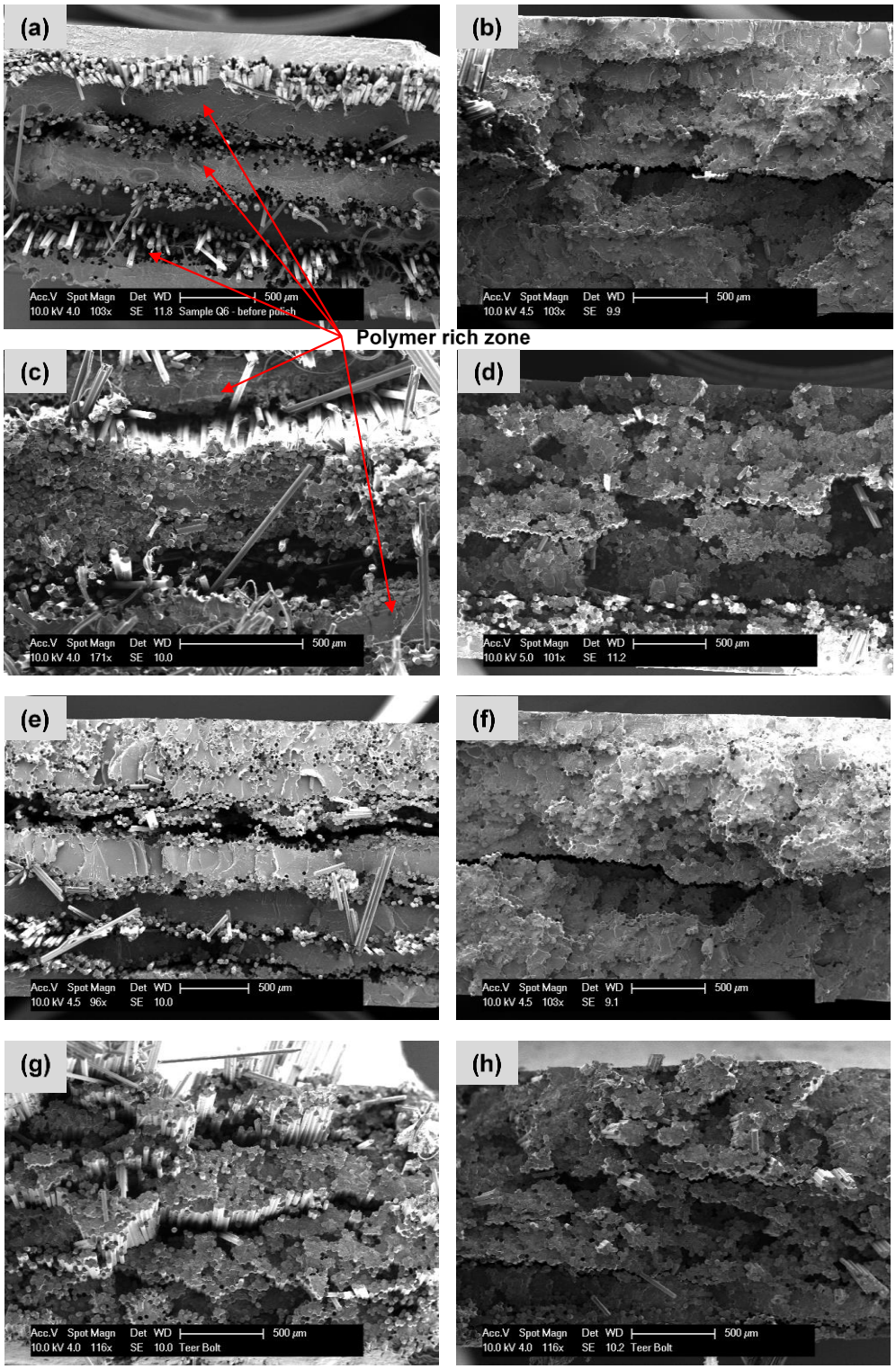

Figure 5.5 *SEM cross section images of the composites fatigue fracture surfaces: (a) D -LS35; (b) D -ISP35; (c) D -LS50; (d) D -ISP50; (e) W -LS35; (f) W -ISP35; (g) W -LS50; (h) W -ISP50 (marker bar length 500 um)*

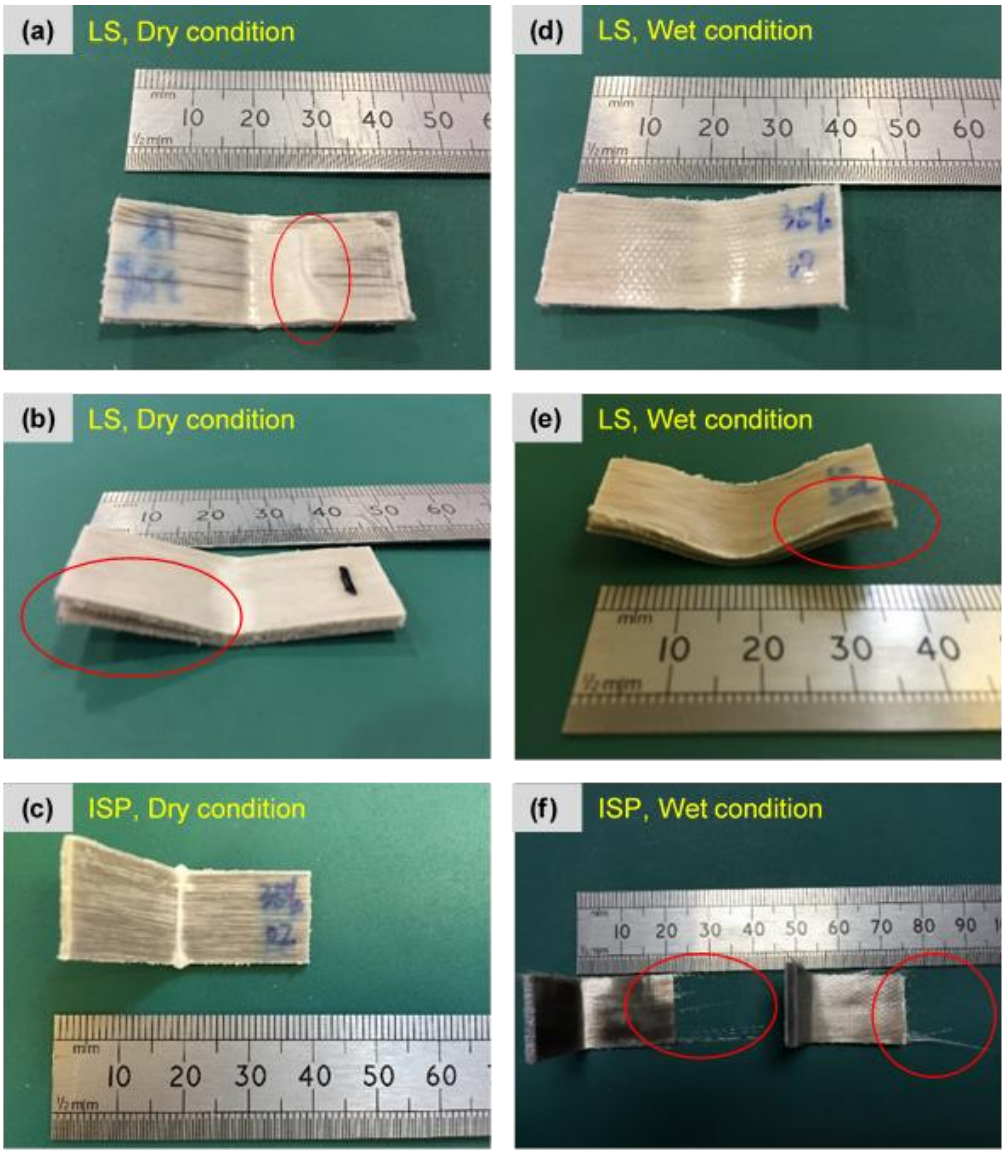

Figure 5.6 *Images taken of LS and ISP composites' after end of fatigue testing cycles: (a) compressive delamination was observed (see red circle); (b) interlaminar shear fracture (see red circle); (c) centre fracture where load was applied; (d) softening of sample observed from wet testing; (e) softening and interlaminar shear fracture observed (see red circle); (f) fibre protrusions were also observed post testing (see red circles) and centre fracture were load was applied.*

5.5. Discussion

This chapter investigated the cyclic flexural fatigue performance of PCL/PGF composites (V_f of 35% and 50%) produced via LS and ISP processes. Environmental conditions were evaluated by performing tests in dry (room temperature) and in wet conditions (immersed in PBS at 37 °C). Fatigue behaviour of the composites was characterised via the classic S-N diagrams, stiffness degradation profiles and SDC.

Table 5.2 summarises the quasi-static flexural properties of the LS and ISP composites in both dry and wet conditions. Testing the samples in wet conditions revealed significant reductions in both the strength and stiffness of the composites, compared to the dry tested samples. Several studies have been conducted on similar PGF composites, which investigated quasi-static mechanical properties in dry and wet conditions. They also reported a distinct decrease in flexural strength and modulus for samples tested in quasi-static wet conditions, and suggested this was due to media attack disrupting the fibre matrix interface and plasticisation [16-18, 158]. However, the ISP composites revealed considerably higher flexural properties compared to the LS composites in both dry and wet conditions. Chapter 4 revealed that a stronger and more robust fibre/matrix interface was achieved using the ISP process as compared to LS, which inhibited PBS media attack and revealed a significant increase in the composites flexural properties (by ~45%).

Depending on the length of the fatigue tests conducted within the wet environment, degradation of the composites (fibre and fibre/matrix interface) could have affected the fatigue life and stiffness profiles during the fatigue tests. The time elapsed during the wet fatigue tests varied between ~30 mins and 2.5

days. According to Figure 4.10, after 3 days immersion within the PBS solution at 37 °C, ISP and LS composites with 35% V_f showed ~14% and ~54% decrease in static flexural modulus respectively, ~32% and ~83% reduction in modulus was found for ISP and LS composites with 50% V_f respectively. Fibre/matrix interface plasticisation was the main cause of those reductions as the PBS diffuse through the interface. It can also be seen from Figure 4.12 that no visible fibre and matrix degradation was found from the SEM images. Therefore, it can be related that the fibre/matrix interface plasticisation is one of the causes for stiffness decline during the wet fatigue tests. However, fibre and matrix degradation itself would have minimum effects during the wet fatigue tests.

On the other hand, fatigue tests conducted within dry environment lasted up to ~12 days to reach catastrophic failure. The major cause for the damage and failure are interface de-bonding and fibre breakage. However, since the tests were performed within the dry environment, no fibre/matrix interface plasticisation and hydraulic degradation of fibre and matrix could have taken place. This is also confirmed by the SEM images in Figure 5.5 (a-d) that no visible fibre and matrix degradation was seen at the cross sections of the composites after the dry fatigue tests.

It also should be noted that the constant cyclic loading accelerated the interface plasticisation degradation and mechanical behaviour of the composites via inducing accumulated damage during the test. Factors influencing the fatigue behaviour were characterised taking into consideration three key factors as discussed below.

5.5.1. Influence of fibre-matrix interface

The S-N diagrams produced revealed the fatigue life profiles with increasing testing stress for all the LS and ISP composites tested (see Figure 5.1). It was immediately apparent that the ISP composites demonstrated a significantly longer fatigue life ($p<0.0001$) than the LS composites at each stress level in both dry and wet conditions. This major increase in fatigue life was attributed to sturdier interfacial bonding promoted by the ISP manufacturing process. De-bonding of the fibre/matrix interface (especially ductile matrices, such as PCL) is widely considered to be the main governing factor of crack propagation, which can lead to the fatigue failure of fibre reinforced composites [180, 214, 215]. Weak interfacial properties can allow de-bonding and friction sliding between fibre and matrix to occur readily upon crack propagation, which can lead to matrix cracks (in this case delamination, see Figures 5.6a and b) without major fibre fractures [189, 205]. Conversely, a stronger fibre/matrix interface could inhibit interfacial sliding and lead to direct fibre fractures along with cracks in the matrix, without inducing significant de-bonding of the fibre/matrix interface (see Figure 5.6c) [189, 205, 214]. This difference in behaviour was apparent when comparing LS and ISP composites, as illustrated by the failure cross sections in Figure 5.5. LS composites showed significant fibre pull-out and ISP composites had clear fibre fractures, which demonstrated that a stronger fibre/matrix interface for the ISP samples had been achieved. Several studies have investigated the effects of the fibre/matrix interface on the fatigue behaviour of glass or carbon fibre reinforced composites. These studies applied coupling agents on fibre surfaces to promote stronger interfacial bonding with the polymer matrices and consequently significantly longer fatigue lives (ranging from 5% - 20%) were achieved [181,

182, 215, 216]. It should be noted that improvements in fibre/matrix interfacial properties in this work were achieved via the ISP manufacturing process alone, and without the use of coupling or sizing agents. This suggests that the ISP process can promote strong interfacial bonding of fibre reinforced composites and has huge potential to further improve the mechanical properties with use of appropriate coupling agents [35].

The variation in SDC was applied in this fatigue analysis to monitor the anisotropic composites' CAS for damage initiation during fatigue loading. Figures 5.4a and b both indicated that the ISP composites retained distinctly higher ($p<0.01$) normalised critical load for damage initiation than the LS composites at equivalent V_f, indicating that the fatigue damage initiation of the composites was postponed by the application of ISP process. This suggested that the improvement of interfacial strength led to higher critical applied loads (60% - 70% under dry condition and 20%-30% under wet condition) for the on-set of progressive composite fatigue damage. Similar behaviour was also reported by Gassan *et al.* [182] on investigations of tension-tension fatigue of natural fibre reinforced composites (made by resin transfer moulding), where 10%-30% increase in values of CAS for damage initiation were achieved via application of alkaline and saline coupling agents. Flexural fatigue studies conducted on UD glass fibre reinforced epoxy composites revealed that a stronger fibre/matrix interface via treatment using a commercial silane coupling agent delayed the matrix cracking, thus increasing the fatigue life of the UD composites by ~20% [217, 218].

It was also observed that the LS composites had significantly lower failure strain ($p<0.05$) than the ISP composites (equivalent V_f), which exhibited that the ISP

composites could sustain increased plastic deformation and damage than their LS counterparts before fatigue failure (see Figure 5.2). Similar findings were reported for unidirectional glass fibre composites, for which failure strain increased with improved fibre/matrix interfacial properties by applying saline coupling agents [217]. From Figures 5.2a and b, a sudden increase in the failure strain was observed for both LS and ISP composites, where the critical stress levels for the onset of the failure strain increase were found to be identical to the critical loading levels in SDC (60% and 50% of UFS for D-ISP35/50 and D-LS35/50 respectively, 40% for all composites in wet conditions). This relationship between SDC and failure strain for the PCL/PGF composites provided strong evidence that the critical stresses for onset of significant fatigue damage observed in this analysis correlated well and was taken into consideration.

5.5.2. Influence of fluid immersion

It was also observed that the wet testing conditions led to a significant decrease ($p<0.0001$) in the fatigue life of the PCL/PGF composites, with a 10 and 9-fold reduction observed in LS and ISP composites respectively (see Figure 5.1). Deterioration of the fatigue strength in wet conditions was also noted as the slopes of the S-N diagram became significantly steeper from dry to wet conditions (represented by coefficient ‘b’, in Table 5.3). Fluids, such as water and PBS solution, are able to diffuse into fibre reinforced composites and weaken both the matrix as well as the fibre-matrix interface [219]. Our previous study [17] showed that plasticisation of the fibre/matrix interface for both LS and ISP PCL/PGF composites occurred readily in PBS at 37 °C. Degradation of PGFs at or near the PGF fibre/matrix interface within PBS solution can further influence the fibre/matrix bonding leading to reduction of composite mechanical properties.

Degradation of the fibre/matrix interface is known to increase the damage accumulation rate under cyclic fatigue loading, hence significantly reducing fatigue life [219, 220]. Similar reductions in fatigue life were also reported by several studies on glass and carbon fibre reinforced composites and degradation of fibre/matrix interface was stated as the main cause [219, 221-223]. Liao *et al.* [221] performed flexural fatigue studies on UD pultruded E-glass/vinyl ester composites in water and NaCl solutions at ambient temperature. They observed significant reductions in fatigue life at low stresses in both media. McBagonluri *et al.* [222] also investigated UD pultruded E-glass/vinyl ester composites subjected to flexural environmental fatigue tests performed in a fluid cell within salt water at 65 °C. They reported that fatigue life was considerably reduced (~55%) due to fluid immersion. Furthermore, a flexural fatigue study conducted by Sumsion *et al.* [224] on UD graphite/epoxy composites in air and in water at ambient temperature, revealed a substantial reduction in fatigue life (~47%) which was suggested to be caused by water attack of fibre/matrix interface.

It was further observed that at high testing stress levels (70% & 80% of UFS), there were no vast difference of the composites fatigue life between dry and wet testing conditions (see Figure 5.1). A significant difference only began to emerge when the composites were tested at lower stress levels (30%~60% of UFS). This behaviour suggested that damage accumulation progressed slower at lower stress levels for LS and ISP composites. Meanwhile, higher stress levels resulted in stress-dependent fatigue behaviour leading to faster damage accumulation. This behaviour was also reported by Liao *et al.* [221] investigating fatigue behaviour of E-glass/vinyl ester composites, which showed that the composites fatigue life was stress-dominated at higher stress levels.

It was evident from Figure 5.3a that, in the dry environment, an initial increase in stiffness at the early stage of the composites' fatigue life (~5% of N_f) had occurred, before the gradual decline to failure. One possible explanation was due to the presence of voids and void tunnels inside the composites, which had perhaps closed due to the applied cyclic loading, making the composites more compact and stiffer. This explanation was supported by the fact that the LS composites showed a larger increase in stiffness than the ISP composites (see Figure 5.3a), and it was previously reported that LS composites generally possessed higher void content than their ISP counterparts [17]. However, it is very difficult to observe or measure this behaviour during the fatigue tests, which distinctive proves of the voids collapsing were not found.

Another possible explanation for this observation could be due to reorientation of any initially off-axis fibre filaments. During the fibre manufacture, the initial fibres collected on the fibre winding drum were sprayed with PCL solution (mixed with Chloroform) to maintain alignment. However, the removal of PCL coated fibre from the drum and the insertion into the composite manufacturing moulds could have caused some fibres to become misaligned. Furthermore, since the phosphate glass fibre mat was bound with PCL prior to moulding, the high temperature and pressure during LS and ISP composites manufacture could have induces a level of off-axis fibre filaments, which could have potentially become unidirectionally reoriented during the fatigue cyclic loading, consequently leading to the initial increase in stiffness observed. Similar behaviour was observed in natural fibre reinforced polyester composites, in which the fibrils of the plant fibre reoriented during tensile fatigue tests and initially increased the composite stiffness [225, 226]. In addition, Betanzos *et al.* [168] applied cyclic

pressure during the compression moulding stage of PLA/PGF composites, where the composites showed significantly lower void levels, stronger fibre/matrix interfacial bonding, more uniform fibre alignment and an increase in flexural modulus. It must be noted that the initial stiffness increase was not expected and is rarely observed, further investigations into this cause will be required.

However, Figure 5.3b showed that the stiffness increase diminished in wet conditions, replaced by a significant decrease in stiffness from the beginning of the fatigue tests. The same change in stiffness variation was also observed when composites were tested at higher stress levels (> 50% UFS) in dry conditions. Both variations can be explained by the earlier onset and faster progress of fatigue damage caused by media attack and increased testing stresses. With the fibre/matrix de-bonding and/or fibre fractures occurring inside the composites, the effects of voids and void channels closing and/or fibre filament reorientation were insignificant. Moreover, fibre/matrix interface failure occurs readily near the void sites, which could considerably reduce the chances of voids closing due to cyclic loading [147, 227].

The wet environment also had a clear effect on the PCL/PGF composites' fatigue failure modes. Figure 5.6 showed that the dominant failure mode in the dry condition was compressive delamination and interlaminar shear fracture for the LS composites, whilst a clean centre fracture was observed for the ISP composites. Immersion in PBS at 37 °C led to a distinctly more ductile behaviour (composite softening) for both LS and ISP composites, which resulted from significant weakening of the fibre matrix interfaces. Figure 5.6f even showed the fibres sliding out sideways as the loading cycles continued, indicating loss of the fibre/matrix interface had occurred. Comparing Figures 5.2a and b, the overall

strain to failure was significantly increased ($p<0.01$) by the introduction of PBS for both LS and ISP composites, which correlated well with the change from brittle to more ductile dominated failure mode. This suggested that considerably more plastic deformation and fatigue damage had occurred in wet conditions. The immersion in PBS solution also led to lower CAS values (see Table 5.4), which indicated that earlier onset of progressive fatigue damage had occurred for the wet composites.

5.5.3. Influence of fibre content

It is well known that the mechanical properties of fibre reinforced composites can be adjusted by varying their V_f. The behaviour of fibre reinforced composites under cyclic loading is also significantly affected by fibre content [228, 229]. In the dry condition, the static data in Table 5.2 showed that the UFS increased with increasing V_f for both LS and ISP composites. Meanwhile, in the wet condition, the UFS decreased with increasing V_f for both LS and ISP composites. As mentioned earlier, the reduction in UFS was mainly caused by plasticisation due to PBS ingress along the fibres disrupting the fibre/matrix interface, which severely reduced interfacial strength, and hence the reduction in UFS was seen. With increasing fibre content, there was much greater fibre/matrix interfacial area, hence the reduction of UFS was found to be more substantial in the higher volume fraction composites.

Regardless of the testing conditions, it can be seen from Figures 5.1a and b that the composites' fatigue life decreased significantly ($p<0.01$) with increasing fibre content for both LS and ISP composites. Many studies have reported that composite fatigue performance tends to deteriorate with increasing fibre content [230-232]. There are three main reasons responsible for this reduction: (i)

increased fibre-fibre interactions, (ii) increased fibre/matrix interfaces and (iii) increased regions with high local V_f resulting from increased fibre bundle compaction. Although it is widely recognized that the enhancement of composite mechanical properties result from effective stress transfer through fibre/matrix interfaces, it must also be noted that the fibre/matrix interface is also the region subject to the largest stress/strain variation [180]. Thus, micro-cracks mostly tend to initiate and grow from the interfaces [180]. Comparing Figures 5.5a and c to b and d, it was evident that PGFs were significantly more compacted with much more fibres close to or touching each other in the 50% V_f composites in comparison to the 35% V_f composites. This resulted in higher stress/strain gradients at the interface and hence accelerated crack propagation, reducing fatigue life.

In dry conditions, both LS and ISP composites demonstrated a higher CAS value for damage initiation with increasing fibre content (see Table 5.4). However, in wet conditions, a lower CAS value was noted with increasing fibre content for both of the LS and ISP composites (see Table 5.4). This suggested that increasing fibre content could lead to lower stress thresholds for onset of composite fatigue failure in wet conditions. On the other hand, no significant difference ($p>0.05$) was found in the degradation rate of composites fatigue strength (b coefficient) between 35% and 50% V_f composites when the same manufacturing process was applied (see Table 5.3). This indicated that the degradation rate of fatigue strength could be independent from fibre content for both LS and ISP PCL/PGF composites. This behaviour also suggested that increasing fibre content didn't have a significant effect on the rate of fatigue damage accumulation. Similar behaviour of fibre reinforced composites was also

reported by Shah *et al.* [233] where no significant variation in degradation rate of fatigue strength was noted due to varying fibre content for natural fibre composites.

This chapter reports for the first time the cyclic fatigue behaviour of fully bioresorbable PCL/PGF composites. Studies demonstrated that ISP composites had a significantly longer flexural fatigue life ($p<0.0001$) and superior fatigue damage resistance in comparison to their LS counterparts. The presence of media (PBS in this case) substantially reduced the performance of the PCL/PGF composites in both fatigue life and damage resistance. Increasing fibre content (from 35% to 50%) also resulted in reduced fatigue life, but no significant difference was observed for the degradation of composites fatigue strength and damage accumulation behaviours. Amongst all the composites investigated, the ISP35 samples showed a minimum fatigue life of 10^5 and 10^6 cycles up to 50% test stress levels in dry and wet conditions respectively (see Figure 5.1). The ISP35 also maintained at least 50% of its initial stiffness and strength (~6.5 GPa; ~ 85 MPa) at the end of the fatigue tests in both dry and wet conditions (see Figure 5.3), which was comparable to the flexural properties of human cortical bone (5 – 23 GPa; 35-250 MPa) [189]. Therefore, it can be advised that the fatigue life and the degradation profile of fatigue strength observed for ISP35 composites were well matched with human cortical bone, suggesting their potential suitability for bone fracture fixation applications.

5.6. Conclusions

Wet and dry fatigue behaviour of PCL/PGF composites (ISP and LS) was investigated in this chapter. Significantly longer flexural fatigue life ($p<0.0001$) and superior fatigue damage resistance were observed for ISP composites in

comparison with LS composites in both dry and wet conditions, which indicated that the ISP process promoted considerably stronger interfacial bonding than the LS process. Immersion in PBS during the flexural fatigue tests resulted in significant reduction ($p<0.0001$) of the composites fatigue life, earlier onset of fatigue damage and faster damage propagation. This was attributed to interface plasticisation (fibre/matrix) caused by PBS diffusion, which resulted in severely weakened interfacial strength, thus adversely affecting both the quasi-static and fatigue performances of the PCL/PGF composites. Regardless of testing conditions, increasing fibre content (from 35% to 50%) resulted in shorter fatigue life for the PCL/PGF composites. However, the degradation rate of fatigue strength and damage accumulation rate were not significantly affected by increasing the fibre content. Interlaminar shear fracture and clean centre fracture were observed as the dominant failure modes for LS and ISP composites respectively in the dry condition. Meanwhile, media immersion resulted in both LS and ISP composites being softened during the fatigue tests, which led to a more ductile failure mode.

In conclusion, this chapter demonstrated for the first time the flexural cyclic fatigue behaviour of fully bioresorbable ISP and LS PCL/PGF composites. ISP35 maintained at least 50% of its flexural strength and modulus after the fatigue tests, which was well within the range of the mechanical properties of the human cortical bone.

Chapter 6. Heated *In-situ* Polymerisation *vs.* Laminate Stacking for Fully Bioresorbable PGF Reinforced PLA Based Polymer Composites: *In-vitro* Degradation, Mechanical Retention and Cytocompatibility Behaviour

6.1. Summary

Composites (PLA and PLA-PCL copolymer as matrix) with 35% V_f were manufactured via ISP and, as a comparison group, PLA composites with the same V_f were produced via a conventional LS process. The PLA-PCL copolymers exhibited relatively lower glass transition temperature (T_g) values compared to neat PLA, which resulted in accelerated reduction in mechanical properties of the PLA-PCL/PGF composites, with both the flexural strength and modulus decreased below the range of mechanical properties for human cortical bone within 7 days immersion within PBS. The accelerated degradation behaviour also found the PLA-PCL/PGF composites to have a negative impact on the cell viability. Furthermore, ~22% and ~13% higher initial (non-degraded) flexural strength and modulus values were achieved by ISP PLA/PGF composites compared to LS counterparts (~450 MPa and ~24 GPa for ISP PLA/PGF composites vs. ~310 MPa and ~18 GPa for LS PLA/PGF composites respectively). ISP PLA/PGF composites also achieved significantly prolonged mechanical retention (up to 15 days, $p<0.01$) during degradation within PBS at 37 °C in comparison to the LS counterparts. Good cell viability was found for the ISP PLA/PGF composites throughout the cytocompatibility study. Conclusively,

PLA/PGF composites manufactured via heated ISP process exhibited the most attractive combination of mechanical retention profiles and cytocompatibility performances for the intended application of bone fracture fixation devices.

6.2. Introduction

Previous studies (chapter 4 and 5) showed that the room temperature ISP process has its ability in enhancing the mechanical and degradation performances of PGF reinforced polymer composites. However, taking into consideration the properties of human bone, the PGF reinforced composites produced via room temperature ISP using PCL as matrix material resulted in flexural modulus and strength ranging from 5 – 14 GPa and 70 – 160 MPa respectively (significantly lowered after 1 day immersion within PBS at 37 °C, see Chapter 4), thus making the PCL/PGF composites suitable for applications in cancellous bone repair (for which the modulus & strength ranged between 0.4 – 1.5 GPa and 7 – 40 MPa respectively) [20, 36, 88]. However, the properties of these composites were still not sufficient to support cortical bone repair (modulus & strength properties ranging between 5 – 23 GPa and 35 – 250 MPa respectively) [46, 47].

The mechanical performance of these composites was limited to the low virgin matrix properties of PCL, for which approximately ~0.35 GPa and ~20 MPa have been reported for the flexural modulus and strength, respectively [17, 192, 234]. By contrast, PLA exhibits much higher mechanical properties, with ~4 GPa and ~100 MPa respectively for flexural modulus and strength [29, 68, 158, 167]. PLA/PGF composites manufactured via LS process also revealed significantly higher flexural properties than PCL/PGF composites, with flexural modulus and

strength values of ~18 GPa and ~300 MPa respectively (with 35% V_f) having been reported [16, 18].

In this chapter, a novel heated ISP system was established for the first time to manufacture PLA/PGF composites. Initially copolymerisation of PLA-PCL/PGF composites with two different compositions (9:1 and 8:2 for mass ratio of PLA to PCL) were explored to reduce the temperature requirements to liquefy the monomer mixture and to make processing easier, whilst retaining a high proportion of the PLA matrix material. Following the successful development of PLA-PCL *in-situ* copolymerisation, ISP for manufacture of neat PLA composites was also developed. PLA/PGF composites were produced via LS to serve as a control group. The composites produced were evaluated via *in-vitro* degradation, mechanical, chemical, thermal, imaging and cytocompatibility analysis to assess their suitability for bone fracture fixation applications.

6.3. Materials and methods

6.3.1. Materials

Please refer to Section 3.3 for details.

6.3.2. Polymerisation characterisation

6.3.2.1. Kinetic study

The detailed procedures were described in Section 3.9.1.2.

6.3.2.2. Viscosity study

The detailed procedures were detailed in Section 3.9.2.

6.3.3. Phosphate based glass and glass fibre production

Detailed parameters and procedures were stated in Section 3.4 and 3.5 for phosphate glass and its glass fibre production respectively.

6.3.4. PGF reinforced composites manufacture

6.3.4.1. Laminate stacking for PLA/PGF composites production

Detailed procedures were presented in Section 3.6.2.

6.3.4.2. PLA-PCL *in-situ* copolymerisation

Detailed procedures were carried out as described in Section 3.10. Reaction parameters for PLA-PCL and PLA polymerisation are detailed in Table 6.1.

Table 6.1 *Reaction parameters for PLA-PCL and PLA polymerisation*

Sample code	Molar ratio of [(Di-lactide : ε-caprolactone) : Benzyl alcohol : $Sn(Oct)_2$]; Reaction Temperature
ISP-PLA ISP-35%	[(1000 : 0) : 0.1 : 1]; 160 °C
ISP-9-1 ISP-35%-9-1	[(900 : 100) : 0.1 : 1]; 160 °C
ISP-8-2 ISP-35%-8-2	[(800 : 200) : 0.1 : 1]; 160 °C

6.3.4.3. PLA *in-situ* polymerisation

Please refer to Section 3.10 and Table 6.1 for detailed procedures.

6.3.5. Characterization

6.3.5.1. Burn off test

Please refer to Section 3.13.6 for detailed procedures.

6.3.5.2. Differential Scanning Calorimetry (DSC)

Please refer to Section 3.13.8 for detailed procedures.

6.3.5.3. Degradation study

The details for the specimen preparation and property measurement were listed in Section 3.13.1. The equipment and specifications for flexural testing were

detailed in section 3.13.2. The molecular weight variation during the degradation study was also monitored via the GPC, which was detailed in Section 3.13.3.

6.3.5.4. Scanning Electron Microscopy (SEM)

Please refer to Section 3.13.5 for detailed procedures.

6.3.5.5. Neutral Red Cytocompatibility Study

Please refer to Section 3.13.9 for detailed procedures.

6.3.5.6. Statistical Analysis

Please refer to Section 3.13.10 for detailed procedures.

6.4. Results

6.4.1. Kinetic study for PLA polymerisation

6.4.1.1. Effects of catalyst concentration

Figure 6.1 shows the monomer conversion of PLA reached ~98% at ~130 mins, ~170 mins and ~270 mins when the concentration of the catalyst $Sn(Oct)_2$ was 0.0138 mol/L, 0.0069 mol/L and 0.00138 mol/L respectively (reaction temperature and initiator benzyl alcohol concentration were kept constant). No significant polymerisation induction time was observed for all PLA polymerisations.

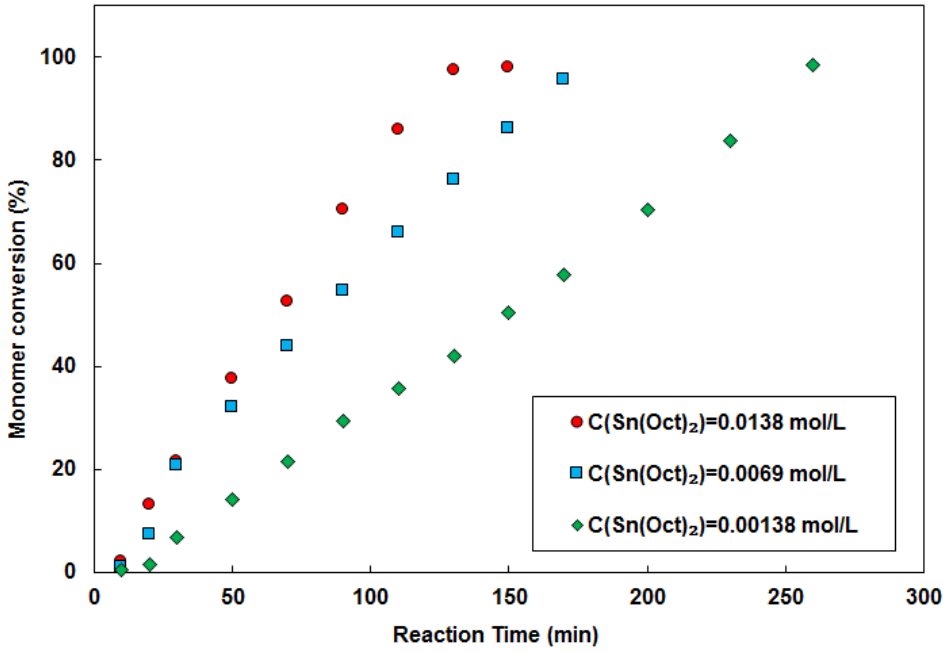

Figure 6.1 *Monomer conversion rate at various $Sn(Oct)_2$ concentrations for PLA polymerisation (benzyl alcohol concentration kept at 0.00115 mol/L and the polymerisation temperature kept at 160 °C)*

Figure 6.2 demonstrates the molecular weight (M_w) against the monomer conversion during polymerisation with all 3 catalyst concentrations. With all 3 catalyst concentrations for PLA polymerisation, the M_w all reached ~40000 Da when the monomer conversion is close to complete (>95%). It should be noted that the PDI for all PLA polymerisation during kinetic study was ~1.5.

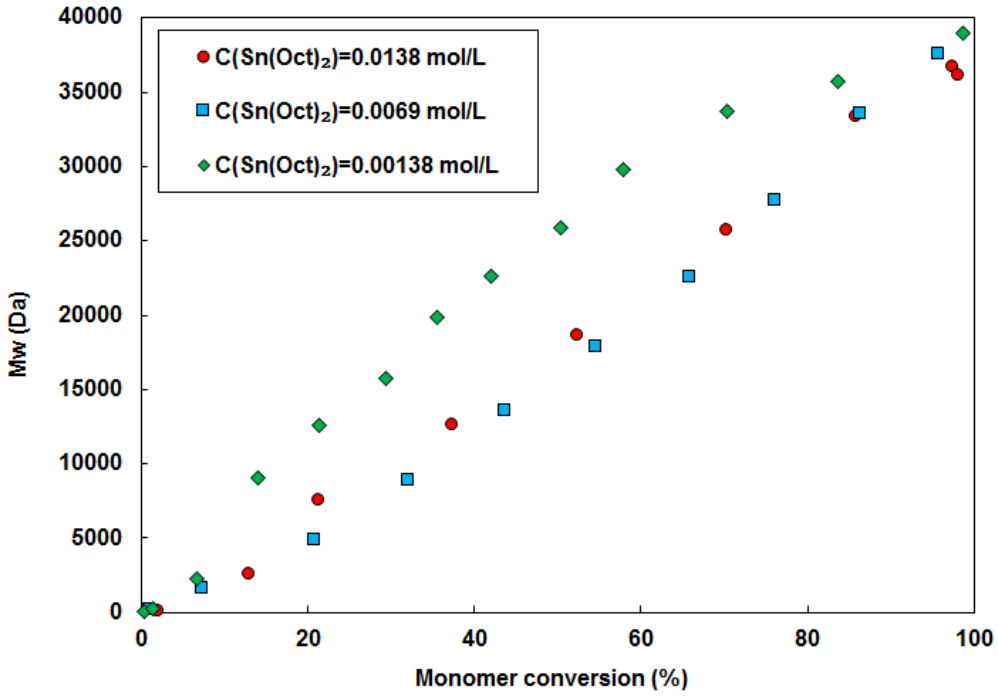

Figure 6.2 *M_w against monomer conversion rate at various $Sn(Oct)_2$ concentrations for PLA polymerisation (benzyl alcohol concentration kept at 0.00115 mol/L and the polymerisation temperature kept at 160 °C)*

6.4.1.2. Effects of initiator concentration

According to Figure 6.3, the monomer conversion of the PLA polymerisation with different benzyl alcohol concentrations all reached ~98% after ~130 mins (reaction temperature and $Sn(Oct)_2$ concentration kept constant). No difference with statistical significance ($p>0.05$) was observed between all 3 monomer conversion profiles.

Figure 6.4 shows that the M_w reached ~10000 Da, ~36000 Da and ~59000 Da when the monomer conversion was ~98% with concentration of the initiator being 0.0115 mol/L, 0.0023 mol/L and 0.00115 mol/L respectively.

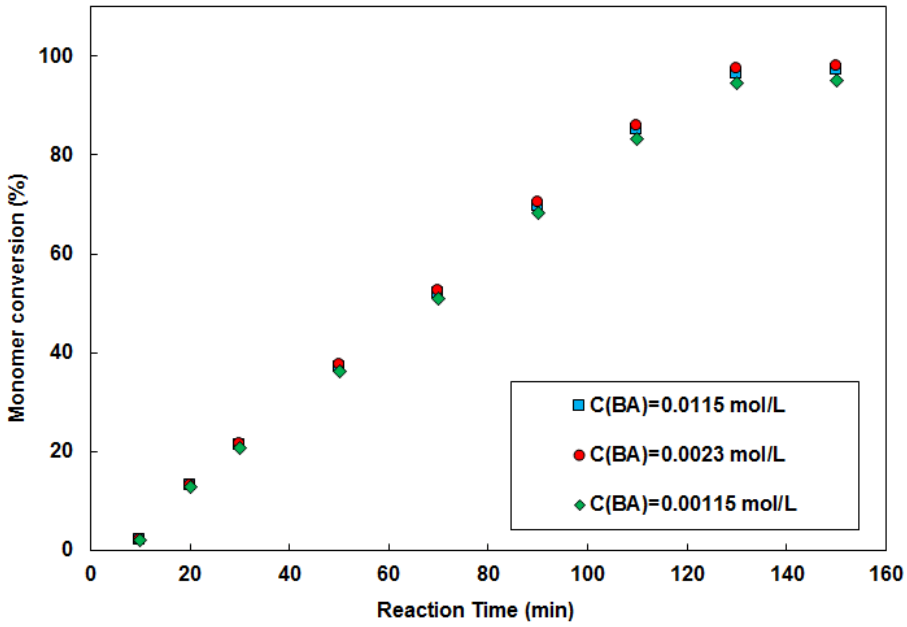

Figure 6.3 *Monomer conversion at various benzyl alcohol concentrations for PLA polymerisation ($Sn(Oct)_2$ concentration kept at 0.0138 mol/L and the polymerisation temperature kept at 160 °C)*

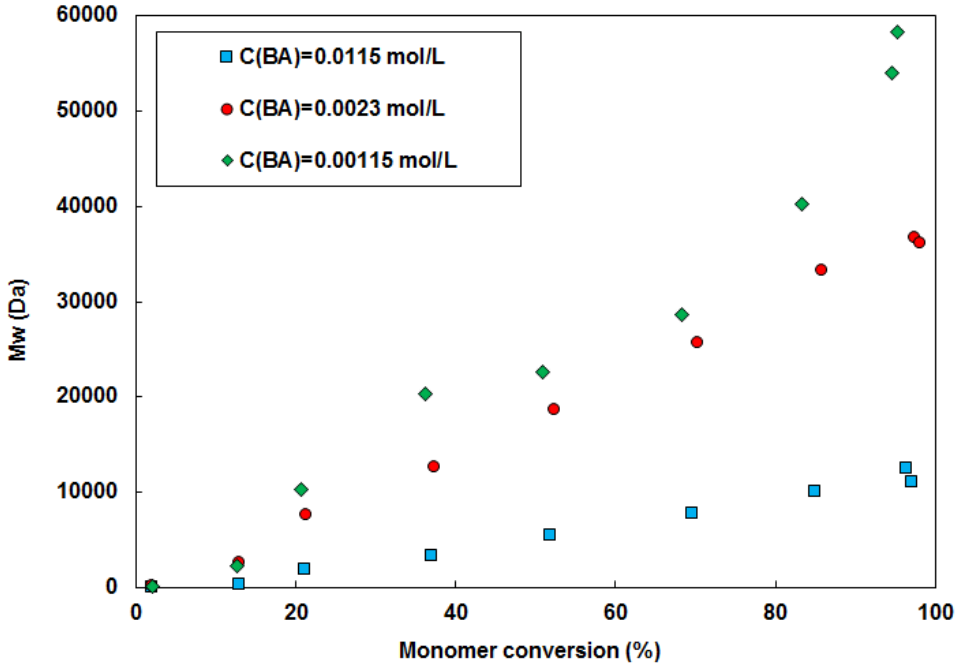

Figure 6.4 *M_w against monomer conversion rate at various Benzyl alcohol concentrations for PLA polymerisation ($Sn(Oct)_2$ concentration kept at 0.0138 mol/L and the polymerisation temperature kept at 160 °C)*

6.4.1.3. Effects of polymerisation temperature

Figure 6.5 demonstrates that the monomer conversion of PLA reached ~98% at ~120 mins, ~160 mins and ~280 mins when the reaction temperature was 160 °C, 140 °C and 120 °C respectively.

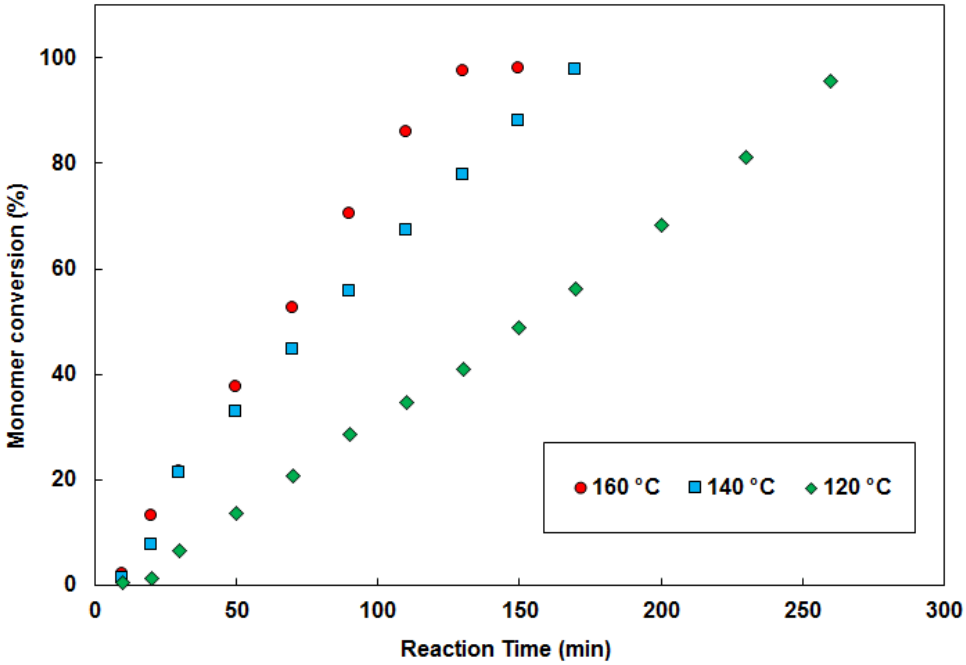

Figure 6.5 *Monomer conversion at various reaction temperatures for PLA polymerisation ($Sn(Oct)_2$ concentration kept at 0.0138 mol/L and benzyl alcohol concentration kept at 0.00115 mol/L)*

Regarding to Figure 6.6, when the monomer conversion reached ~98%, M_w of ~45000 Da was obtained when PLA was polymerised at 120 °C, 140 °C and 160 °C.

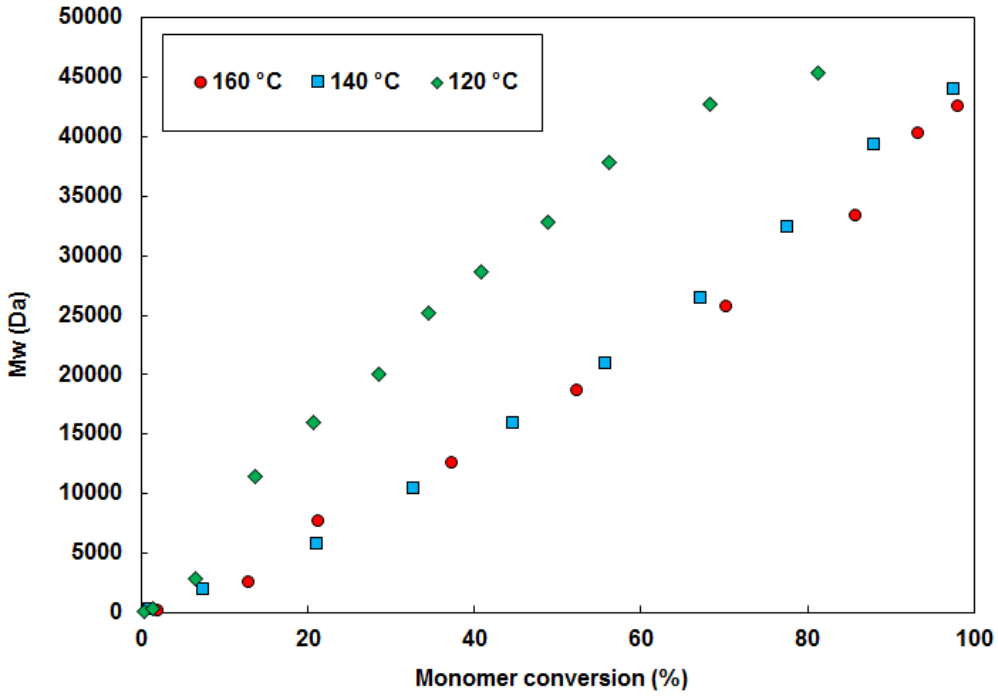

Figure 6.6 *M_w against monomer conversion rate at various reaction temperature for PLA polymerisation ($Sn(Oct)_2$ concentration kept at 0.0138 mol/L and benzyl alcohol concentration kept at 0.00115 mol/L)*

6.4.2. Kinetic study for PLA-PCL copolymerisation

Figure 6.7 illustrates the monomer conversion of PLA reached ~98% after approximately 3 hours for both PLA-PCL copolymerisation with different weight ratios between PLA and PCL (8:2 and 9:1). However, it took ~26 hours and ~28 hours for PCL to reach ~98% monomer conversion with 8:2 and 9:1 weight ratios of PLA:PCL respectively. It should be noted that the final M_w and PDI for all PLA-PCL copolymerisation (monomer conversion > 95%) during kinetic study was ~40000 Da and ~1.4 respectively.

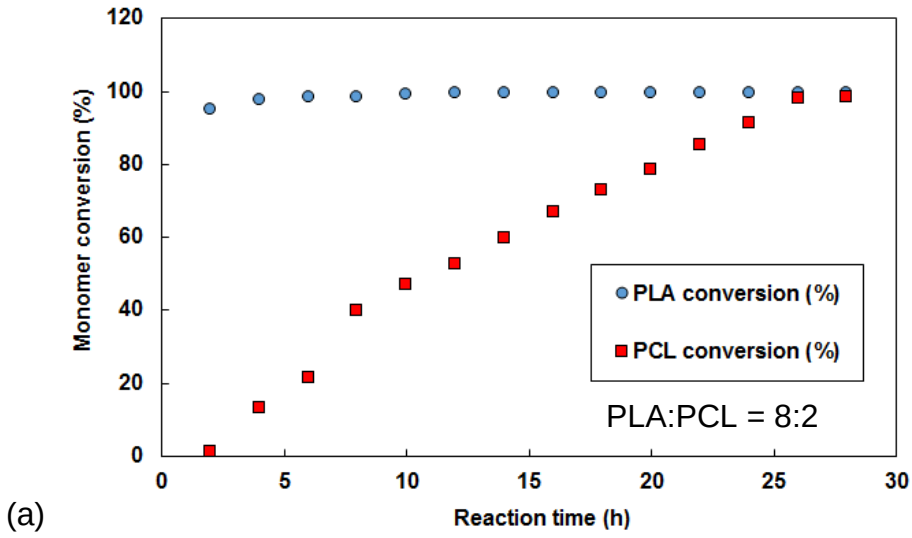

(a)

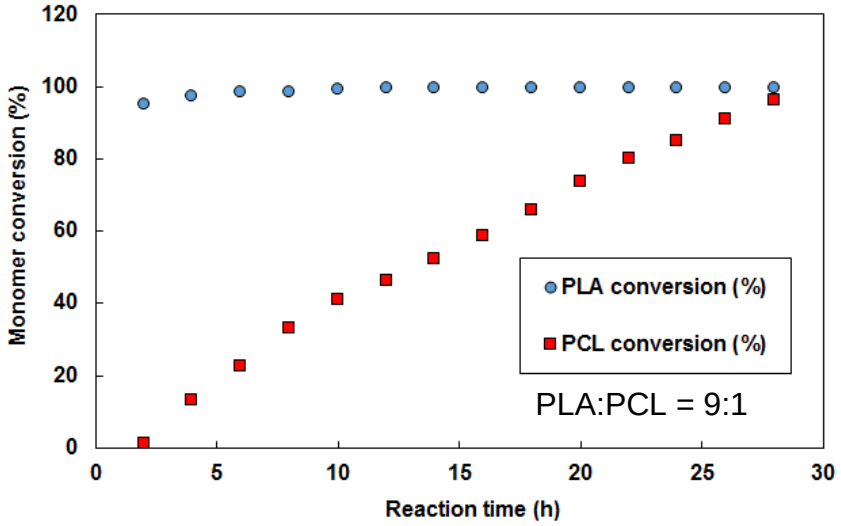

(b)

Figure 6.7 *Monomer conversion of PLA and PCL against reaction time during random PLA-PCL copolymerisation: weight ratio of PLA:PCL (a) 8:2; (b) 9:1 ($Sn(Oct)_2$ concentration kept at 0.0138 mol/L and benzyl alcohol concentration kept at 0.00115 mol/L, reaction temperature kept at 160 °C for all PLA-PCL copolymerisation)*

6.4.3. Viscosity study

Figure 6.8 shows the shear viscosity behaviour for neat monomer ε-caprolactone (CL), neat monomer di-lactide (LA) and their mixtures with increasing temperature. The shear viscosity was monitored from 95 °C as the LA only starts to melt at 95 °C. The shear viscosity of neat CL was measured from 25 °C and

remained the same at ~7 mm^2/s between 25 °C and 170 °C. Meanwhile, the shear viscosity of neat LA gradually decreased from ~1150 mm^2/s (at ~95 °C) to ~10 mm^2/s (at ~160 °C) with increasing temperature. Moreover, the shear viscosity for the mixtures of LA and CL (weight ratio of LA:CL = 8:2 and 9:1) reduced to ~10 mm^2/s at lower temperatures of ~120 °C and ~140 °C respectively.

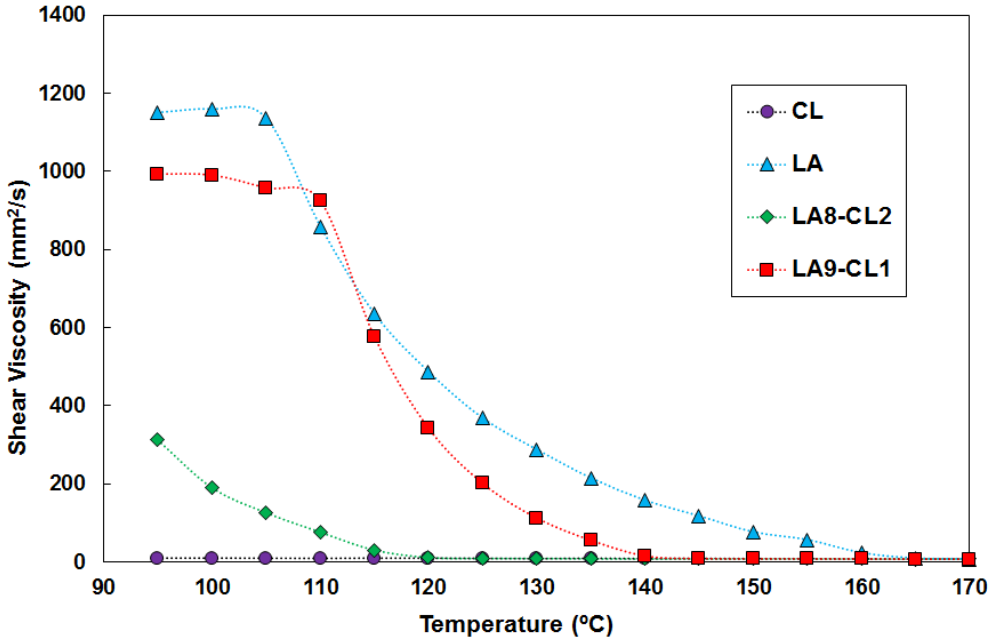

Figure 6.8 *Shear viscosity variation with increasing temperature for neat ε-caprolactone (CL), neat di-lactide (LA) and their mixture (weight ratio of LA:CL = 8:2 and 9:1 for LA8-CL2 and LA9-CL1 respectively)*

6.4.4. Composites fibre volume fraction

Details of the polymers and polymer composite plates produced with their respective sample codes are listed in Table 6.2.

Table 6.2 *Details of resulted polymer and polymer composites with their respective code*

Sample code	Manufacture process	Sample type
LS-PLA	Laminate Stacking (LS)	Neat PLA
LS-35%		PLA/PGF composites
ISP-9-1	*In-situ* Polymerisation (ISP)	Neat copolymer (PLA:PCL = 9:1 Weight fraction)
ISP-8-2		Neat copolymer (PLA:PCL = 8:2 Weight fraction)
ISP-35%-9-1		PLA-PCL/PGF composites
ISP-35%-8-2		PLA-PCL/PGF composites
ISP-PLA		Neat PLA
ISP-35%-PLA		PLA/PGF composites

Table 6.3 shows the actual V_f for all LS and ISP composites obtained from burn-off tests. The determined V_f values were similar to the theoretically expected values (35%).

Table 6.1 *Expected and actual fibre volume fractions of Composites (actual V_f calculated from burn off tests)*

Composites Code	Expected V_f	Actual V_f
LS-35%	35%	33% ± 2%
ISP-35%-PLA		34% ± 1%
ISP-35%-9-1		33% ± 1%
ISP-35%-8-2		35% ± 1%

6.4.5. DSC results

The estimated T_g (from Flory-Fox equation, equation 10 in Section 3.13.8, where -60°C was used for neat PCL [235]) and actual T_g values of PLA, PCL and the PLA-PCL copolymers obtained from DSC measurement are presented in Table 6.4. The DSC traces are presented in Figure 6.9. Differences of 7–10% were found between the actual and estimated T_g values for both ISP-9-1 and ISP-8-2 copolymers. The T_g values of the PLA-PCL copolymers decreased with increasing amounts of PCL within the copolymer composition. Both LS-PLA and ISP-PLA showed very similar T_g values ($p>0.05$) which also agreed with literature values [236].

Table 6.2 *Glass transition temperature estimation and actual values for PLA-PCL copolymers*

Sample Code	Estimated T_g (°C)	Actual T_g (°C)	Reference
PCL	- 60	N/A	[235]
LS-PLA	65	63	[236]
ISP-PLA		62	
ISP-9-1	44	47	This study
ISP-8-2	28	31	This study

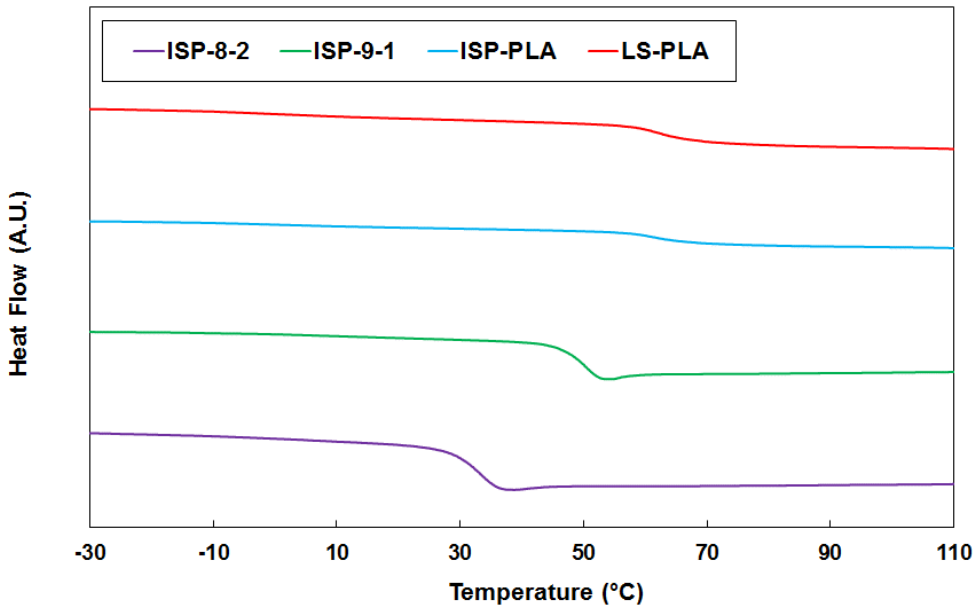

Figure 6.9 *DSC heat flow traces of PLA and PLA-PCL copolymers*

6.4.6. Degradation study

6.4.6.1. Retention of flexural properties

It can be seen from Figure 6.10a and b that both LS-PLA and ISP-PLA maintained their flexural strength (~105 MPa) and modulus (~4 GPa) profiles during the 28-

day immersion period, and no significant differences ($p>0.05$) were observed between LS-PLA and ISP-PLA. In contrast, flexural strength and modulus values of the ISP-9-1 copolymer decreased by ~64% and ~70% respectively within 7 days of immersion (see Figure 6.10a and b), after which a plateau was observed until the end of the study. Similarly, the ISP-8-2 copolymer showed a reduction of ~64% and ~86% in strength and modulus respectively after 1 day of degradation, after which they also maintained a plateau for the duration of the study. In addition, the ISP-9-1 copolymer had significantly higher flexural properties as compared to the ISP-8-2 copolymer ($p<0.01$) over the duration of this study. However, both PLA-PCL copolymers revealed significantly lower strength and modulus ($P<0.0001$) values as compared to the neat PLA samples.

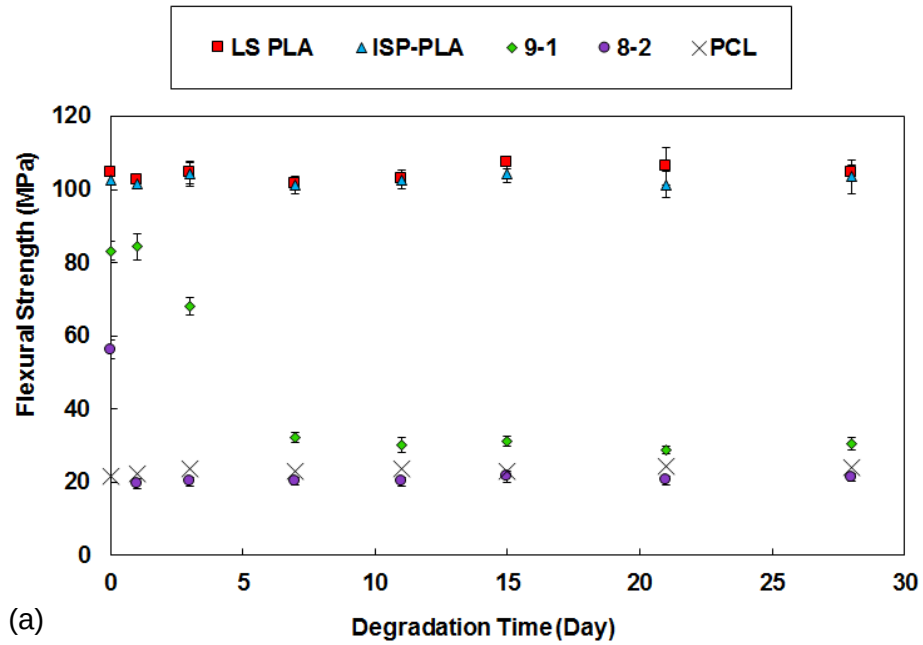
LS PLA
ISP-PLA
9-1
8-2
PCL
Flexural Strength (MPa)
120
100
80
60
40
20
0
0
5
10
15
20
25
30
Degradation Time (Day)

(a)

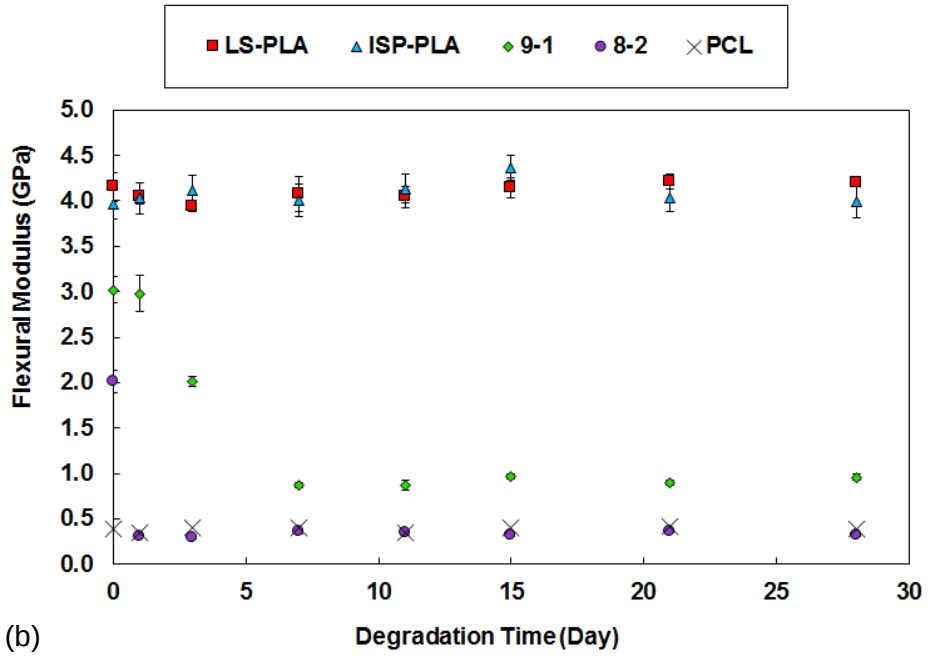
LS-PLA
ISP-PLA
9-1
8-2
PCL
Flexural Modulus (GPa)
5.0
4.5
4.0
3.5
3.0
2.5
2.0
1.5
1.0
0.5
0.0
0
5
10
15
20
25
30
Degradation Time (Day)

(b)

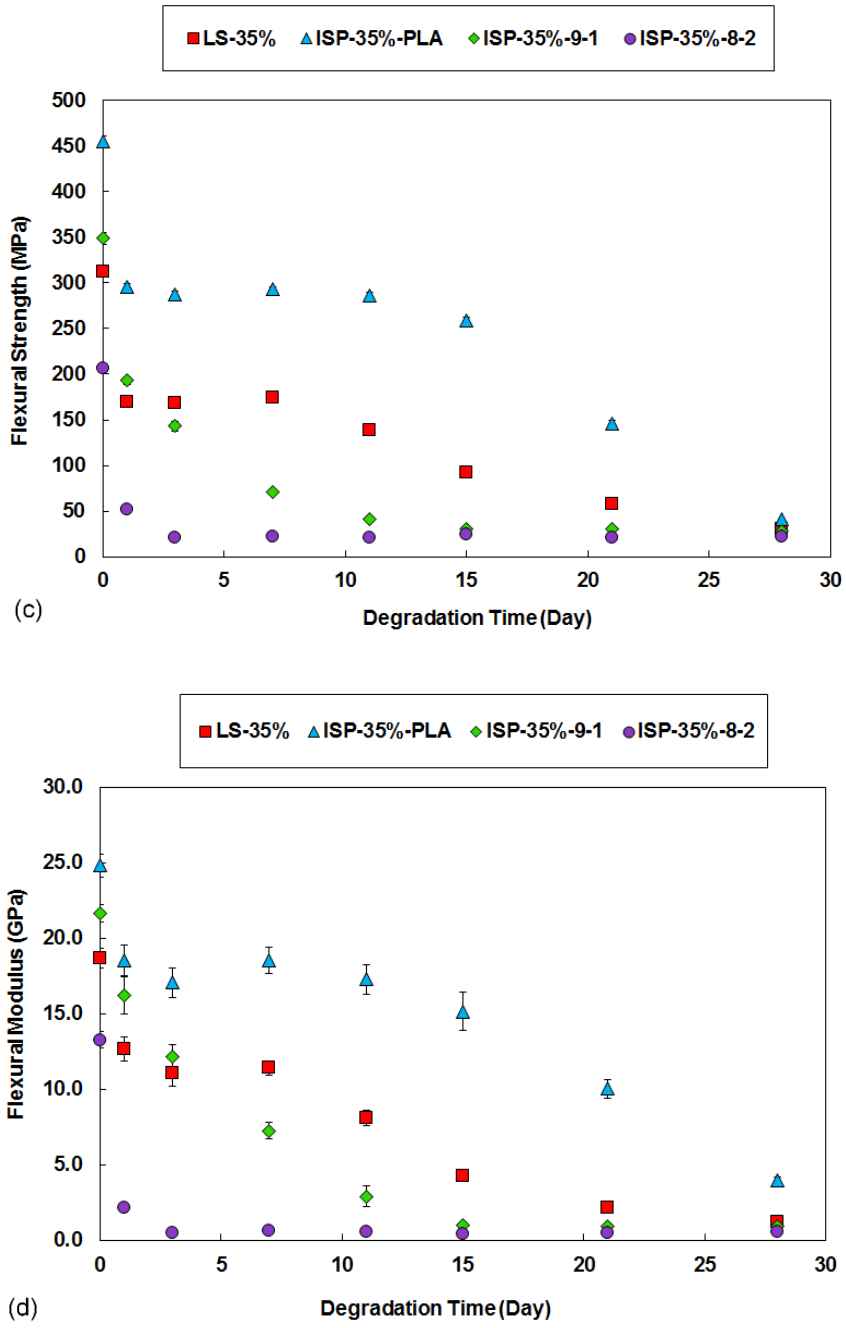

Figure 6.10 *Retention of flexural properties during degradation. For PLA-PCL copolymers and neat PLA: (a) flexural strength; (b) flexural modulus; For PGF reinforced PLA-PCL copolymer and PLA composites: (c) Flexural strength; (d) flexural modulus (PLA-PCL copolymers and their composites were produced via ISP, the neat PLA and their composites was produced via both LS and ISP and denoted separately as LS-PLA, LS-35% and ISP-PLA, ISP-35%-PLA).*

From Figures 6.10c and d, the initial flexural strength and modulus (for dry samples at day 0) of ISP-35%-PLA composite increased by approximately 4 and 6-fold compared to ISP-PLA respectively, whilst the LS-35% composite showed only 3 and 4-fold increase in both strength and modulus with the reinforcement of PGFs compared to LS-PLA. The ISP-35%-PLA composite achieved ~450 MPa strength and ~25 GPa modulus (see Figure 6.10c and d), which were ca. 30% higher ($p<0.01$) than LS-35% composite with the same fibre content. Sharp decreases in flexural strength and modulus were seen for both LS and ISP composites after 1-day immersion in PBS at 37 °C, varying from ~30% for ISP-35%-PLA to ~75% for ISP-35%-8-2. After the reduction, the flexural strength and modulus of LS-35% and ISP-35%-PLA composites reached a plateau until day 7 and day 15 respectively, followed by further gradual reductions until day 28. On the other hand, ISP-35%-9-1 and ISP-35%-8-2 exhibited a gradual decrease in flexural properties from day 1 until day 15 and day 3 respectively, after which their flexural strength and modulus values decreased to ~20 MPa and ~0.5 GPa (lower even than neat PLA, see Figure 4a and 4b) and maintained this value until the end of the study.

6.4.6.2. Water uptake, mass loss and pH variations

Figure 6.11a shows that ISP-PLA and LS-PLA achieved a stable level of water uptake (~0.5%) during the study period. Whereas water uptake for both the ISP-9-1 and ISP-8-2 copolymers revealed a step increase from *ca.* 1% to *ca.* 1.5 and 2% respectively at day 11 followed by a plateau until the end of the study. Both the ISP-9-1 and ISP-8-2 copolymers displayed considerably higher water uptake profiles ($p<0.05$) in comparison to the LS-PLA and ISP-PLA.

In addition, distinctively higher water uptake profiles ($p<0.01$) were seen for the PGF reinforced composites (see Figure 6.12a) when compared to the neat PLA and PLA-PCL copolymers at all time points. Figure 6.12a shows that the water uptake profiles for the composites LS-35%, ISP-35%-PLA and ISP-35%-9-1 revealed a two-stage profile: i) a slow increase up to 7 days reaching ~1%, ii) followed by a fast increase up to 17-24% by the end of the study, with the exception of the ISP-35%-8-2 composite which revealed a sharp linear increase in water uptake throughout the experiment.

The mass loss profiles (see Figure 6.11b) for the PLA-PCL copolymers and neat PLA revealed a gradual increase over the degradation study, although the ISP-8-2 copolymer revealed a significantly higher level of mass loss ($p<0.05$) from day 15 in comparison to the other samples investigated. Meanwhile, LS-PLA, ISP-PLA and ISP-9-1 all had similar mass loss profiles throughout the study period ($p>0.05$). The PLA-PCL copolymers and neat PLA lost between 0.4 - 0.7% of their initial weights after 28 days immersion in PBS at 37 °C. Figure 6.12b showed that the ISP-35%-8-2 composite underwent a gradual and continuous increase in mass loss reaching 18% at day 28. Conversely, two-stage profiles were observed for the other composites: low rate of mass loss until day 11, followed by a fast increase in the mass loss reaching between 12 - 16% by day 28. In comparison, it was seen that all the composite samples experienced substantially higher mass loss ($p<0.0001$) than the neat PLA and PLA-PCL copolymers over the course of the study.

Figure 6.11c showed that the pH of the degradation media for all the PLA and PLA-PCL copolymers did not change significantly ($p>0.05$) and remained approximately neutral throughout the study period. It should be noted that PBS

media was replaced every 3 days during the degradation study. However, both the ISP-9-1 and ISP-8-2 copolymers had lower pH profiles (~4%, $p<0.05$) than LS-PLA and ISP-PLA. It was also noted from Figure 6.12c that all the composite samples exhibited a gradual decrease in pH to 6.5-7 from day 0 to day 28 and that the pH of the degradation media for ISP-35%-9-1 and ISP-35%-8-2 copolymer composites decreased below 7 after one week of immersion in PBS.

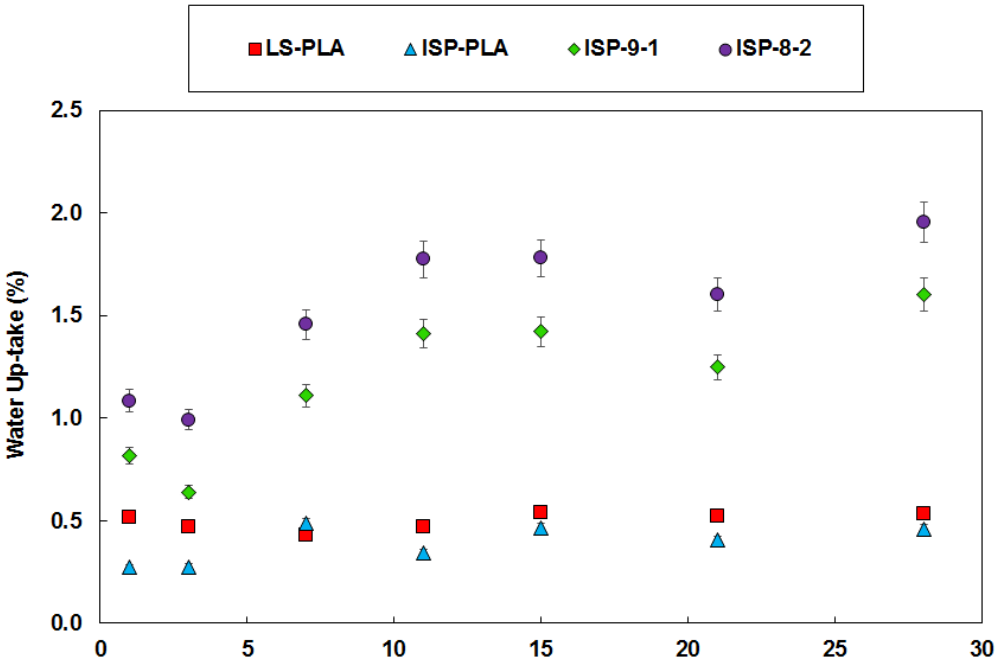
LS-PLA
ISP-PLA
ISP-9-1
ISP-8-2
Water Up-take (%)
Degradation Time (Day)
0.0
0.5
1.0
1.5
2.0
2.5
0
5
10
15
20
25
30

(a)

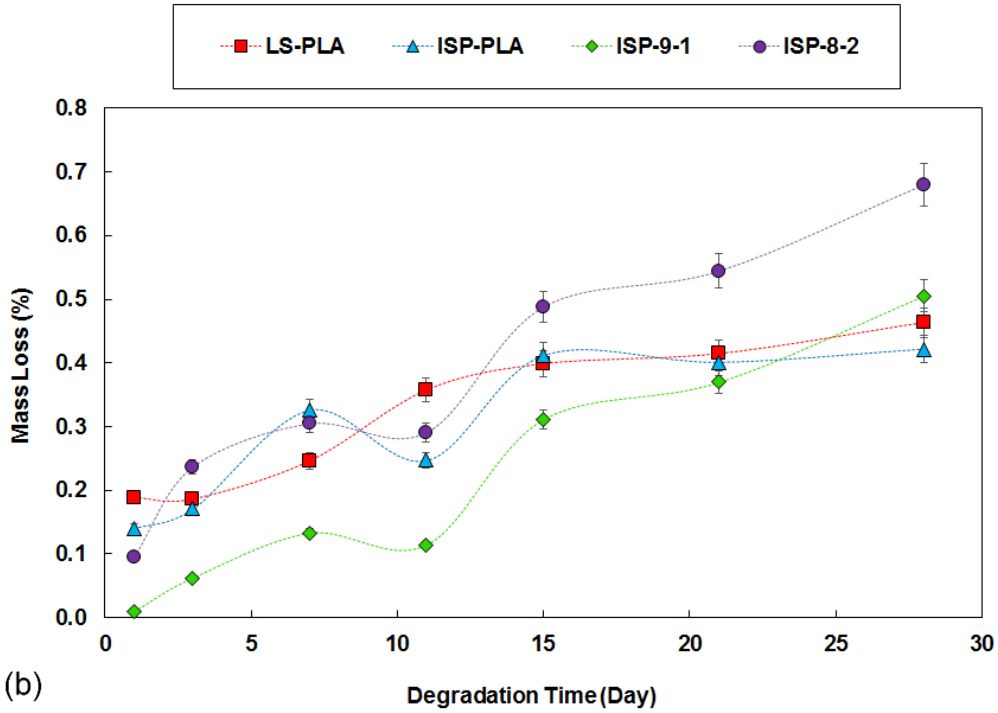
LS-PLA
ISP-PLA
ISP-9-1
ISP-8-2
Mass Loss (%)
Degradation Time (Day)
0.0
0.1
0.2
0.3
0.4
0.5
0.6
0.7
0.8
0
5
10
15
20
25
30

(b)

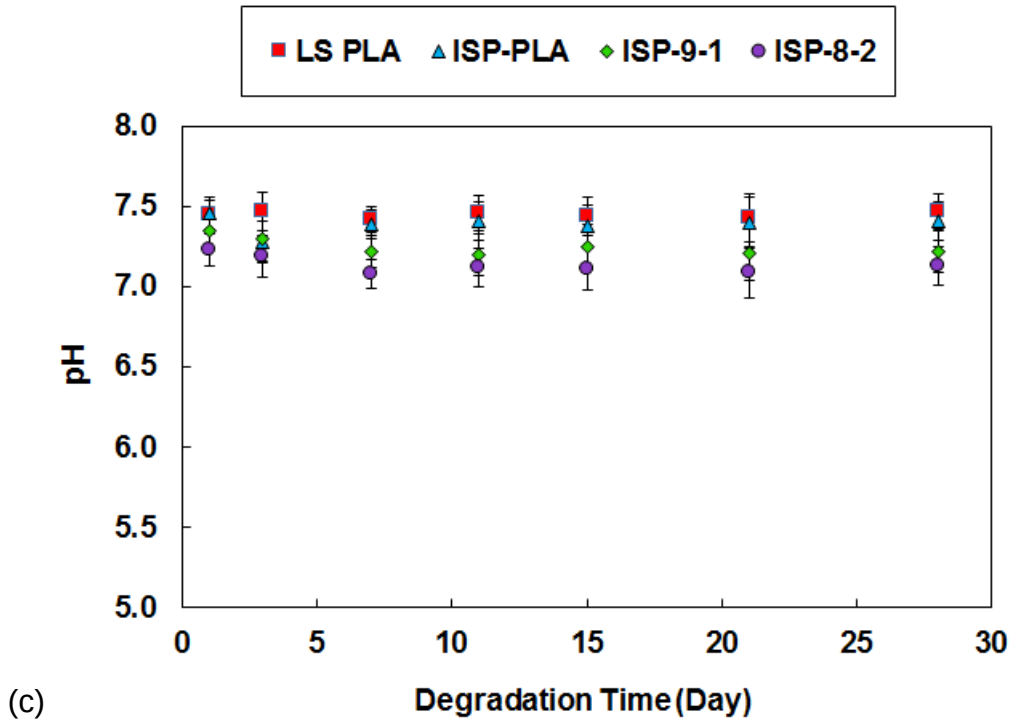

(c)

Figure 6.11 *Degradation behaviour of PLA-PCL copolymers and neat PLA (PLA-PCL copolymers were produced via the ISP* process*, and the neat PLA was produced via both LS and ISP* process *and have been denoted as LS-PLA and ISP-PLA): (a) shows the water uptake variation versus degradation time; (b) shows the mass loss variation versus degradation time (dotted lines have been added as a guideline for the eye); (c) shows the variation in pH of PBS versus degradation time.*

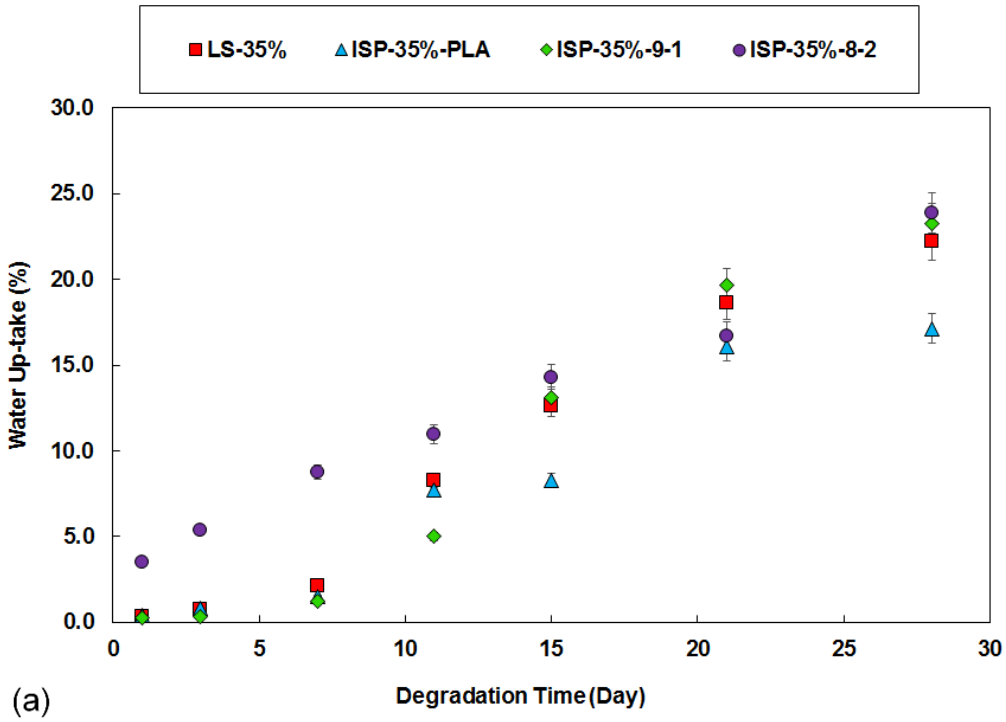
LS-35%
ISP-35%-PLA
ISP-35%-9-1
ISP-35%-8-2
Water Up-take (%)
Degradation Time (Day)
0.0
5.0
10.0
15.0
20.0
25.0
30.0
0
5
10
15
20
25
30

(a)

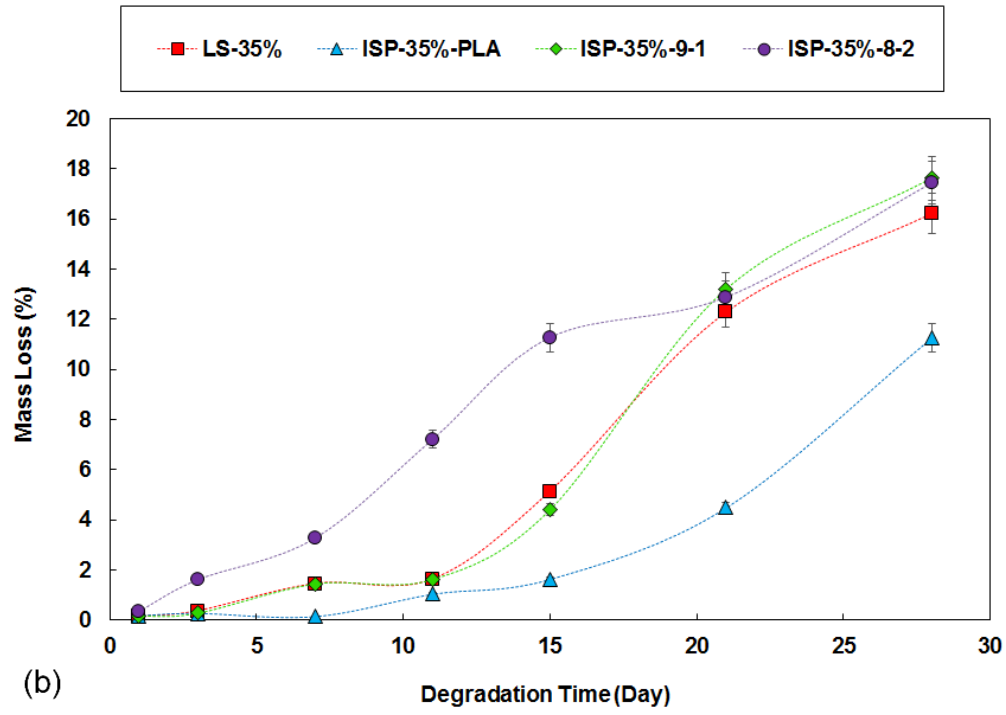
LS-35%
ISP-35%-PLA
ISP-35%-9-1
ISP-35%-8-2
Mass Loss (%)
Degradation Time (Day)
0
2
4
6
8
10
12
14
16
18
20
0
5
10
15
20
25
30

(b)

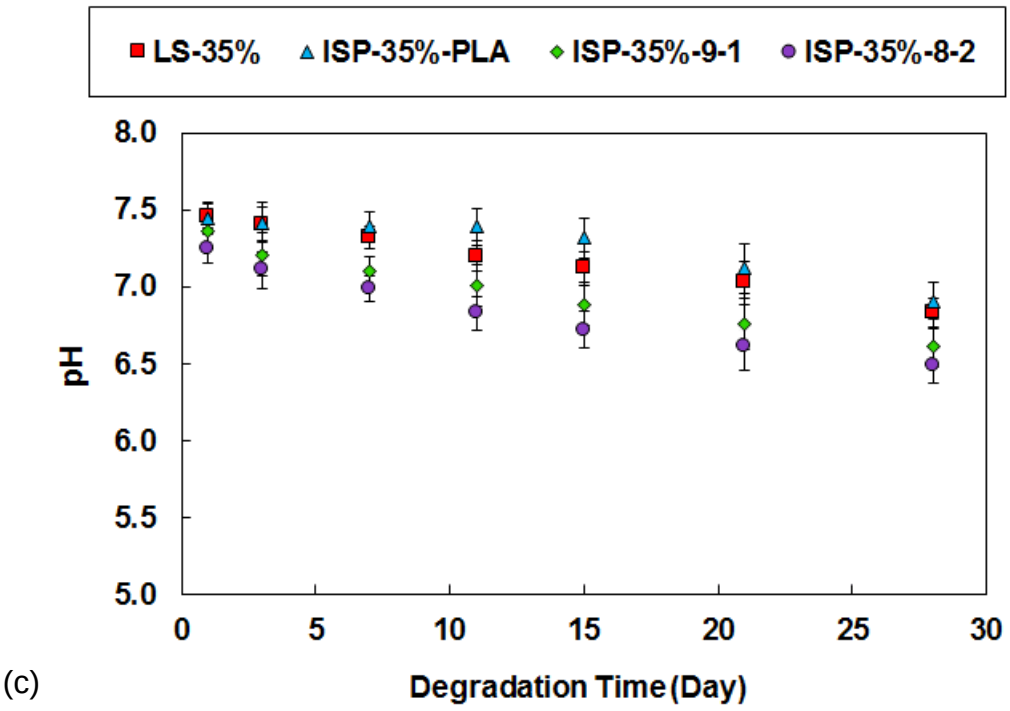

(c)

Figure 6.12 *Degradation behaviour of PGF reinforced PLA-PCL copolymers and neat PLA composites (PGF reinforced PLA-PCL copolymer composites were produced via ISP, the PGF reinforced neat PLA composites was produced via both LS and ISP and have been denoted as LS-35% and ISP-35%-PLA): (a) shows the water uptake variation versus degradation time; (b) shows the mass loss variation versus degradation time (dotted lines have been added as a guideline for the eye); (c) shows the variation in pH of PBS versus degradation time.*

6.4.6.3. Molecular weight variations

It can be seen from both Figure 6.13a and b that the LS-PLA polymer and LS-35% composite had significantly higher molecular weight (40%-50%, $p<0.0001$) than the ISP polymer, copolymers and their PGF composites. ISP-PLA revealed significantly higher molecular weight (~17%, $p<0.01$) in comparison to both the ISP-9-1 and ISP-8-2 copolymers. Similarly, significantly higher molecular weight ($p<0.01$) was also observed for the ISP-35%-PLA in comparison to ISP-35%-9-1 and ISP-35%-8-2.

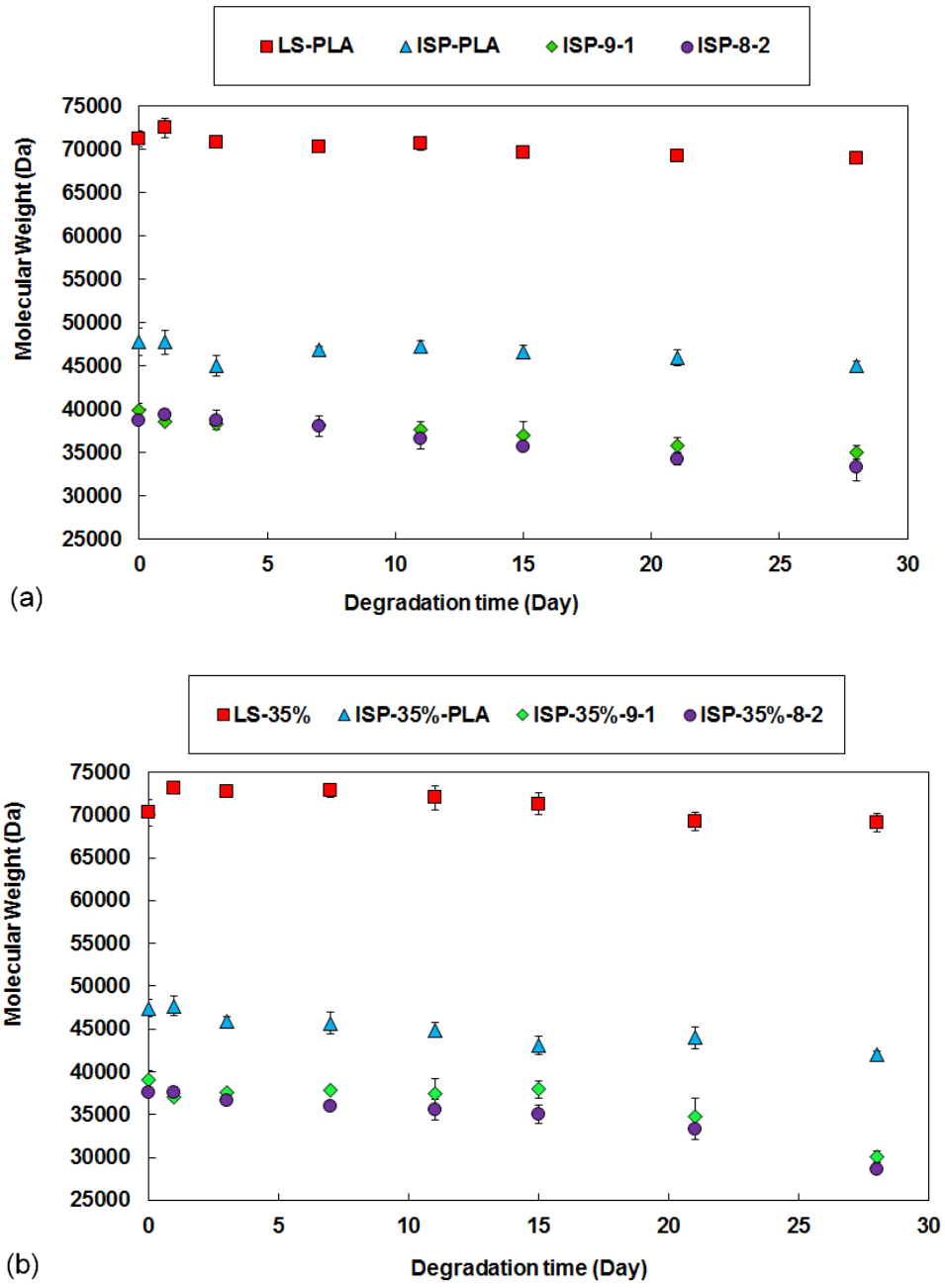

Figure 6.13 *Variation in molecular weight against degradation time for: (a) PLA-PCL copolymers and neat PLA; (b) PGF reinforced PLA-PCL copolymer and PLA composites (PLA-PCL copolymers were produced via ISP, the neat PLA was produced via both LS and ISP and denoted separately as LS-PLA and ISP-PLA).*

A gradual decline in molecular weight over time was found for all the PLA-PCL copolymers, neat PLA and their composite samples. Neat PLA (LS-PLA and ISP-

PLA) and their PGF reinforced copolymers (LS-35% and ISP-35%-PLA) exhibited a slight reduction (3%-5% at day 28) in the molecular weight versus degradation time. Whereas, the PLA-PCL copolymers (ISP-9-1 and ISP-8-2) and their composites (ISP-35%-9-1 and ISP-35%-8-2) exhibited a considerable reduction after day 15 (10%-19% at day 28). In addition, no significant differences ($p>0.05$) in molecular weight were seen for all the PGF reinforced composites when compared with their respective neat polymer or copolymer equivalents.

6.4.7. SEM

Figure 6.14 shows SEM micrographs for the cross sections of the composites during the immersion study, where day 0, day 11 and day 28 are presented. It can be seen for all composites that PGF gradually degraded over time forming channels within the composite structure. Significant fibre degradation could be seen from day 11 for LS-35% and ISP-35%-9-1 composites (see Figure 6.14-a2 and c2). In comparison, ISP-35%-PLA showed no significant fibre degradation at day 11 (see Figure 6.14-b2), with noticeable fibre degradation only observed from day 15. Meanwhile, a substantial amount of fibre degradation was observed from day 7 for ISP-35%-8-2 until day 28 (see Figure 6.14-d3). Furthermore, the LS composites revealed extensive dry fibre bundles and polymer rich zones (see Figure 6.14-a1). In contrast, ISP composites showed good fibre distribution without any significant dry fibre bundles and polymer rich zones (see Figure 6.14-b1, c1 and d1).

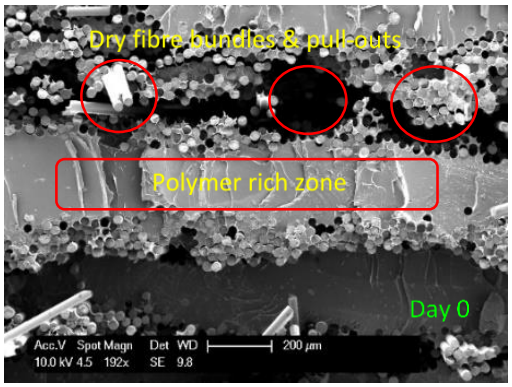

(a1)

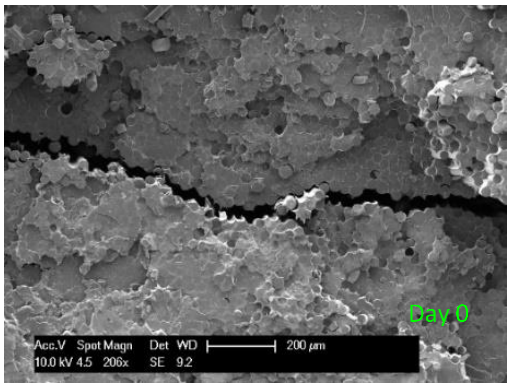

(b1)

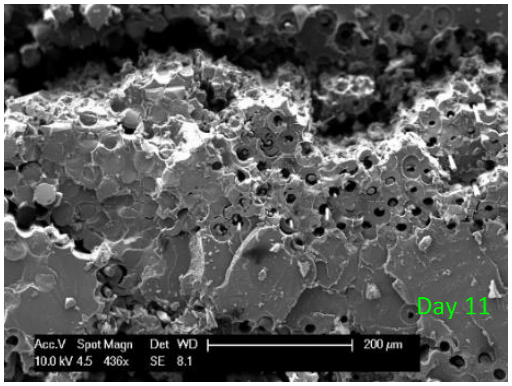

(a2)

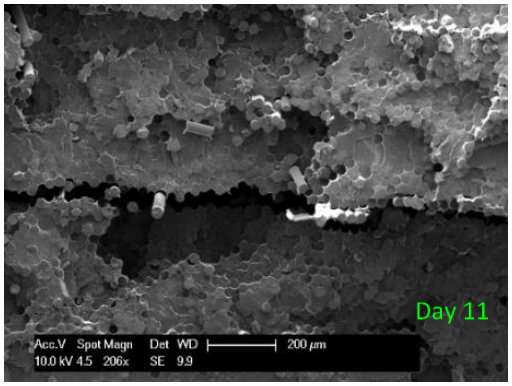

(b2)

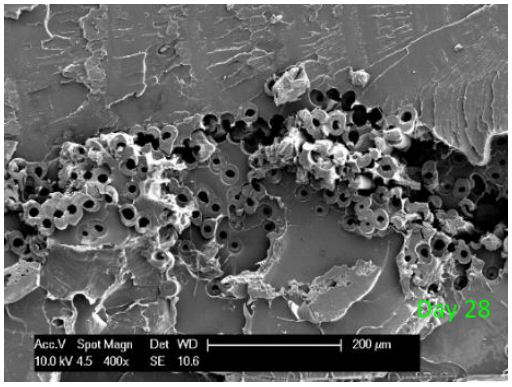

(a3)

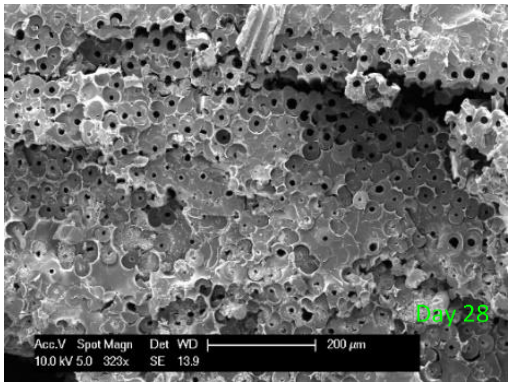

(b3)

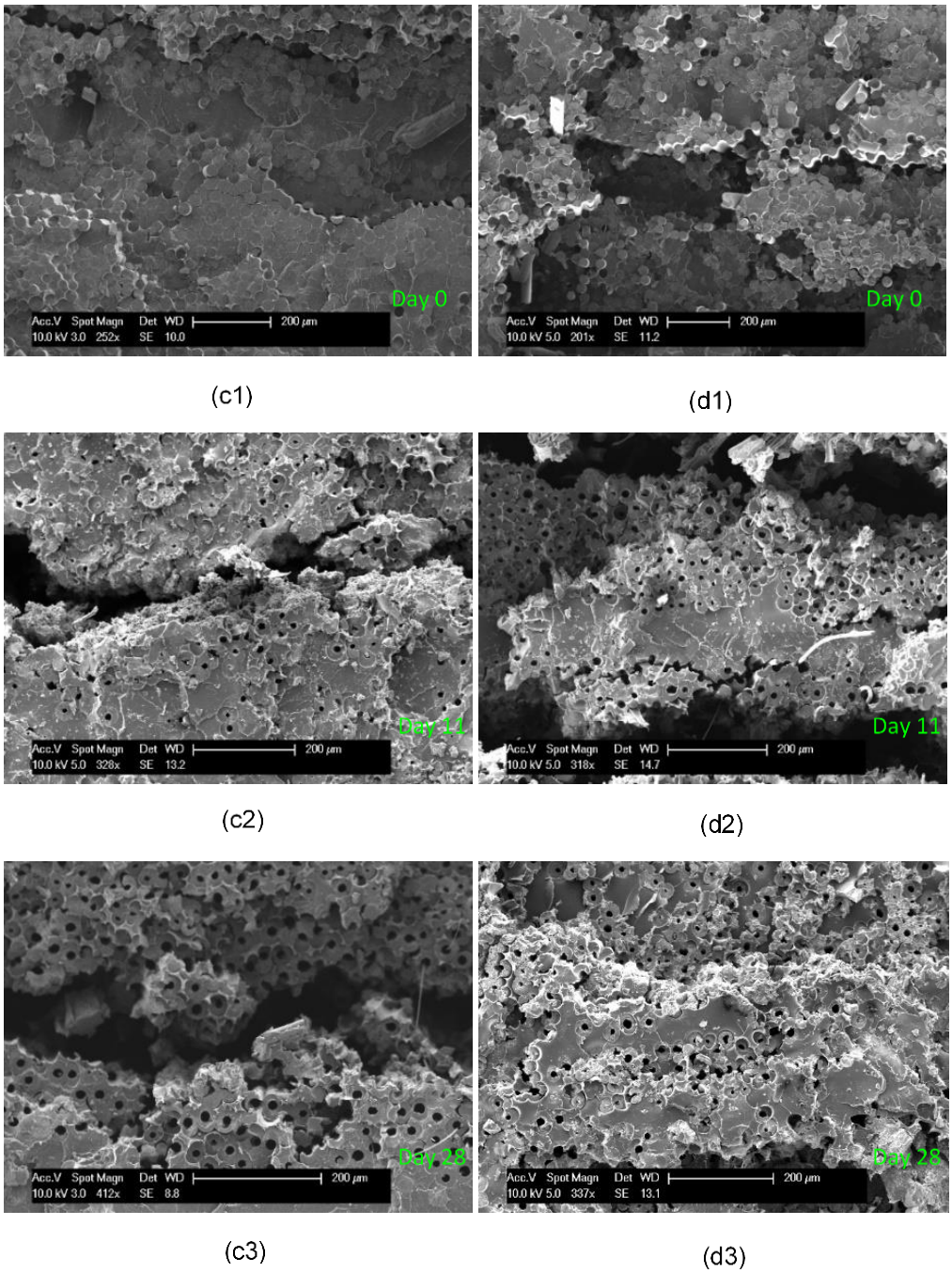

Figure 6.14 *SEM cross section images of the composites during degradation, at day 0, day 11 and day 28: (a1-a3) LS-35%; (b1-b3) ISP-35%; (c1-c3) 9-1-35%; (d1-d3) 8-2-35%. (marker bar length 200 um)*

6.4.8. Cytocompatibility results

Figure 6.15 demonstrates MG63 cell viability when exposed to degradation by-products of neat PLA, PLA-PCL copolymers and their PGF composites via a 7-day neutral red cytotoxicity study. According to ISO 10933, materials are

considered cytotoxic when the neutral red cell viability is lower than 70% of the control. It can be seen that the LS-PLA, ISP-PLA, LS-35% and ISP-35%-PLA samples showed good cell viability throughout the 7-day study. ISP-9-1 and ISP-8-2 appeared to show some level of negative response after being exposed to 1-day immersion by-products, after which their cell viability improved significantly ($p<0.01$) at day 3 and day 7. Thus, the immersion study by-products of neat PLA, PLA-PCL copolymers, LS-35% and ISP-35%-PLA composites were considered to be viable for cells. Conversely, ISP-35%-8-2 and ISP-35%-9-1 composites showed negative responses on MG63 cells during the whole 7-day study.

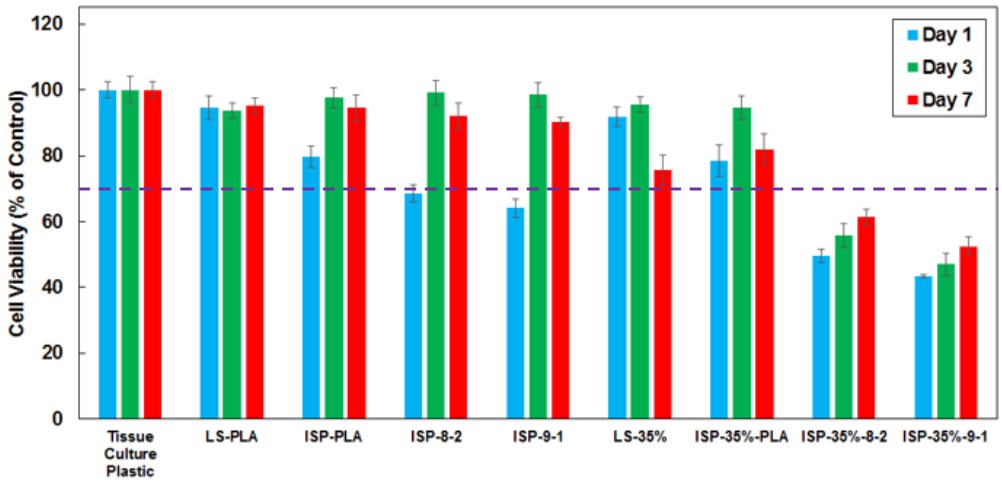

Figure 6.15 *Neutral red cell viability for PLA-PCL copolymers, PLA and their PGF composites (Purple dashed line indicates the lower limit of samples being considered as viable for the cells, 'Day' represents days of elution)*

6.5. Discussion

LS process has been conventionally employed to manufacture PGF reinforced fully bioresorbable composites. However, these LS composites suffered from rapid loss of mechanical properties when immersed within aqueous environments due to their relatively poor fibre/matrix interfacial bonding, which has thus far limited its application for use as bone fracture fixation devices [17, 18, 175]. ISP

process was proposed to overcome the issues experienced with LS, and was initially developed for PCL/PGF composites in Chapter 4 [17, 237]. PCL/PGF composites manufactured via ISP revealed significantly enhanced mechanical properties (~160 MPa and ~14 GPa of flexural strength and modulus respectively for composites with 35% V_f) and more importantly, prolonged mechanical property retention during immersion in PBS in comparison to LS composites was also observed [17].

Despite the significantly improved mechanical properties for PCL/PGF composites via ISP, they are still not sufficient for applications involving human cortical bone fracture fixation (as modulus & strength properties of cortical bone have been reported to range between 7 – 23 GPa and 50 – 250 MPa, respectively) [46, 48]. Hence, PLA was investigated as the matrix material to replace PCL since PLA is mechanically (~4 GPa and ~100 MPa for flexural strength and modulus) significantly stronger than PCL (~0.35 GPa and ~20 MPa for flexural strength and modulus) [22, 27, 157, 192]. However, to manufacture PLA/PGF composites via the ISP process, the monomer must be in a low viscosity state for the ISP process to work effectively. Since di-lactide (the monomer of PLA) is a solid at room temperature (and has a ~95 °C melting point), a new ISP process had to be developed.

In this chapter, the ISP process was initially established to produce PLA-PCL copolymers and their PGF reinforced composites, then developed further for use with neat PLA and their composites. The heated ISP manufacturing process developed had substantial influence on the PLA-PCL copolymers, neat PLA and their PGF reinforced composites, as discussed below.

6.5.1. Polymerisation kinetics

Since PLA and PCL both belong to the same family of aliphatic polyester (similar chemical structures), the reaction mechanism for the ring opening polymerisation of PLA and PCL is similar. In this work, PCL, PLA and PLA-PCL copolymers were all *in-situin-situ* polymerised via the same catalyst ($Sn(Oct)_2$) and initiator (benzyl alcohol), which coordination insertion is the main reaction mechanism for their polymerisation [74, 179].

Similar to the PCL polymerisation kinetic study detailed in Chapter 4, three key factors were studied to obtain the optimal polymerisation parameters for PLA, including reaction temperature, catalyst and initiator concentration within the monomer mixture. Since the reaction mechanism between PCL and PLA polymerisation is comparable, similar effects of varying those three key factors are expected between PCL and PLA ring opening polymerisation.

Figure 6.1 indicated that the PLA polymerisation rate increased with increasing amount of catalyst within the reaction system. However, according to Figure 6.2, catalyst concentration did not have any significant effect on the molecular weight of the resulted PLA, where ~40000 Da was achieved for all three catalyst concentrations when monomer conversion reached ~98%. Therefore, 0.0138 mol/L of catalyst $Sn(Oct)_2$ concentration was selected to maximize the polymerisation rate for PLA.

Identical monomer conversion profiles ($p>0.05$) can be seen from Figure 6.3 with PLA polymerisation proceeded with 3 different initiator concentrations, which indicated that the initiator concentration did not affect the PLA polymerisation rate. However, the molecular weight of the resulted PLA increased with decreasing

amount of initiator in the polymerisation system (see Figure 6.4), which revealed that the molecular weight of PLA could be directly controlled by altering the initiator concentration within the polymerisation reaction. As such, in order to yield PLA with targeted molecular weight, 0.00115 mol/L of initiator benzyl alcohol concentration was chosen.

With increasing polymerisation temperature, the PLA polymerisation rate increased significantly (see Figure 6.5), however, no significant variation of the molecular weight of PLA was observed (see Figure 6.6). Therefore, 160 °C was used as the neat PLA polymerisation temperature in order to pursue the ideal polymerisation rate for ISP process.

Conclusively, in order to ensure an effective PLA polymerisation system for the successful development of heated ISP process, molar ratio of [1000:0.1:1; 160 ºC] ([Monomer : Initiator : Catalyst; Reaction temperature]) was chosen as the final reaction parameters for neat PLA polymerisation in this work, which is the equivalent of $Sn(Oct)_2$ and benzyl alcohol concentration to be 0.0138 mol/L and 0.00115 mol/L respectively. The reaction time for complete PLA polymerisation (>98% monomer conversion) with the chosen reaction parameters is 3 hours, based on the kinetic studies (see Figure 6.1).

The reaction kinetics of PLA-PCL copolymerisation with two weight ratios (weight ratio of PLA:PCL = 9:1 and 8:2) were investigated. Since both ε-caprolactone and di-lactide were presented simultaneously during the copolymerisation, random copolymerisation are expected, as extensively reported in the literature, which follows the same ring opening mechanism as neat PCL and PLA polymerisation [11, 79, 238-240]. Since the major component within the targeted PLA-PCL

copolymer is PLA, the reaction temperature, catalyst and initiator concentration used for PLA-PCL copolymerisation were kept the same as for neat PLA polymerisation, which are stated earlier. This will ensure the resulted PLA-PCL copolymers to have consistent molecular weights and PDIs in comparison to neat PLA polymerisation.

It is evident from Figure 6.7 that the polymerisation of PLA initiated (~15 mins at 160 ^{o}C) significantly earlier than PCL polymerisation (~3 hours at 160 ^{o}C) during the copolymerisation. Moreover, the monomer conversion for PLA polymerisation reached ~98% at ~3 hours, only until then the PCL polymerisation initiated and reached ~98% monomer conversion after 26 - 28 hours at 160 ^{o}C (see Figure 6.7). This copolymerisation behaviour during PLA-PCL random copolymerisation is reported in the previous investigations, which PLA polymerisation often initiates firstly, follow by PCL polymerisation initiation when PLA polymerisation is mostly completed (monomer conversion > 95%) [44, 79, 239, 241]. This polymerisation sequential order originated from the difference in the bonding energy of the monomer ring between di-lactide and ε-caprolactone, which ε-caprolactone has a stronger monomer ring than di-lactide in terms of bonding energy, and the catalyst would favour to insert and open the monomer ring with weaker bonding (in this case di-lactide) [239, 241]. Moreover, comparing Figure 6.7a and b, the complete PCL polymerisation time (monomer conversion > 95%) increased by ~2 hours when the weight percentage of PCL within the PLA-PCL copolymer decreased from 20% to 10%, suggesting the decrease of PCL content within PLA-PCL copolymerisation could prolong the complete copolymerisation time.

Overall, based on the kinetic study for PLA-PCL copolymerisation, the reaction time for complete PLA-PCL copolymerisation was determined as 26 hours and

28 hours at 160 °C for PLA-PCL copolymers with weight ratio as 8:2 and 9:1 (PLA: PCL) respectively.

6.5.2. Effects of PLA-PCL copolymerisation

To effectively develop an ISP process, the monomer must ideally be in a low viscosity state to achieve sufficient fibre impregnation, such as ε-caprolactone monomer (CL) which is liquid at room temperature [17]. As the di-lactide monomer (LA) has a melting point at ~95 °C, significantly higher operating temperatures would be required for developing the ISP process for PLA, which also introduced many difficulties into the manufacturing process development.

In order to achieve a monomer mixture which retained a similar viscosity to neat CL, and to reduce the higher operating temperatures required, copolymerisation of CL and LA was considered. Initially, 10% and 20% weight fraction of CL was mixed with LA (denoted as LA8-CL2 and LA9-CL1 respectively), and their shear viscosity was measured between 95 °C and 170 °C. Figure 6.8 revealed that LA8-CL2 and LA9-CL1 reached similar viscosity to neat CL (~10 mm^2/s) at ~120 °C and ~140 °C respectively, in comparison to ~160 °C for neat LA, which suggested that a significant reduction ($p<0.0001$) in operating temperature could be achieved via mixing LA with CL, in comparison to using LA alone.

Moreover, Figure 6.8 also revealed that with increasing amount of CL, the viscosity profile of the monomer mixture versus increasing temperature decreased significantly ($p<0.0001$), following the order of neat LA > LA9-CL1 > LA8-CL2. The reduction in viscosity may have been as a result of the mild miscibility between LA and CL (LA can slightly dissolve within CL), which led to the relatively lower viscosity of the monomer mixture when compared to neat LA

at the same temperature [242, 243]. Vion *et al.* also reported a noticeable miscibility of L-lactide and ε-caprolactone in their study, in which the miscibility increased with increasing polymerisation temperature (between 140 °C to 180 °C) [241]. Overall, the studies above showed that adding LA to CL was highly beneficial in reducing the working temperature of the heated ISP process when compared to neat LA, thus making PLA-PCL copolymerisation more applicable for use in the ISP process.

However, as well as affecting the viscosity of the monomer mixture, the addition of CL to LA also caused a reduction in the T_g of the resulting copolymers (see Table 6.4 and Figure 6.9). An approximate ~21% and ~50% reduction in T_g was seen for ISP-9-1 and ISP-8-2 copolymers respectively, when compared to ISP-PLA alone. This behaviour was expected as PCL (T_g = -60 °C) has a significantly lower T_g value than PLA (~60 °C), and according to the Flory-Fox equation (see equation 10 in Section 3.13.8), the T_g values of their copolymers should theoretically have been between these two values [235, 244, 245]. From Table 6.4, the measured values of T_g for ISP-9-1 and ISP-8-2 were ~10% and ~11% higher than the estimated values from the Flory-Fox equation, which indicated that the actual PLA content within the resultant PLA-PCL copolymers was slightly higher than anticipated, and could have led to the higher T_g values. The relatively lower T_g values of the PLA-PCL copolymers had a dramatic influence on their mechanical retention and degradation behaviour, as discussed further below.

After the successful implementation of PLA-PCL copolymerisation, the ISP process was further developed to investigate neat LA monomer transfer, so that neat PLA/PGF composites could be manufactured. To achieve a suitable melt viscosity for neat LA, an operating temperature of 160 °C was required (see

Figure 6.8). However, high operating temperatures required use of high temperature materials (such as PTFE tubing, stainless steel pressure port, etc as mentioned in Section 3.10) to develop the heated ISP process for neat PLA.

During the initial trails, in which particularly the lengthy pre-heating procedure (up to ~1 hour) induced a low level of LA polymerisation and considerably increased the melt viscosity (which blocked transfer of the monomer within the tubing and slowed down the transfer rate). This premature polymerisation of LA resulted in relatively poor fibre impregnation and significant void formations within the initial PLA/PGF composites produced. However, the formation of defects within ISP-PLA and ISP-35%-PLA were reduced significantly by carefully adjusting the balance between the operating temperature and the polymerisation rate, which enabled successful implementation of the heated ISP process for PLA. The mechanical properties and cytocompatibility of the resultant ISP PLA/PGF composites are discussed and compared to LS PLA/PGF composites below.

6.5.3. Degradation and mechanical retention behaviour

6.5.3.1. PLA-PCL copolymers and their composites

Although the PLA-PCL copolymerisation was beneficial for reducing the ISP operating temperatures, the reduction in T_g values (~47 °C and ~31 °C for ISP-9-1 and ISP-8-2 respectively) of these copolymers (in comparison to LS-PLA and ISP-PLA, see Table 6.4) were found to be sufficiently low enough to adversely affect their degradation and mechanical property retention. PLA-PCL copolymers, ISP-9-1 and ISP-8-2, exhibited significantly lower initial flexural properties in comparison to both LS-PLA and ISP-PLA (see Figure 6.10a and b), where a decrease of ~20% and ~45% was seen for both flexural strength and modulus respectively. This reduction in mechanical properties was suggested to be due to

the component PCL (~20 MPa and ~0.4 GPa), which has significantly lower mechanical properties than PLA (~105 MPa and ~4 GPa) [17, 192]. Tsuji *et al.* investigated the tensile properties of PLA-PCL blended films produced via solvent casting, and reported a ~40% decrease in tensile strength for the blended films (50% PLA and 50% PCL in weight) when compared to neat PLA films [177, 246]. They also used rule of mixtures to predict the tensile strength of the blended films and reportedly achieved relatively accurate estimations.

Both ISP-9-1 and ISP-8-2 also revealed a significant decrease in their flexural properties during immersion in PBS at 37 °C (see Figure 6.10a and b), as a sharp reduction to ~20 MPa and ~0.4 GPa after 1-day immersion was seen for ISP-8-2, whilst a more gradual decrease to ~30 MPa and ~0.9 GPa after 7-days was observed for ISP-9-1. Their mechanical retention profiles also revealed that the level and rate of reduction in flexural properties for ISP-8-2 was significantly higher ($p<0.01$) than ISP-9-1, and the reductions observed were attributed to their T_g values (~47 °C and ~31 °C respectively), which were near or below the degradation temperature (37 °C). It is well understood that the physical states of any amorphous polymers are affected as their temperature gets closer to the T_g, which could in turn affect their mechanical properties [247]. Since the T_g of ISP-8-2 was ~30% lower than ISP-9-1 and was even lower than the degradation temperature (37 °C), the mechanical property deterioration for ISP-8-2 was expected to be more severe than ISP-9-1, as observed. The biodegradation behaviour of solution-casted PLA-PCL films within soil at 25 °C was investigated up to 2 months by Tsuji *et al.* [177] and they reported an accelerated tensile strength reduction with increasing amount of PCL (25%, 50%, 75% in weight) within the PLA-PCL copolymer composition, for which the reduction in T_g of the

copolymers was stated to be the major cause for reduction observed. Felfel *et al.* [158] investigated the degradation behaviour of neat PLA in three different temperatures (21 °C, 37°C and 50 °C) within PBS up to 56 days and reported no significant variation in PLA flexural strength before and after degradation at 21 °C, whilst ~20% and ~99% reduction was observed at 37 °C and 50 °C respectively, demonstrating that temperatures (nearer T_g) accelerated PLA degradation.

ISP-8-2 and ISP-9-1 also showed a significantly higher level of media absorption and mass loss than both the LS-PLA and ISP-PLA (see Figure 6.11a and b), which were mainly attributed to the difference in PBS diffusion rate between the neat PLA and PLA-PCL copolymers. Since the T_g of the copolymers was closer or below the degradation temperature, they allowed accelerated diffusion of PBS during immersion, which in turn increased the media absorption. Siparsky *et al.* [248] compared the water transport behaviour between neat PLA and PLA-PCL copolymer (PLA:PCL = 7:3 in weight) and reported significantly higher diffusion coefficient of water within the PLA-PCL copolymer when compared to neat PLA. They also stated that the PLA-PCL at test temperature (37 °C and 50 °C) became considerably softer and more vulnerable to water diffusion, which they attributed to the higher level of water absorption. Further evidence can be found in the molecular weight variation (see Figure 6.13a), where ISP-9-1 and ISP-8-2 showed ~10% and ~12% reduction respectively in molecular weight after 28-days immersion in PBS, whilst only ~2% reduction was seen for both LS-PLA and ISP-PLA. The main degradation mechanism of aliphatic polyesters, such as PCL, PLA and PLA-PCL copolymers, is hydrolysis, which media/water molecules react with vulnerable bonds within the polymer chains, result in chain scission and thus reduction in molecular weight [192, 249]. The increase in PBS absorption within

the PLA-PCL copolymers accelerated the hydrolytic degradation leading to faster reduction in molecular weight, and to the increase in mass loss observed (see Figure 6.11b). Similar behaviour was reported by Cohn *et al.* [239] for PLA-PCL copolymer (25%-30% PCL weight fraction) which degraded significantly faster than both neat PLA and PCL within PBS at 37 °C, where ~50% reduction in molecular weight was seen after 75 days, 5 and 12 months for PLA-PCL copolymers, neat PLA and PCL respectively. Lipik *et al.* [250] investigated the mass loss of PLA-PCL block copolymers (molar ratio of PLA:PCL = 1:1, 9:1 and 1:9) during degradation in PBS at 37 °C. A higher amount of mass loss was found with increasing PCL content within the PLA-PCL copolymers, which was attributed to PBS accelerated hydrolytic degradation.

Since PLA-PCL copolymers were used as the matrix material of ISP-35%-9-1 and ISP-35%-8-2, the effects of the decreased T_g also directly reflected on the degradation and mechanical property retention of their respective copolymer composites. Significant mechanical reinforcing effects were observed with the inclusion of PGF for the PLA-PCL copolymers, where an initial flexural strength and modulus of ISP-35%-9-1 and ISP-35%-8-2 was found to be ~310 MPa plus ~18 GPa and ~200 MPa plus ~13 GPa respectively (see Figures 6.10c and d). It is well known that the mechanical properties of any fibre reinforced polymer composites are directly dependent on both the properties of the fibre and the matrix material, where the rule of mixtures can be commonly applied to theoretically estimate the final mechanical properties of the fibre reinforced polymer composites [145]. Therefore, the neat PLA composites (LS-35% in this case) should theoretically have higher mechanical properties than the PLA-PCL copolymer composites, since the matrix LS-PLA showed significantly higher

mechanical properties than both ISP-9-1 and ISP-8-2 (see Figure 6.10a and b). However, Figures 6.10c and d revealed that both the flexural strength and modulus of ISP-35%-9-1 was significantly higher ($p<0.01$) than LS-35%. Since the rule of mixtures assumes an ideal fibre/matrix interfacial bonding, the mechanical property difference observed would suggest that ISP-35%-9-1 had stronger fibre/matrix interfacial bonding in comparison to LS-35%, which led to the higher mechanical properties observed, despite having lower mechanical properties for its neat matrix material. Supporting evidence can be found when comparing the cross-sectional SEM images of these composites. LS-35% (see Figure 6.14-a1) showed extensive dry fibre bundles and fibre pull-out, which suggested a weak fibre/matrix interfacial bonding. In contrast, Figure 6.14-c1 (for ISP-35%-9-1 sample) exhibited even fibre distribution with individual fibres fully impregnated by the matrix, suggesting that a more robust fibre/matrix interfacial bonding had been achieved. The SEM images clearly demonstrated that the ISP process produced considerably stronger fibre/matrix interfaces in comparison to the conventional LS process. It should also be noted that no sizing or coupling agents were used during any of these studies.

Figures 6.10c and d showed fast reduction in both strength and modulus of the PLA-PCL copolymer composites during the first 7-days immersed in PBS. The degradation profiles of ISP-35%-9-1 and ISP-35%-8-2 were also significantly higher and faster ($P<0.01$) in both flexural strength and modulus when compared to ISP-35%-PLA. The flexural strength and modulus of ISP-35%-9-1 reduced to ~50 MPa and ~6 GPa respectively after 7 days degradation, whilst ~50 MPa and ~2 GPa was seen for ISP-35%-8-2 after only 1-day in PBS. These reductions were not deemed suitable for application as fracture fixation devices, as the

mechanical properties for human cortical bone have been reported as 5–23 GPa and 35–250 MPa, for modulus & strength respectively. SEM images suggested earlier onset of PGF breakdown occurred for ISP-35%-8-2 (see Figure 6.14-c2) and ISP-35%-9-1 (see Figure 6.14-d2) in comparison with ISP-35%-PLA (see Figure 6.14-b2). The faster mechanical reductions and PGF breakdown most likely resulted from the low T_g of the PLA-PCL copolymer matrix being closer to the degradation temperature compared to neat PLA matrix (LS-PLA and ISP-PLA), leading to faster diffusion rates of the media to reach the fibre/matrix interface. This also correlated with the water uptake and mass loss profiles (see Figure 6.12a and b), where faster onset of increase and significantly higher overall profiles ($p<0.01$) for both ISP-35%-9-1 and ISP-35%-8-2 were observed when compared to ISP-35%-PLA. Overall, the ISP-35%-9-1 and ISP-35%-8-2 composites were more prone to liquid attack due to their lower T_g values, which made their mechanical retention performance less favourable for bone fracture fixations.

6.5.3.2. Neat PLA and PLA/PGF composites

The neat PLA produced via both LS and ISP, revealed similar initial flexural strength and modulus ($p>0.05$, ~105 MPa and ~4 GPa) (see Figure 6.10a and b). ISP-PLA and LS-PLA also maintained both their flexural strength and modulus throughout the 28-day degradation study.

The inclusion of PGFs increased the initial flexural strength and modulus values significantly (see Figures 6.10c and d), which ranged from ~300 MPa & ~17 GPa (for LS-35%) to ~450 MPa and ~24 GPa (for ISP-35%-PLA). These properties were comparable to human cortical bone, which suggested that these PGF composites could potentially be suitable for applications in hard tissue repair.

However, all the PGF composites suffered from a decrease ($p<0.0001$) in both flexural strength and modulus after 1 day of degradation in PBS at 37 °C. This degradation behaviour of PGF reinforced PCL and PLA composites has been investigated previously and similar initial mechanical reductions have been reported, where loss of fibre/matrix interface and plasticisation of the matrix was suggested as the main cause [17, 18, 157, 168, 251].

Previous work by the authors has shown that PCL/PGF composites produced via ISP possess enhanced mechanical and degradation properties in comparison to the LS composites [17]. It is clear from Figures 6.10c and d that ISP-35%-PLA achieved ~22% and ~13% increase in the initial (non-degraded) flexural strength and modulus respectively compared to LS-35%. After the initial reduction observed after 1-day immersion in PBS, the ISP-35%-PLA still maintained a flexural strength and modulus of ~300 MPa and ~17 GPa respectively, for 15 days. Whilst the LS-35% only managed to maintain ~160 MPa and ~11 GPa of flexural strength and modulus respectively, over 7 days. This evidence suggests that the heated ISP process promoted considerably prolonged mechanical property retention post media immersion for PLA/PGF composites, and the flexural properties of ISP-35%-PLA (after initial reduction) were still well-suited for application as fracture fixation devices.

The SEM images for the LS-35% composite cross-sections revealed polymer rich zones and dry fibre bundles (including fibre pull-out) as seen in Figure 6.14-a1, suggesting poor fibre impregnation and thus weak fibre/matrix interfacial bonding. In contrast, Figure 6.14-b1 exhibited highly uniform fibre distribution across the composite thickness for ISP-35%-PLA, without noticeable dry fibre bundles. This indicated excellent fibre wet out and hence a significantly enhanced fibre/matrix

interface for ISP composites. This enhancement of fibre/matrix interfacial bonding via ISP was also supported by the water-uptake and mass loss profiles, where significantly lower levels and slower rate of increase were seen for ISP-35%-PLA in comparison to LS-35% (see Figure 6.12a and b). These observations showed that the ISP process promoted a stronger and more fluid resistant fibre/matrix interface than LS process, which in turn led to the enhancements in the mechanical property retention and degradation profiles observed.

Secondary reduction in flexural properties was seen for both LS-35% and ISP-35%-PLA after day 11 and day 15 respectively, which was suggested to be due to the breakdown of PGFs within the composites. It is evident from Figure 6.14 (a2-3, b3, c2-3, d2-3) that hollow microtube-like structures were formed after degradation of the PGFs. This breakdown of PGF coincided with an increase in water uptake and mass loss of the composites (see Figure 6.12a and b). Similar degradation behaviour of PGF composites has been reported in previous studies, where major PGF fibre breakdown occurred between 7 and 21 days of immersion with PBS at 37 °C [16, 17, 25, 157].

The LS-PLA showed significantly higher molecular weight profiles ($p<0.0001$) than ISP-9-1, ISP-8-2 and ISP-PLA (see Figure 6.13a). The reaction environment during polymerisation was considered to be the main cause for this difference in molecular weight. Commercial grade PLA was used during LS production, which was produced simultaneously with strictly controlled temperature, proper agitation and under inert gas protection. However, the novel ISP process developed was designed to be a single-step production process, for which the agitation and inert gas protection was not feasible. The relatively less-controlled

reaction environment during ISP process resulted in less control over the polymerisation, which most likely led to the lower molecular weight achieved.

The inclusion of PGFs altered the molecular weight variation of both the PLA and PLA-PCL copolymers during degradation study. ISP-35%-PLA and LS-35% lost ~5% of their initial molecular weight after 28 days of degradation, whereas ~2% loss was observed for LS-PLA and ISP-PLA (see Figure 6.13a and b). Moreover, the molecular weight for both ISP-35%-9-1 and ISP-35%-8-2 decreased ~20% more than ISP-9-1 and ISP-8-2 after 28 days of degradation. These results suggested that the PGF breakdown products may have accelerated the degradation of the matrix (neat PLA and PLA-PCL copolymers), via catalytic hydrolysis due to the acidic nature of PGF degradation by-products. Supporting evidence can be observed in the pH variations of PBS (see Figures 6.11c and 6.12c), where no significant change ($p>0.05$) for neat matrix materials (PLA and PLA-PCL copolymers) was observed, whilst all PGF composites exhibited gradual decrease in pH. The pH reduction could have been caused by the polymer degradation and/or formation of phosphoric acid due to PGF breakdown, which in turn caused the acceleration for degradation of the matrix and thus the faster reduction in the molecular weight [15, 17, 175]. This finding was also reported by the author in Chapter 4 [17], where PGF breakdown catalysed and accelerated the molecular weight reduction of neat PCL matrix. However, it is necessary to mention that the degradation by-products are directly dependant on the formulation of the PGF, formulations maintaining neutral pH profiles during degradation have been developed in our group [133, 159, 170].

Those studies demonstrated that the degradation and mechanical retention behaviour of ISP-PLA-35% was well suited for applications as bone fracture

fixation devices. However, it should be noted that no coupling agents were applied on the PGFs, which the mechanical enhancement was achieved solely via ISP process.

6.5.4. Cytocompatibility tests

The biocompatibility and cytotoxicity of PLA and PCL have been well investigated and reported in the literature, and both are FDA approved materials, and have been used extensively in biomedical applications [11, 174, 252].

6.5.4.1. PLA-PCL copolymers and their composites

It can be seen from Figure 6.15 that both ISP-9-1 and ISP-8-2 showed significantly lower cell viability ($p<0.01$) after being exposed to day 1 degradation products, after which an increase in cell viability was observed when exposed to day 3 and day 7 degradation products. Release of any residual monomer present from the polymerisation reaction (for the ISP process) was considered to be responsible for the reduction in cell viability of ISP-9-1 and ISP-8-2 at day 1. Both di-lactide and ε-caprolactone monomers are known to hydrolyse rapidly in water into hydroxycarboxylic acids that generally display low cytotoxicity and have been shown to cause eye irritation [253]. Evidence for potential leaching of residual monomer was observed in the pH variations (see Figure 6.11b). Both ISP-9-1 and ISP-8-2 showed significantly lower pH profiles ($p<0.05$) in comparison to neat PLA (LS-PLA and ISP-PLA) from day 1, which suggested the release of di-lactide and ε-caprolactone (including oligomers or lactic acid) from the PLA-PCL copolymers, originating from the polymer/copolymer production process. Appropriate solvent extraction of residual monomers is usually carried out during industrial production of commercial grade PLA, which was used in the LS process in this work [254, 255]. In contrast, the ISP process was designed for a single-

step production process, where effective removal of residual monomer without deforming the sample was difficult. Furthermore, since the T_g of the PLA-PCL copolymers were closer to or below the immersion temperature in comparison to ISP-PLA, which may have allowed leaching of residual monomer, and in turn led to the lower cell viability observed at day 1.

Significant improvements in cell viability at later time points (3 and 7 days) for ISP-9-1 and ISP-8-2 were seen from Figure 6.15. It should be noted that the cell culture media was changed at day 1, 3, and 5 in this study to ensure the media was refreshed. The increase in cell viability after day 1 suggests that any residual monomer present had leached out after incubation in DMEM for 24h at 37 °C. Woodruff *et al.* [192] reviewed the hydrolysis degradation of PCL (within distilled water and PBS at 37°C and 50 °C) and suggested that the surface oligomers and carboxyl groups could freely diffuse into the surrounding media. Consequently, an effective surface monomer extraction process at ~37 °C via media immersion for PLA-PCL copolymers produced via ISP could be conducted. However, these composites would not be suitable for the load-bearing applications intended, as highlighted above.

The ISP-35%-9-1 and ISP-35%-8-2 exhibited considerably lower ($p<0.01$) cell viability than ISP-9-1 and ISP-8-2 respectively (see Figure 6.15). Studies have reported that PGFs are biocompatible, which the glass formulation used in this work has been investigated and reported to show good cell (MG63) response [13, 159, 170]. Due to the reduced T_g of the co-polymers and the test temperature used (i.e. 37°C), the degradation process of the PLA-PCL copolymer composites would have been accelerated and creating an acidic environment. This environment would have also facilitated relatively faster breakdown of the fibre

reinforcements via an autocatalytic effect within the cell culture media, which in turn had a negative impact on the cells [5, 13, 167].

6.5.4.2. Neat PLA and PLA/PGF composites

It is apparent from Figure 6.15 that both LS-PLA and ISP-PLA exhibited positive cell viability during the cytocompatibility study, where comparable results ($p>0.05$) with the tissue culture plastic control were observed.

No significant difference ($p>0.05$) was found in cell viability between the LS-PLA and LS-35%, as well as between ISP-PLA and ISP-35%-PLA at day 1 and day 3, which suggested that the inclusion of PGF did not alter the cell response during immersion within DMEM at 37 °C. This also supported the auto-catalytic effects suggested above. At day 7, LS-35% and ISP-35%-PLA showed lower cell viability ($p<0.05$) in comparison with LS-PLA and ISP-PLA respectively, which were still above the minimum cytocompatibility threshold of 70% according to standard ISO 10933.

In summary, the above studies showed for the first time that an ISP process for PLA reinforced with phosphate-glass fibres, with significantly superior mechanical and mechanical property retention in PBS at 37°C, in comparison to its laminate stacked alternative could be achieved. Furthermore, the neutral red elution study showed that both the LS-35% and ISP-35%-PLA exhibited positive cell response, which makes them the more appropriate choice for the intended biomedical applications.

6.6. Conclusions

In this chapter, a novel heated ISP process was successfully developed to manufacture fully bioresorbable PLA-PCL copolymers and PLA based PGF reinforced composites.

Whilst PLA-PCL copolymerisation was beneficial in decreasing the operating temperature for the heated ISP process, it also significantly decreased the T_g values for ISP-9-1 (~41 °C) and ISP-8-2 (~37 °C) when compared to neat PLA (~60 °C). The reduction in T_g correlated with an accelerated degradation in the mechanical properties of the PLA-PCL copolymer composites, with the flexural strength and modulus of the ISP-35%-9-1 and ISP-35%-8-2 decreased within 7 days to be lower than the mechanical properties of human cortical bone. The accelerated degradation behaviour also adversely affected their cytocompatibility performance, where both ISP-35%-9-1 and ISP-35%-8-2 were found to have a negative impact on the MG63 cells during the 7-day neutral red elution study.

ISP-35%-PLA achieved ~450 MPa and ~24 GPa for initial (non-degraded) flexural strength and modulus respectively, which was ca. 22% and ca. 13% higher than LS-35% respectively. ISP-35%-PLA also maintained its flexural strength and modulus at ~300 MPa and ~17 GPa respectively after the initial reduction (1-day immersion within PBS at 37 °C) until day 15, with the flexural properties maintained well matched with the mechanical properties of human cortical bone. The mechanical enhancement and prolonged retention was attributed to the significantly enhanced fibre/matrix interfacial adhesion achieved from the ISP process. This matched with the SEM observations, where LS-35% showed extensive dry fibres and pull-out, whilst ISP-35%-PLA exhibited uniform fibre distribution with no noticeable fibre pull-outs. Furthermore, both LS-35% and

ISP-35%-PLA exhibited positive cell viability throughout the cytocompatibility study.

Considering the mechanical property retention profiles in conjunction with initial cytocompatibility study, ISP-35%-PLA exhibited the most favourable performance for the intended applications in hard tissue repair.

Chapter 7. Overall Conclusions and Future Work

7.1. Overall conclusions

This work established and developed a novel, one-step ISP process intended for the manufacture of fully bioresorbable PGF reinforced composites (to be applied to PCL and PLA matrix composites), and characterised the material behaviour (including long term fatigue performance) of the resulted composites to demonstrate the advantages of the established ISP process over the conventional LS process. In comparison to LS process, the ISP process provided composites with enhanced fluid resistance and the retention of the mechanical performance, as well as maintaining good biocompatibility, to make the resulted composites mechanically more applicable for the intended hard tissue repair applications.

It should be noted that ISP process requires the monomer to be in a low viscosity state to work effectively. For PLA based matrix material, its monomer is solid at room temperature and requires extensive heating to be applied for the ISP process. The heating brought many technical difficulties not only to the heated ISP process development, but also to the polymerisation chemistry for the PLA based matrix material. To the author's best knowledge, the establishment of the heated ISP process for the manufacture of fully bioresorbable PLA based composites has not been investigated and is fully novel.

The following major conclusions can be summarized from this thesis:

A novel, single step ISP process was successfully developed in this work to manufacture fully bioresorbable composites. Initially, room temperature ISP process was established to produce PCL/PGF composites, which sophisticated moulding design and novel injection runner system (to prevent fibre movement and maintain alignment during moulding) was developed. Secondly, a novel heated ISP process was established based on the room temperature ISP process so that PLA-PCL copolymer composites can be manufactured. Automatic heating system, power control system, molten monomer transfer system, degassing system and moulding system were designed for the first time. Finally, the heated ISP process was further enhanced to fit with manufacturing of PLA/PGF composites, which a temperature up to 160 ^{o}C can be realized on the developed ISP system.

The application of the ISP process enabled significantly stronger fibre/matrix interfacial bonding in comparison to LS process, where even fibre distribution across the composites cross section area without noticeable dry fibre bundles was observed. The enhanced fibre/matrix interfaces led to the reduced media uptake & mass loss, prolonged mechanical property retention and higher initial flexural properties. On the one hand, ISP PCL/PGF composites achieved ~14 GPa and ~160 MPa for initial (non-degraded) flexural modulus and strength respectively with 35% V_f. Those mechanical properties were within the range of the mechanical properties of human cancellous bone, suggesting the suitability of the ISP PCL/PGF composites for cancellous bone repair applications. On the other hand, ISP PLA/PGF composites with 35% V_f showed initial flexural modulus and strength of ~24 GPa and ~450 MPa respectively. After the fluid immersion,

the ISP PLA/PGF composites maintained its flexural strength and modulus at ~300 MPa and ~17 GPa up to 15 days, which those mechanical properties are well matched with the human cortical bone. In addition, Good cytocompatibility was also observed for the ISP PLA/PGF composites.

The application of ISP process is proved to be able to enhance not only static mechanical properties, but also dynamic long term mechanical properties, which is of vital importance for the success application of the fully bioresorbable composites in the field of hard tissue repair. ISP PCL/PGF composites demonstrated ~10-fold flexural fatigue life in both dry and wet environment in comparison to the LS PCL/PGF composites, with ~4 million and ~300000 flexural fatigue life before failure achieved in dry and wet environment respectively for 35% V_f ISP PCL/PGF composites. The fatigue behaviour of all tested composites indicated that fluid immersion significantly reduced the fatigue life of the PCL/PGF composites and caused earlier onset of fatigue damage and faster damage propagation. Moreover, regardless of the testing environment, increase in fibre content could lead to shorter fatigue life for fully bioresorbable PCL/PGF composites.

In conclusion of the whole work, considering the degradation and mechanical retention profile (short and long term) in conjunction with initial cytocompatibility results, the ISP PLA/PGF composites were accounted as the most favourable fully bioresorbable composites for the use in hard tissue repair. The ISP process showed clear advantages over LS process in promoting stronger fibre/matrix interfaces, which can be applied to all PCL and PLA based composites.

7.2. Future work

7.2.1. Heated ISP process

- A fully automatic ISP system should be developed, from monomer mixing to composites demoulding. Since the clear advantages of the heated ISP process has been demonstrated in this thesis, it should be used as the standard manufacturing process, instead of conventional LS process, for production of fully bioresorbable polymer composites. However, the current operation of heated ISP process is highly dependent on experiences, time consuming (preparation can take more than 12 hours) and the quality control of the end composites is relatively difficult. Thus, the establishment of the automatic ISP system is called for.
- It can be seen that the polymerisation time for both PCL (~24 hours) and PLA (~3 hours) is rather long, which limits the industry scale-up of the ISP process for fully bioresorbable composites production. The current ISP process is time consuming and only can yield a very low production rate. Microwave heating, instead of conventional heating, can be applied to shorten the polymerisation time. It has been reported in the literature that the selective microwave heating can shorten the PCL polymerisation time to ~10 mins (monomer conversion >95%) [190, 256]. However, in order to use microwave heating, the moulding system has to be made by material that is microwave transparent, such as PTFE, PEEK or silicone glass. This kind of moulding system has to be specifically designed and can be rather expensive.
- Moulds with complicated-shaped cavity can be made to produce composites implant with various shapes and features, such as rods, bend-

plate, plate with screw holes, etc. Those designs are closer to the design of the implants currently used, which will help to understand the use experience of the implant composites better. It also possesses the potential to make mould cavity directly from CT scans of patients, and to make patient-tailored composite implants.

7.2.2. Long term fatigue behaviour characterisation

- High cycle flexural fatigue analysis was performed on the PCL/PGF composites in this work. Similar fatigue analysis can be applied on PLA/PGF composites produced via both LS and ISP. This analysis will give the essential fatigue behaviour for PLA/PGF composites, including the fatigue life and fatigue damage tolerance. Fatigue tests should also be performed in both the dry and wet environment.
- Only one stress ratio (R=0.1) was used in the flexural fatigue tests performed in this work. However, in order to fully capture the high cycle fatigue behaviour of both the LS and ISP composites with PCL and PLA matrix, flexural fatigue tests should be performed with various stress ratio (i.e. R=0.2,0.5,0.8). Fatigue tests with various R ratios should yield constant life diagram for the composites characterised, which the constant life diagram should provide good predications of the fatigue life and effective service time during applications.

7.2.3. Fibre/matrix interface improvements

- ISP process developed has demonstrated its ability to significantly enhance the fibre/matrix interfacial bonding for fully bioresorbable composites, which the increase in the mechanical properties was solely resulted from the nature of the ISP process. To further improve the

mechanical properties of the composites and prolong their mechanical retention, the development of appropriate coupling agent should be carried out. The coupling agent should be easy to apply, biocompatible and induce enhanced bonding between the fibre and matrix. Since ISP process involves live polymerisation, it is possible to introduce surface initiated polymerisation from the coupling agent on the fibre surfaces [257]. In this case, chemical bonding can be achieved between fibre and matrix by the combination of coupling agent and ISP process, which theoretically should yield composites with significantly improved mechanical properties.

References

1. Evans, S. and P. Gregson, *Composite technology in load-bearing orthopaedic implants.* Biomaterials, 1998. **19**(15): p. 1329-1342.
2. Heimke, G. and P. Griss, *Ceramic implant materials.* Medical and Biological Engineering and Computing, 1980. **18**(4): p. 503-510.
3. Sailer, I., et al., *A systematic review of the performance of ceramic and metal implant abutments supporting fixed implant reconstructions.* Clinical Oral Implants Research, 2009. **20**: p. 4-31.
4. Huttunen, M., et al., *Fiber-reinforced bioactive and bioabsorbable hybrid composites.* Biomedical Materials, 2008. **3**(3).
5. Parsons, A.J., et al., *Phosphate Glass Fibre Composites for Bone Repair.* Journal of Bionic Engineering, 2009. **6**(4): p. 318-323.
6. Sun, H., et al., *The in vivo degradation, absorption and excretion of PCL-based implant.* Biomaterials, 2006. **27**(9): p. 1735-1740.
7. Salih, V., et al., *Development of soluble glasses for biomedical use Part II: The biological response of human osteoblast cell lines to phosphate-based soluble glasses.* Journal of Materials Science: Materials in Medicine, 2000. **11**(10): p. 615-620.
8. Manhart, J., et al., *Mechanical properties of new composite restorative materials.* Journal of Biomedical Materials Research, 2000. **53**(4): p. 353-361.
9. Li, S. and M. Vert, *Biodegradation of Aliphatic Polyesters*, in *Degradable Polymers*, G. Scott, Editor. 2002, Springer Netherlands. p. 71-131.
10. Hasegawa, S., et al., *A 5–7 year in vivo study of high-strength hydroxyapatite/poly(l-lactide) composite rods for the internal fixation of bone fractures.* Biomaterials, 2006. **27**(8): p. 1327-1332.
11. Ramot, Y., et al., *Biocompatibility and safety of PLA and its copolymers.* Advanced drug delivery reviews, 2016. **107**: p. 153-162.
12. Mohammadi, M.S., et al., *Effect of phosphate-based glass fibre surface properties on thermally produced poly(lactic acid) matrix composites.* J Mater Sci Mater Med, 2011. **22**(12): p. 2659-72.
13. Ahmed, I., et al., *Processing, characterisation and biocompatibility of iron-phosphate glass fibres for tissue engineering.* Biomaterials, 2004. **25**(16): p. 3223-3232.
14. Haque, P., et al., *Influence of compatibilizing agent molecular structure on the mechanical properties of phosphate glass fiber-reinforced PLA composites.* Journal of Polymer Science Part A: Polymer Chemistry, 2010. **48**(14): p. 3082-3094.
15. Sharmin, N., et al., *Effect of boron oxide addition on fibre drawing, mechanical properties and dissolution behaviour of phosphate-based glass fibres with fixed 40, 45 and 50 mol% P2O5.* Journal of Biomaterials Applications, 2014. **29**(5): p. 639-653.
16. Ahmed, I., et al., *Retention of mechanical properties and cytocompatibility of a phosphate-based glass fiber/polylactic acid composite.* Journal of Biomedical Materials Research Part B: Applied Biomaterials, 2009. **89B**(1): p. 18-27.
17. Chen, M., et al., *In-situ polymerisation of fully bioresorbable polycaprolactone/phosphate glass fibre composites: In vitro degradation*

and mechanical properties. Journal of the mechanical behavior of biomedical materials, 2016. **59**: p. 78-89.
18. Felfel, R.M., et al., *In vitro degradation, flexural, compressive and shear properties of fully bioresorbable composite rods.* Journal of the Mechanical Behavior of Biomedical Materials, 2011. **4**(7): p. 1462-1472.
19. Brauer, D., et al., *Degradable phosphate glass fiber reinforced polymer matrices: mechanical properties and cell response.* Journal of Materials Science: Materials in Medicine, 2008. **19**(1): p. 121-127.
20. Daniels, A.U., et al., *Mechanical properties of biodegradable polymers and composites proposed for internal fixation of bone.* Journal of Applied Biomaterials, 1990. **1**(1): p. 57-78.
21. Colquhoun, R. and K.E. Tanner, *Mechanical behaviour of degradable phosphate glass fibres and composites—a review.* Biomedical Materials, 2016. **11**(1): p. 014105.
22. Ramakrishna, S., et al., *Biomedical applications of polymer-composite materials: a review.* Composites Science and Technology, 2001. **61**(9): p. 1189-1224.
23. Imai, Y., M. Nagai, and M. Watanabe, *Degradation of composite materials composed of tricalcium phosphate and a new type of block polyester containing a poly(L-lactic acid) segment.* Journal of Biomaterials Science, Polymer Edition, 1999. **10**(4): p. 421-432.
24. Mano, J.F., et al., *Bioinert, biodegradable and injectable polymeric matrix composites for hard tissue replacement: state of the art and recent developments.* Composites Science and Technology, 2004. **64**(6): p. 789-817.
25. Parsons, A., et al., *Mechanical and degradation properties of phosphate based glass fibre/PLA composites with different fibre treatment regimes.* Science and Engineering of Composite Materials, 2010. **17**(4): p. 243-260.
26. Furukawa, T., et al., *Biodegradation behavior of ultra-high-strength hydroxyapatite/poly (l-lactide) composite rods for internal fixation of bone fractures.* Biomaterials, 2000. **21**(9): p. 889-898.
27. Maurus, P.B. and C.C. Kaeding, *Bioabsorbable implant material review.* Operative Techniques in Sports Medicine, 2004. **12**(3): p. 158-160.
28. Madhavan Nampoothiri, K., N.R. Nair, and R.P. John, *An overview of the recent developments in polylactide (PLA) research.* Bioresource Technology, 2010. **101**(22): p. 8493-8501.
29. Majola, A., et al., *Absorption, Biocompatibility, and Fixation Properties of Polylactic Acid in Bone Tissue: An Experimental Study in Rats.* Clinical Orthopaedics and Related Research, 1991. **268**: p. 260-269.
30. Uhthoff, H.K. and F.L. Dubuc, *Bone Structure Changes in the Dog Under Rigid Internal Fixation.* Clinical Orthopaedics and Related Research, 1971. **81**: p. 165-170.
31. Mauffrey, C., et al., *External Fixation in Orthopedic Traumatology*. 2012, London: Springer.
32. Langer, R., *Tissue Engineering: A New Field and Its Challenges.* Pharmaceutical Research, 1997. **14**(7): p. 840-841.
33. Hubbell, J.A., *Biomaterials in Tissue engineering.* Nature Publishing Company, 1995. **13**(6): p. 565-576.
34. Christian, P., et al., *Monomer transfer moulding and rapid prototyping methods for fibre reinforced thermoplastics for medical applications.*

Composites Part A: Applied Science and Manufacturing, 2001. **32**(7): p. 969-976.
35. Jiang, G., et al., *Preparation of poly(ε-caprolactone)/continuous bioglass fibre composite using monomer transfer moulding for bone implant.* Biomaterials, 2005. **26**(15): p. 2281-2288.
36. Cowin, S.C., *Bone mechanics handbook (second edition)*. 2nd ed.: CSC Press LLC.
37. Hancox, N.M., *Biology of bone*. 1972, New York: Cambridge University Press.
38. Noor, Z., et al., *Assessment of microarchitecture and crystal structure of hydroxyapatite in osteoporosis.* Universa Medicina, 2011. **30**(1): p. 7-14.
39. Kanis, J.A., *Primer on the Metabolic Bone Diseases and Disorders of Mineral Metabolism.* Clinical Endocrinology, 2000. **52**(4): p. 526-526.
40. Burger, E.H. and J. Klein-Nulend, *Responses of Bone Cells to Biomechanical Forces in Vitro.* Advances in Dental Research, 1999. **13**(1): p. 93-98.
41. Lanyon, L.E., *Osteocytes, strain detection, bone modeling and remodeling.* Calcified Tissue International, 1993. **53**(1): p. S102-S107.
42. Göpferich, A., *Mechanisms of polymer degradation and erosion.* Biomaterials, 1996. **17**(2): p. 103-114.
43. Rivera-Denizard, O., et al., *Biocompatibility studies of human fetal osteoblast cells cultured on gamma titanium aluminide.* Journal of Materials Science: Materials in Medicine, 2008. **19**(1): p. 153-158.
44. Middleton, J.C. and A.J. Tipton, *Synthetic biodegradable polymers as orthopedic devices.* Biomaterials, 2000. **21**(23): p. 2335-2346.
45. Sawhney, G., *Fundamental of biomedical engineering*. 2007: New Delhi : New Age International. 273.
46. *The Mechanical Properties of Cortical Bone*, ed. D.T. Reilly and A.H. Burstein. Vol. 56. 1974. 1001-1022.
47. Reilly, D.T., A.H. Burstein, and V.H. Frankel, *The elastic modulus for bone.* Journal of Biomechanics, 1974. **7**(3): p. 271-275.
48. Rho, J.-Y., L. Kuhn-Spearing, and P. Zioupos, *Mechanical properties and the hierarchical structure of bone.* Medical Engineering & Physics, 1998. **20**(2): p. 92-102.
49. Williams, D.F., *The Williams dictionary of biomaterials*. 1999: Liverpool University Press.
50. Navarro, M., et al., *Biomaterials in orthopaedics.* Journal of The Royal Society Interface, 2008. **5**(27): p. 1137-1158.
51. Hench, L.L. and J.M. Polak, *Third-Generation Biomedical Materials.* Science, 2002. **295**(5557): p. 1014-1017.
52. Boyan, B.D., et al., *Role of material surfaces in regulating bone and cartilage cell response.* Biomaterials, 1996. **17**(2): p. 137-146.
53. Furlong, R. and J. Osborn, *Fixation of hip prostheses by hydroxyapatite ceramic coatings.* Journal of Bone & Joint Surgery, British Volume, 1991. **73-B**(5): p. 741-745.
54. Park, J. and R.S. Lakes, *Biomaterials: an introduction*. 2007: Springer.
55. Pietrzak, W.S., D.R. Sarver, and M.L. Verstynen, *Bioabsorbable Polymer Science for the Practicing Surgeon.* Journal of Craniofacial Surgery, 1997. **8**(2): p. 87-91.

56. Shih, C., *Chain-end scission in acid catalyzed hydrolysis of poly (d,l-lactide) in solution.* Journal of Controlled Release, 1995. **34**(1): p. 9-15.
57. Merkli, A., et al., *Biodegradable polymers for the controlled release of ocular drugs.* Progress in polymer science, 1998. **23**(3): p. 563-580.
58. Angela, L.S., et al., *Strategies in Aliphatic Polyester Synthesis for Biomaterial and Drug Delivery Applications*, in *Degradable Polymers and Materials: Principles and Practice (2nd Edition)*. 2012, American Chemical Society. p. 237-254.
59. Albertsson, A.C., *Degradable Aliphatic Polyesters*. 2002: Springer.
60. Ikada, Y. and H. Tsuji, *Biodegradable polyesters for medical and ecological applications.* Macromolecular rapid communications, 2000. **21**(3): p. 117-132.
61. Köpnick, H., et al., *Polyesters*, in *Ullmann's Encyclopedia of Industrial Chemistry*. 2000, Wiley-VCH Verlag GmbH & Co. KGaA.
62. Ritz, J., et al., *Caprolactam*, in *Ullmann's Encyclopedia of Industrial Chemistry*. 2000, Wiley-VCH Verlag GmbH & Co. KGaA.
63. Pitt, C. and A. Schindler, *Capronor--a biodegradable delivery system for levonorgestrel.* 1984.
64. Tomihata, K., et al., *A new resorbable monofilament suture.* Polymer Degradation and Stability, 1998. **59**(1–3): p. 13-18.
65. Hutmacher, D.W., et al., *Mechanical properties and cell cultural response of polycaprolactone scaffolds designed and fabricated via fused deposition modeling.* Journal of Biomedical Materials Research, 2001. **55**(2): p. 203-216.
66. Cristescu, R., et al., *Polycaprolactone biopolymer thin films obtained by matrix assisted pulsed laser evaporation.* Applied Surface Science, 2007. **253**(15): p. 6476-6479.
67. Pitt, C.G., et al., *Aliphatic polyesters. I. The degradation of poly(ε-caprolactone) in vivo.* Journal of Applied Polymer Science, 1981. **26**(11): p. 3779-3787.
68. Kulkarni, R.K., et al., *Biodegradable poly(lactic acid) polymers.* Journal of Biomedical Materials Research, 1971. **5**(3): p. 169-181.
69. van Natta F.J., Hill J.W., and C. W.H., *Study on the polymerization of ε-caprolactone.* Journal of American Chemcail Society, 1934. **56**: p. 455-457.
70. Young, D. and F. Hostettler, *Polyesters from Lactone.* Union Carbide F-40, 1962: p. 147.
71. Löfgren, A., et al., *Recent Advances in Ring-Opening Polymerization of Lactones and Related Compounds.* Journal of Macromolecular Science, Part C, 1995. **35**(3): p. 379-418.
72. Rozenberg, B.A., *Cationic polymerization of ε-caprolactone in the presence of diols via activated monomer mechanism.* Makromolekulare Chemie. Macromolecular Symposia, 1992. **60**(1): p. 177-188.
73. Kricheldorf, H.R., J.M. Jonté, and R. Dunsing, *Polylactones, 7. The mechanism of cationic polymerization of β-propiolactone and ε-caprolactone.* Die Makromolekulare Chemie, 1986. **187**(4): p. 771-785.
74. Kricheldorf, H.R., M. Berl, and N. Scharnagl, *Poly(lactones). 9. Polymerization mechanism of metal alkoxide initiated polymerizations of lactide and various lactones.* Macromolecules, 1988. **21**(2): p. 286-293.

75. Okamoto, Y., *Cationic ring-opening polymerization of lactones in the presence of alcohol.* Makromolekulare Chemie. Macromolecular Symposia, 1991. **42-43**(1): p. 117-133.
76. Lyudvig, Y.B., et al., *Cationic polymerization of lactones in the presence of hydroxyl-containing compounds.* Acta Polymerica, 1983. **34**(11-12): p. 754-761.
77. Hofman, A., S. Słomkowski, and S. Penczek, *Structure of active centers and mechanism of the anionic polymerization of lactones.* Die Makromolekulare Chemie, 1984. **185**(1): p. 91-101.
78. Agarwal, S., et al., *Rare earth metal initiated ring-opening polymerization of lactones.* Macromolecular rapid communications, 2000. **21**(5): p. 195-212.
79. Duda, A., et al., *Block and random copolymers of ε-caprolactone.* Polymer Degradation and Stability, 1998. **59**(1–3): p. 215-222.
80. Dubois, P., et al., *Macromolecular engineering of polylactones and polylactides. 4. Mechanism and kinetics of lactide homopolymerization by aluminum isopropoxide.* Macromolecules, 1991. **24**(9): p. 2266-2270.
81. Garlotta, D., *A Literature Review of Poly(Lactic Acid).* Journal of Polymers and the Environment, 2001. **9**(2): p. 63-84.
82. Hartmann, M.H., *High Molecular Weight Polylactic Acid Polymers*, in *Biopolymers from Renewable Resources*, D. Kaplan, Editor. 1998, Springer Berlin Heidelberg. p. 367-411.
83. Gupta, A.P. and V. Kumar, *New emerging trends in synthetic biodegradable polymers – Polylactide: A critique.* European Polymer Journal, 2007. **43**(10): p. 4053-4074.
84. Sinclair, R.G., *Blends of polyactic acid*. 1993, Google Patents.
85. Noda, M. and H. Okuyama, *Thermal catalytic depolymerization of poly (L-lactic acid) oligomer into LL-lactide: effects of Al, Ti, Zn and Zr compounds as catalysts.* CHEMICAL AND PHARMACEUTICAL BULLETIN-TOKYO-, 1999. **47**: p. 467-471.
86. Gupta, B., N. Revagade, and J. Hilborn, *Poly(lactic acid) fiber: An overview.* Progress in polymer science, 2007. **32**(4): p. 455-482.
87. Athanasiou, K.A., et al., *Orthopaedic applications for PLA-PGA biodegradable polymers.* Arthroscopy: The Journal of Arthroscopic & Related Surgery, 1998. **14**(7): p. 726-737.
88. Rokkanen, P.U., et al., *Bioabsorbable fixation in orthopaedic surgery and traumatology.* Biomaterials, 2000. **21**(24): p. 2607-2613.
89. Drumright, R.E., P.R. Gruber, and D.E. Henton, *Polylactic acid technology.* Advanced materials, 2000. **12**(23): p. 1841-1846.
90. Avinc, O. and A. Khoddami, *Overview of Poly(lactic acid) (PLA) fibre.* Fibre Chemistry, 2010. **42**(1): p. 68-78.
91. Auras, R.A., et al., *Poly (lactic acid): synthesis, structures, properties, processing, and applications*. Vol. 10. 2011: John Wiley & Sons.
92. Graves, G.A. and B. Kumar, *Bioabsorbable glass fibers for use in the reinforcement of bioabsorbable polymers for bone fixation devices and artificial ligaments*. 1986, Google Patents.
93. Nouvel, C., et al., *Controlled synthesis of amphiphilic biodegradable polylactide-grafted dextran copolymers.* Journal of Polymer Science Part A: Polymer Chemistry, 2004. **42**(11): p. 2577-2588.

94. Nijenhuis, A.J., D.W. Grijpma, and A.J. Pennings, *Lewis acid catalyzed polymerization of L-lactide. Kinetics and mechanism of the bulk polymerization.* Macromolecules, 1992. **25**(24): p. 6419-6424.
95. Dahlmann, J. and G. Rafler, *Biodegradable polymers. 7th comm. On the mechanism of ring-opening polymerization of cyclic esters of aliphatic hydroxycarboxylic acids by means of different tin compounds.* Acta Polymerica, 1993. **44**(2): p. 103-107.
96. Kricheldorf, H.R., I. Kreiser-Saunders, and C. Boettcher, *Polylactones: 31. Sn(II)octoate-initiated polymerization of L-lactide: a mechanistic study.* Polymer, 1995. **36**(6): p. 1253-1259.
97. Kowalski, A., A. Duda, and S. Penczek, *Kinetics and Mechanism of Cyclic Esters Polymerization Initiated with Tin(II) Octoate. 3.† Polymerization of l,l-Dilactide.* Macromolecules, 2000. **33**(20): p. 7359-7370.
98. Kricheldorf, H.R. and D.-O. Damrau, *Polylactones, 37. Polymerizations of L-lactide initiated with Zn(II) L-lactate and other resorbable Zn salts.* Macromolecular Chemistry and Physics, 1997. **198**(6): p. 1753-1766.
99. Kowalski, A., A. Duda, and S. Penczek, *Polymerization of l,l-Lactide Initiated by Aluminum Isopropoxide Trimer or Tetramer.* Macromolecules, 1998. **31**(7): p. 2114-2122.
100. Jacobsen, S., et al., *Polylactide (PLA)—a new way of production.* Polymer Engineering & Science, 1999. **39**(7): p. 1311-1319.
101. Dobrzynski, P., J. Kasperczyk, and M. Bero, *Application of calcium acetylacetonate to the polymerization of glycolide and copolymerization of glycolide with ε-caprolactone and l-lactide.* Macromolecules, 1999. **32**(14): p. 4735-4737.
102. Zhong, Z., et al., *Calcium methoxide initiated ring-opening polymerization of ε-caprolactone and L-lactide.* Polymer Bulletin, 2001. **46**(1): p. 51-57.
103. Kricheldorf, H. and A. Serra, *Polylactones.* Polymer Bulletin, 1985. **14**(6): p. 497-502.
104. Nakayama, A., et al., *Synthesis and degradability of a novel aliphatic polyester: poly(β-methyl-δ-valerolactone-co-L-lactide).* Polymer, 1995. **36**(6): p. 1295-1301.
105. Dunsing, R. and H. Kricheldorf, *Polylactones.* Polymer Bulletin, 1985. **14**(6): p. 491-495.
106. Chamberlain, B.M., et al., *Polymerization of Lactide with Zinc and Magnesium β-Diiminate Complexes: Stereocontrol and Mechanism.* Journal of the American Chemical Society, 2001. **123**(14): p. 3229-3238.
107. Bero, M., J. Kasperczyk, and Z.J. Jedlinski, *Coordination polymerization of lactides, 1. Structure determination of obtained polymers.* Die Makromolekulare Chemie, 1990. **191**(10): p. 2287-2296.
108. Dittrich, W. and R. Schulz, *KINETICS AND MECHNISM FOR RING-OPENING POLYMERIZATION OF L (-)-LACTIDE.* Angewandte Makromolekulare Chemie, 1971. **15**: p. 109-&.
109. Eguiburu, J.L., et al., *Ring-Opening Polymerization of l-Lactide Initiated by (2-Methacryloxy)ethyloxy−Aluminum Trialkoxides. 1. Kinetics.* Macromolecules, 1999. **32**(25): p. 8252-8258.
110. Ryner, M., et al., *Mechanism of Ring-Opening Polymerization of 1,5-Dioxepan-2-one and l-Lactide with Stannous 2-Ethylhexanoate. A Theoretical Study.* Macromolecules, 2001. **34**(12): p. 3877-3881.

111. Zhang, X., et al., *Mechanism of lactide polymerization in the presence of stannous octoate: The effect of hydroxy and carboxylic acid substances.* Journal of Polymer Science Part A: Polymer Chemistry, 1994. **32**(15): p. 2965-2970.
112. Duda, A., et al., *Polymerizations of ε-caprolactone and L,L-dilactide initiated with stannous octoate and stannous butoxide— a comparison.* Macromolecular Symposia, 2000. **153**(1): p. 41-53.
113. Göpferich, A. and J. Tessmar, *Polyanhydride degradation and erosion.* Advanced Drug Delivery Reviews, 2002. **54**(7): p. 911-931.
114. Li, S., *Hydrolytic degradation characteristics of aliphatic polyesters derived from lactic and glycolic acids.* Journal of Biomedical Materials Research, 1999. **48**(3): p. 342-353.
115. An, Y.H., S.K. Woolf, and R.J. Friedman, *Pre-clinical in vivo evaluation of orthopaedic bioabsorbable devices.* Biomaterials, 2000. **21**(24): p. 2635-2652.
116. Tsuchida, J., et al., *Structure of Ternary Aluminum Metaphosphate Glasses.* The Journal of Physical Chemistry C, 2011. **115**(44): p. 21927-21941.
117. Karabulut, M., et al., *Mechanical and structural properties of phosphate glasses.* Journal of Non-Crystalline Solids, 2001. **288**(1): p. 8-17.
118. Brow, R.K., *Review: the structure of simple phosphate glasses.* Journal of Non-Crystalline Solids, 2000. **263–264**(0): p. 1-28.
119. Ahmed, I., et al., *Phosphate glasses for tissue engineering: Part 1. Processing and characterisation of a ternary-based P< sub> 2</sub> O< sub> 5</sub>–CaO–Na< sub> 2</sub> O glass system.* Biomaterials, 2004. **25**(3): p. 491-499.
120. Knowles, J., K. Franks, and I. Abrahams, *Investigation of the solubility and ion release in the glass system K< sub> 2</sub> O–Na< sub> 2</sub> O–CaO–P< sub> 2</sub> O< sub> 5</sub>.* Biomaterials, 2001. **22**(23): p. 3091-3096.
121. Pickup, D.M., et al., *New sol–gel synthesis of a (CaO) 0.3 (Na 2 O) 0.2 (P 2 O 5) 0.5 bioresorbable glass and its structural characterisation.* Journal of Materials Chemistry, 2007. **17**(45): p. 4777-4784.
122. Knowles, J.C., *Phosphate based glasses for biomedical applications.* Journal of Materials Chemistry, 2003. **13**(10): p. 2395-2401.
123. Martin, S., *Review of the structures of phosphate glasses.* ChemInform, 1991. **22**(17).
124. Hoppe, U., *A structural model for phosphate glasses.* Journal of Non-Crystalline Solids, 1996. **195**(1–2): p. 138-147.
125. Neel, E.A.A., et al., *Structure and properties of strontium-doped phosphate-based glasses.* Journal of The Royal Society Interface, 2009. **6**(34): p. 435-446.
126. Griffith, A.A., *The phenomena of rupture and flow in solids.* Philosophical transactions of the royal society of london. Series A, containing papers of a mathematical or physical character, 1921: p. 163-198.
127. Walter, G., et al., *The structure of CaO–Na2O–MgO–P2O5 invert glass.* Journal of Non-Crystalline Solids, 2001. **296**(3): p. 212-223.
128. Brauer, D.S., et al., *Effect of TiO2 addition on structure, solubility and crystallisation of phosphate invert glasses for biomedical applications.* Journal of Non-Crystalline Solids, 2010. **356**(44–49): p. 2626-2633.

129. Bunker, B., G. Arnold, and J.A. Wilder, *Phosphate glass dissolution in aqueous solutions.* Journal of Non-Crystalline Solids, 1984. **64**(3): p. 291-316.
130. Gao, H., T. Tan, and D. Wang, *Dissolution mechanism and release kinetics of phosphate controlled release glasses in aqueous medium.* Journal of Controlled Release, 2004. **96**(1): p. 29-36.
131. Abou Neel, E.A., et al., *Effect of iron on the surface, degradation and ion release properties of phosphate-based glass fibres.* Acta Biomaterialia, 2005. **1**(5): p. 553-563.
132. Delahaye, F., et al., *Acid dissolution of sodium–calcium metaphosphate glasses.* Journal of Non-Crystalline Solids, 1998. **242**(1): p. 25-32.
133. Ahmed, A., et al., *Preparation and characterization of antibacterial P2O5–CaO–Na2O–Ag2O glasses.* Journal of Biomedical Materials Research Part A, 2011. **98**(1): p. 132-142.
134. Parsons, A.J., et al., *Mimicking Bone Structure and Function with Structural Composite Materials.* Journal of Bionic Engineering, 2010. **7, Supplement**(0): p. S1-S10.
135. Franks, K., et al., *Investigation of thermal parameters and crytallisation in a ternary CaO–Na< sub> 2</sub> O–P< sub> 2</sub> O< sub> 5</sub>-based glass system.* Biomaterials, 2001. **22**(5): p. 497-501.
136. Salih, V., et al., *Development of soluble glasses for biomedical use Part II: The biological response of human osteoblast cell lines to phosphate-based soluble glasses.* Journal of Materials Science: Materials in Medicine, 2000. **11**(10): p. 615-620.
137. Bitar, M., et al., *Soluble phosphate glasses: in vitro studies using human cells of hard and soft tissue origin.* Biomaterials, 2004. **25**(12): p. 2283-2292.
138. Navarro, M., M.P. Ginebra, and J.A. Planell, *Cellular response to calcium phosphate glasses with controlled solubility.* Journal of Biomedical Materials Research Part A, 2003. **67**(3): p. 1009-1015.
139. Abou Neel, E.A., W. Chrzanowski, and J.C. Knowles, *Effect of increasing titanium dioxide content on bulk and surface properties of phosphate-based glasses.* Acta Biomaterialia, 2008. **4**(3): p. 523-534.
140. Abou Neel, E.A., et al., *A Facile Synthesis Route to Prepare Microtubes from Phosphate Glass Fibres.* Advanced materials, 2007. **19**(19): p. 2856-2862.
141. Choueka, J., et al., *Effect of annealing temperature on the degradation of reinforcing fibers for absorbable implants.* Journal of Biomedical Materials Research, 1995. **29**(11): p. 1309-1315.
142. Cozien-Cazuc, S., et al., *Effects of aqueous aging on the mechanical properties of P40Na20Ca16Mg24 phosphate glass fibres.* Journal of Materials Science, 2008. **43**(14): p. 4834-4839.
143. Cozien-Cazuc, S., et al., *Real-time dissolution of P< sub> 40</sub> Na< sub> 20</sub> Ca< sub> 16</sub> Mg< sub> 24</sub> phosphate glass fibers.* Journal of Non-Crystalline Solids, 2009. **355**(50): p. 2514-2521.
144. Lin, S.T., et al., *Development of bioabsorbable glass fibres.* Biomaterials, 1994. **15**(13): p. 1057-1061.
145. Hull, D. and T. Clyne, *An introduction to composite materials*. 1996: Cambridge university press.

146. Smith, P. and J. Yeomans, *Benefits of Fiber and Particulate Reinforcement.* Materials Science and Engineering, 2009. **2**: p. 133-154.
147. Thomason, J.L., *The interface region in glass fibre-reinforced epoxy resin composites: 2. Water absorption, voids and the interface.* Composites, 1995. **26**(7): p. 477-485.
148. Wan, Y., et al., *In vitro degradation behavior of carbon fiber-reinforced PLA composites and influence of interfacial adhesion strength.* Journal of Applied Polymer Science, 2001. **82**(1): p. 150-158.
149. Zimmerman, M., J.R. Parsons, and H. Alexander, *The design and analysis of a laminated partially degradable composite bone plate for fracture fixation.* Journal of biomedical materials research, 1987. **21**(A3 Suppl): p. 345-361.
150. Saidpour, S.H., *Assessment of carbon fibre composite fracture fixation plate using finite element analysis.* Annals of biomedical engineering, 2006. **34**(7): p. 1157-1163.
151. Boccaccini, A.R., et al., *Polymer/bioactive glass nanocomposites for biomedical applications: a review.* Composites Science and Technology, 2010. **70**(13): p. 1764-1776.
152. Boccaccini, A.R. and V. Maquet, *Bioresorbable and bioactive polymer/Bioglass® composites with tailored pore structure for tissue engineering applications.* Composites Science and Technology, 2003. **63**(16): p. 2417-2429.
153. Pirhonen, E. and P. Törmälä, *Coating of bioactive glass 13-93 fibres with biomedical polymers.* Journal of materials science, 2006. **41**(7): p. 2031-2036.
154. De Diego, M.A., N.J. Coleman, and L.L. Hench, *Tensile properties of bioactive fibers for tissue engineering applications.* Journal of Biomedical Materials Research Part A, 2000. **53**(3): p. 199-203.
155. Kim, H.W., H.E. Kim, and J.C. Knowles, *Production and Potential of Bioactive Glass Nanofibers as a Next-Generation Biomaterial.* Advanced Functional Materials, 2006. **16**(12): p. 1529-1535.
156. Pirhonen, E., et al., *Manufacturing, mechanical characterization, and in vitro performance of bioactive glass 13–93 fibers.* Journal of Biomedical Materials Research Part B: Applied Biomaterials, 2006. **77**(2): p. 227-233.
157. Ahmed, I., et al., *Weight loss, ion release and initial mechanical properties of a binary calcium phosphate glass fibre/PCL composite.* Acta Biomaterialia, 2008. **4**(5): p. 1307-1314.
158. Felfel, R., et al., *Accelerated in vitro degradation properties of polylactic acid/phosphate glass fibre composites.* Journal of Materials Science, 2015. **50**(11): p. 3942-3955.
159. Ahmed, I., et al., *Cytocompatibility and effect of increasing MgO content in a range of quaternary invert phosphate-based glasses.* J Biomater Appl, 2010. **24**(6): p. 555-75.
160. Kharazi, A.Z., M. Fathi, and F. Bahmany, *Design of a textile composite bone plate using 3D-finite element method.* Materials & Design, 2010. **31**(3): p. 1468-1474.
161. Bagheri, Z.S., et al., *Biomechanical properties of an advanced new carbon/flax/epoxy composite material for bone plate applications.* Journal of the mechanical behavior of biomedical materials, 2013. **20**: p. 398-406.

162. Guo, H., et al., *Effect of epoxy coatings on carbon fibers during manufacture of carbon fiber reinforced resin matrix composites.* Materials & Design, 2010. **31**(3): p. 1186-1190.
163. Schambron, T., A. Lowe, and H.V. McGregor, *Effects of environmental ageing on the static and cyclic bending properties of braided carbon fibre/PEEK bone plates.* Composites Part B: Engineering, 2008. **39**(7): p. 1216-1220.
164. Nassif, G.A.A., *Effect of weave structure and weft density on the physical and mechanical properties of micro polyester woven fabrics.* Life Science Journal, 2012. **9**(3): p. 1326-1331.
165. Fujihara, K., et al., *Performance study of braided carbon/PEEK composite compression bone plates.* Biomaterials, 2003. **24**(15): p. 2661-2667.
166. Fujihara, K., et al., *Feasibility of knitted carbon/PEEK composites for orthopedic bone plates.* Biomaterials, 2004. **25**(17): p. 3877-3885.
167. Hasan, M., et al., *Cytocompatibility and Mechanical Properties of Short Phosphate Glass Fibre Reinforced Polylactic Acid (PLA) Composites: Effect of Coupling Agent Mediated Interface.* Journal of Functional Biomaterials, 2012. **3**(4): p. 706-725.
168. Barrera Betanzos, F., et al., *Cyclic pressure on compression-moulded bioresorbable phosphate glass fibre reinforced composites.* Materials & Design, 2016. **100**: p. 141-150.
169. Han, N., et al., *Influence of screw holes and gamma sterilization on properties of phosphate glass fiber-reinforced composite bone plates.* Journal of biomaterials applications, 2013. **27**(8): p. 990-1002.
170. Sharmin, N., et al., *Cytocompatibility, mechanical and dissolution properties of high strength boron and iron oxide phosphate glass fibre reinforced bioresorbable composites.* Journal of the mechanical behavior of biomedical materials, 2016. **59**: p. 41-56.
171. NV, C. *Corbion Annual Report 2013*. 2013.
172. Ahmed, I., et al., *Phosphate glasses for tissue engineering: part 2. Processing and characterisation of a ternary-based P 2 O 5–CaO–Na 2 O glass fibre system.* Biomaterials, 2004. **25**(3): p. 501-507.
173. Felfel, R.M., et al., *Investigation of crystallinity, molecular weight change, and mechanical properties of PLA/PBG bioresorbable composites as bone fracture fixation plates.* Journal of Biomaterials Applications, 2012. **26**(7): p. 765-789.
174. Felfel, R.M., et al., *In vitro degradation and mechanical properties of PLA-PCL copolymer unit cell scaffolds generated by two-photon polymerization.* Biomedical Materials, 2016. **11**(1): p. 015011.
175. Ahmed, I., et al., *Composites for bone repair: phosphate glass fibre reinforced PLA with varying fibre architecture.* Journal of Materials Science: Materials in Medicine, 2011. **22**(8): p. 1825-1834.
176. Khan, R.A., et al., *Degradation and interfacial properties of iron phosphate glass fiber-reinforced PCL-based composite for synthetic bone replacement materials.* Polymer-Plastics Technology and Engineering, 2010. **49**(12): p. 1265-1274.
177. Tsuji, H., A. Mizuno, and Y. Ikada, *Blends of aliphatic polyesters. III. Biodegradation of solution-cast blends from poly(L-lactide) and poly(ε-caprolactone).* Journal of Applied Polymer Science, 1998. **70**(11): p. 2259-2268.

178. Siparsky, G.L., K.J. Voorhees, and F. Miao, *Hydrolysis of Polylactic Acid (PLA) and Polycaprolactone (PCL) in Aqueous Acetonitrile Solutions: Autocatalysis.* Journal of environmental polymer degradation, 1998. **6**(1): p. 31-41.
179. Kricheldorf, H.R., I. Kreiser-Saunders, and A. Stricker, *Polylactones 48. SnOct2-Initiated Polymerizations of Lactide: A Mechanistic Study.* Macromolecules, 2000. **33**(3): p. 702-709.
180. Vassilopoulos, A.P. and T. Keller, *Fatigue of fiber-reinforced composites*. 2011: Springer Science & Business Media.
181. van den Oever, M. and T. Peijs, *Continuous-glass-fibre-reinforced polypropylene composites II. Influence of maleic-anhydride modified polypropylene on fatigue behaviour.* Composites Part A: Applied Science and Manufacturing, 1998. **29**(3): p. 227-239.
182. Gassan, J., *A study of fibre and interface parameters affecting the fatigue behaviour of natural fibre composites.* Composites Part A: Applied Science and Manufacturing, 2002. **33**(3): p. 369-374.
183. Reifsnider, K.L., K. Schulte, and J.C. Duke, *Long-term fatigue behavior of composite materials*, in *Long-term behavior of composites*. 1983, ASTM International.
184. Adams, R.D. and D.G.C. Bacon, *Measurement of the flexural damping capacity and dynamic Young's modulus of metals and reinforced plastics.* Journal of Physics D: Applied Physics, 1973. **6**(1): p. 27.
185. Xu, H., et al., *Biodegradable Composites: Ramie Fibre Reinforced PLLA-PCL Composite Prepared by in Situ Polymerization Process.* Polymer Bulletin, 2008. **61**(5): p. 663-670.
186. Corden, T.J., et al., *Physical and biocompatibility properties of poly-ε-caprolactone produced using in situ polymerisation: a novel manufacturing technique for long-fibre composite materials.* Biomaterials, 2000. **21**(7): p. 713-724.
187. Edwards, K.L., *An overview of the technology of fibre-reinforced plastics for design purposes.* Materials & Design, 1998. **19**(1–2): p. 1-10.
188. Corden, T.J., et al., *Initial development into a novel technique for manufacturing a long fibre thermoplastic bioabsorbable composite: in-situ polymerisation of poly-ε-caprolactone.* Composites Part A: Applied Science and Manufacturing, 1999. **30**(6): p. 737-746.
189. Bao, G. and Y. Song, *Crack bridging models for fiber composites with slip-dependent interfaces.* Journal of the Mechanics and Physics of Solids, 1993. **41**(9): p. 1425-1444.
190. Irvine, D., et al., *Enhanced 'In-situ' Catalysis via Microwave Selective Heating: Catalytic Chain Transfer Polymerisation.* RSC Advances, 2014.
191. Slivka, M.A., C.C. Chu, and I.A. Adisaputro, *Fiber-matrix interface studies on bioabsorbable composite materials for internal fixation of bone fractures. I. Raw material evaluation and measurement of fiber—matrix interfacial adhesion.* Journal of Biomedical Materials Research, 1997. **36**(4): p. 469-477.
192. Woodruff, M.A. and D.W. Hutmacher, *The return of a forgotten polymer—Polycaprolactone in the 21st century.* Progress in Polymer Science, 2010. **35**(10): p. 1217-1256.
193. Haltia, A.-M., et al., *Self-reinforcement and hydrolytic degradation of amorphous lactic acid based poly(ester-amide), and of its composite with*

sol-gel derived fibers. Journal of Materials Science: Materials in Medicine, 2002. **13**(10): p. 903-909.
194. Liu, X., et al., *Mechanical, degradation and cytocompatibility properties of magnesium coated phosphate glass fibre reinforced polycaprolactone composites.* Journal of Biomaterials Applications, 2014. **29**(5): p. 675-687.
195. Fung, Y.-C., *Biomechanics: mechanical properties of living tissues*. 2013: Springer Science & Business Media.
196. Wang, X., et al., *The role of collagen in determining bone mechanical properties.* Journal of Orthopaedic Research, 2001. **19**(6): p. 1021-1026.
197. Thomason, J.L. and L. Yang, *Temperature dependence of the interfacial shear strength in glass-fibre epoxy composites.* Composites Science and Technology, 2014. **96**: p. 7-12.
198. Yang, L. and J.L. Thomason, *Effect of silane coupling agent on mechanical performance of glass fibre.* Journal of Materials Science, 2013. **48**(5): p. 1947-1954.
199. Yang, L. and J.L. Thomason, *Development and application of micromechanical techniques for characterising interfacial shear strength in fibre-thermoplastic composites.* Polymer Testing, 2012. **31**(7): p. 895-903.
200. Liao, K., et al., *Long-term durability of fiber-reinforced polymer-matrix composite materials for infrastructure applications: a review.* Journal of advanced materials, 1998. **30**(4): p. 3-40.
201. Vauthier, E., et al., *Interactions between hygrothermal ageing and fatigue damage in unidirectional glass/epoxy composites.* Composites Science and Technology, 1998. **58**(5): p. 687-692.
202. Jones, C., et al. *The environmental fatigue behaviour of reinforced plastics*. in *Proceedings of the Royal Society of London A: Mathematical, Physical and Engineering Sciences*. 1984. The Royal Society.
203. Malpot, A., F. Touchard, and S. Bergamo, *Influence of moisture on the fatigue behaviour of a woven thermoplastic composite used for automotive application.* Materials & Design, 2016. **98**: p. 12-19.
204. Caprino, G. and A. D'Amore, *Flexural fatigue behaviour of random continuous-fibre-reinforced thermoplastic composites.* Composites Science and Technology, 1998. **58**(6): p. 957-965.
205. Cox, B.N. and D.B. Marshall, *CRACK BRIDGING IN THE FATIGUE OF FIBROUS COMPOSITES.* Fatigue & Fracture of Engineering Materials & Structures, 1991. **14**(8): p. 847-861.
206. Hamad, W.Y., *On the mechanisms of cumulative damage and fracture in native cellulose fibres.* Journal of Materials Science Letters, 1998. **17**(5): p. 433-436.
207. Aghazadeh Mohandesi, J. and B. Majidi, *Fatigue damage accumulation in carbon/epoxy laminated composites.* Materials & Design, 2009. **30**(6): p. 1950-1956.
208. Shiri, S., M. Yazdani, and M. Pourgol-Mohammad, *A fatigue damage accumulation model based on stiffness degradation of composite materials.* Materials & Design, 2015. **88**: p. 1290-1295.
209. Lu, J., et al., *Simulation of the fatigue behaviour of a power plant steel with a damage variable.* International Journal of Mechanical Sciences, 2015. **100**: p. 145-157.

210. Mao, H. and S. Mahadevan, *Fatigue damage modelling of composite materials.* Composite Structures, 2002. **58**(4): p. 405-410.
211. Wu, F. and W. Yao, *A fatigue damage model of composite materials.* International Journal of Fatigue, 2010. **32**(1): p. 134-138.
212. Gamstedt, E.K., L.A. Berglund, and T. Peijs, *Fatigue mechanisms in unidirectional glass-fibre-reinforced polypropylene.* Composites Science and Technology, 1999. **59**(5): p. 759-768.
213. Lu, J., W. Sun, and A. Becker, *Material characterisation and finite element modelling of cyclic plasticity behaviour for 304 stainless steel using a crystal plasticity model.* International Journal of Mechanical Sciences, 2016. **105**: p. 315-329.
214. Ramakrishnan, V. and N. Jayaraman, *Mechanistically based fatigue-damage evolution model for brittle matrix fibre-reinforced composites.* Journal of Materials Science, 1993. **28**(20): p. 5592-5602.
215. Keusch, S., H. Queck, and K. Gliesche, *Influence of glass fibre/epoxy resin interface on static mechanical properties of unidirectional composites and on fatigue performance of cross ply composites.* Composites Part A: Applied Science and Manufacturing, 1998. **29**(5): p. 701-705.
216. Subramanian, S., et al., *Influence of fiber-matrix interphase on the long-term behavior of graphite/epoxy composites*, in *Composite Materials: Testing and Design: Twelfth Volume*. 1996, ASTM International.
217. Shih, G.C. and L.J. Ebert, *The effect of the fiber/matrix interface on the flexural fatigue performance of unidirectional fiberglass composites.* Composites Science and Technology, 1987. **28**(2): p. 137-161.
218. Bledzki, A., G. Wacker, and H. Frenzel, *Effect of surface-treated glass fibres on the dynamic behavior of fibre-reinforced composites.* Mechanics of composite materials, 1994. **29**(5): p. 429-433.
219. Kotsikos, G., et al., *Environmentally enhanced fatigue damage in glass fibre reinforced composites characterised by acoustic emission.* Composites Part A: Applied Science and Manufacturing, 2000. **31**(9): p. 969-977.
220. Houghton, W., et al. *NDE of composite rotor blades during fatigue testing*. in *Proceedings of the Helicopter Society of America Conference, St. Louis*. 1980.
221. Liao, K., C.R. Schultheisz, and D.L. Hunston, *Long-term environmental fatigue of pultruded glass-fiber-reinforced composites under flexural loading.* International journal of fatigue, 1999. **21**(5): p. 485-495.
222. McBagonluri, F., et al., *Characterization of fatigue and combined environment on durability performance of glass/vinyl ester composite for infrastructure applications.* International journal of fatigue, 2000. **22**(1): p. 53-64.
223. Shan, Y. and K. Liao, *Environmental fatigue behavior and life prediction of unidirectional glass–carbon/epoxy hybrid composites.* International Journal of Fatigue, 2002. **24**(8): p. 847-859.
224. Sumsion, H. and D. Williams, *Effects of environment on the fatigue of graphite-epoxy composites*, in *Fatigue of composite materials*. 1975, ASTM International.
225. Shah, D.U., *Developing plant fibre composites for structural applications by optimising composite parameters: a critical review.* Journal of Materials Science, 2013. **48**(18): p. 6083-6107.

226. Shah, D.U., *Damage in biocomposites: Stiffness evolution of aligned plant fibre composites during monotonic and cyclic fatigue loading.* Composites Part A: Applied Science and Manufacturing, 2016. **83**: p. 160-168.
227. Chambers, A.R., et al., *The effect of voids on the flexural fatigue performance of unidirectional carbon fibre composites developed for wind turbine applications.* International Journal of Fatigue, 2006. **28**(10): p. 1389-1398.
228. Chandra, R., S. Singh, and K. Gupta, *Damping studies in fiber-reinforced composites–a review.* Composite structures, 1999. **46**(1): p. 41-51.
229. Saravanos, D.A. and C.C. Chamis, *Unified micromechanics of damping for unidirectional and off-axis fiber composites.* Journal of Composites, Technology and Research, 1990. **12**(1): p. 31-40.
230. Mandell, J.F., R.M. Reed, and D.D. Samborsky, *Fatigue of fiberglass wind turbine blade materials*.
231. Samborsky, D.D., *Fatigue of E-glass fiber reinforced composite materials and substructures*. 1999, Citeseer.
232. Boller, K.H., *Effect of tensile mean stresses on fatigue properties of plastic laminates reinforced with unwoven glass fibers*. 1964, DTIC Document.
233. Shah, D.U., et al., *Fatigue life evaluation of aligned plant fibre composites through S–N curves and constant-life diagrams.* Composites Science and Technology, 2013. **74**: p. 139-149.
234. Lam, C.X.F., et al., *Evaluation of polycaprolactone scaffold degradation for 6 months in vitro and in vivo.* Journal of Biomedical Materials Research Part A, 2009. **90A**(3): p. 906-919.
235. Koleske, J.V. and R.D. Lundberg, *Lactone polymers. I. Glass transition temperature of poly-ε-caprolactone by means on compatible polymer mixtures.* Journal of Polymer Science Part A-2: Polymer Physics, 1969. **7**(5): p. 795-807.
236. Södergård, A. and M. Stolt, *Properties of lactic acid based polymers and their correlation with composition.* Progress in Polymer Science, 2002. **27**(6): p. 1123-1163.
237. Chen, M., et al., *Wet and dry flexural high cycle fatigue behaviour of fully bioresorbable glass fibre composites: In-situ polymerisation versus laminate stacking.* Composites Science and Technology, 2017. **150**: p. 1-15.
238. Huang, M.-H., S. Li, and M. Vert, *Synthesis and degradation of PLA–PCL–PLA triblock copolymer prepared by successive polymerization of ε-caprolactone and dl-lactide.* Polymer, 2004. **45**(26): p. 8675-8681.
239. Cohn, D. and A. Hotovely Salomon, *Designing biodegradable multiblock PCL/PLA thermoplastic elastomers.* Biomaterials, 2005. **26**(15): p. 2297-2305.
240. Jacquier, V., et al., *Functionalized poly(ε-caprolactone) and copolymers with ethylene oxide through heterogeneous anionic coordinated polymerization. NMR characterization and crystallinity.* Macromolecular Chemistry and Physics, 1996. **197**(4): p. 1311-1324.
241. Vion, J.M., et al., *Synthesis, characterization, and miscibility of caprolactone random copolymers.* Macromolecules, 1986. **19**(7): p. 1828-1838.
242. Vanhoorne, P., et al., *Macromolecular engineering of polylactones and polylactides. 7. Structural analysis of copolyesters of iε-caprolactone and*

L- or D,L-lactide initiated by triisopropoxyaluminum. Macromolecules, 1992. **25**(1): p. 37-44.
243. In't Veld, P.J.A., et al., *Melt block copolymerization of ε-caprolactone and L-lactide.* Journal of Polymer Science Part A: Polymer Chemistry, 1997. **35**(2): p. 219-226.
244. Martin, O. and L. Avérous, *Poly(lactic acid): plasticization and properties of biodegradable multiphase systems.* Polymer, 2001. **42**(14): p. 6209-6219.
245. Wood, L.A., *Glass transition temperatures of copolymers.* Journal of Polymer Science, 1958. **28**(117): p. 319-330.
246. Tsuji, H. and Y. Ikada, *Blends of aliphatic polyesters. I. Physical properties and morphologies of solution-cast blends from poly(DL-lactide) and poly(ε-caprolactone).* Journal of Applied Polymer Science, 1996. **60**(13): p. 2367-2375.
247. Williams, M.L., R.F. Landel, and J.D. Ferry, *The Temperature Dependence of Relaxation Mechanisms in Amorphous Polymers and Other Glass-forming Liquids.* Journal of the American Chemical Society, 1955. **77**(14): p. 3701-3707.
248. Siparsky, G.L., et al., *Water transport in polylactic acid (PLA), PLA/ polycaprolactone copolymers, and PLA/polyethylene glycol blends.* Journal of environmental polymer degradation, 1997. **5**(3): p. 125-136.
249. Lyu, S. and D. Untereker, *Degradability of Polymers for Implantable Biomedical Devices.* International Journal of Molecular Sciences, 2009. **10**(9): p. 4033-4065.
250. Lipik, V.T., et al., *Thermoplastic biodegradable elastomers based on ε-caprolactone and l-lactide block co-polymers: A new synthetic approach.* Acta Biomaterialia, 2010. **6**(11): p. 4261-4270.
251. Sharmin, N., et al., *Effect of Boron Addition on the Thermal, Degradation, and Cytocompatibility Properties of Phosphate-Based Glasses.* BioMed Research International, 2013. **2013**: p. 12.
252. Anderson, J.M. and M.S. Shive, *Biodegradation and biocompatibility of PLA and PLGA microspheres.* Advanced Drug Delivery Reviews, 1997. **28**(1): p. 5-24.
253. Miltenberger, K., *Hydroxycarboxylic Acids, Aliphatic*, in *Ullmann's Encyclopedia of Industrial Chemistry*. 2000, Wiley-VCH Verlag GmbH & Co. KGaA.
254. Södergard, A. and M. Stolt, *Poly (lactic acid): Synthesis, Structures, Properties, Processing and Applications, edited by R. Auras, L.-T. Lim, SEM Selke, and H. Tsuji*. 2010, John Wiley and Sons, NJ, USA.
255. Lunt, J., *Large-scale production, properties and commercial applications of polylactic acid polymers.* Polymer Degradation and Stability, 1998. **59**(1–3): p. 145-152.
256. Johnson, M.S., C.D. Rudd, and D.J. Hill, *Microwave assisted resin transfer moulding.* Composites Part A: Applied Science and Manufacturing, 1998. **29**(1): p. 71-86.
257. Xu, F.J., Z.H. Wang, and W.T. Yang, *Surface functionalization of polycaprolactone films via surface-initiated atom transfer radical polymerization for covalently coupling cell-adhesive biomolecules.* Biomaterials, 2010. **31**(12): p. 3139-3147.